

The role of Galectin-3 in the subventricular zone response to demyelination

Doctor of Philosophy Thesis

James Michael Hillis

Magdalen College
Department of Physiology, Anatomy and Genetics
University of Oxford

Trinity Term 2015

For my grandparents.

Abstract

Multiple sclerosis (MS) is a debilitating neurological condition that causes demyelination and axon degeneration. While relapsing forms of the disease have been treatable for many years, progressive forms lack definitive treatment. An hypothesised therapy involves neural stem cells repairing and replacing damaged oligodendrocytes and neurons. The subventricular zone (SVZ) is a known site of adult neurogenesis and is adjacent to the corpus callosum (CC) white matter region. Previous studies have suggested that SVZ stem cells give rise to oligodendrocytes in the demyelinated CC in both MS and its animal models. This thesis examines the hypothesis that the pro-inflammatory molecule Galectin-3 (Gal-3) impacts on the SVZ regenerative response. The thesis firstly shows a juxtaposition of inflammation between the SVZ and CC, with the SVZ becoming less inflamed during cuprizone treatment while the CC becomes more inflamed. This observation occurs with Gal-3+ astrocytes and microglia, CD45+ haematopoietic cells, and PHi3+ proliferating cells. The absence of Gal-3 in knockout transgenic mice does not, however, alter this inflammation. The thesis then shows an increase in knockout mice compared to wild-type mice of myelin basic protein levels in layer six of the motor cortex, as well as suggesting knockout mice have more SVZ cells migrating into the CC. These findings lead to the hypothesis of Gal-3 absence allowing SVZ cells to migrate into the CC and possibly lower cortical layers, and contributing to better remyelination. This mechanism is evaluated further with in vitro studies, which show that Gal-3 enhances neuronal differentiation in SVZ neurosphere cultures. Gal-3 absence does not, however, cause a significant change in the proportion of oligodendrocytes in SVZ neurosphere cultures, or in the number of oligodendrocytes after cuprizone treatment. Overall this thesis provides results that could impact on the best utilisation of SVZ stem cells to treat MS.

Acknowledgements

It is always interesting how one's perception of an activity differs before and after. Before I began this degree, I hoped it would develop my interest in stem cells and provide proficiency in scientific techniques. I did not, however, expect it to deliver a far greater foundation about the philosophy of science. As a medical practitioner, one of my key roles was to answer questions posed (be it determining a diagnosis from symptoms, or treatments from a diagnosis). I quickly learnt that scientists need to ask those questions first. Similar lessons have recurred throughout this degree. As I reflect on this chapter of my life, I feel like I have accomplished my initial aims as well as so much more.

It goes without saying that there are many people to whom I owe my thanks.

A/Prof Francis Szele, my supervisor, is one of the biggest advocates for "proper science" I know. His focus on ensuring his graduate students develop as critical thinkers is relentless. As I lay the foundations for my future research career, this development is the most significant building block I could have asked from him.

Prof Zoltán Molnár also welcomed me into his laboratory. His and his laboratory members' experience was incredibly helpful in planning and performing experiments. His boundless enthusiasm also ensured my experience of the graduate student roller coaster featured more highs than lows.

Timothy Keyes, Joseph Severs and Alec Noar were three undergraduate students who I supervised. Mayara Mundim was a visiting PhD student from the Universidade Federal de São Paulo who I worked directly with. They all brought fresh enthusiasm and ideas to the laboratory. It was a pleasure and a privilege to work with them.

The other members of the Szele laboratory were also a pleasure to work with: István Adorján, Osama Al Dalahmah, Abeer Al-Shammari, Chiara Bardella, Eun Hyuk

Chang, Julie Davies, Martin Ducker, Rachel James, Delia Koennig, Tracy Lane, Yichen Li, James Nicholson, Diana Rostirolla, Bin Sun, Rod Walker, Chris Young and the myriad rotation students. The members of the Molnár laboratory were too: Abigail Avelar, Melissa Bailey, Amanda Cheung, Fernando Garcia Moreno, Ellie Grant, Luiz Guidi, Anna Hoerder-Suabedissen, Kim Korrell, Andre Marques Smith, Isabel Martinez Garay, Jennifer Miller, Helen Stolp, Navneet Vasistha, Wei Zhi Wang and their rotation students.

While I am grateful to members of both laboratories for their advice, Amanda Cheung deserves a special mention. Her calm and patient teaching of laboratory techniques when I began meant I had two feet to stand on. Annette Bergner provided similar hands-on teaching when I undertook a laboratory rotation as an undergraduate. My gratitude to them both is immense.

Beyond the laboratory, the Biomedical Sciences Building staff were always happy and helpful, especially the Szele laboratory animal technicians Laura, Michael, Nick and Rachel, and the NACWOs Adrian, Ange, Denise, James, Richard, Simon and Stephen. I am also grateful for the help and advice of Colin Beesley, Helen Christian, Carlota De Blas Rodriguez, Gabriele De Luca, David Greaves, Asif Iqbal, Mohan Masih, Antonio Miranda, Lynne Scott, Shankar Srinivas, Lewis Taylor, Elizabeth Tunbridge and Richard Yates.

In preparing this thesis, Melissa Bailey, Claire Higgins, Mayara Mundim and Francis Szele proofread drafts and provided feedback. Harriet Keane and Max Marcus guided me in learning how to use Latex.

The University of Oxford "experience" was, in a word, phemarvellous. So many lifelong friendships were forged and so many lifelong memories created. Highlights included bumping and winning blades with the Magdalen College Boat Club, living with phenomenal housemates at the AbingTon, celebrating an Antipodean Christmas in rural Yorkshire, swimming the English Channel with the Mind Your Head relay team, dining at College formal halls, organising events for Cortex Club and the

Magdalen Middle Common Room, trialling with the Oxford University Lightweight Rowing Club, being passionate about mental health awareness with It Gets Brighter, teaching exceptional medical students at Magdalen College, celebrating Hogmanay in Edinburgh, and cycling to France and Wales with Team Malt Loaf.

The Clarendon Fund and James Fairfax - Oxford Australia Scholarship Fund made both the learning and the broader experiences possible. Ailsa and John White are amazing custodians of the latter, and I will fondly remember the lively annual luncheons at St John's College.

Many mentors have guided me on the journey to where I am today. As Isaac Newton once wrote, "If I have seen further it is by standing on the shoulders of giants". The following giants were particularly prominent as I progressed towards and through this degree: Richard Anderson, James Angus, James Best, Ben Canny, John Collins, Rowan Crosbie-Goold, Gabriele De Luca, Dawn DeWitt, Chris Garland, Zoltán Molnár, Kenneth Payne, Tony Shafton, Roger Short, Elsdon Storey, Francis Szele, Zoe Wainer and Heather Young.

My parents, Pam and David, and my step-parents, Di and Doug, have given me the opportunity to live the dream. It is because of them that I constantly need to pinch myself to remind me that the dream is in fact reality. Their upbringing was the best springboard into life imaginable. My partner, Melissa, continues to make me laugh and smile every day. Her energy and excitement are infectious, and bring out the best in me. My sister, Cath, has been a rock of support over the years. Her ears are forever open and her advice forever sincere. My grandparents, Marj, Pat, Don and Ted, have always emphasised the importance of learning and endeavour. This thesis, a landmark in my education, is dedicated to them.

James Michael Hillis

Authorship statement

I contributed to the design, performance and analysis of the experiments for all results included in this thesis.

A/Prof Francis Szele, my supervisor, contributed to the design of experiments and provided guidance on the performance and analysis of them.

Three undergraduate students were supervised by me and contributed to immunohistochemistry experiments. Mr Timothy Keyes, an undergraduate exchange student from Princeton University, volunteered with me in the laboratory. Mr Joseph Severs and Mr Alec Noar, undergraduate medical students, undertook their Final Honour School projects with me. I trained them in immunohistochemistry, microscopy and analysis. Their experiments and results, including figure elements, are included in this thesis.

A visiting doctor of philosophy student, Ms Mayara Mundim from the Universidade Federal de São Paulo, worked directly with me. We worked together on floxed mouse, proliferation assay, differentiation assay and migration assay experiments. We distributed the workload for these experiments between us. I also performed a considerable number of animal procedures for in vivo traumatic brain injury experiments by MM. These experiments have not been included in this thesis.

The developmental expression experiments were a collaboration with Ms Melissa Bailey and Prof Zoltán Molnár who were investigating two genes of their own interest. MB and ZM dissected tissue. MB, other members of the Molnár laboratory and I processed mRNA. MB, Dr Tracy Lane and I performed then analysed the real-time polymerase chain reaction experiments.

The siRNA construct development and SVZ gene expression experiments were a collaboration with Dr Osama Al Dalahmah in the Szele laboratory. We distributed

the workload for these experiments between us.

The human tissue experiments were a collaboration with Mr Richard Yates and A/Prof Gabriele De Luca in the Nuffield Department of Clinical Neurosciences, as well as Dr István Adorján in the Szele laboratory. RY, IA and I performed different parts of the immunohistochemistry experiments. We all contributed to the design and analysis of experiments.

The macrophage chemotaxis experiments were a collaboration with Dr Asif Iqbal, Ms Carlota De Blas Rodriguez, Mr Lewis Taylor and Prof David Greaves. AI, DG, MM, FS and I designed the experiments. AI, CDBR and LT performed the majority of the experiments with input from MM and me. AI and I conducted most of the analysis.

The Theiler's murine encephalomyelitis virus experiments were performed using tissue obtained by Dr Rachel James, a former doctoral student in the Szele laboratory.

All other experiments, including design, performance and analysis, were performed by me with generous guidance from members of the Szele and Molnár laboratories, the University of Oxford, and the greater scientific community.

James Michael Hillis

30 April 2015

Contents

Prologue **i**
Abstract . . . i
Acknowledgements . . . ii
Authorship statement . . . v
Contents . . . vii
Abbreviations . . . xii
List of figures . . . xiv
List of tables . . . xvi

1 Introduction **1**
1.1 The myelin sheath . . . 2
1.1.1 Structure and development of myelin . . . 2
1.1.2 Disruption of myelin . . . 6
1.1.3 Repair of myelin . . . 7
1.2 Multiple sclerosis . . . 9
1.2.1 Epidemiology and aetiology . . . 9
1.2.2 Pathogenesis . . . 11
1.2.3 Current treatment . . . 13
1.2.4 Animal models of demyelination . . . 15
1.3 Stem cell treatment . . . 17
1.3.1 Subventricular zone . . . 18
1.3.2 Stem cells and demyelination . . . 22
1.4 The galectin family . . . 24
1.4.1 Galectin-3 . . . 25
1.4.2 Galectin-3 in the SVZ and demyelination . . . 27
1.5 Research questions . . . 28

2 Methods **29**
2.1 Human tissue . . . 30
2.2 Animals . . . 30
2.2.1 Breeding and maintenance . . . 30
2.2.2 Genotyping . . . 31
2.2.3 Bromodeoxyuridine administration . . . 31
2.2.4 Cuprizone administration . . . 32
2.2.5 TMEV inoculation . . . 33
2.3 Histology . . . 33
2.3.1 Animal tissue preparation . . . 33
2.3.2 Microtome sectioning . . . 33
2.3.3 Fluorescent immunohistochemistry . . . 34
2.3.4 DAB immunohistochemistry . . . 35
2.3.5 X-gal immunohistochemistry . . . 36
2.3.6 Web search for in situ hybridisation and immunohistochemistry 36
2.4 Microscopy . . . 37
2.4.1 Bright-field and epifluorescence microscopy . . . 37
2.4.2 Confocal microscopy . . . 37
2.4.3 Image analysis . . . 37
2.5 Real-time polymerase chain reaction . . . 38

2.5.1 Developmental samples . . . 38
2.5.2 SVZ samples . . . 39
2.6 Molecular techniques . . . 40
2.6.1 siRNA plasmid design and production . . . 40
2.6.2 Transfection of HEK293T cells . . . 41
2.6.3 Western blot . . . 42
2.7 Neurosphere assays . . . 43
2.7.1 Neurosphere assay . . . 43
2.7.2 Proliferation assay . . . 43
2.7.3 Differentiation assay . . . 44
2.8 Migration assays . . . 45
2.8.1 Neuroblast explant assays . . . 45
2.8.2 ACEA xCELLigence real-time migration assay including Biogel macrophage recruitment and flow cytometry . . . 47
2.9 Statistics . . . 48

3 Galectin-3 experimental toolkit development 49
3.1 Introduction . . . 50
3.2 Results . . . 51
3.2.1 Identification of Gal-3^{+}, Gal-3^{-} and Gal-3^{fl} alleles . . . 51
3.2.2 Creation of Gal-$3^{+/+}$ and Gal-$3^{-/-}$ brain library . . . 51
3.2.3 Developmental expression of Gal-3 . . . 53
3.2.4 Characterisation of Gal-3 floxed mouse . . . 58
3.2.5 Creation of siRNA Gal-3 constructs . . . 60
3.3 Discussion . . . 62
3.3.1 Developmental expression of Gal-3 . . . 62
3.3.2 Characterisation of Gal-3 floxed mouse . . . 63

4 Galectin-3 and its role in inflammation 65
4.1 Introduction . . . 66
4.1.1 Relationship of MS with Gal-3 and the SVZ . . . 66
4.1.2 Inflammation in the SVZ . . . 67
4.1.3 Gal-3 interactions with other galectins . . . 68
4.1.4 Research questions . . . 69
4.2 Results . . . 70
4.2.1 Gal-3 expression occurs normally in the human SVZ and increases in the adjacent CC in acute MS plaques . . . 70
4.2.2 Gal-3 expression increases in the mouse CC but decreases in the SVZ after cuprizone treatment . . . 74
4.2.3 Gal-3 expression after cuprizone treatment occurs in GFAP+ astrocytes and CD45+ microglia . . . 76
4.2.4 Gal-3 absence does not alter weight change during cuprizone treatment . . . 79
4.2.5 Haematopoietic cell density follows a similar pattern to Gal-3+ cell density after cuprizone treatment and is not altered by Gal-3 absence . . . 81
4.2.6 CD68-GFP transgenic mice further demonstrate immune cell activation after cuprizone treatment . . . 83
4.2.7 Proliferation also follows a similar pattern to Gal-3+ cell density after cuprizone treatment and is not altered by Gal-3 absence . 84

4.2.8 In vitro proliferation is not altered by Gal-3 absence 87
4.2.9 Reactive astrocytosis increases with cuprizone treatment in the SVZ and CC, and occurs more in the CC in the presence of Gal-3 89
4.2.10 Gal-3 absence is not compensated by other galectins 91
4.3 Discussion 93
4.3.1 Gal-3 presence around the human lateral ventricles 93
4.3.2 Juxtaposition of inflammation in the SVZ and CC after cuprizone treatment 94
4.3.3 Lack of Gal-3 effect on inflammatory cell densities 97
4.3.4 Lack of Gal-3 compensation by other galectins 98
4.3.5 Conclusion 99

5 Galectin-3 and its role in oligodendrogenesis 100
5.1 Introduction 101
5.1.1 SVZ capacity for oligodendrogenesis 101
5.1.2 Gal-3 and oligodendrogenesis 102
5.1.3 OB demyelination in animal models 103
5.1.4 Research questions 103
5.2 Results 104
5.2.1 The density of oligodendrocyte lineage cells changes after cuprizone treatment in the CC, but not in the SVZ or in the absence of Gal-3 104
5.2.2 Gal-3 presence does not enhance oligodendrocyte differentiation after cuprizone treatment 106
5.2.3 Gal-3 enhances neuronal differentiation in vitro 106
5.2.4 Gal-3 absence does not alter MBP levels in the CC after cuprizone treatment 111
5.2.5 Gal-3 absence increases MBP levels in layer six of the motor cortex after cuprizone treatment 113
5.2.6 OB demyelination and remyelination occur in both the cuprizone and TMEV animal models 115
5.3 Discussion 120
5.3.1 Gal-3 role in neuronal differentiation 120
5.3.2 Increased MBP in layer 6 of the Gal-$3^{-/-}$ motor cortex 121
5.3.3 Lack of Gal-3 role in oligodendrocyte differentiation 123
5.3.4 Demyelination in the OB in animal models 124
5.3.5 Conclusion 125

6 Galectin-3 and its role in migration 126
6.1 Introduction 127
6.1.1 Migration of SVZ neuroblasts to the CC 127
6.1.2 Migration of immune cells to the CC 128
6.1.3 Research questions 129
6.2 Results 130
6.2.1 Gal-3 absence increases the number of ectopic neuroblasts in the CC after TMEV in SJL mice 130
6.2.2 Gal-3 absence increases SVZ cells migrating to the CC after cuprizone treatment 132
6.2.3 Gal-3 does not demonstrate a motogenic or chemoattractive effect on neuroblasts in vitro 135

6.2.4 Gal-3 absence does not alter candidate migratory gene expression 137
6.2.5 Gal-3 does not attract murine macrophages in vitro 140
6.3 Discussion 143
6.3.1 Migration of SVZ cells to the CC in the cuprizone model 143
6.3.2 Increased migration to the CC in Gal-3$^{-/-}$ mice 144
6.3.3 Lack of in vitro effect of Gal-3 on migration 146
6.3.4 Conclusion 147

7 Discussion **148**
7.1 Overall comments 149
7.1.1 SVZ response to demyelination 149
7.1.2 Gal-3 impact on the SVZ response to demyelination 151
7.1.3 Gal-3 as a therapeutic candidate 152
7.2 Limitations 154
7.2.1 Postmortem tissue samples 154
7.2.2 Cuprizone as a demyelination model 154
7.2.3 Lack of behavioural studies 156
7.3 Future ideas 156
7.3.1 Immunohistochemistry in cuprizone experiments 156
7.3.2 Floxed Gal-3 mouse 157
7.3.3 Molecular manipulation of Gal-3 157
7.3.4 Heterogeneity between SVZ regions 157
7.3.5 Exogenous stem cells 158
7.4 Concluding remarks 159

Bibliography **160**

Appendices **192**

A Reagent preparation **193**
A.1 Animal tissue preparation 193
A.2 Cell culture 193
A.3 Common laboratory solutions 194
A.4 Immunohistochemistry 194
A.5 Molecular biology 195
A.6 Western blot 195
A.6.1 Buffers 195
A.6.2 Gels 196

B Computer scripts **197**
B.1 ImageJ macros 197
B.1.1 CC immunohistochemistry quantification 197
B.1.2 MBP threshold quantification 197
B.1.3 Neuorosphere proliferation quantification 198
B.1.4 Explant assay quantification 199
B.2 SPSS syntax 201
B.2.1 Student's t-test 201
B.2.2 One-way ANOVA 201
B.2.3 Two-way ANOVA 202
B.2.4 Repeated measures ANOVA 203

C Repeated measures ANOVA statistics **205**
C.1 PHi3+ cells in the SVZ and CC after cuprizone treatment 205
C.2 Olig2+ cells in the SVZ after cuprizone treatment 209
C.3 MBP threshold values in the cortex after cuprizone treatment 211
C.4 MBP threshold values in the OB after cuprizone treatment 215
C.5 MBP threshold values in the OB after TMEV 218
C.6 BrdU+ cells in the SVZ and CC after cuprizone treatment 224

Abbreviations

AEP	anterior entopeduncular area
ANOVA	analysis of variance
A-P	anterior-posterior
BBB	blood-brain barrier
β-Gal	β-Galactosidase
BMP	bone morphogenetic protein
BrdU	bromodeoxyuridine
CC	corpus callosum
CGE	caudal ganglionic eminence
CNS	central nervous system
CRD	carbohydrate recognition domain
CSF	cerebrospinal fluid
DAPI	4',6-diamidino-2-phenylindole
Dcx	doublecortin
df	degrees of freedom
dH_2O	distilled water
DMEM	Dulbecco's Modified Eagle's Medium
DNA	deoxyribonucleic acid
E	embryonic day
EAE	experimental autoimmune encephalomyelitis
EBV	Epstein-Barr Virus
EDTA	ethylene diamine tetraacetic acid
EGF	epidermal growth factor
EGFR	epidermal growth factor receptor
EtOH	ethanol
FBS	foetal bovine serum
FGF	fibroblast growth factor including basic (bFGF)
Gal	Galectin
GFAP	glial fibrillary acidic protein
GFP	green fluorescent protein
GST	glutathione-s-transferase
HBSS	Hank's balanced salt solution
HLA	human leucocyte antigen
HRP	horseradish peroxidase
HSCT	haematopoietic stem cell transplantation
IL	interleukin
IP	intraperitoneal
iPSC	induced pluripotent stem cell
LGE	lateral ganglionic eminence
LRP2	lipoprotein receptor related protein 2
MBP	myelin basic protein
MCAO	middle cerebral artery occlusion
MCT	monocarboxylate transporter
MGAT5	mannosyl (alpha-1,6-)-glycoprotein beta-1,6-N-acetyl-glucosaminyltransferase
MGE	medial ganglionic eminence
MOG	myelin oligodendrocyte glycoprotein
MRI	magnetic resonance imaging

MS	multiple sclerosis
MSC	mesenchymal stem cell
NB-A+	Neurobasal A+
NB-GF	Neurobasal A+ with growth factors
NOS	nitric oxide synthase including inducible (iNOS) and neuronal (nNOS)
Nrg1	neuregulin 1
OB	olfactory bulb
OPC	oligodendrocyte precursor cell
P	postnatal day
PB	phosphate buffer
PBS	phosphate buffered saline
PCR	polymerase chain reaction
PDGF	platelet derived growth factor
PDGF-Rα	platelet derived growth factor receptor α
PFA	paraformaldehyde
PHi3	phosphohistone H3
Pi-3K	phosphatidylinositol-3-kinase
PLP	proteolipid protein
PMD	Pelizaeus-Merzbacher disease
PMI	postmortem interval
PNS	peripheral nervous system
PPMS	primary progressive multiple sclerosis
PRMS	progressive relapsing multiple sclerosis
pSil	pSilencer 2.0-U6 linear expession vector
PVDF	polyvinylidene fluoride
RIN	RNA integrity number
RNA	ribonucleic acid including messenger (mRNA) and small interfering (siRNA)
RRMS	relapsing remitting multiple sclerosis
RT-PCR	real-time polymerase chain reaction
SEM	standard error of the mean
Shh	Sonic hedgehog
SGZ	subgranular zone
SPMS	secondary progressive multiple sclerosis
SVZ	subventricular zone
TBI	traumatic brain injury
TBS	tris-buffered saline
TBS-T	tris-buffered saline with 0.5% Tween
T_c	cell cycle length
TMEV	Theiler's murine encephalomyelitis virus
TNF-α	tumour necrosis factor alpha
Th	T-helper
UVR	ultraviolet radiation
VEGF	vascular endothelial growth factor
WB	Western blot

List of figures

1 Introduction
1.1 Myelin sheath structure . . . 2
1.2 OPC origins in the forebrain . . . 3
1.3 Global MS prevalence . . . 10
1.4 MS pathophysiology . . . 12
1.5 Stem cell revolution . . . 17
1.6 Subventricular zone . . . 19
1.7 Galectin categories . . . 25

2 Methods
2.1 Oligodendrocyte density during cuprizone treatment . . . 32
2.2 RMS explant dissection . . . 46

3 Galectin-3 experimental toolkit development
3.1 Gal-3 wild-type, knockout and floxed alleles . . . 52
3.2 Developmental expression of Gal-3 . . . 54
3.3 Developmental RT-PCR experiment design . . . 56
3.4 Gal-3 developmental RT-PCR . . . 57
3.5 LacZ expression in Gal-$3^{fl/fl}$ mice . . . 59
3.6 Transfection of HEK293T cells with Gal-3 overexpression and shRNA plasmids . . . 61

4 Galectin-3 and its role in inflammation
4.1 Gal-3 expression occurs normally in the SVZ and increases in the adjacent CC after MS . . . 72
4.2 Gal-3 is expressed predominantly in hyperacute and acute MS lesions . 73
4.3 Gal-3 expression increases in the CC but decreases in the SVZ after cuprizone treatment . . . 75
4.4 LacZ expression increases in the CC of Gal-$3^{fl/+}$ mice after cuprizone treatment . . . 77
4.5 Gal-3 expression after cuprizone treatment occurs in GFAP+ astrocytes and CD45+ microglia . . . 78
4.6 Gal-3 absence does not alter weight change during cuprizone treatment 80
4.7 CD45+ cell density follows a similar pattern to Gal-3+ cell density after cuprizone treatment and is not altered by Gal-3 absence . . . 82
4.8 CD68-GFP transgenic mice further demonstrate immune cell activation after cuprizone treatment . . . 85
4.9 Proliferation follows a similar pattern to Gal-3+ cell density after cuprizone treatment and is not altered by Gal-3 absence . . . 86
4.10 In vitro proliferation is not altered by Gal-3 absence . . . 88
4.11 Reactive astrocytosis increases with cuprizone treatment in the SVZ and CC, and occurs more in the CC in the presence of Gal-3 . . . 90
4.12 Gal-3 absence is not compensated by other galectins . . . 92

5 Galectin-3 and its role in oligodendrogenesis
5.1 The density of oligodendrocyte lineage cells changes after cuprizone treatment in the CC, but not in the SVZ or in the absence of Gal-3 . . 105

5.2 Gal-3 presence does not enhance oligodendrocyte differentiation after cuprizone treatment . . . 107
5.3 Gal-3 enhances neuronal differentiation in vitro . . . 108
5.4 Gal-3 absence does not alter MBP levels in the CC after cuprizone treatment . . . 112
5.5 Gal-3 absence increases MBP levels in layer six of the motor cortex after cuprizone treatment . . . 114
5.6 Cuprizone causes consistent demyelination then remyelination in the OB 116
5.7 TMEV causes less consistent demyelination then remyelination in the OB than cuprizone . . . 118

6 Galectin-3 and its role in migration
6.1 Gal-3 absence increases the number of ectopic neuroblasts in the CC after TMEV in SJL mice . . . 131
6.2 Gal-3 absence increases SVZ cells migrating to the CC after cuprizone treatment . . . 133
6.3 Gal-3 does not demonstrate a motogenic or chemoattractive effect on neuroblasts in vitro . . . 136
6.4 Gal-3 absence does not alter candidate migratory gene expression. . . . 139
6.5 Gal-3 does not attract murine macrophages in vitro . . . 141

7 Discussion
7.1 Key findings of thesis . . . 150

List of tables

1 Introduction
1.1 Causes of CNS demyelination 6

2 Methods
2.1 Genotyping primer sequences 31
2.2 Primary antibodies for fluorescent immunohistochemistry 34
2.3 Primary antibodies for DAB immunohistochemistry 35
2.4 QuantiTect primer assays 39
2.5 TaqMan gene expression assays 40
2.6 siRNA sequences 41
2.7 Primary antibodies for WB 42
2.8 Primary antibodies for fluorescent immunocytochemistry 45

3 Galectin-3 experimental toolkit development
3.1 Brain library of Gal-$3^{+/+}$ and Gal-$3^{-/-}$ brains 53

4 Galectin-3 and its role in inflammation
4.1 Human control and MS cases 71

Appendices

C Repeated measures ANOVA statistics
PHi3+ cells in the SVZ and CC after cuprizone treatment
C.1 Means 205
C.2 Sphericity testing 205
C.3 Main effects and interactions 206
C.4 Pairwise comparisons for Region * Treatment in the SVZ 207
C.5 Pairwise comparisons for Region * Treatment in the CC 208

Olig2+ cells in the SVZ after cuprizone treatment
C.6 Means 209
C.7 Sphericity testing 209
C.8 Main effects and interactions 210

MBP threshold values in the cortex after cuprizone treatment
C.9 Means 211
C.10 Sphericity testing 211
C.11 Main effects and interactions 212
C.12 Pairwise comparisons for Cortical Layer * Treatment 213
C.13 Pairwise comparisons for Cortical Region * Cortical Layer * Genotype . 214

MBP threshold values in the OB after cuprizone treatment
C.14 Means 215
C.15 Sphericity testing 215
C.16 Main effects and interactions 216
C.17 Pairwise comparisons for OB Region * Treatment 217

MBP threshold values in the OB after TMEV
C.18 Means 218
C.19 Sphericity testing 219
C.20 Main effects and interactions 219
C.21 Pairwise comparisons for A-P Axis within A-P Axis * OB Region * Treatment interaction 220
C.22 Pairwise comparisons for Treatment within A-P Axis * OB Region * Treatment interaction 222

BrdU+ cells in the SVZ and CC after cuprizone treatment
C.23 Means 224
C.24 Sphericity testing 225
C.25 Main effects and interactions 225
C.26 Pairwise comparisons for Genotype within Length * Treatment * Genotype interaction in the SVZ 226
C.27 Pairwise comparisons for Treatment within Length * Treatment * Genotype interaction in the SVZ 226
C.28 Pairwise comparisons for Length within Length * Treatment * Genotype interaction in the SVZ 227
C.29 Pairwise comparisons for Region * Treatment interaction in the SVZ . . 227
C.30 Pairwise comparisons for Genotype within Region * Length * Genotype interaction in the SVZ 228
C.31 Pairwise comparisons for Length within Region * Length * Genotype interaction in the SVZ 229
C.32 Pairwise comparisons for Length in the CC 230
C.33 Pairwise comparisons for Region * Treatment in the CC 230

1

Introduction

Contents

1.1 The myelin sheath 2
1.1.1 Structure and development of myelin 2
1.1.2 Disruption of myelin 6
1.1.3 Repair of myelin 7
1.2 Multiple sclerosis 9
1.2.1 Epidemiology and aetiology 9
1.2.2 Pathogenesis 11
1.2.3 Current treatment 13
1.2.4 Animal models of demyelination 15
1.3 Stem cell treatment 17
1.3.1 Subventricular zone 18
1.3.2 Stem cells and demyelination 22
1.4 The galectin family 24
1.4.1 Galectin-3 25
1.4.2 Galectin-3 in the SVZ and demyelination 27
1.5 Research questions 28

1.1 The myelin sheath

The myelin sheath is a crucial component of the central and peripheral nervous systems (CNS/PNS; von Virchow, 1854). It encircles neuronal axons and increases the efficiency of nerve impulse conduction. The cells that contain it, oligodendrocytes in the CNS and Schwann cells in the PNS, also provide trophic support to neurons. Its loss results from myriad pathophysiologic processes and leads to impaired signalling, axon degeneration and clinical symptoms. Multiple sclerosis (MS), which affects more than 100,000 people in the United Kingdom, is the most common human disease that damages myelin (Multiple Sclerosis Society, 2014). Current MS research targets all aspects of the pathophysiologic pathway, and stem cells offer particular hope in repairing and replacing damaged myelin.

This introduction, and indeed this thesis, investigate demyelination and remyelination, the potential for stem cell treatment from the subventricular zone (SVZ) neural stem cell niche, and the role of the pro-inflammatory protein Galectin-3 (Gal-3).

1.1.1 Structure and development of myelin

The myelin sheath is an extension of cell membranes and segmentally encircles axons between nodes of Ranvier (Figure 1.1). Low conductivity is a key characteristic for myelin, which its structure provides: 40-50% water and a dry weight incorporating

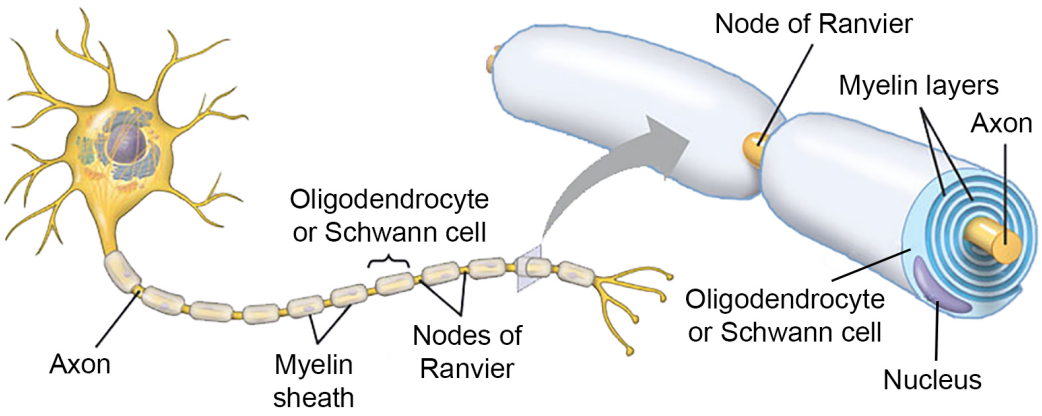


Figure 1.1: **Myelin sheath structure.** Diagram demonstrating myelin sheath structure. Adapted from Kennebecasis Valley High School (2015).

lipids (70-85%) and proteins (15-30%; Finean, 1957; Siegel et al., 1999). The lipids include cholesterol, galactolipids (predominantly galactocerebroside), phospholipids and plasmalogens (Norton and Autilio, 1966). The proteins include myelin basic protein (MBP; Kornguth and Anderson, 1965; Laatsch et al., 1962), myelin oligodendrocyte glycoprotein (MOG; Quarles et al., 1972), and proteolipid protein (PLP; Folch and Lees, 1951). As mentioned above, the myelin sheath is produced by, and contained within, oligodendrocytes in the CNS and Schwann cells in the PNS. A single cortical oligodendrocyte myelinates ∼60 axonal segments (known as internodes), which can be on multiple axons (Chong et al., 2012).

The low conductivity inhibits a myelinated axon segment from depolarising. When a neuron is depolarised, electrical signals instead jump from one node of Ranvier to the next in a process called saltatory conduction (Huxley and Stämpfli, 1949). That enables action potentials to travel faster while using less energy: myelinated Aα neurons conduct impulses at 72-120m/s, thinly myelinated Aδ neurons at 4-36m/s and unmyelinated C fibres at 0.4-2.0m/s (Gasser and Erlanger, 1927; Kandel et al., 2000).

Forebrain oligodendrocytes, which are the focus of this thesis, develop in three waves in mice (Figure 1.2; Fancy et al., 2011; Kessaris et al., 2006). From embryonic day 12.5 (E12.5), oligodendrocyte precursor cells (OPCs) appear in the medial ganglionic

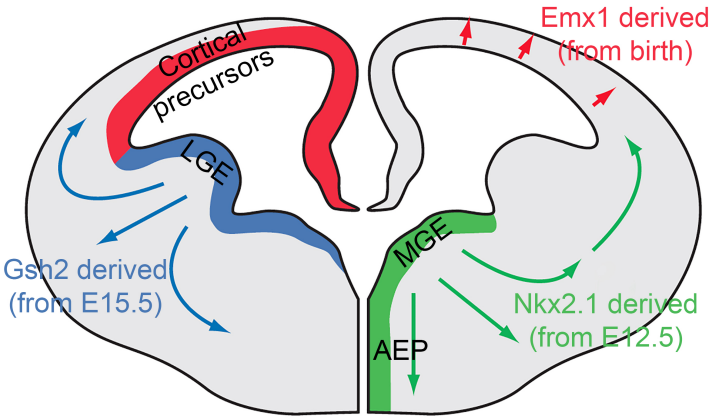


Figure 1.2: **OPC origins in the forebrain.** Diagram demonstrating development of OPCs in the embryonic mouse brain. Note that OPCs also develop from the CGE, which is a fusion of the MGE/LGE caudal to this diagram. Adapted from Fancy et al. (2011).

eminence (MGE) and anterior entopeduncular area (AEP) of the ventral forebrain. They originate from Nkx2.1-expressing neuroepithelium and migrate throughout the telencephalon in a ventral-to-dorsal manner. From E15.5, Gsh2-expressing OPCs are produced in the lateral and caudal ganglionic eminences (LGE and CGE) before spreading through the telencephalon. From birth, a third population of OPCs, derived from Emx1-expressing cortical precursors, appears in the cortex. This population gives rise to ∼80% of corpus callosum (CC) oligodendrocytes, while the other ∼20% originate from the Gsh2-expressing OPCs (Tripathi et al., 2011). These two populations have indistinguishable electrical properties (Tripathi et al., 2011).

OPCs can differentiate into myelinating oligodendrocytes, but a proportion remain undifferentiated. In adult brain grey matter, the number of OPCs is approximately equal to the number of oligodendrocytes (each ∼3-4% of total cells in cortex and ∼5% in hippocampus; Dawson et al., 2003). In spinal cord white matter, there are more mature oligodendrocytes (a ratio of 5:1 or ∼37% compared to ∼7.5% of total cells in dorsal column white matter). These OPCs continue to replicate at postnatal day 60 (P60) with a cell cycle of ∼10 days in the CC and ∼36 days in the motor cortex (Young et al., 2013). Their ability to proliferate and differentiate is also not diminished by injury (Penderis et al., 2003a). Interestingly, human oligodendrocytes are normally only generated until age 5 (Yeung et al., 2014). Their population then remains largely stable throughout life with an annual turnover of only 1 in 300 (Yeung et al., 2014).

Multiple factors regulate the phases of oligodendrocyte development including the lineage specification of undifferentiated stem cells and maturation of OPCs into myelinating oligodendrocytes. Many of these mechanisms recur in adult neurogenesis and are therefore of interest to this thesis (Fancy et al., 2011).

The main oligodendrocyte specification pathway of ventral OPCs involves the morphogen Sonic hedgehog (Shh) and basic helix-loop-helix transcription factor Olig2 (Lu et al., 2000; Orentas et al., 1999; Poncet et al., 1996; Pringle et al., 1996). Shh was initially demonstrated to be a necessary signal in ventral oligodendrocyte specification in chick neural tube explants (Pringle et al., 1996). Recently it was shown in human

in vitro studies to increase the proportion of oligodendrocytes in cultures of mixed cortical and radial glial cells (Mo and Zecevic, 2009; Ortega et al., 2013). It increases the Nk homeodomain proteins Nkx6.1 and Nkx6.2, which then increase Olig2 (Liu et al., 2003; Novitch et al., 2001). In turn, Olig2 regulates transcription of genes involved in both ventral and dorsal oligodendrocyte specification, including via the chromatin remodelling enzyme Smarca4/Brg1 (Lu et al., 2002; Yu et al., 2013; Yue et al., 2006; Zhou et al., 2001). Olig2 is additionally regulated upstream by sulfatase 1 and Indian hedgehog b (Chung et al., 2013; Touahri et al., 2012).

Olig2 maintains expression throughout the oligodendrocyte lineage, and also has a role in oligodendrocyte differentiation (Lu et al., 2002; Zhou et al., 2001). Its downstream targets include Sox10, which can directly induce the myelin genes MBP and PLP, and myelin gene regulatory factor and zinc finger protein 191, which are transcription factors required for mature oligodendrocytes to myelinate (Emery et al., 2009; Howng et al., 2010; Koenning et al., 2012; Liu et al., 2007; Stolt et al., 2002). Olig2 and Sox10 interact with Nkx2.2, which can induce PLP expression (Qi et al., 2001; Zhou et al., 2001). Separately Sox8 may have a role in differentiation and Sox9 induces Sox10 expression, although Sox9 levels disappear before final maturation (Finzsch et al., 2008; Stolt et al., 2004, 2003). Olig1, another basic helix-loop-helix transcription factor, enhances differentiation by increasing expression of MBP and PLP, and decreasing transcription of glial fibrillary acidic protein (GFAP; Lu et al., 2002; Xin et al., 2005).

Further mechanisms of oligodendrocyte specification and differentiation include the inhibitory transcription factors Id2 and Id4 downstream of bone morphogenetic protein 4 (BMP4), and neuronal activity through synapses onto OPCs (Bergles et al., 2000; Samanta and Kessler, 2004; Wang et al., 2001). A more detailed discussion is, however, beyond the scope of this thesis. An experimental consideration of proteins involved with oligodendrocyte development is that they can identify differentiation stage. This technique and subsequent experiments are expanded on in Chapter 5.

1.1.2 Disruption of myelin

The myelin sheath can be disrupted in multiple ways. Dysmyelination refers to congenitally defective myelin that never provides normal myelination. The most common cause, Pelizaeus-Merzbacher disease (PMD), is an X-linked condition involving the PLP gene (Gencic et al., 1989; Merzbacher, 1910; Pelizaeus, 1885). Demyelination, in contrast, refers to normal myelin that is subsequently destroyed. The aetiologies of CNS demyelination are outlined in Table 1.1 with primary demyelinating disorders such as MS being the most common cause. Similar pathogenic processes affect the PNS including the primary demyelinating disorders Guillain-Barré syndrome and chronic inflammatory demyelinating polyneuropathy (Lewis, 2012; Vriesendorp, 2014).

Aetiology	**Disease**
Hereditary disorders	Phenylketonuria and other aminoacidurias Tay-Sachs, Niemann-Pick, and Gaucher diseases Hurler syndrome Krabbe disease and other leukodystrophies Adrenoleukodystrophies Adrenomyeloneuropathy Leber hereditary optic atrophy and related mitochondrial disorders
Hypoxia and ischaemia	Carbon monoxide toxicity and other syndromes of delayed hypoxic cerebral demyelination Progressive subcortical ischaemic demyelination
Nutritional deficiencies	Osmotic demyelination syndrome (formerly called central pontine myelinolysis) Demyelination of the CC (Marchiafava-Bignami disease) Vitamin B12 deficiency
Direct viral invasion of CNS	Progressive multifocal leukoencephalopathy Subacute sclerosing panencephalitis Tropical spastic paraparesis/HTLV-1-associated myelopathy
Primary demyelinating disorders	Recurrent, progressive disorders (MS and its variants) Monophasic disorders such as optic neuritis, acute transverse myelitis, acute disseminated encephalomyelitis, and acute haemorrhagic leukoencephalitis Neuromyelitis optica
Toxins	Alcohol Ethambutol

Table 1.1: **Causes of CNS demyelination.** Adapted from Apatoff (2014).

The primary demyelinating disorders are a focus of this thesis. They follow similar patterns of immune-mediated inflammation and destruction with subsequent axonal degeneration. This pathophysiology will be considered in the context of MS in Section 1.2.2 on p11.

It is conceptually important, however, to understand that damage to the myelin sheath results in axonal degeneration because of decreased trophic and metabolic factors from oligodendrocytes (Nave, 2010). This process can occur in addition to, and independently from, axonal degeneration due to myelin loss. Initial clues for this mechanism came from PLP1 or 2',3'-cyclic nucleotide phosphodiesterase deficient mice that maintain myelination but have progressive axonal degeneration (Griffiths et al., 1998; Lappe-Siefke et al., 2003). A recent study used diphtheria toxin to selectively induce apoptosis in oligodendrocytes, and showed axonal injury without widespread myelin loss (Oluich et al., 2012). The mechanism of metabolic and trophic support is still being elucidated and one possibility involves the lactate transporter monocarboxylate transporter 1 (MCT1). It is hypothesised to export lactate or pyruvate from oligodendrocytes, which MCT2 on axons then internalises for the axon to use. Anatomical studies have shown MCT1 and MCT2 expression in oligodendrocytes and axons respectively (Lee et al., 2012; Rinholm et al., 2011). Functional studies have shown that MCT1 downregulation causes axonopathy, while oligodendrocyte produced lactate is quickly utilised by neighbouring cells such as neurons (Fünfschilling et al., 2012; Lee et al., 2012).

1.1.3 Repair of myelin

The process of repair for damaged myelin is known as remyelination. It restores saltatory conduction, and occurs in both mice and humans (Patani et al., 2007; Patrikios et al., 2006; Smith et al., 1979). It features similar signals to initial myelin development such as Olig2 and Nkx2.2, and the term 'recapitulation' has been used to describe the relationship of remyelination with developmental myelination (Fancy et al., 2011, 2004; Smith et al., 1979). There are, however, a number of key differences.

The first difference relates to the thickness of myelin. Normally the thickness and internodal length of myelin is roughly proportional to axonal diameter. With remyelination, however, myelin is much thinner and its width is typically constant regardless of axon size (Fancy et al., 2011). This difference is believed to be due to the cell-signalling protein neuregulin 1 (Nrg1), a decrease of which normally causes hypomyelination in brains and an overexpression of which causes hypermyelination (Brinkmann et al., 2008; Taveggia et al., 2008). Resistance to Nrg1 appears after demyelination, with an infusion or overexpression of Nrg1 failing to induce hypermyelination (Brinkmann et al., 2008; Penderis et al., 2003b). Other signals that normally increase myelination include the signal transducer enzyme phosphatidylinositol-3-kinase (Pi-3K) and the serine/threonine kinase Akt (Flores et al., 2008; Harrington et al., 2010; Narayanan et al., 2009). An increase in Pi-3K, similar to Nrg1, does not alter remyelination (Harrington et al., 2010).

The second difference is that the effectiveness of remyelination decreases with age: studies of MS patients have shown less remyelination with disease longevity as well as clinical progression that correlates with age independent of the initial disease course (Confavreux and Vukusic, 2006; Goldschmidt et al., 2009). This decline occurs because OPCs have a decreased ability to recruit histone deacetylases to relevant promoter regions, resulting in an accumulation of transcriptional inhibitors and a diminished ability to differentiate into oligodendrocytes (Shen et al., 2008). Myelin debris also inhibits OPC differentiation (Kotter et al., 2006). In chronic MS tissue, these processes result in an increased number of quiescent OPCs (Wolswijk, 1998). Interestingly, recent experiments using heterochronic parabiosis (connecting the blood streams of a young and old mouse) have restored remyelination in the older mouse, suggesting that systemic cells and factors can overcome this inefficiency (Ruckh et al., 2012).

The third difference is that remyelination can make axons more vulnerable to damage in the short-term: while they are still restoring their metabolic capacity, high-frequency impulses can cause sodium accumulation and toxicity (Smith, 2006). This vulnerability results from abnormal aggregation of voltage-gated sodium channels, which is in turn

due to abnormalities with the cell adhesion molecule neurofascin (Coman et al., 2006; Howell et al., 2006). A consequential, beneficial effect is that sodium channel blockers provide neuroprotection (Black et al., 2006; Kapoor et al., 2003).

The final key difference is that OPCs originate from different sources in adults including adult neurogenic stem cell niches. This thesis focuses on remyelination from the SVZ, and stem cells are discussed in more detail in Section 1.3 on p17.

1.2 Multiple sclerosis

MS was first alluded to by Robert Carswell as "a remarkable lesion of the spinal cord accompanied with atrophy" (Carswell, 1838). It has since been termed 'multiple sclerosis' (meaning 'many scars') and refers to the disseminated, demyelinated plaques that appear in CNS white matter (Charcot, 1868). Symptoms depend on the neuroanatomical location of demyelination, and today the diagnosis is made using clinical history, magnetic resonance imaging (MRI) and cerebrospinal fluid (CSF) analysis as outlined by the McDonald criteria (McDonald et al., 2001; Polman et al., 2011). Current treatments are limited and are described further below.

MS may be classified into different stages (Lublin et al., 1996). Relapsing remitting MS (RRMS) features clearly defined relapses with recovery, either full or with sequelae, and no progression during remission. Primary progressive MS (PPMS) progresses from the onset with occasional plateaus and minor improvements. Secondary progressive MS (SPMS) begins as RRMS before becoming progressive. Progressive relapsing MS (PRMS) is similar to PPMS but with clear acute relapses.

1.2.1 Epidemiology and aetiology

MS affects more than 100,000 people in the United Kingdom and an estimated 2.3 million people worldwide (Figure 1.3; Multiple Sclerosis International Federation, 2013; Multiple Sclerosis Society, 2014). It has a mean age of onset of 28-32 and generally becomes clinically apparent between 15 and 45 years of age (Goodin, 2014). It occurs

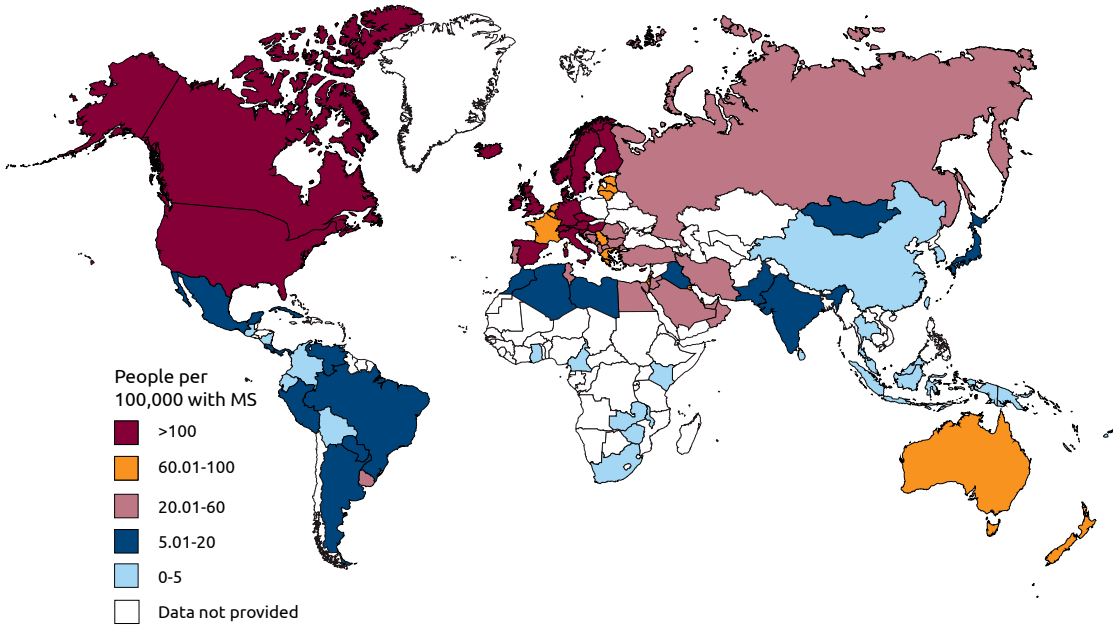


Figure 1.3: **Global MS prevalence.** MS prevalence rates in 2013. Adapted from Multiple Sclerosis International Federation (2013).

approximately twice as commonly in women compared to men (ratio 1.4 in 1955 to 2.3 in 2000; Alonso and Hernán, 2008). It clusters in families with a recurrence risk of 18.2% in monozygotic twins and 2.7% in siblings (O'Gorman et al., 2012). It also clusters in geographic regions, particularly as a latitude gradient whereby incidence increases with distance from the equator (Simpson et al., 2011).

The exact aetiology of MS is unknown. The familial clustering, however, suggests a genetic basis (Ebers et al., 1995). The regional clustering suggests both a genetic and population-level environmental basis (Dean et al., 2008; Dyment et al., 2006).

Fourteen genome wide association studies have now been performed for MS (Sawcer et al., 2014, for review). The largest, including 9,772 MS cases and 17,376 controls, identified 57 susceptibility loci (International Multiple Sclerosis Genetics Consortium et al., 2013, 2011). The genes associated with these loci predominantly affect the immune system, especially T-helper (Th) cells, by encoding proteins for cytokine pathways, co-stimulation and signal transduction. They also encode for proteins related to Vitamin D metabolism and MS monoclonal antibody targets (natalizumab and daclizumab, explained further on p14). Interestingly, only two genes are related to neurodegeneration independently of inflammation. The allele with the strongest

effect is human leucocyte antigen (HLA)-DRB1*15:01 with an odds ratio of 3.1, while HLA-A*02:01 confers protection with an odds ratio of 0.73.

Proposed environmental causes include viruses, geography and Vitamin D deficiency. Epstein-Barr Virus (EBV) is the most likely viral candidate, and hypothesised mechanisms are antigen mimicry, immortalisation of B-cell clones and cytotoxic T-cell activity against virally infected B-cells (Bagert, 2009). EBV-caused infectious mononucleosis has a relative risk of 2.3 for developing MS (Thacker et al., 2006). It is, however, difficult to prove a direct causal link as the virus most likely precedes symptoms by many years or decades, and 84% of the general population are seropositive for EBV antibodies (although 100% of people with MS are; Larsen et al., 1985).

Vitamin D deficiency, including lack of sunlight, has been shown to increase MS risk (Munger et al., 2004; van der Mei et al., 2003). One possible mechanism is via a Vitamin D responsive element in the HLA-DRB1*15 promoter (Ramagopalan et al., 2009). In addition, living at a latitude farther from the equator, where there is less ultraviolet radiation (UVR), increases risk (Simpson et al., 2011). Similarly, northern hemisphere babies born in April, who would have been in utero during winter with less UVR, have a higher risk (Dobson et al., 2012). The same occurs in the southern hemisphere with babies born in November-December (Staples et al., 2010). Smoking is also a risk factor for MS (Riise et al., 2003).

1.2.2 Pathogenesis

The pathognomonic features of MS are inflammation, demyelination and axon degeneration (Figure 1.4; Compston and Coles, 2008). Inflammation involves accumulation of peripheral T-cells, B-cells and macrophages, and local microglia (Lucchinetti et al., 2000). Initially the blood-brain barrier (BBB) is disrupted, which can be seen radiologically through increased MRI enhancement (Goodkin et al., 1998). Th17-cells, which are driven by interleukin-23 (IL-23) and secrete IL-17, then cross the BBB to increase BBB inflammation and cause neurodegeneration (Kebir et al.,

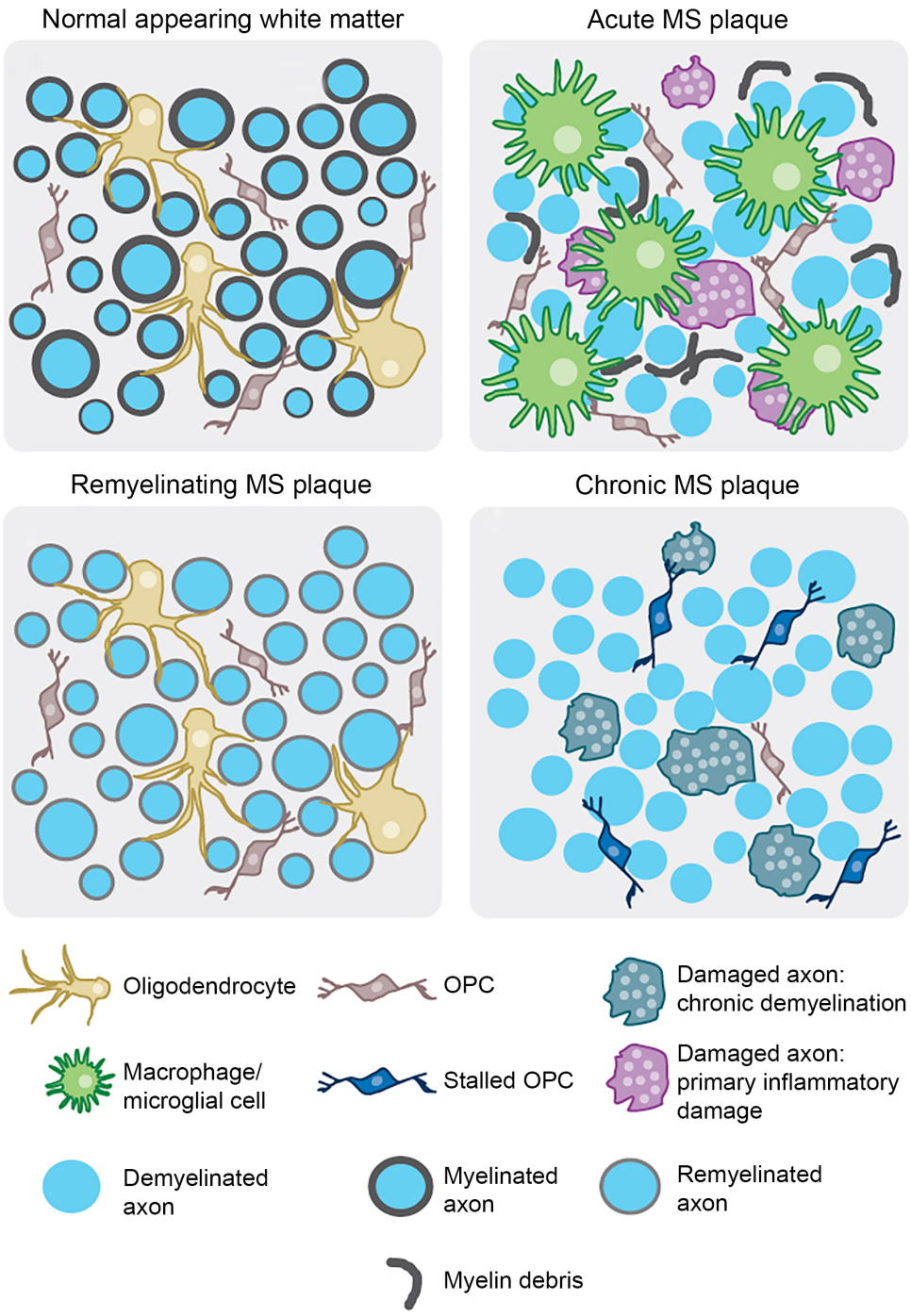


Figure 1.4: **MS pathophysiology.** Diagram demonstrating MS pathophysiology. Adapted from Fancy et al. (2011).

2007; Langrish et al., 2005; Tzartos et al., 2008; Vaknin-Dembinsky et al., 2006). The release of cytokines by these cells recruits further inflammatory cells including local microglia. Meanwhile, $CD4^{+}CD25^{hi}$ T-cells, which normally suppress immune cells, have decreased function (Viglietta et al., 2004).

While MS is an autoimmune disease, there is no single autoimmune target. Antibodies

against the potassium channel KIR4.1, which oligodendrocytes and astrocytes express, are present in 46.9% of people with MS (Srivastava et al., 2012). Antibodies directed against neurofascin inhibit axonal conduction and are present in approximately one-third of MS patients especially those with progressive MS (Mathey et al., 2007). A higher proportion of reactive T-cells directed against MBP and PLP occur in people with MS (Zhang et al., 1994). In addition, T-cells against MBP have been demonstrated in MS plaques (Oksenberg et al., 1993).

The inflammatory milieu causes demyelination and axon degeneration via cytokines, oxidative stress, mitochondrial dysfunction and altered ion channel activity (Friese et al., 2014). Microglia produce tumour necrosis factor alpha (TNF-α), resulting in oligodendrocyte cytotoxicity (Zajicek et al., 1992). MS plaques contain neuronal nitric oxide synthase (nNOS) and reactive nitrogen species, with oxidative damage being evident in neurons and oligodendrocytes (Haider et al., 2011; Zeis et al., 2009). Multiple mitochondrial genes, and the function of mitochondrial respiratory chain complexes, are decreased in the MS motor cortex (Dutta et al., 2006). Ion channels implicated in MS include sodium channels such as acid-sensing ion channels (Craner et al., 2004; Shields et al., 2012; Vergo et al., 2011), calcium channels such as glutamate-stimulated receptors (Kornek et al., 2001; Newcombe et al., 2008), and non-selective ion channels (Schattling et al., 2012). All of these processes likely converge on the process of Wallerian degeneration, whereby the axon distal to the inflammatory site degenerates (Dziedzic et al., 2010).

1.2.3 Current treatment

Management of MS involves both symptomatic and disease-modifying treatments. Symptoms include cognitive dysfunction, immobility and spasticity with treatments incorporating allied health services, such as physiotherapy and occupational therapy, medications and rarely surgery. Disease-modifying treatments target inflammation and are most relevant to relapsing MS (RRMS and PRMS), where they can be considered as acute or ongoing treatments. In progressive MS (PPMS and SPMS), disease-modifying

treatments are largely ineffective and only temporarily slow progress (Olek, 2014).

The mainstay of acute treatment is glucocorticoid steroids. Methylprednisolone has a protective effect against disease progression or stability (odds ratio 0.37; Citterio et al., 2000), and can be given orally or intravenously with equal efficacy (Barnes et al., 1997). It does, however, have a broad side effect profile associated with long-term use including hypertension, diabetes and osteoporosis. Plasma exchange can be used for acute MS refractory to glucocorticoid steroids (Weinshenker et al., 1999). It has its own side effects related to fluid and electrolyte imbalances, and exposure to donor plasma.

The most common ongoing treatments for relapsing MS are interferons, glatiramer and monoclonal antibodies. Interferons, particularly interferon beta-1a and beta-1b, decrease the rate of MS relapses by ∼25-35% through an unknown immunomodulatory mechanism likely involving T-cells (Dhib-Jalbut and Marks, 2010; Ebers et al., 1998; IFNB Multiple Sclerosis Study Group et al., 1993). Common side effects include injection site reactions, flu-like symptoms and asymptomatic liver dysfunction (Ebers et al., 1998). Glatiramer is antigenically similar to MBP, with which it competes in binding to T-cells (Webb et al., 1973). It promotes Th2 suppressor cells as well and causes a 29% reduction in relapse rate (Johnson et al., 1995; Vieira et al., 2003). Its adverse effects include injection site reactions and a transient self-limited systemic reaction with flushing and/or chest pain (Johnson et al., 1995). Alemtuzumab is a monoclonal antibody directed against the lymphocyte surface protein CD52, and is more effective than interferon beta (Cohen et al., 2012; Coles et al., 2012). It does, however, have a significant side effect profile that limits its wider use including infections, autoimmunity (particularly thyroid disorders) and immune thrombocytic purpura (Cohen et al., 2012; Coles et al., 2012).

The search is on for treatments of progressive MS and stem cell treatment is one possibility. It is considered in Section 1.3 on p17.

1.2.4 Animal models of demyelination

There are two major issues in researching neurological conditions like MS. Firstly, the human brain is difficult to assess in real-time: it is hard to access for tissue sampling and, even if it can be accessed, there are ethical considerations in obtaining brain tissue. While imaging technologies like MRI continue to improve, they do not provide molecular or even cellular resolution. A large number of studies use postmortem tissue, although it regularly contains only end-stage disease. Secondly, with an unknown aetiology, it is not possible to create an exact animal model. A number of demyelination models therefore exist and can be broadly classified as purely autoimmune, toxin-induced or virus-induced (Denic et al., 2011). None of them, however, completely replicate the pathogenesis of MS.

The main autoimmune model is experimental autoimmune encephalomyelitis (EAE), which is the original, and most extensively studied, demyelination model (Rivers and Schwentker, 1935; Rivers et al., 1933). It can be used in rodents and non-human primates (Bernard and Carnegie, 1975; Rivers et al., 1933), and glatiramer was initially discovered through it (Teitelbaum et al., 1971). EAE involves immunisation, typically with a myelin protein (MBP, MOG, or PLP), which then elicits a peripheral T-cell response (Constantinescu et al., 2011). Similar to MS, that T-cell response involves IL-17, IL-23 and Th17-cells (Cua et al., 2003; Langrish et al., 2005). Demyelination and remyelination may then occur (Constantinescu et al., 2011). The major criticism of EAE is that a number of agents that successfully treat it then fail to treat MS (Sriram and Steiner, 2005). An example is interferon gamma, which benefits EAE yet induces relapses in people with MS (Billiau et al., 1988; Panitch et al., 1987). There are evidently pathophysiologic differences between EAE and MS, beginning with inoculation in EAE compared to a likely viral cause in MS.

Cuprizone (bis-cyclohexanone-oxaldihydrazone), which this project uses, causes toxin-induced demyelination (Blakemore, 1972). It is a copper-chelator administered systemically in mouse chow, although its exact mechanism is unknown especially

as supplemental copper does not reverse its effect (Carlton, 1967). It is, however, known to impair mitochondrial respiration with the hypothesis that oligodendrocytes are preferentially targeted in the CNS due to their large size and metabolic demand (Matsushima and Morell, 2001; Venturini, 1973). The main downside of cuprizone is that it is not immunologically-mediated, and it maintains an intact BBB with no T-cell infiltration (Bakker and Ludwin, 1987; Kondo et al., 1987). It therefore offers a model of demyelination rather than the immune aetiology of MS. A key advantage of cuprizone is its reversibility, allowing remyelination to be predictably induced by returning mice to control chow. It also induces demyelination in many brain regions including the CC, cortex, striatum, thalamus, midbrain and cerebellum (Blakemore, 1972; Silvestroff et al., 2010). Interestingly, both resident microglia and peripheral macrophages are present following cuprizone-induced demyelination (McMahon et al., 2002). Cuprizone also attenuates EAE through a separate mechanism of inhibiting T-cell responses (Emerson et al., 2001).

Lysolecithin is the other main toxin-induced model (Hall, 1972). It causes focal demyelination then remyelination through injection into the relevant neuroanatomical region (Jeffery and Blakemore, 1995). It is closely related to phospholipase A_2, which is known to predispose myelin to proteolytic breakdown (Banik et al., 1976). This model involves B- and T-cells, and their presence enhances remyelination (Bieber et al., 2003). Similar to MS, that remyelination is slower in older animals (Shields et al., 1999). The key disadvantages of lysolecithin are that it only elicits focal demyelination and its aetiology is not immune-mediated.

Theiler's murine encephalomyelitis virus (TMEV) is a viral model of MS (Theiler, 1937). It is typically inoculated by intracerebral injections, and initially infects neurons leading to flaccid paralysis. This process peaks after one week before resolving after a further one-two weeks (Lipton, 1975). Genetically susceptible mice such as the SJL strain may then develop a second phase whereby TMEV infects and persists in oligodendrocytes causing chronic demyelination (Lipton, 1975; Rodriguez et al., 1983). The TMEV model therefore best resembles progressive MS. It also draws similarities

with MS in that it is caused by a virus, including with subsequent autoimmunity (Miller et al., 1997). Key disadvantages include that the chronic phase occurs primarily in the spinal cord rather than the brain, and that it does not provide as good a model of RRMS as EAE (Lipton, 1975).

1.3 Stem cell treatment

Stem cells have been trumpeted as a treatment that could revolutionise medicine (Figure 1.5). By the strictest definition, they are undifferentiated cells that can self-renew and give rise to progenitors that go onto differentiate into any mature cell type. Many researchers, however, consider them to encompass self-renewing cells with a restricted lineage. Neural stem cells are typically tripotent with the potential to become neurons, astrocytes or oligodendrocytes.



Figure 1.5: **Stem cell revolution.** Magazine covers demonstrating the hype surrounding stem cell treatment possibilities.

There are two key neural stem cell niches in the adult brain: the SVZ surrounding the lateral ventricles and the subgranular zone (SGZ) in the dentate gyrus (Altman and Das, 1965; Ray et al., 1993; Reynolds and Weiss, 1992). Other sources have also been reported: parenchymal OPCs, which become active and proliferate in response to demyelination (Di Bello et al., 1999; Levine and Reynolds, 1999); the hypothalamus, where they have a role in weight control (Kokoeva et al., 2005; Markakis et al., 2004; Pencea et al., 2001); and, recently, the striatum, although debate surrounds their

existence (Ernst et al., 2014; Wang et al., 2014). Neural lineage cells can additionally be derived from induced pluripotent stem cells (iPSCs), embryonic stem cells or via direct transformation (Bain et al., 1995; Dimos et al., 2008; Takahashi and Yamanaka, 2006; Vierbuchen et al., 2010).

This introduction focuses on the relevant aspects to this thesis: SVZ stem cells and the broader use of stem cells in treating demyelination. It should, however, be noted how quickly this research field is progressing: iPSCs were first reported in 2006 and the first human trial with them occurred in 2014 for macular degeneration (Cyranoski, 2014; Takahashi and Yamanaka, 2006).

1.3.1 Subventricular zone

As mentioned above, the SVZ is a region of adult neurogenesis that lines the lateral ventricles (Figure 1.6A and B; Altman and Das, 1965; Ihrie and Álvarez-Buylla, 2011). It contains neural stem cells that begin as slowly-dividing, astrocyte-like primary progenitors before becoming transit amplifying cells and then neuroblasts (Doetsch et al., 1999). Normally neuroblasts migrate in chains along the rostral migratory stream (RMS) to become GABAergic or dopaminergic interneurons in the olfactory bulb (OB; Doetsch and Álvarez-Buylla, 1996; Rousselot et al., 1995). Distinct stem cell populations within the SVZ give rise to specific interneuron types (Merkle et al., 2014, 2007), and the continuous supply of interneurons is essential for olfactory learning and memory (Sakamoto et al., 2014).

The SVZ has a unique anatomy, and can be divided into three layers (Figure 1.6C; Lim and Álvarez-Buylla, 2014). The outer layer, which is adjacent to the lateral ventricles, contains ependymal cells and the apical processes of neural stem cells. The ependymal cells function as the blood-CSF barrier and have cilia to direct CSF flow. The majority are in fact multiciliated, postmitotic and derived from radial glial cells (Spassky et al., 2005), while a small proportion are biciliated with complex basal bodies (Mirzadeh et al., 2008). Both types are arranged in a pinwheel formation around the neural

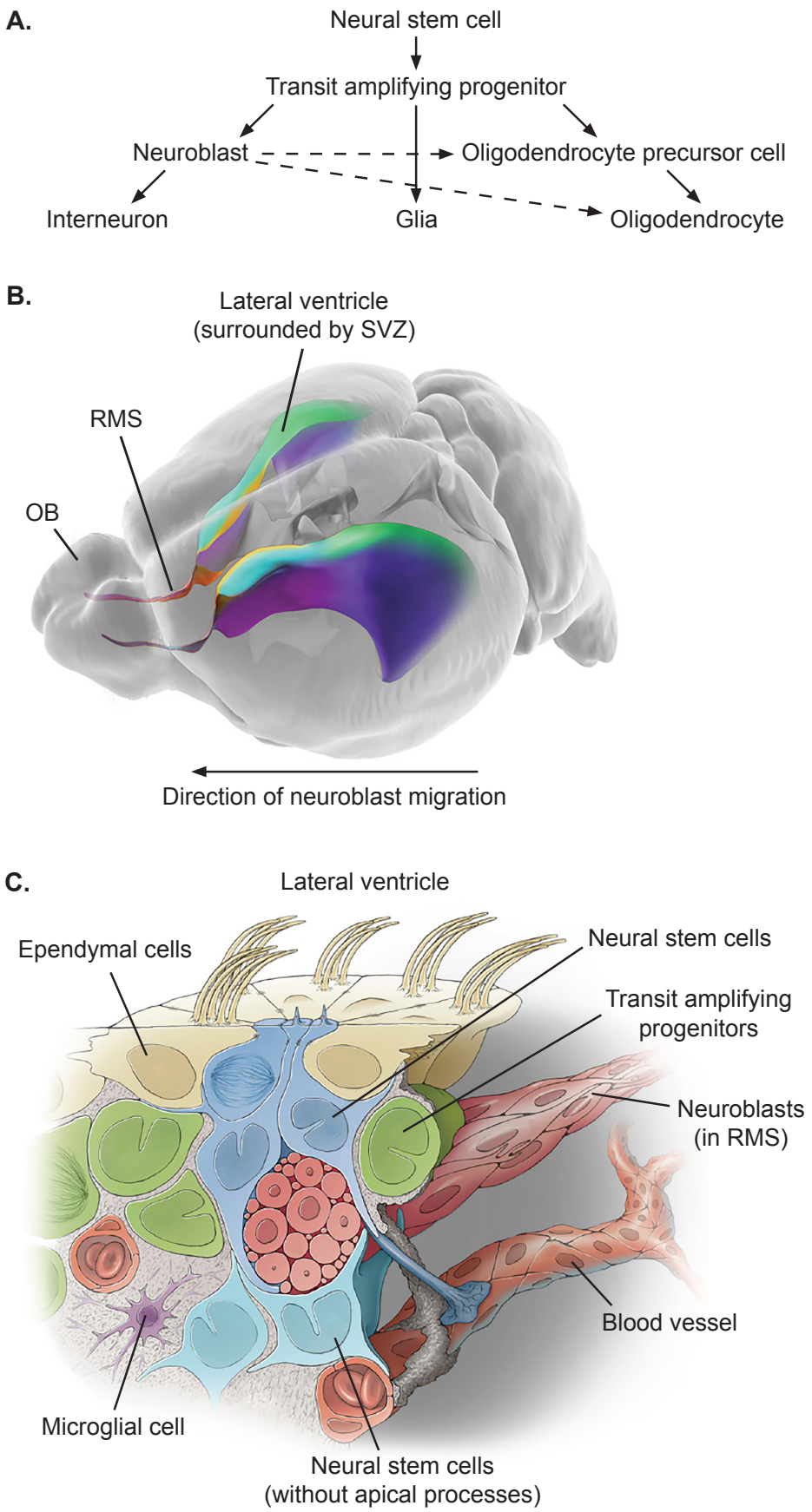


Figure 1.6: **Subventricular zone.** **A,** Flow chart showing tripotentiality of neural stem cells. **B,** Diagram showing anatomy of the SVZ, RMS and OB. **C,** Diagram showing anatomy within the SVZ. Diagrams adapted from Ihrie and Álvarez-Buylla (2011).

stem cell apical processes that contain a single, non-motile cilium (Mirzadeh et al., 2008). These cilia allow stem cells to receive signals from the CSF, such as Shh, which induces neurogenesis in the ventral SVZ (Tong et al., 2014). The middle layer comprises the cell bodies of the neural stem cells, as well as the transit amplifying progenitors and neuroblasts. The migrating chains of neuroblasts are surrounded by a scaffold of astrocytes (Jankovski and Sotelo, 1996). There are also haematopoietic microglia, which fulfil a phagocytic and immune surveillance role, and a subset of neural stem cells that do not contain apical processes, which appear to be less functionally important than those that do (Doetsch et al., 1997). The inner layer contains basal endfeet from the stem cells, which contact blood vessels and are hypothesised to receive further signals (Mirzadeh et al., 2008). Interestingly, the neural stem cells can regulate the diameter and blood flow of these vessels (Lacar et al., 2012).

SVZ stem cells are a largely quiescent population (Morshead et al., 1994). Indeed, in humans they only proliferate and give rise to migrating neuroblasts until 18 months of age (Sanai et al., 2011). After this time, they exhibit only trace levels of proliferation in vivo and leave behind a hypocellular gap in place of migrating neuroblasts (Sanai et al., 2011, 2004). They do, however, maintain the capacity to proliferate in vitro and can also be reactivated in diseases such as MS (Nait-Oumesmar et al., 2007; Sanai et al., 2004). They are also largely quiescent in mice but not to the same extent as in humans (Morshead et al., 1994). This difference likely stems from the greater importance of olfactory sensation and OB plasticity in mice. Once the stem cells become active, they upregulate Nestin and epidermal growth factor receptor (EGFR), and commence proliferating (Codega et al., 2014). Neural stem cells undergo a round of division with a cell cycle length (T_c) of 17 hours to give rise to transit amplifying progenitors (Ponti et al., 2013). They then proliferate three times with T_c = ∼18-25 hours, before neuroblasts divide once or twice with T_c = 18 hours and commence migration to the OB.

The signals regulating the SVZ originate from the blood, CSF and local cells. Small molecules in the blood can enter the SVZ, particularly in the vicinity of transit

amplifying progenitors (Tavazoie et al., 2008). Parabiotic experiments have been shown to reverse the age related decline in proliferation (Katsimpardi et al., 2014). As described earlier, CSF signals can be transmitted via the cilia on apical processes of neural stem cells (Tong et al., 2014). They may also be transmitted by ependymal cells, which as an example contain the low-density lipoprotein receptor related protein 2 (LRP2); LRP2 is a receptor for BMP4 and its absence leads to impaired SVZ proliferation (Gajera et al., 2010). Local signals include dopamine, which increases transit amplifying progenitor proliferation (Kim et al., 2010), and GABA, which is released from neuroblasts and decreases proliferation of neural stem cells (Liu et al., 2005). Recent optogenetic experiments have shown choline acetyltransferase positive neurons within the SVZ are necessary and sufficient to control neural stem cell proliferation (Paez-Gonzalez et al., 2014).

A detailed description of all mechanisms regulating the SVZ is beyond the scope of this introduction (see Ihrie and Álvarez-Buylla, 2011, for further review). It is worthwhile noting, however, that many key developmental regulators are recapitulated in adult neurogenesis. Signalling pathways include Wnt/beta-catenin (Adachi et al., 2007; Piccin and Morshead, 2011), Shh (Ahn and Joyner, 2005; Machold et al., 2003) and BMP/noggin (Lim et al., 2000); growth factors include epidermal growth factor (EGF; Kuhn et al., 1997; Reynolds and Weiss, 1992), fibroblast growth factor (FGF; Kuhn et al., 1997; Reynolds and Weiss, 1992), platelet derived growth factor (PDGF; Jackson et al., 2006) and vascular endothelial growth factor (VEGF; Zhang et al., 2003); and transcription factors include the neurogenic Dlx2 (Petryniak et al., 2007), Mash1 (Parras et al., 2004), NeuroD1 (Gao et al., 2009) and Pax6 (Hack et al., 2005).

The SVZ has the capacity to produce oligodendrocytes, and under normal physiologic conditions the ratio of oligodendrocytes to neurons varies from 1:3 to 1:30 depending on the location (Menn et al., 2006). This ratio increases following demyelination in the adjacent CC, and this process will be expanded on in the next section (Menn et al., 2006; Nait-Oumesmar et al., 1999; Picard-Riera et al., 2002). Transit amplifying cells expressing Olig2 give rise to oligodendrocytes (Hack et al., 2005; Marshall et al., 2005;

Menn et al., 2006), and EGF, FGF and pigment epithelium derived factor enhance this fate-choice (Azim et al., 2012; Gonzalez-Perez et al., 2009; Sohn et al., 2012). Additionally, neuroblasts may be redirected by chordin to become oligodendrocytes, as was shown after intraventricular chordin infusion in mice with green fluorescent protein (GFP) labelled neuroblasts (Jablonska et al., 2010).

1.3.2 Stem cells and demyelination

Stem cell use in demyelination was traditionally thought to have the aim of replacing lost oligodendrocytes; the first myelin transplantation experiments used Schwann cells from the sciatic nerve to repopulate lysolecithin-damaged oligodendrocytes in rats and cats (Blakemore, 1977). The region of demyelination had been irradiated first to diminish repair by local OPCs. It is now recognised, however, that stem cells also exert a beneficial immunomodulatory effect to decrease demyelination and axonal damage (Pluchino et al., 2005). This concept is referred to as functional multipotency (Teng et al., 2011), and the stem cells that have been investigated in human studies include haematopoietic, mesenchymal and neural. They may be derived endogenously and can also be transplanted, although the former currently appears more promising (Franklin and Ffrench-Constant, 2010).

Haematopoietic stem cell transplantation (HSCT) use in MS aims to reset the immune system and remove self-reactive immune cells (Ikehara et al., 1985; Marmont, 1994). It involves ablating immune cells with immunosuppression before transplanting allogenic or autologous haematopoietic stem cells. There have been over twenty studies to date involving over 500 patients (Sola-Valls et al., 2015). These studies have all suggested that HSCT prolongs periods of stable disease, particularly in patients who are younger than 40, have had MS for less than 5 years, demonstrate inflammatory MRI activity and/or are treated during an RRMS phase (Sola-Valls et al., 2015). The mechanism involves altering the T-cell profile with more naive T-cells, fewer central-memory T-cells, decreased IL-17 levels and diminished Th17 responses (Abrahamsson et al., 2013; Darlington et al., 2013; Muraro et al., 2005). Common

adverse effects include fever, engraftment syndrome (involving fever, erythrodermatous skin rash and noncardiogenic pulmonary oedema), enteritis and transient neurological worsening (Reston et al., 2011; Spitzer, 2001). There was a transplant related mortality of 1.3% between 2001 and 2007 (Mancardi and Saccardi, 2008).

Mesenchymal stem cells (MSCs) are obtained from connective tissue such as bone marrow but are by definition non-haematopoietic. They typically give rise to connective tissue cells including osteoblasts and adipocytes, and are also capable of becoming astrocytes, neurons and oligodendrocytes (Hermann et al., 2004; Kopen et al., 1999; Lu et al., 2008; Pittenger et al., 1999; Woodbury et al., 2000). While this fate-choice potential exists, it is more likely that MSCs aid regeneration through secreted factors that act on local stem cells and through decreasing inflammation (Gerdoni et al., 2007; Rivera et al., 2006). MSCs have been shown to benefit EAE in mice (Zappia et al., 2005). In humans, a recent Phase II trial with only nine participants (N = 4 placebo, N = 5 treated) had a non-significant trend for lower frequency of MRI lesions in RRMS (Llufriu et al., 2014). That followed another Phase IIa study in SPMS patients with visual deficits, which resulted in improved visual acuity and visual evoked response latency (Connick et al., 2012). These trials did not cause serious adverse effects.

Endogenous neural stem cell sources include the SVZ and SGZ as described above. SVZ cells have the capacity to migrate to demyelinated regions and differentiate into oligodendrocytes in mice (Nait-Oumesmar et al., 1999). A fate-mapping study showed that they contribute primarily to remyelination in the rostral CC, and that remyelination from SVZ derived oligodendrocytes results in thicker myelin than from OPC derived oligodendrocytes (Xing et al., 2014). In humans with MS, the SVZ is activated and produces more transit amplifying cells, some of which appear committed to becoming oligodendrocytes (Nait-Oumesmar et al., 2007). The SVZ is, however, difficult to artificially recruit due to its location. As with any stem cell population, its recruitment could also lead to cancer if efforts to enhance proliferation go too far. Pharmaceutical or other treatments will therefore need to be anatomically targeted through either delivery into the lateral ventricles or a mechanism of SVZ cell specificity.

They will also require a method to limit their effect size.

Exogenous neural stem cells may also be administered. Mice with EAE show histologic and functional improvement when neural stem cells are administered intravenously or intracerebroventricularly (Pluchino et al., 2003). This effect is due to both regeneration and protection (Pluchino et al., 2003, 2005), and has been replicated in non-human primates with EAE (Pluchino et al., 2009). While no trials have occurred in patients with MS, four children with PMD had foetal neural stem cells directly injected into four locations within the frontal lobe (Gupta et al., 2012). After 12 months, all children had stable or modest gains in motor and mental status function. No serious adverse effects occurred during that period. One difficulty in treating with exogenous neural stem cells is obtaining them. In the PMD study, they were obtained from a donated foetal brain. They may also be derived from ESCs or iPSCs, which could in turn be derived from easily accessible skin fibroblasts. As noted above, the first human iPSC trials occurred last year for macular degeneration (Cyranoski, 2014).

1.4 The galectin family

Galectins are a family of proteins characterised by their ability to bind glycoproteins. They have been implicated in inflammation and disease including in MS (Stancic et al., 2011). They specifically bind β-galactosides and 15 types are currently known (Liu and Rabinovich, 2010). They are located in the cytoplasm, nuclei and mitochondria, and can be secreted extracellularly. Extracellular galectins link cell-surface glycans with other cells, pathogens or the extracellular matrix (Boscher et al., 2011; Elola et al., 2007). These interactions regulate signalling through transmembrane receptors including for integrin and tyrosine kinase. Intracellular galectins have a role in regulation of cell growth, apoptosis and the cell cycle (Boscher et al., 2011; Elola et al., 2007).

Galectins bind glycoproteins through a carbohydrate recognition domain (CRD), and the 15 galectins can be classified into three categories: one CRD (Gal-1, 2, 5, 7, 10,

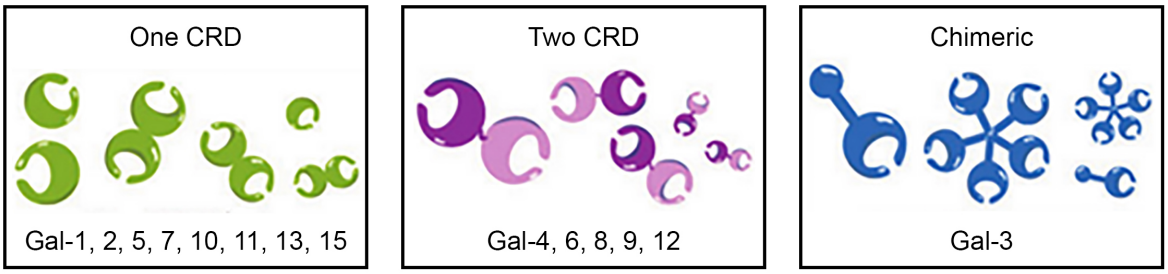


Figure 1.7: **Galectin categories.** Diagrams demonstrating one CRD, two CRD and chimeric galectins. Images adapted from Liu and Rabinovich (2010).

11, 13, 15), two CRD (Gal-4, 6, 8, 9, 12), and chimeric (Gal-3). The one CRD type contains monomers that can dimerise; the two CRD type connects two distinct but homologous CRDs with a polypeptide chain; and the chimeric type can form pentamers and includes a repetitive proline-, glycine- and tyrosine-rich sequence connected to the CRD (Figure 1.7; Jia and Wang, 1988; Liu and Rabinovich, 2010).

The Allen Brain Atlas demonstrated that Gal-3, Gal-8 and Gal-9 were expressed in the SVZ and RMS (Lein et al., 2007). Interestingly, Gal-1 has been reported to be expressed by and increase proliferation of SVZ neural stem cells (Sakaguchi et al., 2006). It was not, however, expressed in the SVZ or RMS in the Allen Brain Atlas. Separately, Gal-3 upregulation was demonstrated in tissue surrounding traumatic brain injury (TBI) lesions by the Szele laboratory. The connection of Gal-3 expression in the SVZ, Gal-3 expression after TBI, and the potential role of Gal-3 in MS as described below have made it a focus for the Szele laboratory and this thesis.

1.4.1 Galectin-3

Gal-3 is encoded by the Lgals3 gene and, as described above, is chimeric with the capacity to form pentamers (Jia and Wang, 1988; Liu and Rabinovich, 2010). It is largely seen as a pro-inflammatory molecule and was initially called Mac-2 in recognition of its expression by macrophages (Ho and Springer, 1982). That expression commences in monocytes and increases dramatically as they differentiate into macrophages (Liu et al., 1995). Gal-3 acts to enhance macrophage phagocytosis of apoptotic neutrophils, and is also a chemoattractant for monocytes and macrophages

(Karlsson et al., 2009; Sano et al., 2000). In neutrophils, it delays apoptosis, enhances phagocytosis, and promotes adhesion to laminin and endothelial cells to facilitate extravasation (Farnworth et al., 2008; Kuwabara and Liu, 1996; Sato et al., 2002). It has similar pro-inflammatory roles in other cells of the innate immune system including mast cells, eosinophils and dendritic cells (Frigeri et al., 1993; Hsu et al., 2009; Truong et al., 1993).

In the adaptive immune system, the role of Gal-3 is less clear. In B-cells, it shifts differentiation from plasma cells to memory cells via a mechanism involving IL-4 and Blimp-1 (Acosta-Rodríguez et al., 2004). In T-cells, extracellular Gal-3 induces apoptosis via the receptors CD7, CD29, CD45 and CD71, while intracellular Gal-3 prevents apoptosis through decreased reactive oxygen species production and maintenance of mitochondrial membrane potentials (Fukumori et al., 2003; Matarrese et al., 2000; Stillman et al., 2006; Yang et al., 1996). Dendritic cells also produce less IL-12 in the presence of Gal-3, leading to decreased Th1 responses (Bernardes et al., 2006). Interestingly, the enzyme that produces the glycosylated branches to which Gal-3 binds, mannosyl (alpha-1,6-)-glycoprotein beta-1,6-N-acetyl-glucosaminyltransferase (MGAT5), increases the threshold for T-cell activation (Demetriou et al., 2001). MGAT5 variants can alter MS disease severity (Brynedal et al., 2010).

Gal-3 additionally has an established role in inducing angiogenesis (Nangia-Makker et al., 2000). The mechanism is through VEGF and basic FGF (bFGF; Markowska et al., 2010).

The main medical conditions associated with Gal-3 are cancer and heart failure. Gal-3 is both a tumour promoter and suppressor: its expression carries a poor prognosis for glioblastoma (Debray et al., 2004) and pancreatic (Xie et al., 2012), nasopharyngeal (Acikalin et al., 2012), colorectal (Endo et al., 2005) and lung (O'Driscoll et al., 2001) cancers, while its presence is beneficial in breast cancer (Castronovo et al., 1996), melanoma (Brown et al., 2012) and chronic lymphocytic leukaemia (Asgarian-Omran et al., 2010). In prostate cancer, nuclear Gal-3 suppresses a tumour but cytoplasmic

Gal-3 promotes a tumour (Califice et al., 2004; van den Brûle et al., 2000). A detailed description of these mechanisms goes beyond the scope of this introduction; in brief, they include cell cycle modulation, altered cell migration and metastasis, and angiogenesis (Song et al., 2014). In heart failure, Gal-3 promotes cardiac fibroblast proliferation, collagen deposition and ventricular dysfunction (Lin et al., 2009; Sharma et al., 2004). Multiple studies suggest that serum Gal-3 is a poor prognostic indicator (Lok et al., 2010; Milting et al., 2008; van Kimmenade et al., 2006).

1.4.2 Galectin-3 in the SVZ and demyelination

Gal-3 has established roles in both the SVZ and demyelination. In the SVZ, Gal-3 is expressed by ependymal cells, astrocytes and a subset of transit amplifying progenitors (Comte et al., 2011). It enhances migration with neuroblasts becoming slower and more exploratory in Gal-$3^{-/-}$ mice, and fewer of them reaching the OB. The SVZ architecture is also distorted in Gal-$3^{-/-}$ mice, with astrocytic processes being thicker and losing their usual parallel orientation to the lateral ventricles. Following middle cerebral artery occlusion (MCAO) in Gal-$3^{-/-}$ mice, the neighbouring striatum shows decreased neovascularisation, endothelial cell proliferation and VEGF expression (Young et al., 2014).

In demyelination and remyelination, Gal-3 impacts both inflammation and oligodendrocyte differentiation. Gal-$3^{-/-}$ mice have a smaller leucocyte infiltrate in the EAE and TMEV models, which manifests with a milder phenotype in EAE (James, 2012; Jiang et al., 2009). These mice also contain fewer activated microglia in the CC following cuprizone treatment (Hoyos et al., 2014). While Gal-3 appears deleterious in demyelination, it seems beneficial for remyelination: recombinant Gal-3 increases differentiation in primary oligodendrocyte cultures, and non-diseased wild-type (Gal-$3^{+/+}$) mice have better myelin integrity than Gal-$3^{-/-}$ mice (Pasquini et al., 2011). In addition to these findings, Gal-3 expression is increased in postmortem MS tissue (Stancic et al., 2011).

Given the links of Gal-3 to both the SVZ and demyelination, it is surprising that the published literature does not link these three areas more frequently. The inflammation literature about Gal-3 and demyelination focuses on white-matter tracts like the CC rather than the SVZ, while the Gal-3 oligodendrocyte differentiation literature mainly used primary oligodendrocyte cultures derived from whole-brain tissue as opposed to just the SVZ (Pasquini et al., 2011). One finding that does draw these areas together occurs after TMEV when more SVZ derived neuroblasts migrate ectopically in the CC in Gal-$3^{-/-}$ compared to Gal-$3^{+/+}$ mice (James, 2012). There is, however, much more to discover.

1.5 Research questions

This background provides paradoxical hypotheses for the role of Gal-3 after demyelination: it worsens demyelination through increasing immune system activation; yet it benefits remyelination by enhancing oligodendrocyte differentiation. In addition, it alters migration of SVZ neuroblasts, which may have implications for remyelination. This thesis aims to clarify these roles and their mechanisms. It primarily focuses on the cuprizone model because of the ability to distinguish demyelination and remyelination phases. It also uses in vitro experiments, tissue from TMEV treated mice, and postmortem control and MS cases. The three broad sets of research questions are:

- How does Gal-3 influence inflammation during both demyelination and remyelination? Does its expression change in the SVZ and CC after cuprizone treatment? Does its absence alter SVZ inflammation?

- How does Gal-3 impact on oligodendrocytes? Does it alter their fate-specification or differentiation? Does it change their function and the level of demyelination or remyelination?

- How does Gal-3 affect neuroblast migration? Does it act as a chemoattractant or repellent? Does its absence alter the destination of neuroblasts following cuprizone treatment?

2

Methods

Contents

2.1 Human tissue 30
2.2 Animals 30
2.2.1 Breeding and maintenance 30
2.2.2 Genotyping 31
2.2.3 Bromodeoxyuridine administration 31
2.2.4 Cuprizone administration 32
2.2.5 TMEV inoculation 33
2.3 Histology 33
2.3.1 Animal tissue preparation 33
2.3.2 Microtome sectioning 33
2.3.3 Fluorescent immunohistochemistry 34
2.3.4 DAB immunohistochemistry 35
2.3.5 X-gal immunohistochemistry 36
2.3.6 Web search for in situ hybridisation and immunohistochemistry 36
2.4 Microscopy 37
2.4.1 Bright-field and epifluorescence microscopy 37
2.4.2 Confocal microscopy 37
2.4.3 Image analysis 37
2.5 Real-time polymerase chain reaction 38
2.5.1 Developmental samples 38
2.5.2 SVZ samples 39
2.6 Molecular techniques 40
2.6.1 siRNA plasmid design and production 40
2.6.2 Transfection of HEK293T cells 41
2.6.3 Western blot 42
2.7 Neurosphere assays 43
2.7.1 Neurosphere assay 43
2.7.2 Proliferation assay 43
2.7.3 Differentiation assay 44
2.8 Migration assays 45
2.8.1 Neuroblast explant assays 45
2.8.2 ACEA xCELLigence real-time migration assay including Biogel macrophage recruitment and flow cytometry 47
2.9 Statistics 48

2.1 Human tissue

Postmortem human tissue was obtained from the Oxford Brain Bank. It had been collected with approval from the relevant ethics committee in accordance with the UK Human Tissue Act. Anatomical blocks including periventricular regions were selected for controls (N = 8) and MS cases with active inflammatory demyelination (N = 8; details including causes of death in Table 4.1 on p71). The average age and postmortem interval (PMI) did not differ significantly between groups (age was 31.00 ± 7.61 for controls vs 44.38 ± 4.79 for MS cases, p = 0.159 for t-test; PMI was 57.00 ± 9.00 hours vs 47.13 ± 9.92 hours, p = 0.473). Tissue preparation including paraffin embedding, microtome sectioning at 10μm and slide mounting was performed by the Oxford Brain Bank.

2.2 Animals

2.2.1 Breeding and maintenance

129Sv and C57Bl6 wild-type mice were obtained through the University of Oxford Biomedical Services Specific Pathogens Free Breeding Unit. Gal-3 knockout mice on a 129Sv background (Gal-$3^{-/-}$) were obtained from Françoise Poirier's laboratory (Institut Jacques Monod, Paris; Colnot et al., 1998). They were bred with 129Sv wild-type mice (referred to as Gal-$3^{+/+}$ in the context of Gal-$3^{-/-}$ mice) to produce heterozygote mice (Gal-$3^{+/-}$). Gal-$3^{+/-}$ mice were subsequently mated with one another to produce Gal-$3^{+/+}$ and Gal-$3^{-/-}$ littermate controls. For experiments using adult animals, these animals were used. For experiments using postnatal animals, the littermate controls were bred with other mice of the same genotype to produce entire litters of Gal-$3^{+/+}$ or Gal-$3^{-/-}$ pups. The day of birth was designated as P0 and, for embryonic animals, the day of vaginal plug detection was E0. Gal-3 floxed heterozygote mice on a C57Bl6NTac background (Gal-$3^{+/fl}$) mice were obtained from MRC Harwell. They were bred with one another to produce floxed homozygote mice (Gal-$3^{fl/fl}$). CD68-GFP and control mice on a C57Bl6 background were provided as adult mice

by Prof David Greaves' laboratory (Sir William Dunn School of Pathology, University of Oxford; Iqbal et al., 2014). Animals were maintained in individually ventilated cages on 12-hour light/dark cycles with free access to food and water. Procedures were performed with University of Oxford Research Ethics Committee approval in accordance with the Animals (Scientific Procedures) Act of 1986 (UK). All efforts were made to minimise animal suffering and distress.

2.2.2 Genotyping

Animal technical staff obtained ear-clip samples. Deoxyribonucleic acid (DNA) was then extracted using the E.Z.N.A. Tissue DNA Kit (Omega Bio-Tek). Five microlitres of DNA was added to 20μL genotyping mastermix (recipe in Appendix A.5 on p195; primers as per Table 2.1). A polymerase chain reaction (PCR) programme was then run: initial denaturation at 94°C for 3 minutes; 35 cycles with denaturation at 94°C for 45 seconds, annealing at 55°C for 30 seconds and elongation at 72°C for 2 minutes; and final elongation at 72°C for 5 minutes. PCR products were separated by agarose gel electrophoresis at 180V for 20 minutes (2% agarose with 0.4μg/mL ethidium bromide in TAE; Sigma-Aldrich for agarose and ethidium bromide; TAE recipe in Appendix A.5). DNA bands were visualised under ultraviolet light.

Strain	**Primer**	**Sequence**	**Amplicon**
Knockout	Common	5'-CACGAACGTCTTTTGCTCTCTGG-3'	
	Gal-3^{+}	5'-TGAAATACTTACCGAAAAGCTGTCTGC-3'	∼300bp
	Gal-3^{-}	5'-GCTTTTCTGGATTCATCGACTGTGG-3'	∼500bp
Floxed	Common	5'-TGGGGATGTCTACCACACCT-3'	
	Gal-3^{+}	5'-CCCATTTCAACCCATAATTCA-3'	284bp
	Gal-3^{fl}	5'-GAACTTCGGAATAGGAACTTCG-3'	146bp

Table 2.1: **Genotyping primer sequences.**

2.2.3 Bromodeoxyuridine administration

Bromodeoxyuridine (BrdU) was prepared at 10mg/mL (recipe in Appendix A.1 on p193). It was administered via intraperitoneal (IP) injection at 50mg/kg in one of two

regimens. To mark proliferating cells at a given point in time, it was given 2 hours before sacrifice. To create label-retaining cells and enable analysis of both proliferation and migration, it was given in six 12-hourly doses at least 3 weeks before sacrifice.

2.2.4 Cuprizone administration

Cuprizone was administered to 8 week old male and female mice ad libitum in chow (International Product Supplies). The CD68-GFP and control mice started receiving cuprizone when they were 9 weeks old, while one Gal-$3^{+/+}$ 6 week control mouse was 10 weeks old. (It was excluded from all analysis except BrdU immunohistochemistry.) A concentration of 0.2% was chosen based on the literature, which also demonstrated that male and female mice had similar demyelination (Taylor et al., 2010). Treated mice received cuprizone chow for 3 or 6 weeks to cause demyelination, or 6 weeks followed by 10 days of control chow to induce remyelination. Control mice received the same chow without cuprizone. The 6 week cuprizone period was chosen as oligodendrocytes decrease greatly by that time, while the speed of oligodendrogenesis should have peaked after ∼10 days of remyelination (Figure 2.1). Mice were weighed weekly to ensure they remained within the 20% weight loss limit of the Procedure Project Licence.

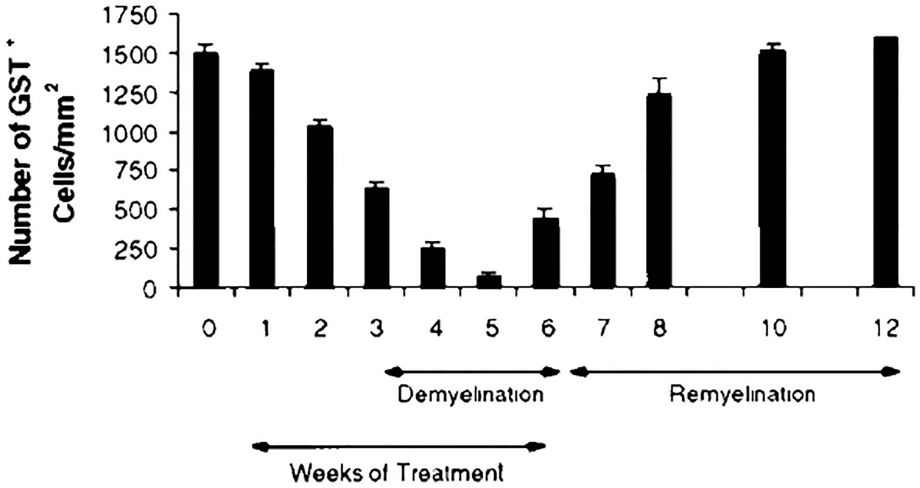


Figure 2.1: **Oligodendrocyte density during cuprizone treatment.** Graph showing how the density of oligodendrocytes in the CC varies after cuprizone and control chow administration. These mice were treated with cuprizone for 6 weeks before returning to control chow. Immunohistochemistry was performed for the Pi isoform of glutathione-s-transferase (GST) to label mature oligodendrocytes. Adapted from Mason et al. (2000).

2.2.5 TMEV inoculation

TMEV was administered to 6-8 week old female mice. They were anaesthetised with 4% isofluorane, and a 27 gauge needle was then used to inject the right posterior cortex with 3×10^6 plaque forming units of BeAN 8386 virus suspended in 0.03mL Hank's balanced salt solution (HBSS). A separate sham group received only HBSS. Mice were monitored daily for changes in neurological status. They were sacrificed 3, 7 or 14 days after the inoculation.

2.3 Histology

2.3.1 Animal tissue preparation

Mice being used for immunohistochemistry were overdosed with IP pentobarbitone, and transcardiacally perfused with cold normal saline (volume in millilitres approximately equal to mouse weight in grams). Brains from younger mice, typically less than P8, were dissected out and post-fixed overnight in 4% paraformaldehyde (PFA) at 4°C. Older mice were transcardiacally perfused with cold PFA (volume similar to normal saline) before brain dissection and post-fixation. Brains were cryoprotected in 30% sucrose in 0.1M phosphate buffer (PB) for 24-60 hours. They were then frozen in dry ice and kept at -80°C. Recipes for animal tissue preparation solutions are provided in Appendix A.1 on p193, and for common laboratory solutions in Appendix A.3 on p194.

2.3.2 Microtome sectioning

Frozen brains were cut into 30μm serial coronal sections on a Leica SM2000R sliding microtome. Sections were stored as free-floating sections in cryoprotectant at -20°C.

2.3.3 Fluorescent immunohistochemistry

Free-floating mouse brain sections were placed in 12 or 24 well plates with a maximum of 8 sections per well. Sections were treated with 50mM glycine in phosphate buffered saline (PBS) for 15 minutes, blocked for 1 hour in PBS+ (PBS with 10% donkey serum and 0.1% Triton X-100), and incubated in primary antibodies diluted in PBS+ at 4°C overnight (primary antibodies in Table 2.2). Each step had 3 × 10 minute PBS washes in between. Sections were then incubated for 1-2 hours with secondary antibodies diluted 1:500 in PBS+ and incubated for 10 minutes in 4',6-diamidino-2-phenylindole (DAPI, 10μg/mL in PBS, Sigma-Aldrich) with 3 × 10 minute PBS washes in between. Sections were rinsed 3 × 10 minutes in PB and mounted on Superfrost Plus slides. Slides were blotted with filter paper for excess fluid, air-dried for 1 hour, and coverslipped (#1.5 thickness) with FluorSave mounting media (Calbiochem). They were then dried at room temperature overnight and stored in slide boxes at 4°C. Immunohistochemistry was performed at room temperature unless otherwise stated and exposure to light was minimised after addition of fluorophores. Secondary antibodies included fluorescent Alexa Fluor 488, 568 and 647 (Life Technologies) and Cy3 (Jackson ImmunoResearch) conjugated antibodies against the host species of the relevant primary antibody. The specificity of secondary antibodies was verified in

Antigen	**Dilution**	**Host**	**Manufacturer**	**Product #**
β-Gal	1:2000	chicken	Abcam	ab9361
BrdU	1:500	sheep	Abcam	ab1893
BrdU	1:500	mouse	Progen	11200
CC1	1:500	mouse	Calbiochem	OP80
CD45	1:500	rat	Chemicon	CBL1326
Dcx	1:100	goat	Santa Cruz	sc-8066
Gal-3	1:100	rabbit	Santa Cruz	sc-20157
Gal-3	1:100	rat	Santa Cruz	sc-23938
GFAP	1:400	rat	Life Technologies	13-0300
Iba1	1:400	goat	Abcam	ab5076
Mash1	1:200	mouse	BD Pharmingen	556604
MBP	1:100	goat	Santa Cruz	sc-13914
Olig2	1:1000	rabbit	Chemicon	AB9610
PHi3	1:400	rabbit	Upstate	06-570

Table 2.2: **Primary antibodies for fluorescent immunohistochemistry.**

every experiment with a no primary antibody control. BrdU samples required antigen retrieval by heating with 1M HCl at 38.5°C for 1 hour.

2.3.4 DAB immunohistochemistry

Human tissue sections were paraffin embedded and slide mounted. They were initially dewaxed through a descending ethanol (EtOH) row (2 minutes each for Xylene (×2), 100% EtOH (×2), 96% EtOH, 90% EtOH, 80% EtOH, 70% EtOH, 60% EtOH, 50% EtOH and distilled water (dH_2O; ×2)). Sections were then placed in a water bath for 10 minutes at 80°C for antigen retrieval and 0.3% H_2O_2 in dH_2O for 10 minutes at room temperature to block endogenous peroxidase activity. Sections were rinsed in PBS for 5 minutes, blocked in PBS with 10% donkey serum for 30 minutes, rinsed in PBS for 5 minutes, and incubated overnight at 4°C in primary antibody diluted in PBS with 10% donkey serum and 0.1% Triton X-100 (primary antibodies in Table 2.3). Sections were then rinsed in PBS for 5 minutes, incubated in biotinylated secondary antibody diluted in PBS for 1 hour, and rinsed in PBS for 5 minutes. Sections were then placed in ABC peroxidase-streptavidin complex (VectaStain Elite ABC Kit, Vector) for 30 minutes, rinsed in PBS for 5 minutes, added to DAB substrate (DAB Substrate Kit, Vector) for ∼3 minutes, and rinsed thoroughly in PBS. Sections were counterstained with haematoxylin, dehydrated through an ascending EtOH row (2 minutes each for 50% EtOH, 60% EtOH, 70% EtOH, 80% EtOH, 90% EtOH, 96% EtOH, 100% EtOH (×2) and Histoclear), and mounted with DePex. Before primary antibody incubation, sections were encircled with ImmEdge wax pen (Vector A-4001) to minimise antibody use. DAB immunohistochemistry for CD68 and PLP followed a modified protocol that included antigen retrieval of microwave heating with citrate buffer (pH 6.0).

Antigen	**Dilution**	**Host**	**Manufacturer**	**Product #**
CD68	1:100	mouse	Dako	M0876
Gal-3	1:400	rabbit	Santa Cruz	sc-20157
Gal-3	1:200	rat	Santa Cruz	sc-23938
PLP	1:1000	mouse	AbD Serotec	MCA839G

Table 2.3: **Primary antibodies for DAB immunohistochemistry.**

2.3.5 X-gal immunohistochemistry

The Gal-3^{fl} allele contained a LacZ construct, which produced β-Galactosidase (β-Gal) driven by the Gal-3 promoter (see allele structure in Figure 3.1 on p52). An initial titration experiment determined that 8 hours of 4% PFA post-fixation at 4°C provided optimal balance between fixation and ongoing β-Gal activity. This result was broadly consistent with published material (Ma et al., 2002). Animal tissue was otherwise prepared and sectioned on a microtome as described above.

Free floating sections were fixed in 0.2% glutaraldehyde on ice for 10 minutes. They were then rinsed in PBS, washed in PBS for 10 minutes, washed in X-gal detergent rinse for 10 minutes (recipe in Appendix A.4 on p194), and incubated overnight at 37°C in 1mg/mL X-gal (Promega) in X-gal staining solution (Appendix A.4). Sections were then post-fixed in 4% PFA for 10 minutes, rinsed in PBS, washed in PBS for 10 minutes, washed in dH_2O for 2×5 minutes, counter-stained with Nuclear Fast Red (Sigma-Aldrich) for $\sim$2 minutes, and washed in dH_2O. They were then mounted as described for fluorescent immunohistochemistry.

2.3.6 Web search for in situ hybridisation and immunohistochemistry

The websites Genepaint.org, Gensat.org and www.brain-map.org (Allen Brain Atlas) were searched for images of the protein Gal-3 and the messenger ribonucleic acid (mRNA) of its gene Lgals3. Sagittal images were examined with a particular focus on the SVZ and RMS.

2.4 Microscopy

2.4.1 Bright-field and epifluorescence microscopy

Bright-field images of human tissue were obtained using a Leica Aperio ScanScope AT Turbo microscope. Images were viewed using Leica Aperio ImageScope software.

Bright-field and epifluorescence images of animal tissue were obtained using two microscopes. One was a Leica DMIRB microscope with a Hamamatsu C4742-95 digital camera. Its images were acquired in Openlab software (Improvision) and processed in Volocity 4 software (PerkinElmer). The other microscope was a Leica DMR microscope with a Leica DFC-500 digital camera. Its images were acquired in Leica Firecam 3.4.1 software. The vast majority of imaging, including all images for threshold analysis, involved using constant camera settings within a given experiment.

2.4.2 Confocal microscopy

Confocal images were obtained on a Zeiss LSM 710 laser scanning confocal microscope using the Z-stack and tile functions as appropriate. They could be analysed in LSM Image Browser 4.2 (Zeiss).

2.4.3 Image analysis

All quantitative image analysis, including image acquisition and quantification, was performed blinded, except for the initial acquisition of CC and cortical MBP images.

For cell counting including calculating densities, cells were analysed in one of two ways: live counting or sample imaging then counting. Live counting was used for BrdU+ and phosphohistone H3 (PHi3+) cells in the SVZ and CC, Olig2+ cells in the SVZ only, and doublecortin (Dcx+) cells in TMEV brains. Sample images were used for all other immunohistochemistry cell counting. Images were viewed in ImageJ (NIH) and counted using macros (see Appendix B.1.1 on p197 for example CC macro script).

These macros allowed images to be opened with only the DAPI channel visible, so that the appropriate region could be selected and cropped without the bias of seeing other channels. The macros then switched the view to the other channels for cell counting.

For scoring of GFAP immunohistochemistry for reactive astrocytosis, two experienced laboratory members independently scored images on ImageJ between 0-10. The criteria included brightness and quantity of fluorescence, and thickness of processes.

For MBP threshold analysis, images were analysed using macros in ImageJ (see Appendix B.1.2 on p197 for cortex macro script). Initially the macro caused only DAPI to be displayed to avoid the bias of seeing other channels. It then allowed the appropriate regions to be selected. For cortical layers, ten regions corresponding to layers 1, 2/3, 4, 5 and 6 in the motor and somatosensory cortices were manually selected using the ROI Manager. The macro then calculated and displayed the intensity histograms for the regions. These histograms were copied to Microsoft Excel and plotted to display the intensity distribution. An appropriate intensity was chosen above which MBP labelling was considered to be positive, and the percentage of pixels with greater intensity was calculated. The CC threshold analysis was performed without the macro but with a similar process. It additionally involved calculating an intensity histogram for the entire image. The maximum and minimum value from the entire image were then used to linearly transform the histograms for the CC, such that the maximum and minimum values were consistent across brains.

2.5 Real-time polymerase chain reaction

2.5.1 Developmental samples

Tissue from nine brain regions (see Figure 3.3A on p56 for diagram) of E15, E18, P2, P10 and adult C57Bl6 mice was dissected and placed in RNAlater® solution (Life Technologies). Embryonic and postnatal tissue was pooled from pups within a litter, while adult tissue was from one mouse. Samples were then stored at -80°C. Each brain region at each time point had biological triplicates. RNA extraction was performed

Protein	Gene	Assay ID
Galectin-3	Lgals3	QT00152558
TFRC	Tfrc	QT00122745

Table 2.4: **QuantiTect primer assays.**

using an RNeasy Mini Kit (Qiagen). RNA integrity was tested using an Agilent RNA 6000 Nano Kit with RNA Integrity Number (RIN) requirement of 8.0. One sample (one replicate of midbrain at P10) had RIN 5.5 and there was insufficient tissue for further RNA extraction. It was therefore included for future processing and, after seeing consistent results with other replicates, was included in final analysis. Reverse transcription was performed using a QuantiTect Reverse Transcription Kit (Qiagen). Real-time polymerase chain reaction (RT-PCR) was performed on a 7900HT Fast Real Time PCR System using QuantiTect Primer Assays (Table 2.4; Life Technologies) and QuantiFast SYBR Green PCR Master Mix (Life Technologies). The protocol followed the 384 well instructions in the QuantiTect Primer Assay Handbook, and used technical triplicates and standard curves.

Data was initially analysed using SDS Software v2.4 (Applied Biosystems) and aberrant replicates were removed. Tfrc had efficiency between 90-110% and $R^2 \geq 0.998$, and Gal-3, which had lower gene expression levels, had a minimum efficiency of 82.60% and $R^2 \geq 0.993$. Data was then exported to Microsoft Excel and SPSS. Statistics were performed using a two-way analysis of variance (ANOVA) for age and brain region as described later.

2.5.2 SVZ samples

SVZ tissue from individual 6 week littermate control Gal-$3^{+/+}$ and Gal-$3^{-/-}$ mice was microdissected in HBSS. The sample was centrifuged to pellet tissue and aspirate excess HBSS. It was snap frozen in liquid nitrogen and stored at -80°C. RNA extraction was again performed using an RNeasy Mini Kit. Before extraction, individual samples were pooled to provide three groups of four animals for each genotype. All samples provided a 260/280 ratio between 2.08 and 2.10, which was considered to provide

Protein	Gene	Assay ID
Galectin-1	Lgals1	Mm00839408_g1
Galectin-3	Lgals3	Mm00802901_m1
Galectin-8	Lgals8	Mm01332239_m1
Galectin-9	Lgals9	Mm00495295_m1
EGFR	Egfr	Mm00433023_m1
CCL2	Ccl2	Mm00441242_m1
CCR2	Ccr2	Mm00438270_m1
MMP9	Mmp9	Mm00442991_m1
B2M	B2m	Mm00437762_m1

Table 2.5: **TaqMan gene expression assays.**

satisfactory RNA quality. Reverse transcription was performed using a High Capacity RNA to cDNA Kit (Applied Biosystems). RT-PCR used TaqMan Gene Expression Assays (Table 2.5; Life Technologies) and TaqMan Gene Expression Master Mix (Life Technologies). It was performed on a 7900HT Fast Real Time PCR System (Applied Biosystems) using technical triplicates and standard curves, and following the TaqMan Gene Expression Master Mix Protocol for 384 well plates.

Similar to developmental samples, data was initially analysed using SDS Software v2.4 and aberrant replicates were removed. All genes had efficiency between 90-110% and $R^2 \geq 0.998$ except for Ccl2 ($R^2 = 0.965$), Ccr2 ($R^2 = 0.948$) and Mmp9 ($R^2 = 0.987$), which had lower gene expression levels compared to other genes. Data was then exported to Microsoft Excel, where individual gene quantities were normalised to B2m and divided by Gal-$3^{+/+}$ quantities to create fold change ratios. Statistics were performed on normalised values using a student's t-test as described later.

2.6 Molecular techniques

2.6.1 siRNA plasmid design and production

Small interfering RNA (siRNA) constructs were produced using a pSilencer 2.0-U6 linear expression vector (pSil; Ambion). Sense and antisense sequences were based on published literature, and the insertion sequence design included BamHI and HindIII restriction sites (Table 2.6; Henderson et al., 2006). pSil plasmids were digested with

Name	Nucleotide start	Exon	Strand	Sequence
shGal3_v1	646	5	sense antisense	5'-GATGTTGCCTTCCACTTTA-3' 5'-CTACAACGGAAGGTGAAAT-3'
shGal3_v2	148	2-3	sense antisense	5'-GCAGACAGCTTTTCGCTTA-3' 5'-CGTCTGTCGAAAAGCGAAT-3'
shGal3_v3	822	6	sense antisense	5'-GGTCAACGATGCTCACCTA-3' 5'-CCAGTTGCTACGAGTGGAT-3'
shGal3_v4	344	3	sense antisense	5'-GGACAGGCTCCTCCTAGTG-3' 5'-CCTGTCCGAGGAGGATCAC-3'

Table 2.6: **siRNA sequences.** Based on Henderson et al. (2006).

BamH1 and HindIII, then linear vector and insertion sequences were conjugated by T4 DNA ligase according to product protocols (New England BioLabs). The plasmids were transformed into Subcloning Efficiency DH5α Competent Cells according to product protocol (Life Technologies). Transformed cells were then seeded on LB agar plates with ampicillin (100μg/mL) and incubated at 37°C overnight. Pipette scrapings from individual colonies were seeded in LB broth with ampicillin, and a QIAprep Spin Miniprep Kit (Qiagen) was used to obtain DNA. Samples were initially screened for successful conjugation with PCR using primers designed against insertion sequences, and then with sequencing by Source BioScience LifeSciences. Transformed cells with a positive sequence were seeded in larger quantities of LB broth with ampicillin, and plasmids were purified using an EndoFree Plasmid Maxi Kit (Qiagen).

2.6.2 Transfection of HEK293T cells

siRNA constructs were evaluated in HEK293T cells cultured in Dulbecco's Modified Eagle's Medium (DMEM; Life Technologies) with 10% foetal bovine serum (FBS) and 1% penicillin/streptomycin. Cells were seeded at 250,000 per well in 6 well plates. After one day, each well was transfected with 500μL OptiMEM (Life Technologies) including 2μg of each plasmid and 10μL Lipofectamine reagent (Life Technologies). pSil plasmids were trialled individually and collectively (2μg total DNA per well). Additional vectors used included pCAGIG and pCAGIG-Gal-3 (developed by Dr Osama Al Dalahmah in

the Szele laboratory) and non-targeting pSil (gift from Dr Stephen Fleenor in A/Prof Jo Begbie's laboratory). Media was changed after 24 hours and cells were harvested after 48 hours. Harvesting initially involved imaging wells using bright-field and fluorescence to measure transfection efficiency. Protein was extracted by pelleting cells, adding lysis buffer (Appendix A.5 on p195), vortexing then centrifuging the homogenate, and aspirating the supernatant. Samples were kept at -80°C.

2.6.3 Western blot

Total protein levels were initially measured using the DC Protein Assay (Bio-Rad) and its Microplate Assay Protocol. Western blot (WB) gels were prepared as resolving and stacking gels in a glass plate casting apparatus (Bio-Rad; WB gel and buffer recipes in Appendix A.6 on p195). Solid gels were then loaded into a running apparatus (Bio-Rad) filled with WB running buffer. Before loading, 30μg total protein samples were heated to 98°C for 3 minutes in a 1:1 dilution in Laemmli Sample Buffer (Bio-Rad). They were then loaded into wells and the gel was run at 140V for approximately 75 minutes. Separated protein was transferred to Immun-Blot polyvinylidene fluoride (PVDF) membranes (Bio-Rad). The PVDF membranes had been activated in methanol for 30 seconds, washed in H_2O for 30 seconds, and placed in WB transfer buffer. They were then assembled adjacent to gels, and between blot paper, in a membrane transfer apparatus (Bio-Rad) in WB transfer buffer. The apparatus was run at 220V at 400mA for approximately 70 minutes. The PVDF membrane was then washed in tris-buffered saline (TBS) with 0.5% Tween (TBS-T), immersed in methanol, dried to fix the protein, immersed in methanol, washed briefly with TBS-T, and blocked for one hour in 5% milk (5g in 100mL TBS-T). The membrane was then incubated in primary antibody at 4°C overnight (primary antibodies in Table 2.7), washed 3 × 10 minutes in TBS-T,

Antigen	**Dilution**	**Host**	**Manufacturer**	**Product #**
β-actin	1:1000	mouse	Sigma-Aldrich	A4700
Gal-3	1:1000	rat	Santa Cruz	sc-23938

Table 2.7: **Primary antibodies for WB.**

incubated in 1:5000 horseradish peroxidase (HRP) conjugated secondary antibodies for 1 hour, and washed 3 × 10 minutes in TBS-T. It was then developed using Immobilon Western Chemiluminescent HRP Substrate (Merck Millipore), and imaged on a ChemiDoc XRS System (Bio-Rad). For testing different antibodies, the blot was stripped by placing in WB stripping buffer for 15 minutes then washing 2 × 5 minutes in PBS and 2 × 5 minutes in TBS-T.

2.7 Neurosphere assays

2.7.1 Neurosphere assay

Primary SVZ cultures were obtained from P4-5 mice. Animals were sacrificed using anaesthesia (hypothermia) followed by decapitation. Whole brains were dissected then cut into 500μm coronal sections using a McIlwain tissue chopper. SVZ was micro-dissected in DMEM and stored on ice until dissection was complete. Cells were dissociated mechanically with iris scissors and enzymatically through Accutase (Sigma, A6964) incubation for 10 minutes at 37°C. Cells were then washed three times in Neurobasal A+ (NB-A+; neurosphere recipes in Appendix A.2 on p193) including centrifugation for 5 minutes at 1200rpm for each wash, suspended in NB-A+ with growth factors (NB-GF), counted, and seeded as described for each assay below. Cultures were incubated at 37°C with 5% CO_2. For passaging, neurospheres were aspirated and then dissociated enzymatically, washed, suspended, counted and seeded.

2.7.2 Proliferation assay

SVZ neurospheres were cultured from Gal-$3^{+/+}$ and Gal-$3^{-/-}$ mice. Primary SVZ cells were seeded in 96 well plates at 10,000 cells in 200μL of NB-GF. They were then cultured for 7 days before whole wells were imaged using an AMF4300 EVOS® FL Imaging System (Life Technologies). Neurospheres were passaged and secondary cells were seeded at 1,000 cells in 200μL of NB-GF. Images were analysed using an ImageJ macro (see Appendix B.1.3 on p198 for macro script). It guided the merging of separate

images to form the whole well image, and the measurement of individual cell diameters.

2.7.3 Differentiation assay

SVZ neurospheres from Gal-$3^{+/+}$ and Gal-$3^{-/-}$ mice were cultured in 6 well Polyheme-coated plates at 200,000 cells in 2mL NB-GF. These plates were prepared by combining ingredients for 10× Polyheme (Appendix A.2), vortexing vigorously, and incubating overnight at 37°C. This solution was then vortexed and diluted to 1× with 95% EtOH. It was added to plates such that it covered the base of wells, and left to dry inside a laminar flow hood. The plates were prepared up to 2 weeks in advance.

Tertiary neurospheres were obtained by passaging neurospheres every 4-5 days. These neurospheres were then passaged, and dissociated cells were seeded in 96 well plates. The plates were pre-treated by coating each well with 100μL of 100μg/mL poly-D-lysine (Sigma-Aldrich, P6403), incubating at 4°C overnight, aspirating excess poly-D-lysine, coating each well with 30μL of 10μg/mL laminin (Sigma-Aldrich, L2020) for 1 hour before use, and aspirating excess laminin. This pre-treatment provided a substrate for cells to adhere to, and the subsequent absence of growth factors allowed cells to differentiate. The cells were initially seeded at 10,000 cells in 30μL of NB-A+ and cultured for 1 hour, so that cells would adhere to the base of wells. A further 170μL NB-A+ was then added including chemicals of interest: retinoic acid (diluted in DMSO; Sigma-Aldrich, R2625), recombinant Gal-3 (diluted in dH_2O; Peprotech, 450-38), DMSO (Sigma-Aldrich, 472301) or dH_2O. Cells were cultured for 6 days.

Differentiated cells were fixed for 15 minutes with 100μL of 4% PFA and washed 3 × 5 minutes in PBS. They were then stored at 4°C until fluorescent immunohistochemistry was performed. At this stage, cells were blocked for 1 hour in PBS+ (PBS with 5% donkey serum and 0.1% Triton X-100 for immunocytochemistry), incubated for 4 hours in primary antibodies in PBS+ (primary antibodies in Table 2.8), washed 3 × 5 minutes in PBS, incubated for 1 hour in secondary antibodies diluted 1:500 in PBS+, washed 3 × 5 minutes in PBS, incubated for 15 minutes in DAPI

Antigen	Dilution	Host	Manufacturer	Product #
GFAP	1:400	rat	Life Technologies	13-0300
MAP2	1:300	mouse	Upstate	05-346
Olig2	1:1000	rabbit	Chemicon	AB9610

Table 2.8: **Primary antibodies for fluorescent immunocytochemistry.**

(10μg/mL in PBS), and washed 3 $\times$ 5 minutes in PB. All steps used 100μL of solution per well except DAPI, which used 50μL per well. Cells were then left to air-dry for $\sim$2 minutes before a drop of FluorSave was added to each well. The entire plate was covered with a PCR plate seal to prevent evaporation and stored at 4°C. Exposure to light was minimised after the addition of fluorophores. Secondary antibodies were fluorescent Alexa Fluor 488, 568 and 647 conjugated antibodies against the host species of the primary antibodies.

Plates were imaged using an AMAFD1000 EVOS® FL Auto Imaging System (Life Technologies). Wells were then blinded and cells were counted in ImageJ. GFAP+ astrocytes and MAP2+ neurons required astrocytic or neuronal morphology in addition to immunofluorescence to be counted. Olig2+ cells were only counted if they were GFAP-/MAP2-.

2.8 Migration assays

2.8.1 Neuroblast explant assays

RMS explants were obtained from P4-5 mice in a similar method to the dissection of SVZ cells for neurospheres. Rather than microdissecting the SVZ, however, the RMS was dissected from rostral coronal sections including in the OB (Figure 2.2; Ward and Rao, 2005). The RMS dissections were cut into smaller cubes with iris scissors to produce the experimental explants. The explants were immersed in 6mg/mL Matrigel (Corning, BD 356231) in NB-A+, before being transferred to a fresh 10μL drop of 3D Matrigel in the centre of a well in a 12 well plate.

A gradient of recombinant Gal-3 (Peprotech, 450-38) or SDF-1 (Peprotech, 300-28A)

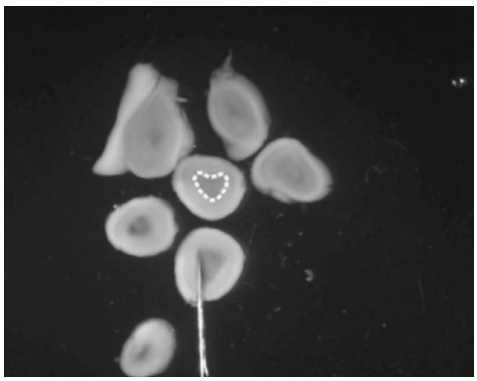


Figure 2.2: **RMS explant dissection.** Image demonstrating dissection of RMS from coronal brain sections. Adapted from Ward and Rao, 2011.

was established in multiple ways. Initially it was attempted with two vertical 200μL pipette tips filled with 5% agarose plugs at each end of the well, and 2μL of 10ng/mL or 100ng/mL SDF-1 injected into one of the plugs. It was then attempted by directly injecting 1μL of 1-100μg/mL Gal-3 or 1μg/mL SDF-1 into the Matrigel with a Hamilton syringe, approximately 1mm from the explant. Finally, agarose beads (Sigma, CL-4B) were used as a source. They were soaked for 24 hours at 4°C in 1μg/mL Gal-3 or 1μg/mL SDF-1. They were also immersed in Matrigel before being transferred to the drop of 3D Matrigel containing an explant. The beads and explant were arranged such that the beads were on one side of the explant and would create a chemical gradient. Once the beads and explant had been added to each well on a plate, they were incubated for 30 minutes at 37°C with 5% CO_2 to allow the Matrigel to solidify. 1mL NB-A+ was then added to each well. A method with 2D Matrigel was also attempted: Matrigel was pipetted into a well then aspirated immediately to create a substrate for the explants, and the beads were secured using high vacuum silicone grease (VWR).

Images were taken of explants after 24 and 48 hours on a Motic AE2000 inverted microscope with Moticam 580 digital camera (Motic). They were then analysed using an ImageJ macro (see Appendix B.1.4 on p199 for macro script and Figure 6.3B on p136 for example analysis). It used colour parameters to determine the regions occupied by both the explant and migratory neuroblasts. It then determined quadrants from the centre of the explant and the number of pixels occupied by neuroblasts in each quadrant. The proximal:distal migration ratio, as well as the total number of pixels occupied by migrating neuroblasts, could then be calculated.

2.8.2 ACEA xCELLigence real-time migration assay including Biogel macrophage recruitment and flow cytometry

Peritoneal macrophages were initially recruited for this experiment from adult male C57Bl6 mice. Mice received an IP injection of 1mL 4% (w/v) Bio-Gel P100 polyacrylamide beads (Bio-Rad) to stimulate peritoneal migration of macrophages. After four days, the mice were sacrificed and underwent peritoneal lavage with 10mL cold PBS with 2mM ethylene diamine tetraacetic acid (EDTA) to collect macrophages. The peritoneal fluid was pooled from 2-3 mice and centrifuged at 250G for 5 minutes to pellet cells. Cells were then resuspended in 10mL chemotaxis buffer (Roswell Park Memorial Institute 1640 Medium with 25mM HEPES, pH 7.4) and cultured overnight in Greiner bacterial petri dishes at 37°C with 5% CO_2. Macrophages should have adhered to the dishes, so dishes were washed with 10mL PBS before macrophages were lifted with PBS containing 10mM EDTA. Cells were then centrifuged at 250G for 5 minutes before resuspension in chemotaxis buffer for use in flow cytometry and the ACEA xCELLigence migration assay.

Flow cytometry was performed using a Dako CyAn ADP flow cytometer and FlowJo software (Tree Star). One million macrophages were washed in PBS then resuspended in flow cytometry buffer (PBS with 2% FBS, 25mM HEPES, 5mM EDTA). They were then incubated in the macrophage marker F4/80 (AbD Serotec, MCA497APCT) for 30 minutes at 4°C before analysis.

The ACEA xCELLigence migration assay used CIM-16 well plates on an xCELLigence RTCA-DP instrument. Similar to transwell assays, it contained 8μm pores with macrophages present above and chemoattractant present below. A volume of 160μL of chemoattractant (10nM CCL2, CCL5, CCL8, CXCL10, Gal-3 and 300nM Gal-3, all recombinant proteins from Peprotech) was loaded into the lower wells before the upper chambers were attached. The upper wells were then filled with 50μL of chemotaxis buffer and 50μL of macrophage cell suspension (4×10^5 cells or 8×10^6 cells/mL). The

assay was run for 4 hours with data points collected every 5 seconds. The parameters measured are described in Section 6.2.5 on p140.

2.9 Statistics

Data from the appropriate quantification was collated into Microsoft Excel. It was then analysed using scripts written for SPSS 21 (scripts in Appendix B.2 on p201). For experiments comparing one factor between two groups, a student's t-test was performed. For experiments comparing one factor between three or more groups, a one-way ANOVA was performed. For experiments comparing two factors, a two-way ANOVA was performed. For experiments comparing two factors for a variable quantified in multiple SVZ or CC anatomical regions, a repeated measures ANOVA was performed. Bonferroni post-hoc tests were used to determine significant pairwise comparisons in ANOVAs. Graphs were produced in Prism 5 (GraphPad) and show mean ± standard error of the mean (SEM). Given the complexity of repeated measures ANOVAs, these results are provided in tables in Appendix C on p205.

3

Galectin-3 experimental toolkit development

Contents

3.1 Introduction 50

3.2 Results 51

3.2.1 Identification of Gal-3^{+}, Gal-3^{-} and Gal-3^{fl} alleles 51

3.2.2 Creation of Gal-$3^{+/+}$ and Gal-$3^{-/-}$ brain library 51

3.2.3 Developmental expression of Gal-3 53

3.2.4 Characterisation of Gal-3 floxed mouse 58

3.2.5 Creation of siRNA Gal-3 constructs 60

3.3 Discussion 62

3.3.1 Developmental expression of Gal-3 62

3.3.2 Characterisation of Gal-3 floxed mouse 63

3.1 Introduction

The Szele laboratory has had an interest in Gal-3 since showing its constitutive expression in the SVZ and upregulation in cortical tissue after TBI (Comte et al., 2011). Its expression in both a neurogenic niche and an inflamed region suggest a significant role in adult brain plasticity. Many doctoral students and post-doctoral researchers in the laboratory have therefore investigated it. Research published to date has focused on in vivo and ex vivo differences between Gal-$3^{+/+}$ and Gal-$3^{-/-}$ mice, and in vitro assays with rGal-3 or Gal-3 function blocking antibodies (Comte et al., 2011; James, 2012; Young, 2011; Young et al., 2014). With broader scientific advances in molecular biology, the Szele laboratory Gal-3 toolkit has also expanded.

This chapter provides details on the technique development that I contributed to, which included:

- Identifying transgenic mouse alleles for genotyping.
- Creating a library of Gal-$3^{+/+}$ and Gal-$3^{-/-}$ brains.
- Determining the expression of Gal-3 during development.
- Characterising a Gal-3 floxed mouse.
- Developing plasmids to knockdown Gal-3 expression.

The Gal-3 floxed mouse, in particular, offers myriad possibilities for future experiments. It is a conditional knockout mouse, which facilitates the removal of critical exons when Cre-recombinase is expressed. If Cre-recombinase is driven by a cell specific promoter, the knockout effect can be limited to cell lineages (Gu et al., 1994). The temporal expression of Cre-recombinase may also be restricted by requiring oestrogen receptor ligand binding (Metzger et al., 1995). Tamoxifen can then be administered at a specific age to elicit the knockout effect. The Gal-3 floxed mouse therefore provides spatial and temporal control of Gal-3 expression, as opposed to the universal effect of a constitutive knockout mouse.

3.2 Results

3.2.1 Identification of Gal-3^{+}, Gal-3^{-} and Gal-3^{fl} alleles

The Szele laboratory has a Gal-3^{-} allele on a 129Sv mouse background strain and Gal-3^{fl} allele on a C57Bl6NTac strain. The Gal-3^{-} allele was developed in the Poirier laboratory using a vector that removed exons II, III and IV through homologous recombination (Figure 3.1A; Colnot et al., 1998). The vector was electroporated into embryonic stem cells, which were then injected into blastocysts to produce germline chimeric mice. Heterozygous progeny of these mice were selected to establish a colony containing the Gal-3^{-} allele. When bred as homozygotes, Gal-3$^{-/-}$ mice were found to be viable and fertile (Colnot et al., 1998).

A Gal-3^{fl} (or Gal-3^{tm1a}) allele was produced using a similar method by MRC Harwell as part of the International Mouse Phenotyping Consortium and International Knockout Mouse Consortium (Figure 3.1B; Bradley et al., 2012; Pettitt et al., 2009; Skarnes et al., 2011). This allele contains loxP sites around exon IV, which allow this exon to be removed with Cre-recombinase. The subsequent knockout allele is referred to as Gal-3^{tm1b}. A broad, multisystem phenotypic screen revealed no phenotype for Gal-3$^{tm1b/tm1b}$ (knockout) mice compared to controls (International Mouse Phenotyping Consortium, 2014).

Primers were produced against the Gal-3^{+}, Gal-3^{-} and Gal-3^{fl} alleles (Table 2.1, p31). They could identify homozygous and heterozygous genotypes for both knockout and floxed mice (Figure 3.1C).

3.2.2 Creation of Gal-3$^{+/+}$ and Gal-3$^{-/-}$ brain library

In order to easily conduct immunohistochemistry on Gal-3$^{+/+}$ and Gal-3$^{-/-}$ brains, I perfused and dissected Gal-3$^{+/+}$ and Gal-3$^{-/-}$ brains at a range of ages (Table 3.1). Most of these mice received a dose of BrdU 2 hours prior to sacrifice. The brains were subsequently dehydrated in 30% sucrose, frozen on dry ice, and stored at -80°C.

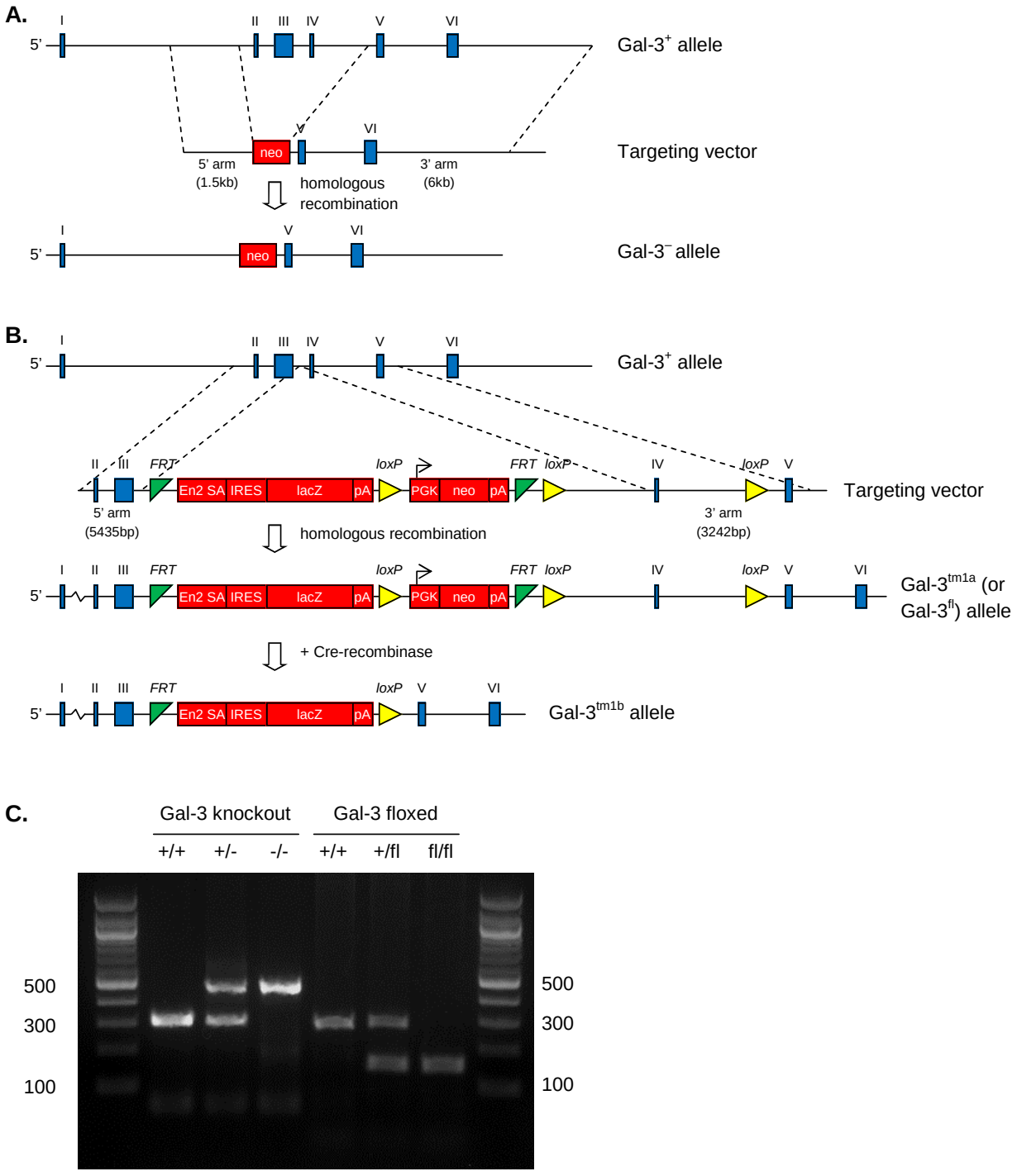


Figure 3.1: **Gal-3 wild-type, knockout and floxed alleles.** **A,** Production of knockout allele from wild-type allele by homologous recombination. Adapted from Colnot et al. (1998). **B,** Production of Gal-3^{tm1a} (or Gal-3^{fl}) and Gal-3^{tm1b} alleles by homologous and Cre-recombinase recombination. Adapted from International Mouse Phenotyping Consortium (2014) and their provided genotyping protocol. Note: targeting vector not to scale. **C,** Gel electrophoresis of genotyping PCR products showing different genotypic combinations for knockout and floxed mice.

Age	Gal-3$^{+/+}$	Gal-3$^{-/-}$
1 week	4	9
2 weeks	6	14
3 weeks	6	14
4 weeks	7	10
5 weeks	4	11
6 weeks	3	20
7 weeks	3	0
8 weeks	14	11

Table 3.1: **Brain library of Gal-3$^{+/+}$ and Gal-3$^{-/-}$ brains.** Table reporting number of brains for each age and genotype.

3.2.3 Developmental expression of Gal-3

Adult neurogenesis recapitulates many developmental events. I therefore wanted to know how Gal-3 is expressed during normal development. In addition, I used postnatal mice for many in vitro experiments in this thesis and I wanted to ensure it is expressed at the relevant ages.

A previous study used in situ hybridisation and immunohistochemistry to show that Gal-3 is expressed in the mouse notochord from E8.5 but not in the CNS until E16.5 (Fowlis et al., 1995). Through a web search of public gene expression databases for Lgals3, I found that Gal-3 is expressed around the lateral ventricles from E15.5 onwards (Figure 3.2). At E15.5, the expression appeared limited to the choroid plexus and endothelial layer. At P7, the expression included a rudimentary RMS. In the adult mouse, Gal-3 was expressed in the choroid plexus, SVZ and RMS.

To further characterise Gal-3 expression in P4 and adult mice, I used the LacZ construct within the Gal-3^{fl} allele to identify cells transcribing Gal-3. These results are described in detail in Section 3.2.4 on p58. Briefly, my findings were largely consistent with published databases. They suggested, however, that the highest transcription occurred in the ependymal cells surrounding the lateral ventricles.

I also examined mRNA levels via RT-PCR on samples taken from nine brain regions

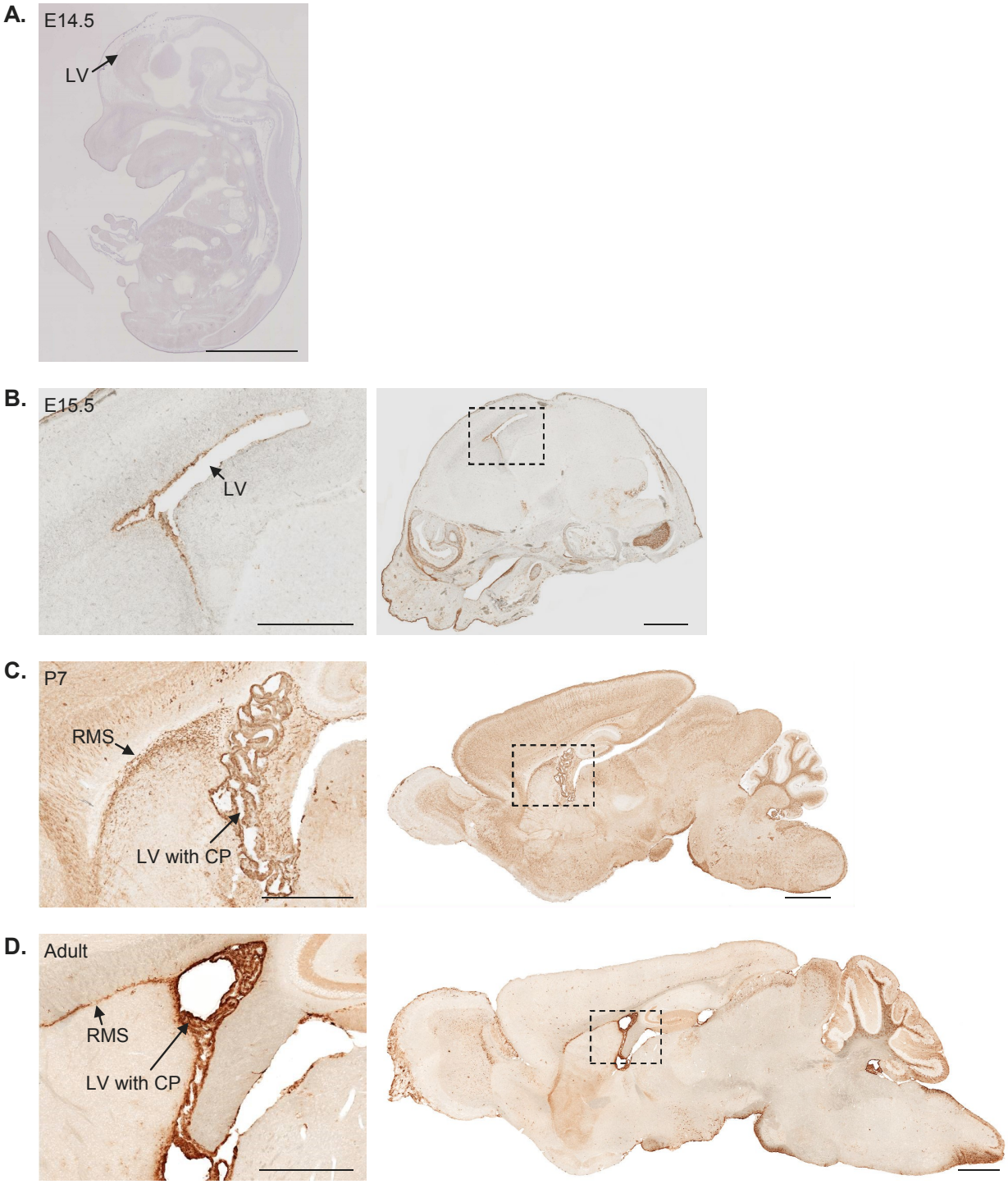


Figure 3.2: **Developmental expression of Gal-3. A,** Sagittal view through E14.5 embryo with in situ hybridisation for Gal-3 from Genepaint.org. Scale bar 1mm. **B to D,** Sagittal views through E15.5 (B), P7 (C) and adult (D) brains from Lgals3-GFP BAC transgenic mice from Gensat.org. Dotted lines show region of high magnification images. Scale bars 500μm for high magnification images and 1mm for low magnification images. LV: lateral ventricle, RMS: rostral migratory stream, CP: choroid plexus.

in E15, E18, P2, P10 and adult mice (Figure 3.3A). By measuring these levels, I hoped to detect Gal-3 transcription below the level of detection for immunohistochemistry.

Initially I verified the mRNA input levels across samples using the housekeeping gene Tfrc. It encodes transferrin receptor protein 1 and should be similar between brain regions (Boda et al., 2009). I found it had no significant differences between brain regions at a given age (Figure 3.3B; $F(8,87) = 1.884$, $p = 0.073$ for main effect in two-way ANOVA for region with N values as reported in the figure legend; $F(32,87) = 1.148$, $p = 0.302$ for interaction with age). Interestingly, however, Tfrc levels did increase with age ($F(4,87) = 59.752$, $p < 0.0005$ for main effect; $p < 0.0005$ for E15, E18 and P2 compared to P10 and adult; $p = 0.001$ for P10 compared to adult). The global increase across brain regions suggested this finding was physiologic rather than an experimental error of providing more starting mRNA. Caution would, however, need to be used in interpreting the Gal-3 results if they showed a similar rise.

Gal-3 mRNA levels were much lower than Tfrc: the cycle threshold values for RT-PCR occurred after approximately 25 cycles for Tfrc and 31 for Gal-3, suggesting a difference of 2^6 (64) times. In spite of that, Gal-3 demonstrated characteristic patterns that resulted in multiple significant differences (Figure 3.4; $F(8,87) = 15.039$, $p < 0.0005$ for main effect of region in two-way ANOVA with N values as reported in Figure 3.3; $F(4,87) = 6.806$, $p < 0.0005$ for main effect of age; $F(32,87) = 2.392$, $p = 0.001$ for interaction of age and region). In other experiments in this thesis, significant interactions in a two-way ANOVA negate any main effects that involve those factors. In this experiment, however, the number of ages and regions meant that there were overall differences that might only gain significance by examining main effects. Equally, an interaction in only a few ages and/or regions would not necessarily negate a main effect. Both the main effects and interactions were therefore considered for pairwise comparisons.

These pairwise comparisons are detailed in Figure 3.4 and there are two key observations to make. Firstly, Gal-3 expression peaked around E18 and P2 overall with this trend appearing in the cortex, hippocampus, striatum and thalamus

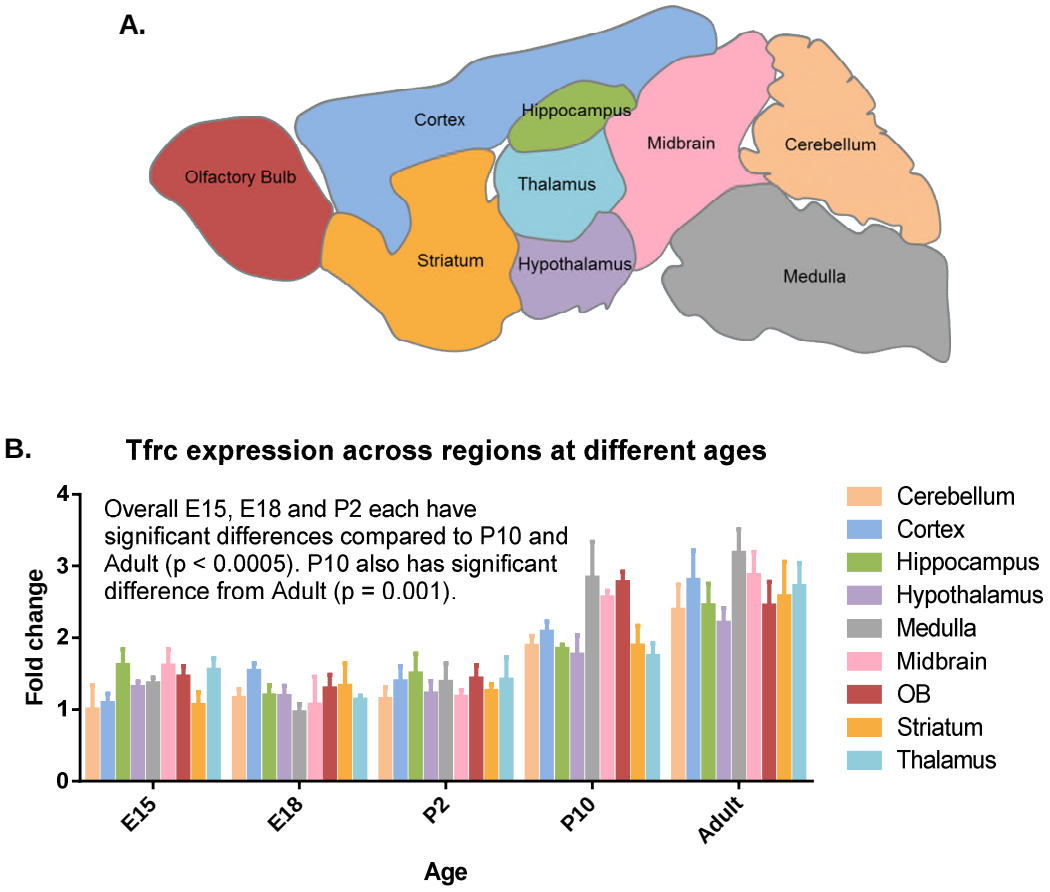


Figure 3.3: **Developmental RT-PCR experiment design. A,** Diagram showing regions of the brain dissected at E15, E18, P2, P10 and adult ages. N = 3 for each region except for cerebellum P10 (N = 2), midbrain E18 (N = 2) and midbrain P2 (N = 2 only for Tfrc). Image adapted from Melissa Bailey in the Molnár laboratory (unpublished). **B,** Graph demonstrating fold change of Tfrc in brain regions at different ages. Fold change values calculated relative to cerebellum E15. Statistics calculated as two-way ANOVA using SPSS. Graph shows mean ± SEM.

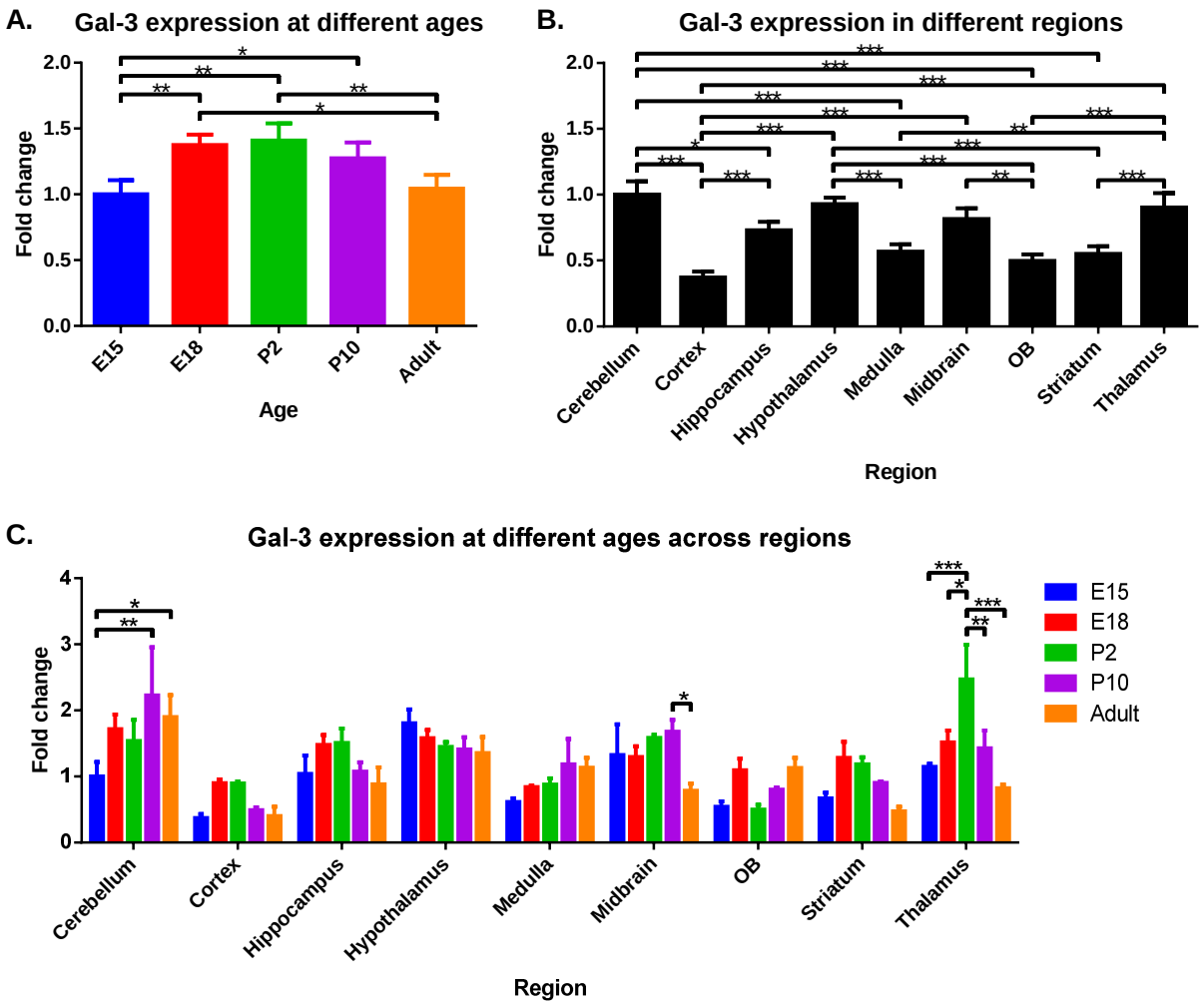


Figure 3.4: **Gal-3 developmental RT-PCR. A to C,** Graphs demonstrating fold change of Gal-3 at different ages for mean across all regions (A), different regions for mean across all ages (B) and different regions for separate ages (C). Fold change values calculated relative to left-most column. Statistics calculated as two-way ANOVA using SPSS. Significant comparisons between regions for a given age not shown in C due to complexity. N values the same as Figure 3.3. Graphs show mean ± SEM. *p $\leq$ 0.05, **p $\leq$ 0.01, ***p $\leq$ 0.001.

(Figure 3.4A and C; $p < 0.05$ overall and in the thalamus; trend not significant in cortex, hippocampus or striatum). Secondly, the regions with the least Gal-3 were the cortex, medulla, OB and striatum (Figure 3.4B; significant comparisons in figure). The cortex and striatum are anatomically the closest regions to the SVZ, while the OB is the destination of SVZ neuroblasts and the hippocampus is the other main neurogenic niche in adults. It is therefore interesting that the level of Gal-3 in these regions decreased as mice became older and/or was minimal compared to other regions. The regions with the highest Gal-3 expression were the cerebellum, hypothalamus, midbrain and thalamus.

3.2.4 Characterisation of Gal-3 floxed mouse

The Gal-3^{fl} allele was produced by MRC Harwell as described in Section 3.2.1 on p51. MRC Harwell then conducted a broad, multi-system phenotypic screen in globally floxed mice (International Mouse Phenotyping Consortium, 2014). It involved measuring parameters for most organ systems. The neurologic system screen, for example, included gait, activity levels and behavioural responses like startle reflex. The entire screen revealed no phenotype when comparing floxed mice to controls.

To ensure appropriate transgene expression in the SVZ, I examined X-gal staining in P4 and adult Gal-$3^{fl/fl}$ brains. The Gal-3^{fl} allele contains a LacZ gene driven by the Gal-3 promoter. It in turn produces β-Gal, which cleaves X-gal to produce a blue stain. Initial fluorescent immunohistochemistry experiments for β-Gal, which would allow co-fluorescent immunohistochemistry, were unsuccessful (results not shown; using protocol of Franco et al., 2012). X-gal immunohistochemistry experiments were used instead. Titration showed that brains could be post-fixed in PFA for 8 hours without losing X-gal intensity, which was broadly in keeping with published literature (Ma et al., 2002).

The findings were largely consistent with known Gal-3 expression (Figure 3.5; $N = 3$ for each age). The OB and RMS at both ages were absent for X-gal, except for occasional

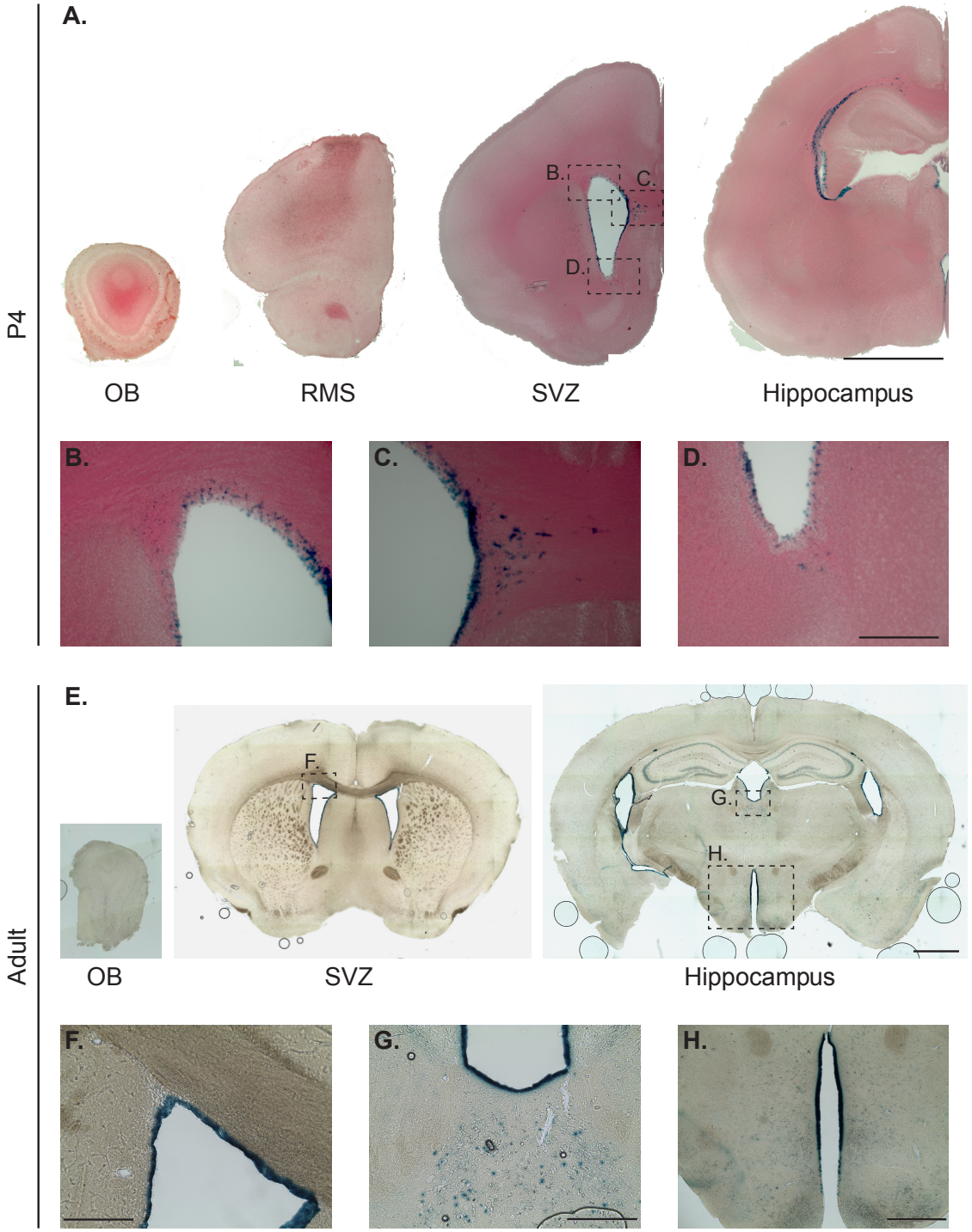


Figure 3.5: **LacZ expression in Gal-3$^{fl/fl}$ mice.** **A,** Representative images of X-gal immunohistochemistry from P4 mice. **B to D,** Higher magnification images of dorsolateral SVZ (B), CC (C) and ventral SVZ (D). **E,** Representative images of X-gal immunohistochemistry from adult mice. **F to H,** Higher magnification images of dorsolateral SVZ (F), dorsal third ventricle (G) and ventral third ventricle (H). N = 3 for each age. Scale bars 1000μm for low magnification images, 400μm for H and 200μm for other high magnification images.

cells in the meninges surrounding the OB. These X-gal+ cells were likely olfactory ensheathing cells, which are known to express Gal-3 (Storan et al., 2004). Sections at the level of the SVZ and hippocampus demonstrated X-gal+ cells surrounding the lateral and third ventricles. Interestingly, X-gal staining was strongest in the ependymal layer, the extent of which had not been reported before. Crucially, there were still some X-gal+ cells evident beyond the ependymal layer in the dorsolateral and ventral SVZ (Figure 3.5B, D and F). In addition, 2 out of 3 of the P4 SVZ sections demonstrated X-gal+ cells extending across the CC (Figure 3.5C). This effect was not seen in the adult.

3.2.5 Creation of siRNA Gal-3 constructs

Gal-3 siRNA constructs were produced to decrease Gal-3 expression during in vivo, ex vivo and in vitro experiments. Four siRNA sequences were designed based on existing Gal-3 siRNA constructs, and conjugated with a pSil linear expression vector (Table 2.6 on p41; Henderson et al., 2006). The plasmids were then transfected into HEK293T cells together with a pCAGIG-Gal-3 overexpression vector (Figure 3.6A; N = 3). GFP was expressed by the pCAGIG-Gal-3 and pCAGIG control vectors, and confirmed adequate transfection efficiency for all conditions (Figure 3.6B).

WBs were performed to assess Gal-3 expression (Figure 3.6C). In the absence of siRNA constructs, the pCAGIG-Gal-3 vector caused a clear increase in Gal-3 expression compared to the pCAGIG control vector. The siRNA constructs decreased Gal-3 expression with efficiency v1 > v2 > v3 > v4. A combination of all four constructs had similar efficiency to v1 alone.

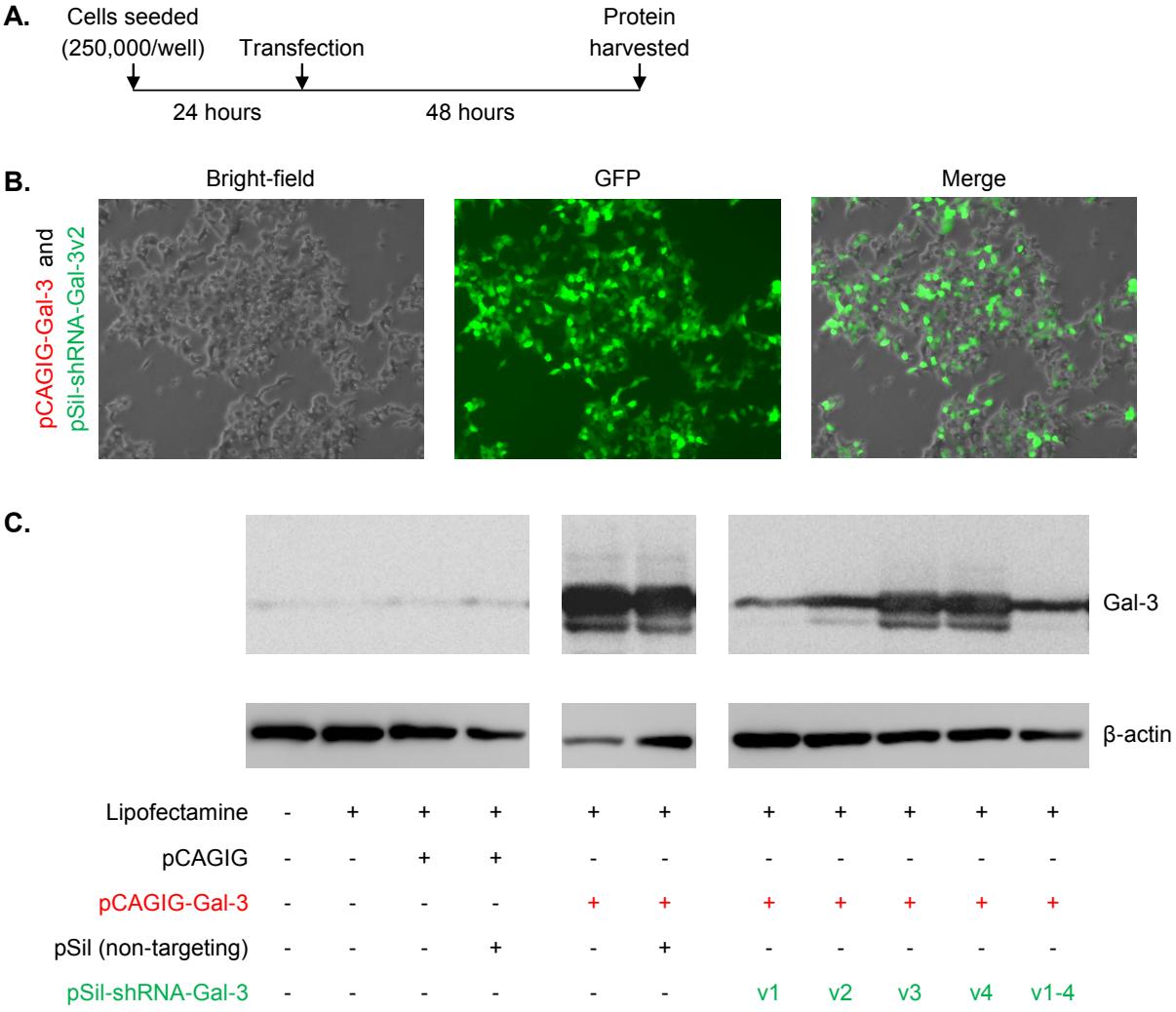


Figure 3.6: **Transfection of HEK293T cells with Gal-3 overexpression and shRNA plasmids.** **A,** Diagram demonstrating timing of experiment. **B,** Images showing transfection efficiency. Scale bar 100μm. **C,** Representative WB showing levels of Gal-3 (31kDa) and β-actin after transfection with different combinations of plasmids. N = 3 for each condition. Overexpression plasmid in red. shRNA knockdown plasmids in green.

3.3 Discussion

The development of this Gal-3 toolkit provided essential experimental reagents for my thesis and Szele laboratory research more broadly. Through the Gal-3 development and floxed animal studies, I also elucidated some interesting findings.

3.3.1 Developmental expression of Gal-3

A search of expression databases demonstrated Gal-3 expression around the lateral ventricles from E15.5 onwards. This result was slightly inconsistent with the literature, which had suggested Gal-3 was not expressed in the CNS until E16.5 (Fowlis et al., 1995). A key rationale for this experiment was, however, to ensure that Gal-3 was expressed in the lateral ventricles at P4, when a number of in vitro experiments were performed. This occurrence appeared correct either way. In mapping the E15.5 expression to neurodevelopment milestones, E15.5 is the commencement of LGE/CGE oligodendrogenesis via Gsh2-expressing OPCs (Kessaris et al., 2006). Had the results in subsequent chapters suggested a role for Gal-3 in adult oligodendrocyte differentiation, it would have been interesting to investigate the embryonic role of Gal-3 and whether it might trigger or facilitate this oligodendrogenesis.

A developmental RT-PCR showed low expression of Gal-3 across brain regions and different ages. This finding was not a huge surprise given previous immunohistochemistry and in situ experiments suggested Gal-3 is selectively expressed by ependymal cells and the SVZ (Comte et al., 2011, and the expression databases described). The SVZ was included in the cortex, striatum, hippocampus and thalamus dissections in these experiments, and any Gal-3 mRNA from the SVZ would have been diluted by other mRNA from surrounding tissue. A similar dilution would have occurred for Gal-3 mRNA from olfactory ensheathing cells due to surrounding OB tissue. A subsequent adult RT-PCR used only SVZ tissue, and verified that Gal-3 expression is much higher there (Section 4.2.10 on p91). An intriguing finding was that Gal-3 expression was lowest in SVZ relevant regions including the cortex, OB

and striatum. It might reflect the reported association of Gal-3 with injury and inflammation (James, 2012; Young et al., 2014). Through being expressed at low levels in normal brain parenchyma, Gal-3 can exert a greater biological effect when it is expressed during injury and inflammation.

The RT-PCR also showed that Gal-3 levels peaked around E18 and P2 both overall and in the cortex, hippocampus, striatum and thalamus. In the cortex, this time period is associated with an influx of microglial cells, which are hypothesised to cull surplus neural precursors (Cunningham et al., 2013; Swinnen et al., 2013). It is likely that these inflammatory cells caused the increased Gal-3 expression, and that a similar process occurred in other brain regions too.

3.3.2 Characterisation of Gal-3 floxed mouse

The floxed mouse characterisation demonstrated that transgene expression was mostly consistent with known Gal-3 expression (Comte et al., 2011, and the expression databases described). As such, it appeared that the transgene is being appropriately expressed by the Gal-3 promoter. Future characterisation will assess the ability to remove the critical exon in the transgene. One experiment involves culturing neurospheres from Gal-$3^{fl/fl}$ mice and nucleofecting dissociated cells with a Cre-recombinase or control plasmid. Gal-3 mRNA and protein levels will be examined with RT-PCR and WB respectively.

The characterisation may also have provided two new findings about Gal-3 expression. Firstly, Gal-3 was expressed by cells within the developing CC. Further co-immunohistochemistry experiments are required to determine the identity and potential roles of these cells. It is also possible that the transgene had off target expression. Secondly, X-gal was most strongly expressed in ependymal cells. While this expression had been shown previously with immunohistochemistry and in situ experiments, the far greater levels compared to the SVZ had not been realised (Comte et al., 2011). Previous dissections for SVZ protein analysis by enzyme linked

immunosorbent assay included the ependymal layer and may need to be reinterpreted with this finding (James, 2012). Future experiments may also consider how ependymal cells contribute to any biological effects in the SVZ.

The floxed mouse provides a novel method to test many experimental hypotheses. In particular, its use with a promoter-specific Cre-recombinase provides spatial control and allows Gal-3 to be knocked out in a select population of cells. Through use with a Cre-recombinase requiring oestrogen receptor ligand binding, the knockout can be temporally controlled.

4

Galectin-3 and its role in inflammation

Contents

4.1 Introduction 66
4.1.1 Relationship of MS with Gal-3 and the SVZ 66
4.1.2 Inflammation in the SVZ 67
4.1.3 Gal-3 interactions with other galectins 68
4.1.4 Research questions 69
4.2 Results 70
4.2.1 Gal-3 expression occurs normally in the human SVZ and increases in the adjacent CC in acute MS plaques 70
4.2.2 Gal-3 expression increases in the mouse CC but decreases in the SVZ after cuprizone treatment 74
4.2.3 Gal-3 expression after cuprizone treatment occurs in GFAP+ astrocytes and CD45+ microglia 76
4.2.4 Gal-3 absence does not alter weight change during cuprizone treatment 79
4.2.5 Haematopoietic cell density follows a similar pattern to Gal-3+ cell density after cuprizone treatment and is not altered by Gal-3 absence 81
4.2.6 CD68-GFP transgenic mice further demonstrate immune cell activation after cuprizone treatment 83
4.2.7 Proliferation also follows a similar pattern to Gal-3+ cell density after cuprizone treatment and is not altered by Gal-3 absence . 84
4.2.8 In vitro proliferation is not altered by Gal-3 absence 87
4.2.9 Reactive astrocytosis increases with cuprizone treatment in the SVZ and CC, and occurs more in the CC in the presence of Gal-3 89
4.2.10 Gal-3 absence is not compensated by other galectins 91
4.3 Discussion 93
4.3.1 Gal-3 presence around the human lateral ventricles 93
4.3.2 Juxtaposition of inflammation in the SVZ and CC after cuprizone treatment 94
4.3.3 Lack of Gal-3 effect on inflammatory cell densities 97
4.3.4 Lack of Gal-3 compensation by other galectins 98
4.3.5 Conclusion 99

4.1 Introduction

Inflammation is a broad term that refers to an immune and vascular response to potentially harmful stimuli. It occurs across species as both a physiologic and pathologic process, and usually involves the extravasation of immune cells into the affected tissue. That extravasation, and the inflammatory response as a whole, are heterogenous to different stimuli. Importantly, it is through inflammation that long-term sequelae of an initial stimulus occur.

The crux of this chapter lies in the convergence of three inflammation concepts. MS and associated animal models are inflammatory disorders with sequelae of demyelination and axon degeneration (see Introduction on p9). Gal-3 is considered a pro-inflammatory molecule with a variety of effects on immune cells (see Introduction on p25). The SVZ has unique inflammatory properties that contribute to its neurogenic potential (Goings et al., 2006, and following subsections). This chapter therefore considers the interaction and overlap of these ideas.

In doing so, Gal-3 fulfils a dual experimental role. It firstly provides a readout of inflammation through its presence in immunohistochemistry experiments; indeed, it was originally thought of as a macrophage marker and was shown to specify a subset of macrophages that phagocytose myelin (Ho and Springer, 1982; Reichert et al., 1994). Secondly, it is a modifiable component of inflammation allowing comparison through Gal-$3^{+/+}$ and Gal-$3^{-/-}$ mice (see Introduction on p25 about its specific roles).

4.1.1 Relationship of MS with Gal-3 and the SVZ

There are some key postmortem studies that link MS with Gal-3 and the SVZ. These studies do not, however, link all three. Stancic et al. (2011) compared control and MS white matter, and showed an increase in Gal-3 mRNA and protein in active plaques. They then used immunohistochemistry to confirm this increase, and demonstrate it occurred in foamy macrophages and hypertrophic astrocytes. They showed that chronic

lesions contain a 'mesh'-like appearance of extracellular Gal-3, which they attributed to astrogliotic scar. They also demonstrated endothelial expression of Gal-3, although it appeared similar in control and MS tissue. As mentioned above, Stancic et al. did not specifically examine Gal-3 in and around the SVZ.

A second postmortem study examined the SVZ in MS. Nait-Oumesmar et al. (2007) showed a two-to-three fold increase in SVZ cell density and proliferation compared to controls. PSA-NCAM+ precursor cells, in particular, were significantly increased in active lesions compared to normal appearing white matter. These precursors were believed to be from the SVZ, and were more common in more proximal lesions to the SVZ. The majority of precursors also expressed Sox9, and some expressed Sox10 and Olig2, which are all markers associated with oligodendrocyte differentiation (see Introduction on p5). These results therefore suggest that SVZ cells can migrate to demyelinated regions in humans and integrate as oligodendrocytes.

In considering these two studies together, active MS lesions feature both increased Gal-3 and more capacity for SVZ cells to integrate as oligodendrocytes. The three have not, however, been examined together.

4.1.2 Inflammation in the SVZ

The SVZ is a unique inflammatory niche. As an example, Goings et al. (2006) reported that SVZ microglia in mice were constitutively active, in contrast to non-activated microglia in the surrounding parenchyma. They hypothesised that SVZ microglia are active to phagocytose the tens of thousands of SVZ cells undergoing apoptosis each day (Lois and Álvarez-Buylla, 1994). Interestingly, when mice underwent cortical aspiration injury, the number of activated microglia increased in the CC and cortex, but remained constant in the SVZ (Goings et al., 2006). If the aspiration included a small part of the SVZ, the number of activated SVZ microglia increased.

The reason that such observations matter is because inflammation can impact on neurogenesis. SVZ co-cultures with microglial cells or microglial conditioned media

reverse the normal decline in the ability of SVZ cultures to produce neuroblasts (Walton et al., 2006). SGZ research has suggested differing responses in acute and chronic inflammation. Acute inflammation with lipopolysaccharide, status epilepticus or irradiation increases microglia yet decreases hippocampal proliferation (Ekdahl et al., 2003; Monje et al., 2003). Chronic inflammation following status epilepticus still increases microglia but, after the initial decrease in proliferation due to acute inflammation, neuroblast formation and the total number of mature neurons return to normal (Bonde et al., 2006). In addition, T-cells are necessary for hippocampal neurogenesis including spatial learning and memory, with T- and B-cell deficient mice experiencing deficits in these areas (Ziv et al., 2006).

Demyelination in the neighbouring CC after cuprizone treatment provides an interesting juxtaposition for the SVZ. The questions arise of whether it experiences increased inflammation like the CC or behaves differently and how that inflammation impacts on proliferation. There is also the question of how Gal-3 impacts on these processes. While Gal-3 is traditionally considered pro-inflammatory and has been shown to increase leucocyte infiltrates in EAE and TMEV (see Introduction on p27), its absence in the normal SVZ causes an inflammatory, reactive astrocytosis (Comte et al., 2011).

4.1.3 Gal-3 interactions with other galectins

The galectin family contains 15 types (see Introduction on p24), and interactions between them are frequently considered. Tsai et al. (2011) demonstrated that Gal-1 and Gal-8 have redundant roles in promoting plasma B-cell formation. Tribulatti et al. (2012) showed that both Gal-1 and Gal-8 have a role in antigen-specific co-stimulation of CD4 T-cells, but Gal-3 antagonises them. Gal-1, Gal-8 and Gal-9 have also been reported in the SVZ previously, and are possible candidates for Gal-3 interaction (Lein et al., 2007; Sakaguchi et al., 2006).

4.1.4 Research questions

Following on from this background, this chapter aimed to answer the following questions:

- Is Gal-3 expressed in proximity to the human SVZ in MS?
- How is inflammation in the SVZ affected by demyelination in the neighbouring CC after cuprizone treatment? What effect does that have on SVZ proliferation?
- Does Gal-3 absence alter inflammation, proliferation or reactive astrocytosis after cuprizone treatment?
- Are there interactions or redundancies between galectins? Do other galectins compensate for Gal-3 absence?

4.2 Results

4.2.1 Gal-3 expression occurs normally in the human SVZ and increases in the adjacent CC in acute MS plaques

To investigate Gal-3 expression in and around the human SVZ, I examined periventricular regions of postmortem tissues. It included both control and MS cases (Table 4.1). As expected, the CC of control tissue demonstrated Gal-3 absence in the parenchyma but presence perivascularly (Figure 4.1A and C). The SVZ also contained Gal-3, which was particularly prominent in the ependymal layer. In MS tissue, Gal-3 expression was increased in and around plaques in the CC (Figure 4.1B and D). The increase was most noticeable perivascularly, where Gal-3+ cells appeared morphologically to be extravasating macrophages. There was an increase throughout the inflamed plaque, with cells appearing as microglia or macrophages. Interestingly, there did not appear to be an increase in SVZ Gal-3 expression unless the SVZ was immediately adjacent to a plaque. The ependymal layer maintained a level of Gal-3 expression in MS cases similar to control cases.

By performing immunohistochemistry on adjacent sections with PLP and CD68 (a macrophage/microglial marker), it was possible to determine Gal-3 expression in particular plaque types (Figure 4.2A; Popescu and Lucchinetti, 2012, for review of histological markers in MS lesion types). Gal-3 was predominantly expressed in hyperacute and acute plaques, where there was a large CD68+ cell infiltrate (Figure 4.2B and C). In chronic plaques, where CD68+ cells formed a clear demarcation of the plaque, Gal-3 also featured at the plaque border and had minimal expression within the plaque (Figure 4.2D). In repaired plaques, where PLP was present but less dense than normal appearing white matter, Gal-3+ cells were present in small quantities throughout the plaque (Figure 4.2E).

	Case #	Age	Gender	PMI	Diagnosis (cause of death)
Controls	C1754	45	M	48	No specific pathology and no evidence of lymphoma (unknown cause of death)
	C3279	50	M	48	None of the features of Alzheimer's disease or any other specific pathology (septicaemia)
	1125/99	27	F	24	Normal brain (sudden death)
	137/05	16	M	72	Normal brain (unknown cause of death but some evidence of oedema)
	1149/00	69	F	96	Normal brain (lung carcinoma)
	1144/94	7	M	72	Normal brain (unknown cause of death but clinical evidence of epilepsy)
	1134/91	21	F	24	Normal brain (acute cardiac failure)
	1105/98	13	M	72	Normal brain (unknown cause of death)
MS cases	B5781	37	F	48	Multiple sclerosis (pulmonary embolism)
	B9860	53	F	24	Multiple sclerosis (cardiac failure)
	B1413	25	F	104	Multiple sclerosis (respiratory arrest)
	B6653	32	M	24	Multiple sclerosis (hypostatic pneumonia)
	B6187	67	F	48	Multiple sclerosis (bronchopneumonia)
	B561	51	F	35	Multiple sclerosis (pulmonary embolism)
	B133	39	M	70	Multiple sclerosis (pneumonia)
	B520	51	M	24	Multiple sclerosis (septicaemia)

Table 4.1: **Human control and MS cases.**

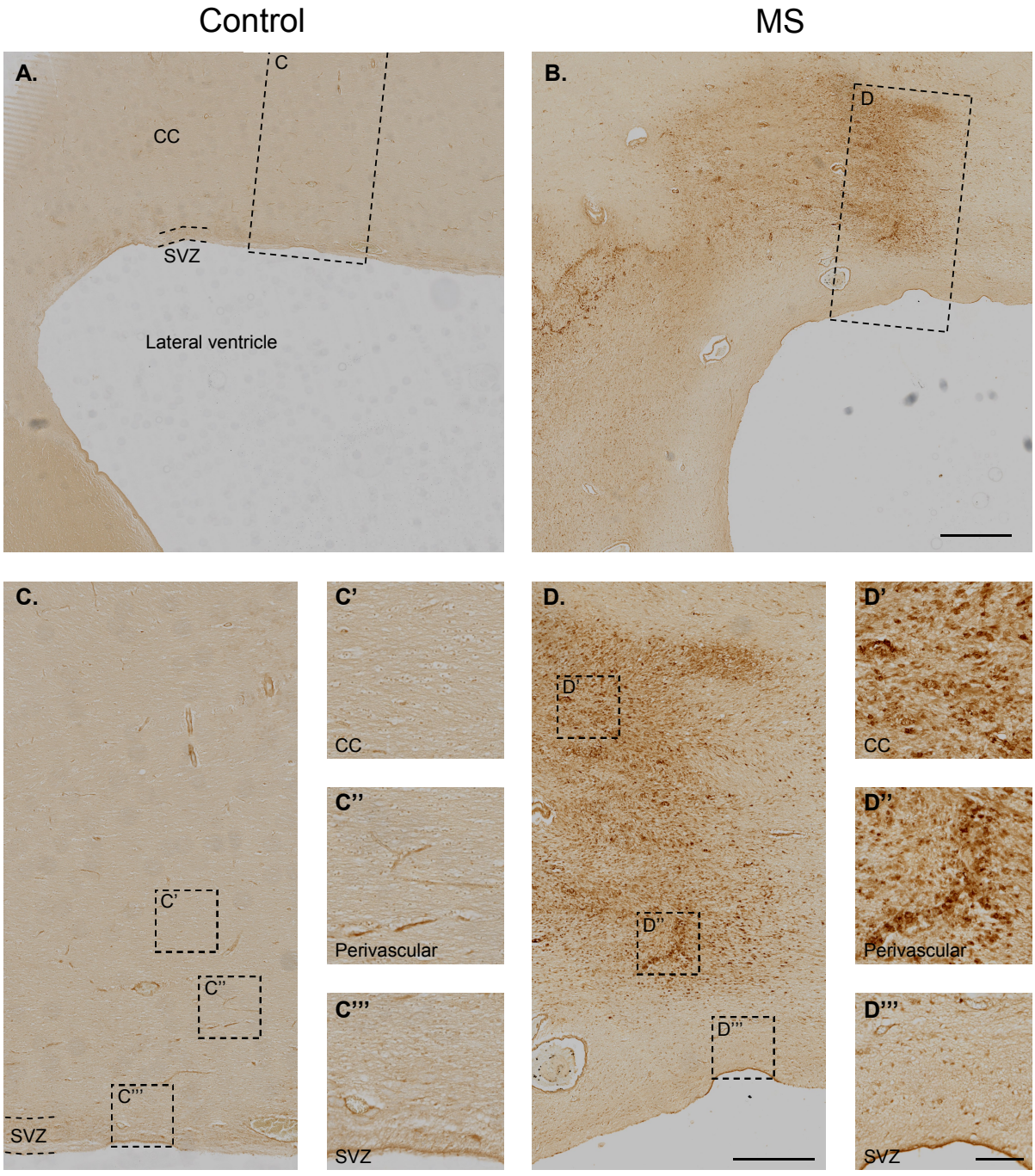


Figure 4.1: **Gal-3 expression occurs normally in the SVZ and increases in the adjacent CC after MS. A and B,** Representative, low magnification images demonstrating differences in Gal-3 immunohistochemistry between control (A) and MS (B) sections. Scale bar 1mm. **C and D,** Medium and high magnification images of Gal-3 immunohistochemistry. Scale bars 500μm (C and D) and 100μm (C′-D‴). Dotted boxes show magnified regions. Dotted parallel lines show representative SVZ.

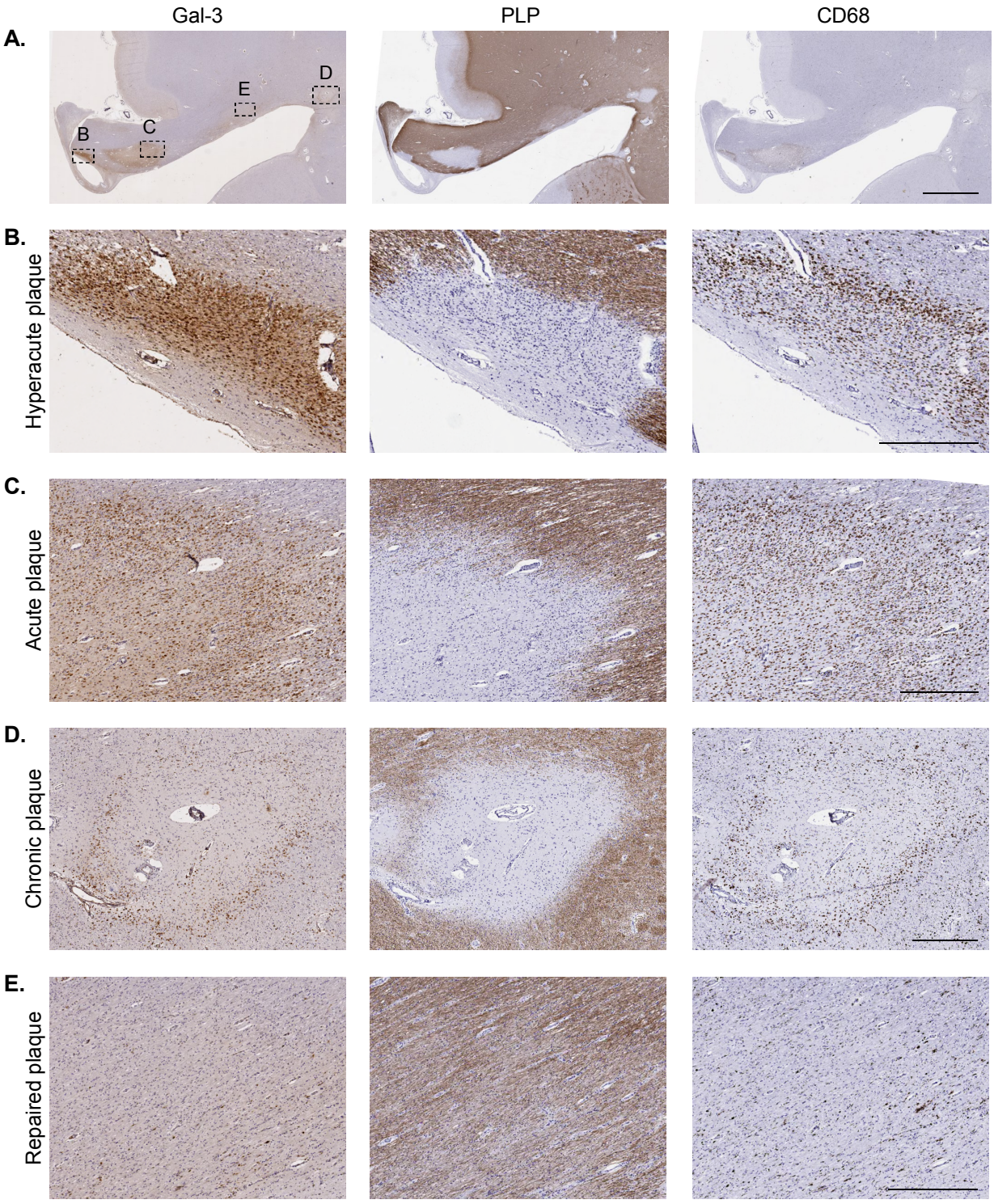


Figure 4.2: **Gal-3 is expressed predominantly in hyperacute and acute MS lesions. A,** Low magnification images of Gal-3, PLP and CD68 immunohistochemistry demonstrating different MS plaques within the same CC. Dotted boxes show magnified regions. Scale bar 5mm. **B to E,** Medium magnification images of Gal-3, PLP and CD68 immunohistochemistry in hyperacute (B), acute (C), chronic (D) and repaired (E) plaques. Scale bars 500μm.

4.2.2 Gal-3 expression increases in the mouse CC but decreases in the SVZ after cuprizone treatment

To further elucidate the presence and role of Gal-3 in the SVZ after demyelination, I used the murine cuprizone demyelination model. Cuprizone was administered ad libitum in chow to Gal-$3^{+/+}$ and Gal-$3^{-/-}$ mice for 3 weeks or 6 weeks to cause demyelination, or 6 weeks followed by 10 days of control chow to cause remyelination (Figure 4.3A; rationale for treatment lengths and cuprizone dilution provided in Methods on p32).

Initially I performed immunohistochemistry to examine Gal-3 expression in the SVZ and CC of Gal-$3^{+/+}$ mice (Figure 4.3B; N = 4 for each group). There were two Gal-3 antibodies that I used: a rat monoclonal antibody and rabbit polyclonal antibody (Table 2.2 on p34). The rat antibody contained less non-specific labelling than the rabbit antibody and was therefore used for comparisons of Gal-3+ cells. The rabbit antibody was used in co-immunohistochemistry experiments that included another antibody raised in rat. A macro was developed and used for these experiments to allow the SVZ or CC to be selected by DAPI immunohistochemistry alone (see Methods on p37). It therefore avoided bias from knowing the density of Gal-3+ cells in the other region.

Control mice contained 2831.39 ± 230.50 Gal-3+ cells/mm^2 in the SVZ yet only 18.13 ± 7.40 cells/mm^2 in the CC (Figure 4.3C, D and E). This finding was consistent with previous Szele laboratory results (Comte et al., 2011). After cuprizone administration, the density of Gal-3+ cells in the SVZ decreased greatly ($F(3,12) = 13.198$, $p < 0.0005$ for one-way ANOVA; 1441.82 ± 255.34 cells/mm^2 for 3-week cuprizone, $p = 0.009$ compared to control; 733.53 ± 250.82 cells/mm^2 for 6-week cuprizone, $p < 0.0005$ compared to control). The density then increased in the remyelination treatment group (1882.54 ± 228.77 cells/mm^2, $p = 0.034$ compared to 6-week cuprizone). The opposite occurred in the CC with the density increasing after demyelination ($F(3,12) = 16.904$, $p < 0.0005$ for one-way ANOVA; 117.87 ± 33.52

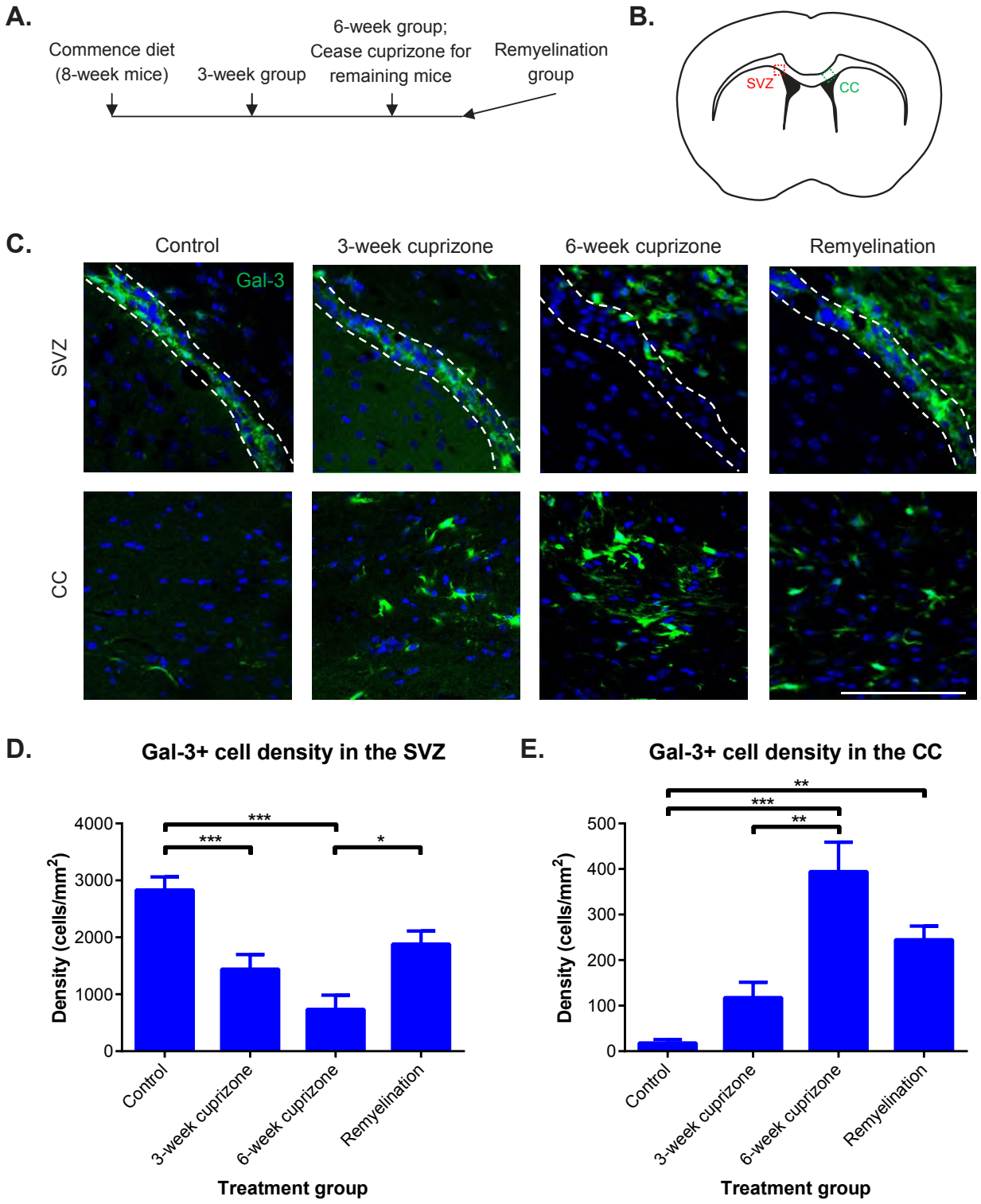


Figure 4.3: **Gal-3 expression increases in the CC but decreases in the SVZ after cuprizone treatment. A,** Schematic showing cuprizone regimen. **B,** Diagram demonstrating regions analysed from the SVZ and CC. **C,** Representative images of Gal-3+ cells in the SVZ and CC after cuprizone treatment. Scale bar 100μm. White dotted lines define SVZ boundaries. **D and E,** Graphs demonstrating the density of Gal-3+ cells in the SVZ (D) and CC (E). Statistics calculated as one-way ANOVA with N = 4. Graphs show mean ± SEM. *p $\leq$ 0.05, **p $\leq$ 0.01, ***p $\leq$ 0.001.

cells/mm^2 for 3-week cuprizone, p = 0.601 compared to control; 394.40 ± 64.70 cells/mm^2 for 6-week cuprizone, p < 0.0005 compared to control and p = 0.002 compared to 3-week cuprizone) before decreasing with remyelination (244.80 ± 30.07 cells/mm^2, p = 0.010 compared to control and p = 0.122 compared to 6-week cuprizone).

The LacZ construct in the Gal-3^{fl} allele was used to verify these results. It showed a clear increase in the CC between control and 6-week cuprizone Gal-3$^{fl/+}$ mice (Figure 4.4; N = 3 for each group). The ependymal layer exhibited strong X-gal immunohistochemistry in both control and 6-week cuprizone mice, and it was not possible to discern any difference in the SVZ.

4.2.3 Gal-3 expression after cuprizone treatment occurs in GFAP+ astrocytes and CD45+ microglia

Having established the altering densities of Gal-3, I wanted to determine which cells expressed Gal-3. I therefore performed co-immunohistochemistry of Gal-3 with GFAP (astrocytes and neural stem cells), Mash1 (transit amplifying progenitors), Dcx (neuroblasts), Olig2 (oligodendrocytes) and CD45/Iba1 (activated microglia). SVZ samples were analysed qualitatively, while CC samples were analysed quantitatively (N ≥ 4 for each treatment group for each co-localisation).

The majority of Gal-3+ cells in both locations were either GFAP+ astrocytes or CD45+ microglia (Figure 4.5A). In the CC, ∼30% of astrocytes were Gal-3+ at any stage (Figure 4.5B; F(3,12) = 0.563, p = 0.649 for one-way ANOVA). The percentage of CD45+/Iba1+ microglia that were Gal-3+ increased as demyelination then remyelination occurred (Figure 4.5C; F(3,24) = 71.875, p < 0.0005 for one-way ANOVA; pairwise comparisons shown in graph). Interestingly, when reversing these percentages to obtain the percentage of Gal-3+ cells that were GFAP+ or CD45+, the aggregates were close to 100% (Figure 4.5D; the aggregates were not necessarily 100% because the co-localisation experiments were conducted separately; CD45

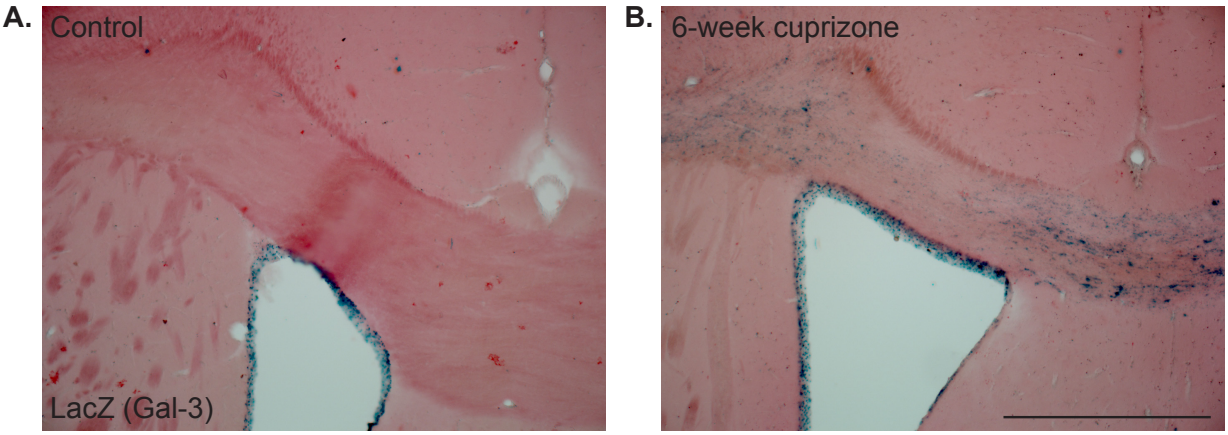


Figure 4.4: **LacZ expression increases in the CC of Gal-3$^{fl/+}$ mice after cuprizone treatment. A and B,** X-gal immunohistochemistry of the dorsolateral SVZ and surrounding CC in control (A) and 6-week cuprizone (B) mice. Scale bar 500μm.

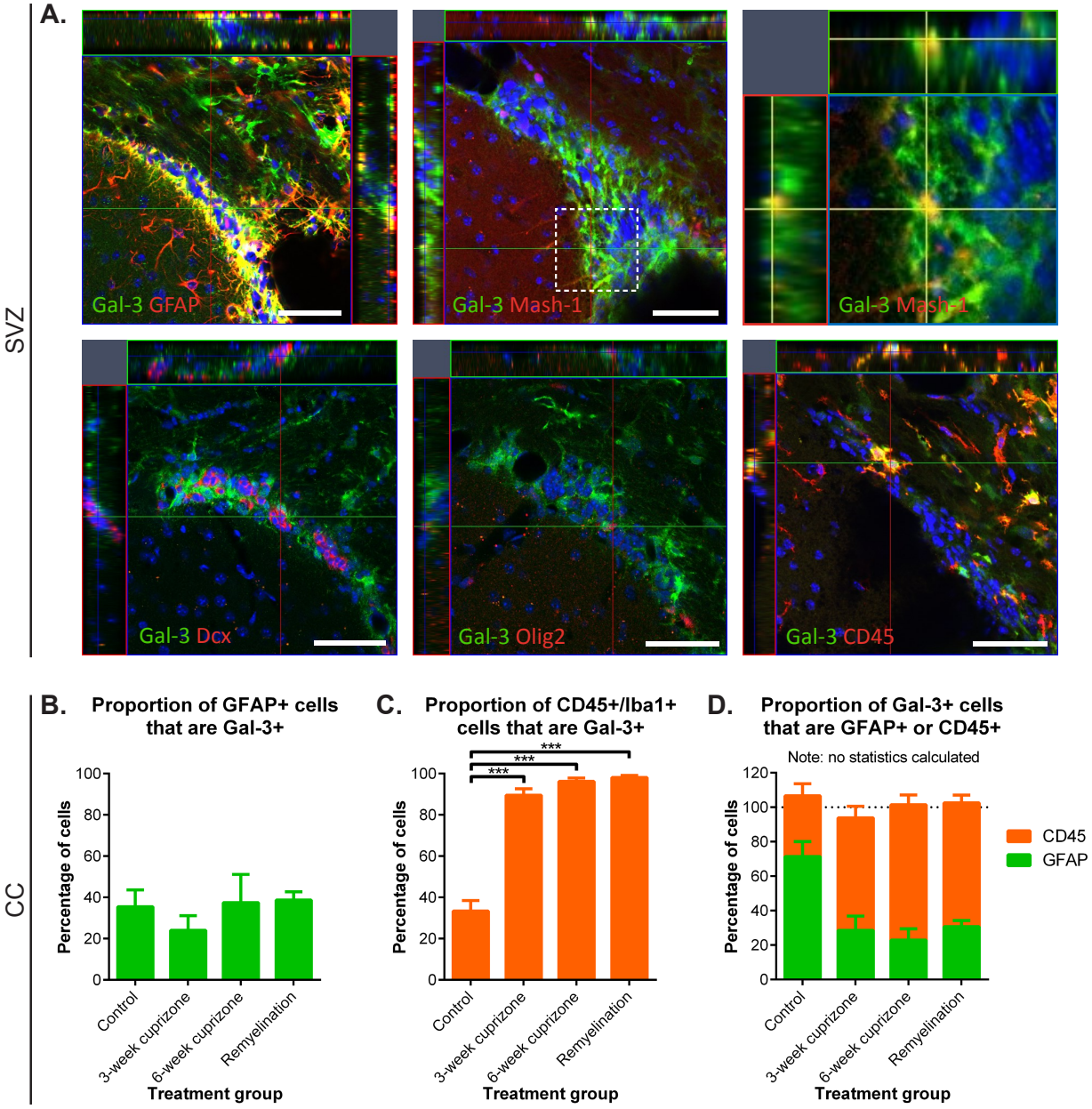


Figure 4.5: **Gal-3 expression after cuprizone treatment occurs in GFAP+ astrocytes and CD45+ microglia.** **A,** Representative images of the SVZ showing Gal-3 co-localisation with GFAP+ astrocytes/neural stem cells, Mash-1+ transit amplifying progenitors and CD45+ haematopoietic cells (which incorporates CD45+/Iba1+ microglia), and lack of Gal-3 co-localisation with Dcx+ neuroblasts and Olig2+ oligodendrocytes. Dotted box shows magnified region. Scale bars 50μm. **B to D,** Graphs showing quantification of co-localisation in the CC. Statistics calculated as one-way ANOVA with N $\geq$ 4 for B and C. No statistics performed for D. Graphs show mean $\pm$ SEM. ***p $\leq$ 0.001. Note that GFAP+ and CD45+ cells were quantified in different experiments, so aggregates in D will not necessarily equal 100%.

immunohistochemistry without Iba1 marked all haematopoietic cells, although the vast majority would have been activated microglia as shown in Section 4.2.5 on p81).

With the other markers, the occasional Mash-1+ transit amplifying progenitor in the SVZ was Gal-3+. There were, however, only four Mash-1+ cells in the CC and one of them was Gal-3+. Dcx+ neuroblasts did not co-express Gal-3 in either location (out of 337 Gal-3+ and 42 Dcx+ cells in the CC, only one was co-labelled). Olig2+ oligodendrocytes similarly did not co-express Gal-3 in either location (out of 337 Gal-3+ and 436 Olig2+ cells in the CC, only two were co-labelled).

4.2.4 Gal-3 absence does not alter weight change during cuprizone treatment

In administering cuprizone to Gal-$3^{+/+}$ and Gal-$3^{-/-}$ mice, I was required to weigh them weekly to assess their welfare. These measurements also provided information to detect clinical differences between genotypes and to assess differences in oral intake. The latter was an important point given that cuprizone was administered in chow and the experimental comparison of genotypes assumed equal doses.

Control mice from both genotypes demonstrated a steady increase in weight of just more than 2% per week (Figure 4.6). Cuprizone treated mice from both genotypes experienced a sharp decrease in weight over the first week before the weight loss plateaued and they steadily regained weight. When remyelination mice were returned to control chow, they experienced a sudden weight gain and approached the weights of control mice.

Equivalence between genotypes was assessed through t-tests and 90% confidence intervals as described by GraphPad Software (2015). The t-tests revealed a significant difference between genotypes in control mice after 2 weeks ($p = 0.018$). Cuprizone treated mice had no significant differences and were therefore considered equivalent based on the t-tests. In examining the confidence intervals of differences in cuprizone treated mice, the largest mean difference was 1.291% after 3 weeks and the largest 90%

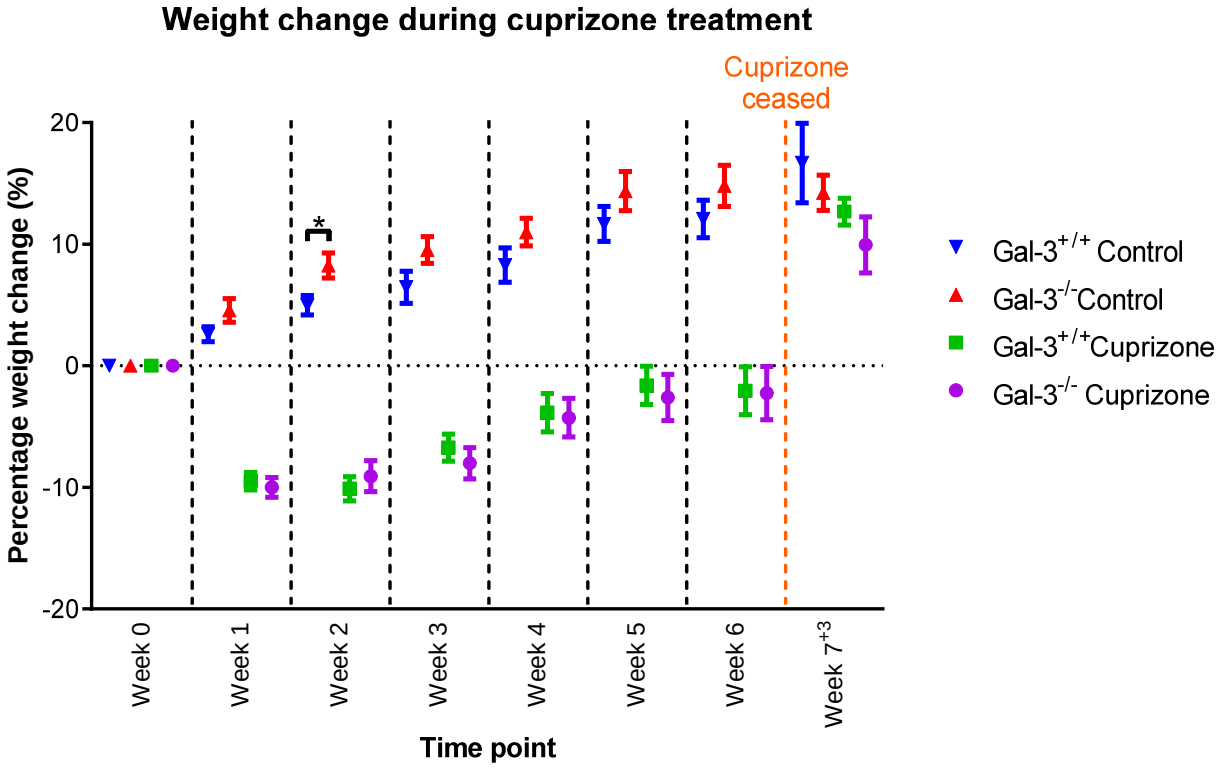


Figure 4.6: **Gal-3 absence does not alter weight change during cuprizone treatment.** Graph demonstrating weight change during cuprizone treatment. Statistics calculated as t-tests comparing Gal-$3^{+/+}$ and Gal-$3^{-/-}$ mice for each treatment and time point. N $\geq$ 8 for each treatment and time point, excluding control mice at Week 7^{+3} for which N = 3. Graph shows mean $\pm$ SEM. *p $\leq$ 0.05.

confidence interval was 5.160% after 6 weeks. These figures were considered within acceptable limits and the genotypes were considered equivalent based on confidence intervals too. The significant difference that occurred between control mice was considered to have happened by chance.

Two cuprizone treated mice exceeded the severity limit of 20% weight loss and were sacrificed during treatment. One was a Gal-$3^{+/+}$ mouse that exceeded the limit after eleven days. The other was a Gal-$3^{-/-}$ mouse that exceeded the limit after nine days.

4.2.5 Haematopoietic cell density follows a similar pattern to Gal-3+ cell density after cuprizone treatment and is not altered by Gal-3 absence

The next step was to evaluate what happens to inflammatory cells in the SVZ and CC after cuprizone treatment, and whether Gal-3 influences any changes. I therefore co-immunolabelled Gal-$3^{+/+}$ and Gal-$3^{-/-}$ cuprizone treated brains with anti-CD45 and Iba1 antibodies. CD45 identifies all haematopoietic cells, while Iba1 is specific to activated microglia (Ito et al., 1998; Ohsawa et al., 2004; Trowbridge and Thomas, 1994).

The changes in the density of CD45+ cells were similar to Gal-3+ cells: it decreased in the SVZ with demyelination yet increased in the CC (Figure 4.7A and B; $N \geq 5$). These differences were confirmed by a two-way ANOVA, which revealed a significant main effect for treatment group in both conditions ($F(3,46) = 4.229$, $p = 0.010$ for SVZ; $F(3,46) = 12.669$, $p < 0.0005$ for CC). In the SVZ, the comparisons that achieved significance were between control and 3-week cuprizone ($p = 0.030$), and control and 6-week cuprizone ($p = 0.046$) treatment groups. In the CC, they were between control and 6-week cuprizone ($p < 0.0005$), control and remyelination ($p < 0.0005$), 3-week cuprizone and 6-week cuprizone ($p = 0.027$), and 3-week cuprizone and remyelination ($p = 0.002$) treatment groups.

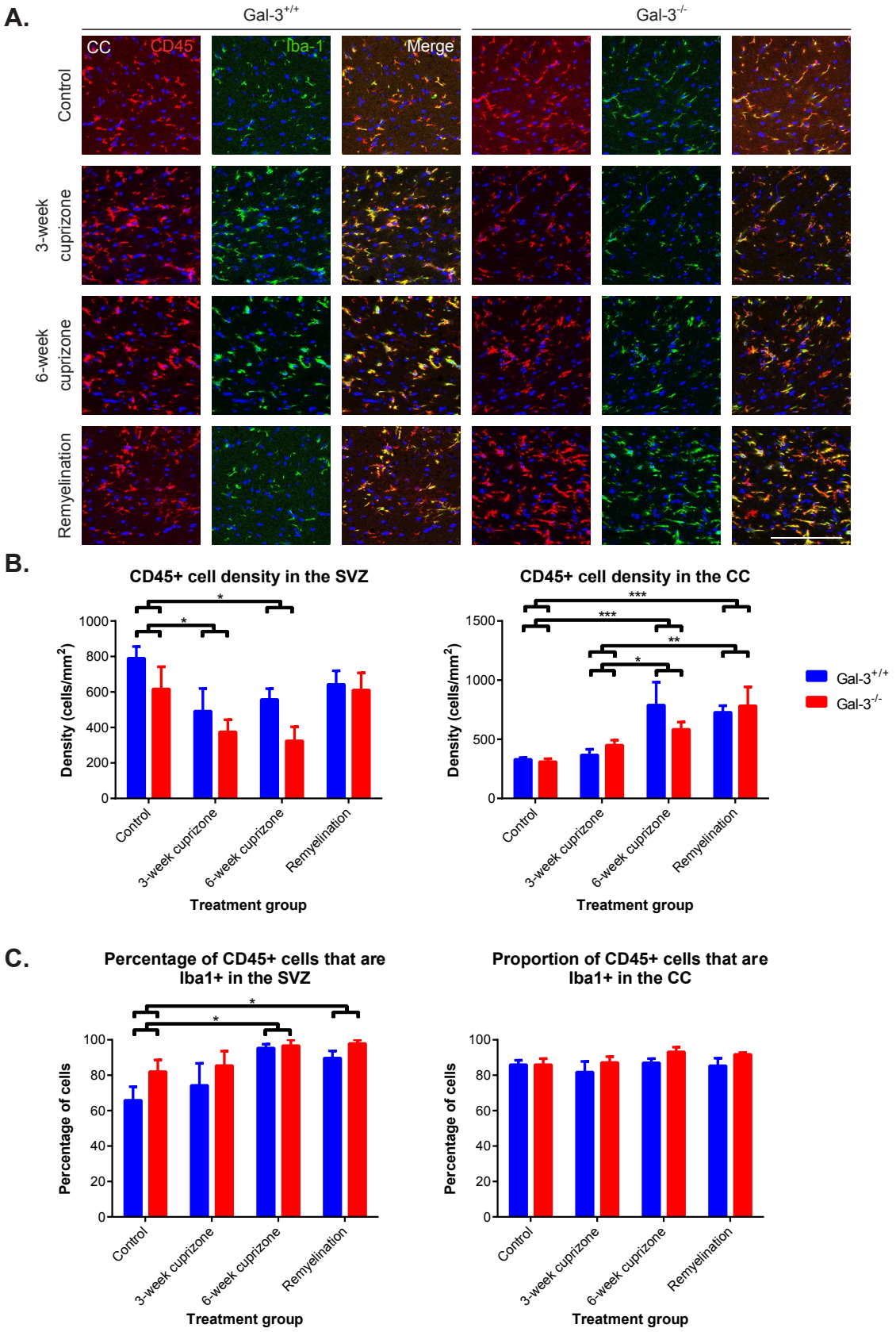


Figure 4.7: **CD45+ cell density follows a similar pattern to Gal-3+ cell density after cuprizone treatment and is not altered by Gal-3 absence. A,** Representative images of CD45 and Iba1 immunohistochemistry in the CC. Scale bar 100μm. **B,** Graphs demonstrating the density of CD45+ cells in the SVZ and CC. **C,** Graphs demonstrating the proportion of CD45+ cells that are Iba1+ in the SVZ and CC. Statistics calculated as two-way ANOVA with N $\geq$ 5. Graphs show mean $\pm$ SEM. *p $\leq$ 0.05, **p $\leq$ 0.01, ***p $\leq$ 0.001.

While there was a trend for Gal-$3^{+/+}$ mice to have more CD45+ cells in the SVZ than Gal-$3^{-/-}$ mice, it was not significant ($F(1,46) = 4.013$, $p = 0.051$ for main effect; $F(3,46) = 0.358$, $p = 0.784$ for interaction with treatment groups). The CC showed no consistent effect for Gal-$3^{+/+}$ compared to Gal-$3^{-/-}$ mice ($F(1,46) = 0.129$, $p = 0.721$ for main effect; $F(3,46) = 0.957$, $p = 0.421$ for interaction with treatment groups).

The large proportion of CD45+ cells that were Iba1+ suggested that the majority were activated microglia: over 60% in each treatment group in the SVZ and over 80% in the CC (Figure 4.7C). As the treatment lengthened, the proportion of CD45+ cells in the SVZ that were Iba1+ increased ($F(3,46) = 4.660$, $p = 0.006$ for main effect). This effect achieved significance between control and 6-week cuprizone ($p = 0.019$), and control and remyelination ($p = 0.035$) treatment groups. Therefore, while the number of CD45+ cells in the SVZ decreased, a greater proportion were activated microglia. The CC did not exhibit a significant difference between treatment groups in the proportion of CD45+ cells that were Iba1+ ($F(3,46) = 0.965$, $p = 0.417$ for main effect; $F(3,46) = 0.473$, $p = 0.702$ for interaction with genotype).

There was also a trend for Gal-$3^{+/+}$ mice to have fewer CD45+ cells that were Iba1+ than Gal-$3^{-/-}$ mice. This trend was, however, not significant ($F(1,46) = 3.139$, $p = 0.083$ for main effect; $F(3,46) = 0.381$, $p = 0.767$ for interaction with treatment groups). The CC exhibited a trend too with Gal-$3^{+/+}$ mice having a smaller proportion of CD45+ cells that were Iba1+. It was not significant as well ($F(1,46) = 3.249$, $p = 0.078$ for main effect; interaction with treatment group as above).

4.2.6 CD68-GFP transgenic mice further demonstrate immune cell activation after cuprizone treatment

In order to further describe inflammation after cuprizone treatment, I used a CD68-GFP transgenic mouse that had recently been developed by the Greaves laboratory (Iqbal et al., 2014). CD68 is expressed only by monocytes and macrophages, although its exact role is unknown (Hume et al., 2010). This mouse therefore

fluorescently labels these cells and allows observation of inflammation in multiple brain regions after cuprizone treatment. This experiment was also the first neurologic experiment in these mice, and an aim was to see if microglia expressed CD68-GFP.

After treating CD68-GFP mice with cuprizone or control chow for 6-weeks, I was able to compare endogenous GFP in similar brain regions (Figure 4.8A to D; N = 3). Control brains contained GFP+ cells in multiple regions including the external plexiform layer, RMS, SVZ and CC. The density of these cells was quite low and they often occurred in isolation. Cuprizone brains demonstrated a large increase in GFP+ cells in the OB especially the granular layer, RMS, and CC including the caudal CC adjacent to the hippocampus.

Given the existence of GFP+ cells in controls and my result that most haematopoietic cells were microglia, it seemed likely that this transgene labelled microglia. I did, however, verify this result through co-immunohistochemistry with CD45 and Iba1. While the majority of CD68+ cells were CD45+/Iba1+ and vice-versa, I was surprised to find a mismatch of immunohistochemistry in the SVZ: Iba1+/CD68- cells existed in control SVZ, yet Iba1-/CD68+ cells existed in 6-week cuprizone SVZ (Figure 4.8E). It had previously been noted that the GFP transgene did not overlap entirely with macrophage markers F4/80 and mCd68 in lung, liver and peritoneal lavage. This discrepancy was therefore not investigated further at this stage.

4.2.7 Proliferation also follows a similar pattern to Gal-3+ cell density after cuprizone treatment and is not altered by Gal-3 absence

Due to the reported impact of inflammation on proliferation (see Section 4.1.2 on p67), I next wanted to investigate proliferation after cuprizone treatment. To do so, I performed immunohistochemistry with an anti-PHi3 antibody, which labels cells during M phase (Shibata and Ajiro, 1993). I then counted the number of PHi3+ cells in four SVZ and two CC regions (Figure 4.9A). These regional results, together with a repeated

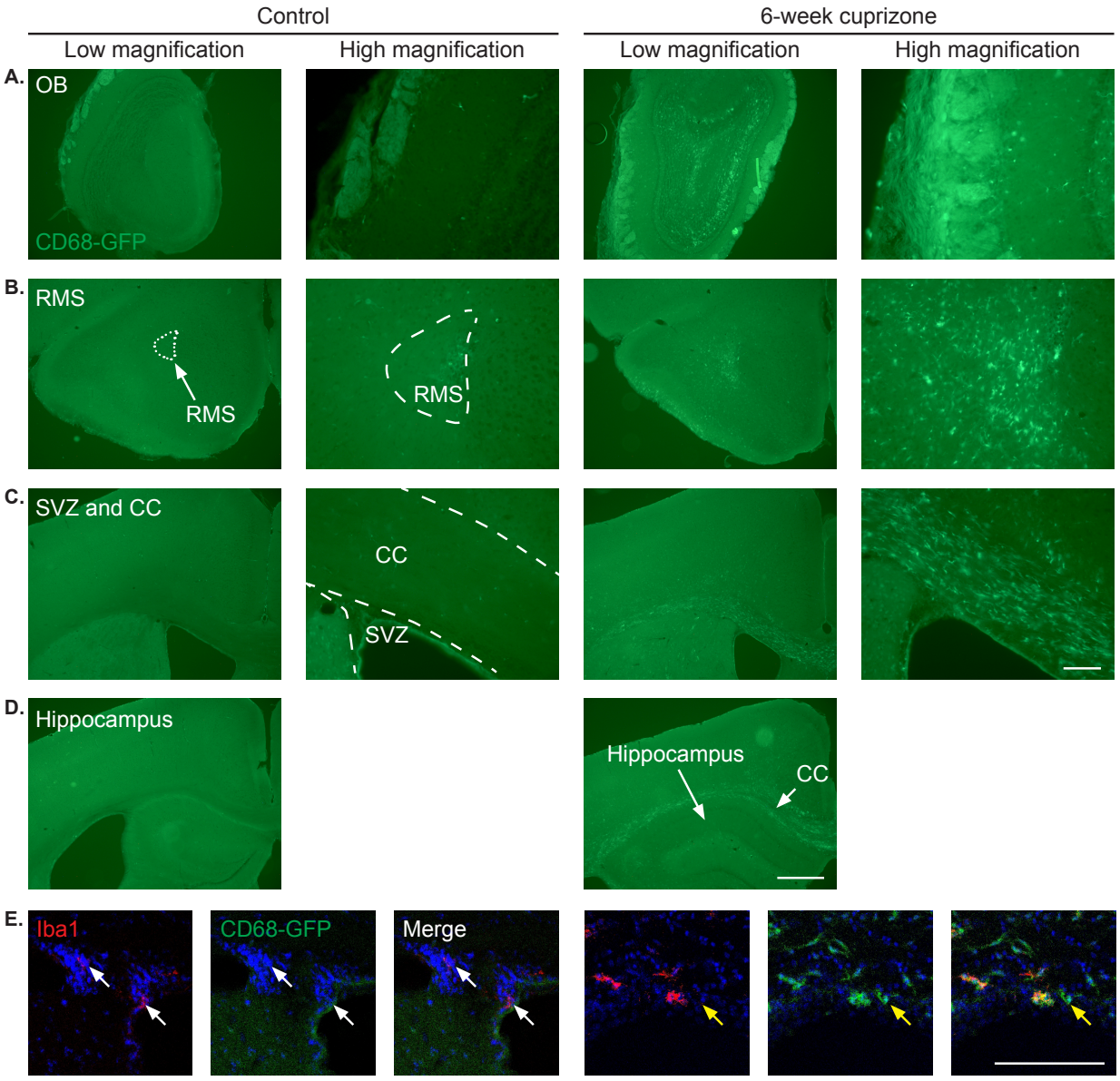


Figure 4.8: **CD68-GFP transgenic mice further demonstrate immune cell activation after cuprizone treatment. A to D,** Representative images of the OB (A), RMS (B), SVZ (C) and hippocampus (D). Annotations provide anatomical orientation. For OB anatomical information, please refer to Figure 5.6 on p116. **E,** Images demonstrating Iba1+/GFP- cells (white arrows) in the SVZ of control mice and Iba1-/GFP+ cells (yellow arrows) in the SVZ of 6-week cuprizone mice. Scale bars 500μm (low magnification) and 100μm (high magnification and co-immunohistochemistry).

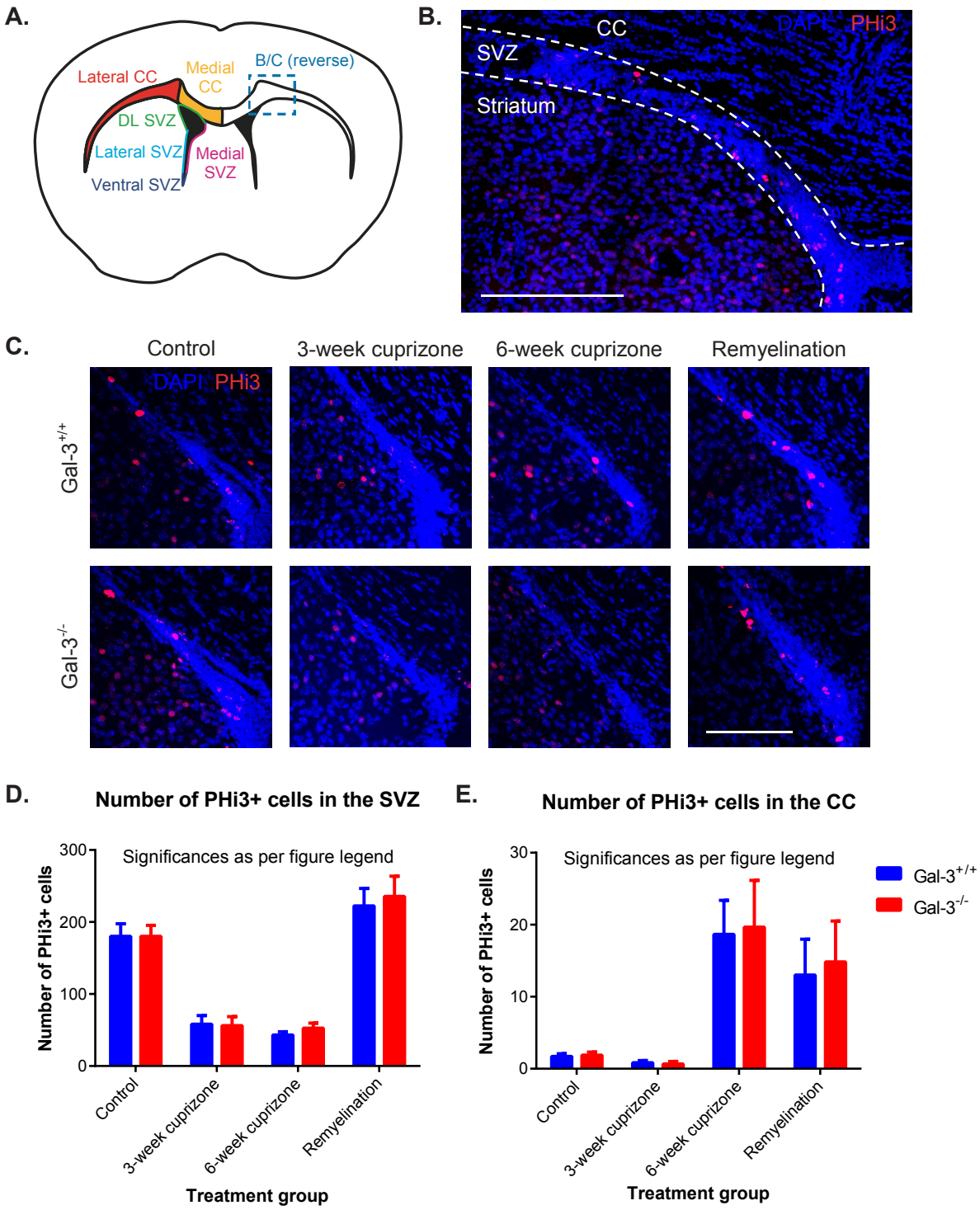


Figure 4.9: **Proliferation follows a similar pattern to Gal-3+ cell density after cuprizone treatment and is not altered by Gal-3 absence. A,** Diagram showing coronal brain regions examined in the SVZ and CC. DL: dorsolateral. **B,** Low magnification image demonstrating PHi3 immunohistochemistry throughout the dorsolateral SVZ in a Gal-$3^{+/+}$ mouse treated with control chow. The striatum contained non-specific background staining, which was not evident in the SVZ or CC. Scale bar 200μm. **C,** Higher magnification images of a portion of the dorsolateral SVZ comparing PHi3+ cells in Gal-$3^{+/+}$ and Gal-$3^{-/-}$ mice across treatment groups. Scale bar 100μm. **D and E,** Quantification of PHi3+ cells in the SVZ (D) and CC (E). Significant differences from repeated measures ANOVA are not displayed on graphs due to complexity, and can instead be found in Appendix C.1 on p205. N $\geq$ 6. Graphs show mean $\pm$ SEM.

measures ANOVA, are detailed in Appendix C.1 on p205.

In the SVZ, the trend of PHi3+ cells was consistent in the four regions, with the number of cells decreasing during demyelination then recovering with remyelination (aggregate values in Figure 4.9B to D; regional values in Table C.1 on p205; $N \geq 5$). These differences were highly significant across regions between most combinations of treatment groups ($p \leq 0.008$ when significant; Table C.4 on p207). The exceptions occurred between 3-week cuprizone and 6-week cuprizone treatment groups in all regions, and between control and remyelination treatment groups in the striatal and ventral SVZ ($p = 1.000$ for each of these comparisons). There were no significant differences involving genotypes (Table C.3 on p206).

In the CC, there was a trend for PHi3+ cells to increase in the 6-week cuprizone treatment group and decrease only slightly in the remyelination treatment group (Figure 4.9E). Interestingly, this effect occurred in the lateral CC with the number of PHi3+ cells in the medial CC remaining close to zero in all groups (Table C.1). There was significance in the lateral CC for differences between all combinations of control or 3-week cuprizone, and 6-week cuprizone or remyelination mice ($p \leq 0.002$ for each comparison; Table C.5 on p208). Similar to the SVZ, there were no significant differences involving genotypes (Table C.3).

4.2.8 In vitro proliferation is not altered by Gal-3 absence

To verify the in vivo lack of difference between Gal-$3^{+/+}$ and Gal-$3^{-/-}$ mice, I also investigated the in vitro effect of Gal-3 absence. I cultured primary SVZ neurospheres that were seeded at clonal density of 10,000 cells per well (Figure 4.10A). After seven days, I counted the number and measured the diameter of neurospheres larger than 50μm (Figure 4.10B). I then passaged the neurospheres, seeded secondary neurospheres at 1,000 cells per well, and analysed these neurospheres the same way.

There were no significant differences between genotypes. The number of neurospheres was consistent between genotypes for primary neurospheres (291.20 ± 26.92, $N = 5$

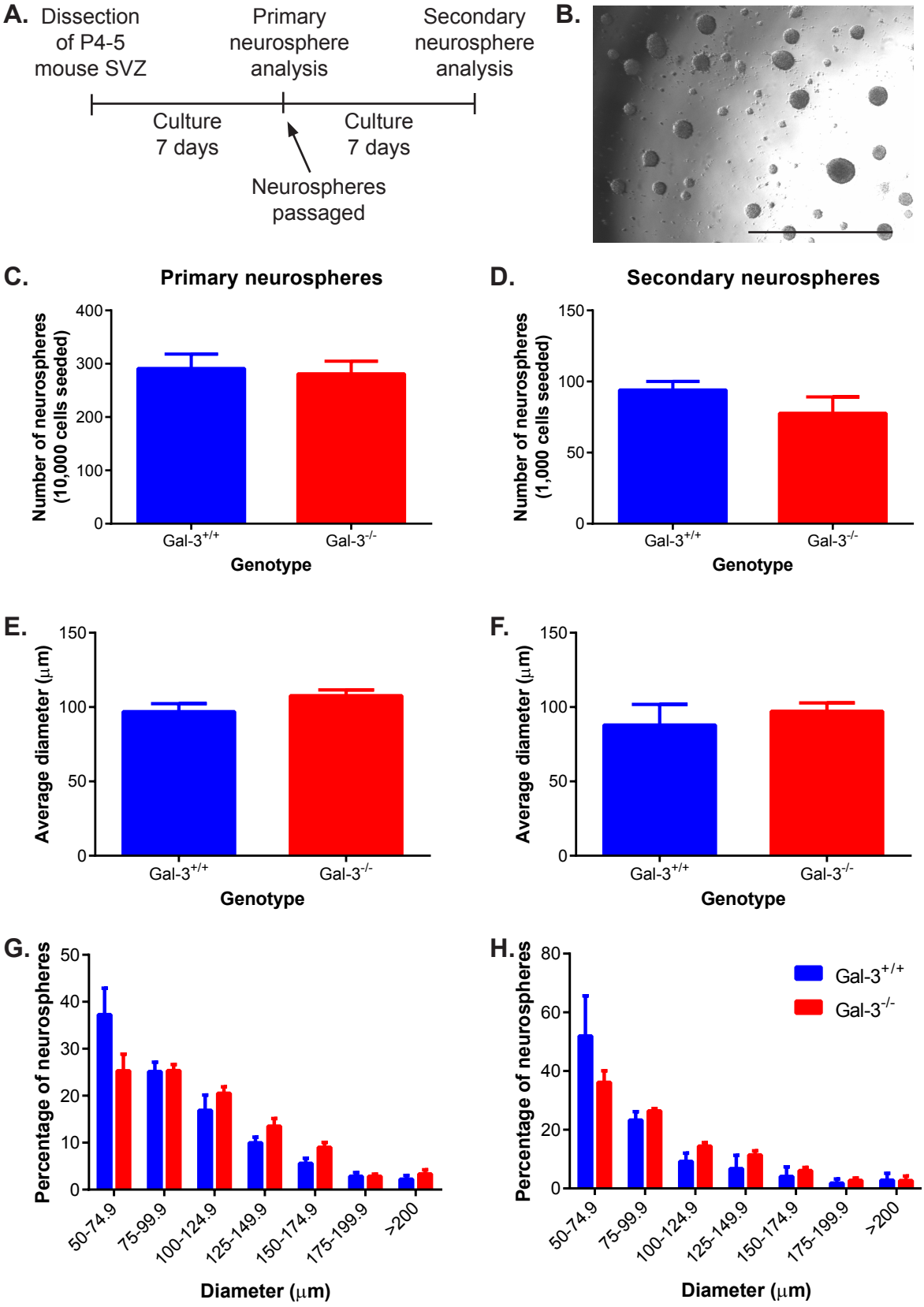


Figure 4.10: **In vitro proliferation is not altered by Gal-3 absence. A,** Diagram showing experimental protocol. **B,** Sample image of primary neurospheres. Scale bar 1mm. **C to H,** Graphs comparing Gal-$3^{+/+}$ and Gal-$3^{-/-}$ mice for number of neurospheres (C and D), average diameter (E and F) and profile of neurosphere sizes (G and H) for primary (C, E and G) and secondary (D, F and H) neurospheres. Statistics performed using t-tests with N = 5 for all groups except Gal-$3^{+/+}$ secondary neurospheres for which N = 3. Graphs show mean ± SEM.

for Gal-$3^{+/+}$ vs 281.20 ± 23.76, N = 5 for Gal-$3^{-/-}$; p = 0.788; Figure 4.10C) and secondary neurospheres (94.00 ± 6.08, N = 3 vs 77.67 ± 11.50, N = 5; p = 0.346; Figure 4.10D). The average diameter was consistent between genotypes for primary neurospheres (96.96 ± 5.35μm vs 107.66 ± 3.86μm; p = 0.143; Figure 4.10E) and secondary neurospheres (87.89 ± 13.91μm vs 97.13 ± 5.66μm; p = 0.493; Figure 4.10F). The profile of neurosphere sizes was consistent between genotypes for primary and secondary neurospheres (p > 0.05 for each comparison; Figure 4.10G and H).

4.2.9 Reactive astrocytosis increases with cuprizone treatment in the SVZ and CC, and occurs more in the CC in the presence of Gal-3

Inflammation also manifests in the brain through activation of astrocytes. Reactive astrocytosis, as this process is known, involves an increase in GFAP production and thickening of astrocytic processes (Middeldorp and Hol, 2011). To analyse it in the cuprizone brains, two blinded laboratory members independently scored SVZ and CC images of GFAP immunohistochemistry between 0-10 (Figure 4.11A and B). The criteria included brightness and quantity of fluorescence, and thickness of processes.

Interestingly, and contrary to published literature, there was more reactive astrocytosis in Gal-$3^{+/+}$ compared to Gal-$3^{-/-}$ mice in the CC (Figure 4.11C; $F(1,47) = 4.340$, $p = 0.043$ for main effect; Comte et al., 2011). In the SVZ, there was a similar, albeit non-significant, trend ($F(1,47) = 2.402$, $p = 0.128$ for main effect; $F(3,47) = 0.070$, $p = 0.976$ for interaction with treatment group).

There were also significant differences between treatment groups, with reactive astrocytosis increasing for longer treatment periods ($F(3,47) = 12.599$, $p < 0.0005$ for main effect in the SVZ; $F(3,47) = 36.694$, $p < 0.0005$ for main effect in the CC). In the SVZ, this effect was significant between control and 3-week cuprizone ($p = 0.048$), 6-week cuprizone ($p < 0.0005$) and remyelination ($p < 0.0005$) treatment groups. In the CC, this effect was significant for all treatment group combinations ($p < 0.002$)

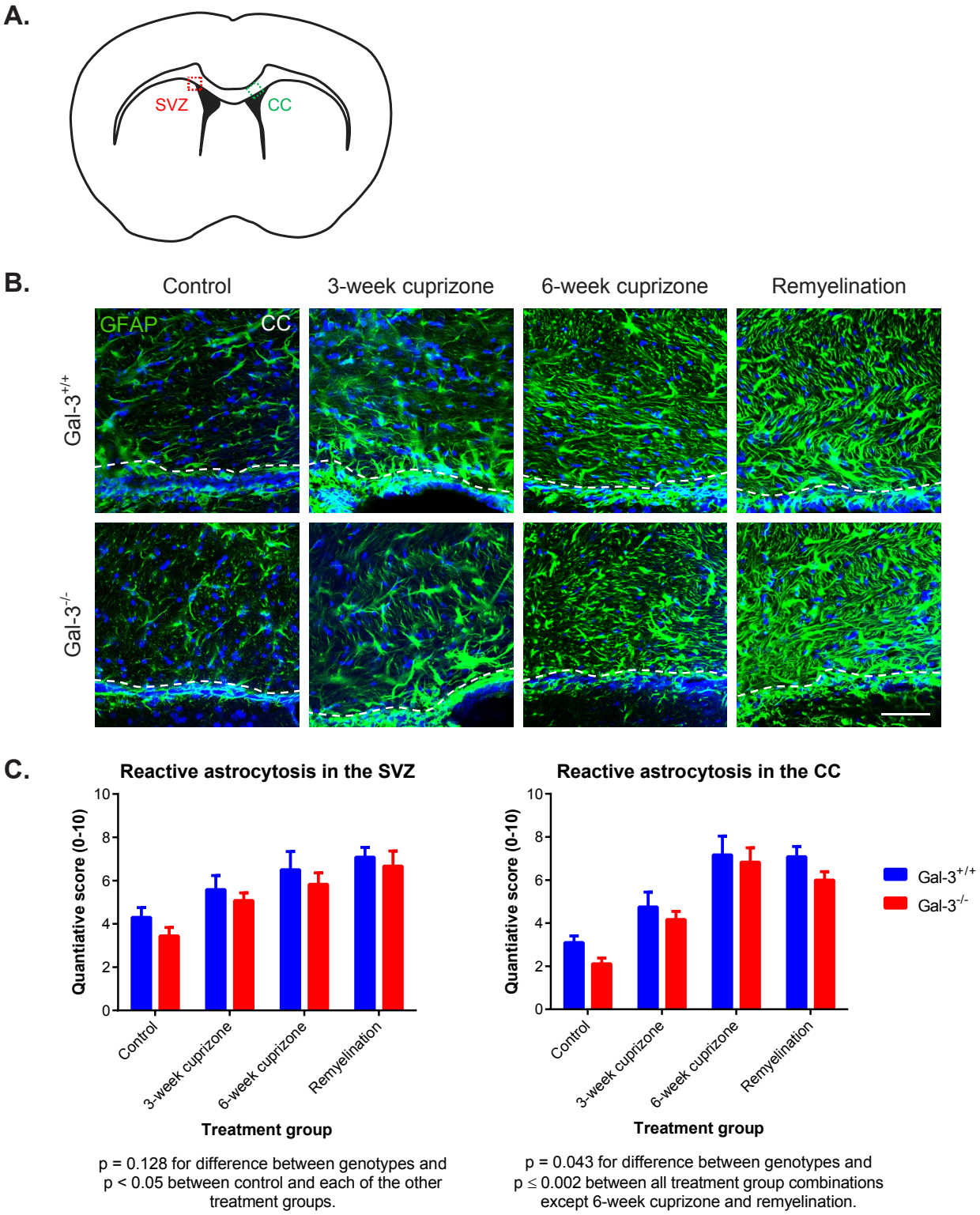


Figure 4.11: **Reactive astrocytosis increases with cuprizone treatment in the SVZ and CC, and occurs more in the CC in the presence of Gal-3. A,** Diagram demonstrating SVZ and CC regions examined. **B,** Representative images of GFAP in the CC after cuprizone treatment. Dotted white line delineates CC from SVZ (note that SVZ was analysed in separate images of dorsolateral SVZ). Scale bar 50μm. **C,** Graphs demonstrating the degree of reactive astrocytosis in the SVZ and CC. One image for each brain was scored between 0-10 by two blinded observers. Statistics calculated as two-way ANOVA using SPSS with N $\geq$ 6. Graphs show mean $\pm$ SEM.

except for between 6-week cuprizone and remyelination ($p = 1.000$). Like the SVZ, there was no significant interaction between genotype and treatment group in the CC ($F(3,47) = 0.235$, $p = 0.872$).

4.2.10 Gal-3 absence is not compensated by other galectins

To investigate the possibility of Gal-3 absence receiving compensation from other galectins, I performed an RT-PCR experiment on SVZ samples from littermate Gal-$3^{+/+}$ and Gal-$3^{-/-}$ mice ($N = 3$ samples per genotype, each sample containing pooled SVZs from 4 mice). The genes included Lgals1, 3, 8 and 9, the respective genes of Gal-1, 3, 8 and 9, which had previously been associated with the SVZ (see Introduction on p25 or Section 4.1.3 on p68 for details). B2m was used as a housekeeping gene and revealed no difference between genotypes ($p = 0.460$ using t-test; Boda et al., 2009, justifies housekeeping gene choice). When the other genes were normalised to B2m, Lgals1, 8 and 9 also showed no difference between genotypes ($p = 0.647$, $p = 0.308$ and $p = 0.443$ respectively; Figure 4.12). As expected, Lgals3 was absent in Gal-$3^{-/-}$ mice ($p < 0.0005$).

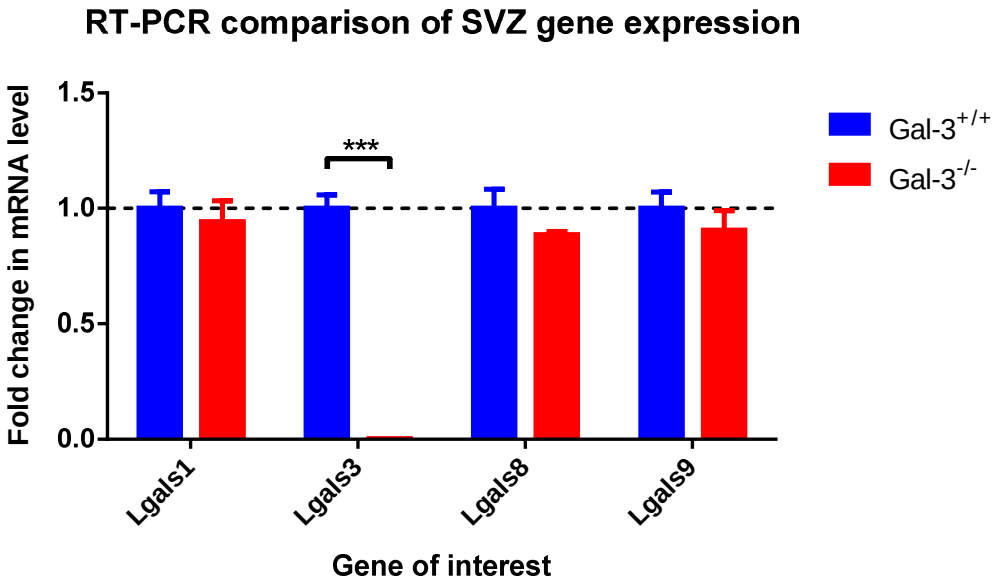


Figure 4.12: **Gal-3 absence is not compensated by other galectins.** Graph showing RT-PCR comparison of SVZ galectin expression in Gal-$3^{+/+}$ and Gal-$3^{-/-}$ mice. It demonstrates fold change compared to Gal-$3^{+/+}$ mice for quantities normalised to the housekeeping gene B2m. Genes include Lgals1, 3, 8 and 9, which correspond to Gal-1, 3, 8 and 9 respectively. Statistics calculated as t-test with N = 3 samples per genotype, each sample containing pooled SVZs from 4 mice. Graph shows mean ± SEM. ***$p \leq 0.001$.

4.3 Discussion

In this chapter, I focused on investigating inflammation in the SVZ and CC after demyelination including how it relates to Gal-3. I showed that Gal-3 is expressed in the human SVZ normally and in the CC in MS. I then demonstrated a juxtaposition of inflammation after cuprizone treatment with it decreasing in the SVZ while increasing in the CC. Gal-3 absence did not impact on inflammation or proliferation, and was not compensated by other galectins.

4.3.1 Gal-3 presence around the human lateral ventricles

The presence of Gal-3 around the human lateral ventricles provides an important translational link from animal studies. It had previously been shown to be present in the mouse SVZ in ependymal cells and astrocytes (see LacZ expression from Gal-3 promoter in Section 3.2.4 on p58; Comte et al., 2011). The current results suggest similar expression in humans with clear labelling of ependymal and SVZ cells. In addition, extravasating macrophages and microglia appear to express Gal-3. These findings would, however, benefit from further co-immunohistochemistry experiments to specify SVZ cell types. In MS, Gal-3 had previously been shown to increase in acute plaques (Stancic et al., 2011). I clarified that this increase occurs in acute plaques adjacent to the SVZ.

From an inflammation perspective, it is no surprise that Gal-3 increases in active plaques. Gal-3 is predominantly associated with the innate immune system, particularly macrophages (Ho and Springer, 1982; Liu et al., 1995). Acute MS lesions, which are characterised by macrophages and activated microglia, would therefore be expected to contain Gal-3 (Lucchinetti et al., 2000). The decrease of Gal-3 expression in more chronic MS plaques might mirror the decrease in macrophages and activated microglia. The Gal-3 decrease might also be causative of the inflammatory cell decrease given that Gal-3 is a chemoattractant of macrophages (Sano et al., 2000).

This chemoattractive role of Gal-3, as well as its ability to enhance phagocytosis in macrophages and neutrophils (Farnworth et al., 2008; Karlsson et al., 2009), suggest that it may have a positively reinforcing role in MS. The subsequent cuprizone experiments, however, indicated that Gal-3 absence did not impact on immune cell presence in the SVZ or CC. While the cuprizone results will be elaborated on shortly, it is worthwhile noting that further human experiments may be relevant. Immunohistochemistry experiments that correlate Gal-3 with a range of inflammatory markers might provide further clues about its role. In vitro studies with human tissue, possibly iPSCs, would likely be needed to prove causation.

An existing correlation is that PSA-NCAM+ cells also increase in acute MS plaques (Nait-Oumesmar et al., 2007). They are believed to migrate to demyelinated regions and integrate as oligodendrocytes. This finding can be interpreted with the results that myelin debris inhibits oligodendrocyte differentiation and that remyelination diminishes with disease longevity (Goldschmidt et al., 2009; Kotter et al., 2006). A question that arises is whether the decrease in Gal-3 in chronic MS plaques leads to decreased myelin clearance by macrophages and microglia, which then leads to impaired migration and/or differentiation of PSA-NCAM+ cells. Chapter 5 on p100 examines the role of Gal-3 in oligodendrocyte differentiation and includes a comparison of myelin levels after cuprizone treatment in Gal-$3^{+/+}$ and Gal-$3^{-/-}$ mice.

4.3.2 Juxtaposition of inflammation in the SVZ and CC after cuprizone treatment

One of the most intriguing results from this chapter was the juxtaposition of inflammation in the SVZ and CC after cuprizone treatment. The densities of Gal-3+ cells and CD45+ haematopoietic cells, as well as the number of PHi3+ proliferating cells, decreased in the SVZ but increased in the CC with cuprizone treatment. The increase in reactive astrocytosis was the only similarity observed in both regions.

An initial hypothesis that should be discounted is a differential effect of cuprizone:

general toxicity and apoptosis in the SVZ versus demyelination and the response to demyelination in the CC. From the MS translational perspective, it is important that the effect of cuprizone treatment on the SVZ is its response to demyelination in the CC rather than toxicity. The delineation of these possibilities through experiments is unlikely to be definitive, because both processes involve inflammation and many relevant cell markers. The lack of Gal-3 increase after MS in human SVZ, however, suggests that this process is not unique to cuprizone. Goings et al. (2006) also showed that SVZ microglia maintain a steady population after cortical aspiration injury in spite of increases in the CC. TMEV results additionally suggest that SVZ toxicity would increase inflammation: SVZ cells are infected with TMEV and there is increased microglial activation in both the SVZ and CC (Goings et al., 2008; James, 2012).

The next hypothesis to consider is that activated microglia simply migrate from the SVZ to the CC. There are three broad possibilities for the increase in microglia observed in the CC: proliferation of local microglia, migration of SVZ microglia and migration of peripheral macrophages. Local microglial proliferation is unlikely because the medial CC, where the CD45+/Iba1+ microglia were sampled, maintained close to zero PHi3+ proliferating cells in all groups. Migration of either SVZ microglia or peripheral macrophages are possibilities. Goings et al. (2006) injected rhodamine-labelled latex microspheres into the lateral ventricles to show SVZ microglia can migrate into the CC. McMahon et al. (2002), meanwhile, demonstrated peripheral macrophages are present in the CNS after cuprizone treatment in spite of an intact BBB. To determine whether the cells are SVZ microglia or peripheral macrophages, a similar labelling strategy of SVZ microglia could be used. Fluorescent peripheral macrophages from CD68-GFP+ mice could also be transplanted into non-fluorescent wild-type cuprizone treated mice.

A key biological outcome is how inflammation affects neurogenesis. Proliferation is one element of neurogenesis, and here it followed the same pattern of changes as microglia. Whether there is a causal link is an interesting question, especially in thinking towards future therapeutics. The correlation between inflammation and proliferation across different conditions is inconsistent though. Cortical aspiration injury maintains SVZ

microglial activation yet decreases SVZ proliferation (Goings et al., 2006, 2002). TMEV increases microglial activation but maintains normal proliferation (Goings et al., 2008). The dysbindin-1 mutant schizophrenia model, which is being researched by Ms Abeer Al-Shammari, a doctoral student in the Szele laboratory, shows decreased microglia in the SVZ after a pro-inflammatory polyI:C injection in only wild-type mice yet decreased proliferation in the SVZ after injection in only dysbindin-1 mutants (unpublished data). These findings, however, show correlation rather than causation. An in vitro experiment demonstrated that co-culture of SVZ cells with microglial cells or microglial conditioned media rescues the normal decline in the production of Tuj1+ neuroblasts (Walton et al., 2006). This finding is consistent with the current experiments. If a preliminary aim of recruiting SVZ cells to demyelinated regions is to increase their proliferation, then one must wonder if the decreased SVZ inflammation seen here is actually detrimental.

An emerging idea is the distinction between between pro-inflammatory M1 and anti-inflammatory M2 microglia (Crain et al., 2013; Kigerl et al., 2009). M1 microglia produce the cytokines inducible NOS (iNOS), TNF-α, IL-1β, and IL-6, and contribute to decreased neurogenesis and apoptosis. M2 microglia produce the cytokines IL-10 and arginase-I, and the growth factor VEGF, and promote neurogenesis and cell survival. Furthermore, M2 microglia have been shown to drive CNS oligodendrocyte differentiation both in vivo and in vitro (Miron et al., 2013). The M1 phenotype has also been shown to predominate in early TMEV spinal cord demyelination, before both M1 and M2 phenotypes are present during the chronic progressive phase (Herder et al., 2015). The juxtaposition of SVZ and CC densities seen here might also involve microglial phenotype. It would seem appropriate that M1 microglia predominate in the CC and M2 microglia in the SVZ, especially if the increase seen in the SVZ in the remyelination group largely features M2 microglia. Further immunohistochemistry experiments could clarify the presence of each microglial phenotype.

The disparity seen with CD68-GFP mice might also be explained by M1 and M2 phenotypic differences. CD68 should be expressed by all macrophages (Barros et al.,

2013), although I noticed the existence of Iba1+/GFP- cells in control mice yet Iba1-/GFP+ cells in cuprizone treated mice. As these experiments were the first in brain tissue for the CD68-GFP mice, it is not known whether the transgene is differentially expressed in microglia. The CD68-GFP mice would therefore also benefit from future immunohistochemistry experiments clarifying microglial phenotype.

4.3.3 Lack of Gal-3 effect on inflammatory cell densities

The lack of difference in inflammatory cells between Gal-$3^{+/+}$ and Gal-$3^{-/-}$ mice was a surprise given that Gal-3 has an established role of increasing inflammation including the number of inflammatory cells in TMEV and EAE (James, 2012; Jiang et al., 2009). As the current experiments occurred, Hoyos et al. (2014) published a paper that investigated the effects of Gal-3 on the CC after cuprizone treatment. They only examined the CC, where they reported Gal-$3^{-/-}$ mice had more microglia but fewer of these microglia were activated. These results are clearly different to the current study and no simple explanation is apparent. Hoyos et al. did perform experiments in a different Gal-3 knockout mouse, which lacked exon V (Hsu et al., 2000). The mouse used here lacked exons II, III and IV (Colnot et al., 1998).

As Hoyos et al. suggest, however, it may be that Gal-3 exerts an effect that does not manifest with a change in inflammatory cell number. In keeping with their finding that Gal-3 enhances microglial activation, Gal-3 is also known to attract human macrophages and enhance macrophage phagocytosis (Karlsson et al., 2009; Sano et al., 2000). Interestingly, MacKinnon et al. (2008) reported that Gal-3 increases M2 macrophage activation. It would therefore be interesting to examine the M1 versus M2 microglial phenotype between genotypes too.

The one experiment where Gal-3 did demonstrate an effect was in reactive astrocytosis: Gal-$3^{+/+}$ mice had a greater degree of reactive astrocytosis than Gal-$3^{-/-}$ mice in the CC. While the general pro-inflammatory effect of Gal-3 might suggest this result was expected, it is inconsistent with the literature. Comte et al. (2011) reported SVZ

reactive astrocytosis in otherwise healthy Gal-3$^{-/-}$ mice. Hoyos et al. (2014) reported more GFAP+ cells in Gal-3$^{-/-}$ mice after 6-weeks of cuprizone treatment, as well as an increase in GFAP protein levels measured by WB. There are multiple methods to quantify reactive astrocytosis and it may be worthwhile performing further analysis using current images.

4.3.4 Lack of Gal-3 compensation by other galectins

The research question about compensation was posed based on similarities between galectins, and previously reported redundancy between Gal-1 and Gal-8 (Tsai et al., 2011). This question became more relevant and directed with the lack of phenotypic findings for Gal-3 absence: with largely consistent findings between Gal-3$^{+/+}$ and Gal-3$^{-/-}$ mice, was something compensating for Gal-3 absence? The results revealed that, if something was, it was not another galectin. The reason may include the different structures of Gal-3 to Gal-1 and Gal-8: Gal-3 is chimeric, while Gal-1 is a one CRD galectin and Gal-8 is a two CRD galectin. The three galectins are known to have different roles more broadly (see Liu and Rabinovich, 2010, for review). In addition, Tribulatti et al. (2012) reported that Gal-3 antagonises Gal-1 and Gal-8. The current experiments did not suggest that Gal-1 and Gal-8 decrease with Gal-3 absence, which might have been expected if they antagonise Gal-3.

One limitation of this experiment is that it was only conducted in healthy, non-diseased Gal-3$^{+/+}$ and Gal-3$^{-/-}$ mice. Given there was also no phenotypic difference in these mice, it is reasonable to expect that any compensation that might exist after cuprizone treatment would occur then too. Gal-1 has, however, been shown to increase SVZ neurogenesis and improve functional recovery after stroke (Ishibashi et al., 2007), and enhance neural stem cell spinal cord transplants (Yamane et al., 2010). Pasquini et al. (2011) also reported that Gal-1 was downregulated while Gal-3 was upregulated as oligodendrocytes differentiate. It might therefore be relevant to check interactions between galectins in cuprizone treated mice. As a broader research topic, it would be interesting to investigate the role of other galectins in SVZ neurogenesis after

demyelination.

4.3.5 Conclusion

The SVZ and CC demonstrated differential effects in inflammation with a similar pattern in proliferation. There may be a biological reason including the loss of pro-inflammatory M1 microglia in the SVZ, and a reciprocal gain in the CC. The SVZ, in contrast, may maintain pro-neurogenic M2 microglia. Gal-3 had a limited effect on inflammation after cuprizone treatment, which was a surprise given its well-documented role in other demyelination models and medical conditions. It did, however, increase reactive astrocytosis in the CC.

5

Galectin-3 and its role in oligodendrogenesis

Contents

5.1 Introduction 101

5.1.1 SVZ capacity for oligodendrogenesis 101

5.1.2 Gal-3 and oligodendrogenesis 102

5.1.3 OB demyelination in animal models 103

5.1.4 Research questions 103

5.2 Results 104

5.2.1 The density of oligodendrocyte lineage cells changes after cuprizone treatment in the CC, but not in the SVZ or in the absence of Gal-3 104

5.2.2 Gal-3 presence does not enhance oligodendrocyte differentiation after cuprizone treatment 106

5.2.3 Gal-3 enhances neuronal differentiation in vitro 106

5.2.4 Gal-3 absence does not alter MBP levels in the CC after cuprizone treatment 111

5.2.5 Gal-3 absence increases MBP levels in layer six of the motor cortex after cuprizone treatment 113

5.2.6 OB demyelination and remyelination occur in both the cuprizone and TMEV animal models 115

5.3 Discussion 120

5.3.1 Gal-3 role in neuronal differentiation 120

5.3.2 Increased MBP in layer 6 of the Gal-$3^{-/-}$ motor cortex 121

5.3.3 Lack of Gal-3 role in oligodendrocyte differentiation 123

5.3.4 Demyelination in the OB in animal models 124

5.3.5 Conclusion 125

5.1 Introduction

The SVZ has the potential to treat conditions like MS by giving rise to oligodendrocytes that remyelinate the CC. This process, called oligodendrogenesis, involves multiple steps. It initially requires the SVZ stem cell population to proliferate, it then requires progenitor cells to differentiate into oligodendrocyte lineage cells, and it finally requires these oligodendrocyte lineage cells to mature as myelinating oligodendrocytes. Each step has unique mechanisms, and Gal-3 has been suggested to have a role in maturation in particular (Pasquini et al., 2011). This chapter therefore focuses on the differentiation and maturation of oligodendrocytes, including subsequent myelination.

5.1.1 SVZ capacity for oligodendrogenesis

The SVZ contributes to oligodendrogenesis in the CC both routinely and after demyelination. It arises developmentally from the MGE, LGE and CGE, which produce Nkx2.1 and Gsh2 derived oligodendrocytes during embryogenesis (see Introduction on p3). The postnatal SVZ continues to give rise to oligodendrocytes in the CC and cortex (Levison and Goldman, 1993). The adult SVZ also gives rise to oligodendrocytes, which can migrate as far as 550μm into the CC in mice (Menn et al., 2006). In addition, a subpopulation of neural stem cells and transit amplifying progenitors express the oligodendrocyte lineage marker Olig2. In the lysolecithin and EAE demyelination models, the SVZ contributes oligodendrocytes for CC remyelination (Nait-Oumesmar et al., 1999; Picard-Riera et al., 2002). Neuroblasts that have migrated into the CC following lysolecithin-induced demyelination also have the capacity to transform into oligodendrocyte lineage cells (Jablonska et al., 2010). These results translate to humans, with PSA-NCAM+ precursor cells migrating from the SVZ to demyelinated white matter in MS (Nait-Oumesmar et al., 2007). The majority of these cells express Sox9, and some express Sox 10 and Olig2, which are markers associated with oligodendrocyte differentiation and maturation.

Two recent studies examined the contribution of the SVZ to CC remyelination in

the cuprizone model. Xing et al. (2014) used Nestin-CreER^{T2} line 5-1:Rosa26-eYFP mice to label Nestin+ SVZ neural stem cells. They also labelled parenchymal PDGF receptor alpha (PDGF-Rα+) OPCs, which are the other population of stem cells that contribute to CC remyelination. They demonstrated that SVZ cells contribute to CC remyelination after cuprizone treatment, particularly in the rostral SVZ. Interestingly, the SVZ derived oligodendrocytes produced significantly thicker myelin compared to OPC derived oligodendrocytes. Guglielmetti et al. (2014) injected iron oxide particles into the lateral ventricles, so that SVZ cells would incorporate these particles and could be tracked with MRI. They also injected a lentivirus encoding both eGFP and a Luciferase reporter to track cells with in vivo bioluminescence imaging. They concluded that SVZ cells did not contribute to CC remyelination at all, although they had focused on the caudal SVZ. The current study therefore focused on the rostral SVZ.

5.1.2 Gal-3 and oligodendrogenesis

Gal-3 has been suggested to play a role in myelination both in vivo and in vitro. Pasquini et al. (2011) showed that Gal-3$^{-/-}$ mice have fewer myelinated axons, with fewer myelin turns and larger g-ratios, than Gal-3$^{+/+}$ mice. They also used oligodendrocyte cell lines to show that Gal-3 both enhances maturation of oligodendrocytes and is upregulated as they do. They only investigated the SVZ to a small extent: they showed that the proportion of O4+ oligodendrocytes in SVZ neurosphere cultures decreases from $\sim$12% of cells obtained from Gal-3$^{+/+}$ mice to $\sim$8% of cells from Gal-3$^{-/-}$ mice. The same laboratory published a further study examining Gal-3 after cuprizone treatment as the research in this thesis was in progress (Hoyos et al., 2014). They showed that there is impaired maturation of oligodendrocytes in Gal-3$^{-/-}$ mice after cuprizone treatment. They also reported spontaneous remyelination after 6-weeks of cuprizone treatment in Gal-3$^{+/+}$ mice. This result did not occur in Gal-3$^{-/-}$ mice, which they attributed to the impaired oligodendrocyte maturation. The focus of Hoyos et al. was, however, on the CC rather than the SVZ. There are therefore many remaining biological questions including what the different roles are for constitutive expression of Gal-3 in the SVZ and de novo

expression in the CC.

5.1.3 OB demyelination in animal models

A side question arose about whether cuprizone treatment or TMEV caused demyelination in the OB. A/Prof Gabriele de Luca in the Nuffield Department of Clinical Neurosciences, with whom I collaborated on human tissue experiments, reported high levels of demyelination in human OB in the demyelinating conditions MS, neuromyelitis optica and acute disseminated encephalomyelitis (DeLuca et al., 2014). This finding carried relevance to this thesis because the SVZ gives rise to OB interneurons. In the human context, it was exceptionally relevant for multiple reasons: the OB provides a potential route of entry for viral and other pathogens that could cause these diseases, the demyelination explains anosmia that frequently occurs in MS, and the demyelination was associated with demyelination and inflammation of adjacent cortex. There are scant references in the literature about whether OB demyelination occurs in animal models. Silvestroff et al. (2010) and Yang et al. (2009) reported that cuprizone was known to have fewer MBP fibres and CNP+ cells in the OB, but did not provide further detail including OB layer specific findings. Wada and Fujinami (1993) showed TMEV has the capacity to infect the brain via the OB, and then spreads faster through the brain than when the cortex is initially infected. I decided to more systematically evaluate myelination in the OB in both the cuprizone and TMEV models.

5.1.4 Research questions

Based on this background, this chapter aimed to answer the following questions:

- Does Gal-3 impact on the SVZ and CC oligodendrocyte populations, including myelin levels, after cuprizone treatment?
- How does Gal-3 impact on the differentiation of SVZ cells in vitro?
- Does the OB undergo demyelination in the cuprizone and TMEV models?

5.2 Results

5.2.1 The density of oligodendrocyte lineage cells changes after cuprizone treatment in the CC, but not in the SVZ or in the absence of Gal-3

To begin with, I investigated the number of oligodendrocyte lineage cells present in the SVZ and CC after cuprizone treatment. I performed immunohistochemistry with the anti-Olig2 antibody, which is a pan-oligodendrocyte lineage cell marker. In the SVZ, I counted the number of cells in regions similar to the number of PHi3+ proliferating cells (Figure 5.1A; $N \geq 6$; detailed regional counts and analysis in Appendix C.2 on p209). In the CC, however, there were too many Olig2+ cells and it was necessary to sample a region from the medial CC.

The SVZ demonstrated no clear trends between different treatment groups or genotypes (Figure 5.1B for overall SVZ results; Table C.6 on p209 for regional SVZ results). The total number of Olig2+ cells per SVZ was $\sim$100 for all groups. This lack of effect was confirmed by a repeated measures ANOVA, which showed no significance for main effects or interactions involving treatment groups or genotypes (Table C.8 on p210).

The CC, in contrast, showed a clear effect of cuprizone treatment but not of genotype. The density of Olig2+ cells decreased in both Gal-$3^{+/+}$ and Gal-$3^{-/-}$ mice after 3-weeks cuprizone treatment before recovering to baseline at 6-weeks (Figure 5.1C). The density in the remyelination group of Gal-$3^{-/-}$ mice had a possible further increase, although there was a large SEM for this result. A two-way ANOVA revealed a significant main effect for treatment ($F(3,47) = 7.532$, $p \leq 0.0005$), with post-hoc comparisons showing this significance occurred for the decrease between control and 3-week cuprizone ($p = 0.024$), and the increases between 3-week cuprizone and 6-week cuprizone ($p = 0.011$) or remyelination ($p \leq 0.0005$) treatment groups. There was no significant difference between genotypes (either main effect ($F(1,47) = 1.471$, $p = 0.231$) or interaction with treatment ($F(3,47) = 0.681$, $p = 0.568$)).

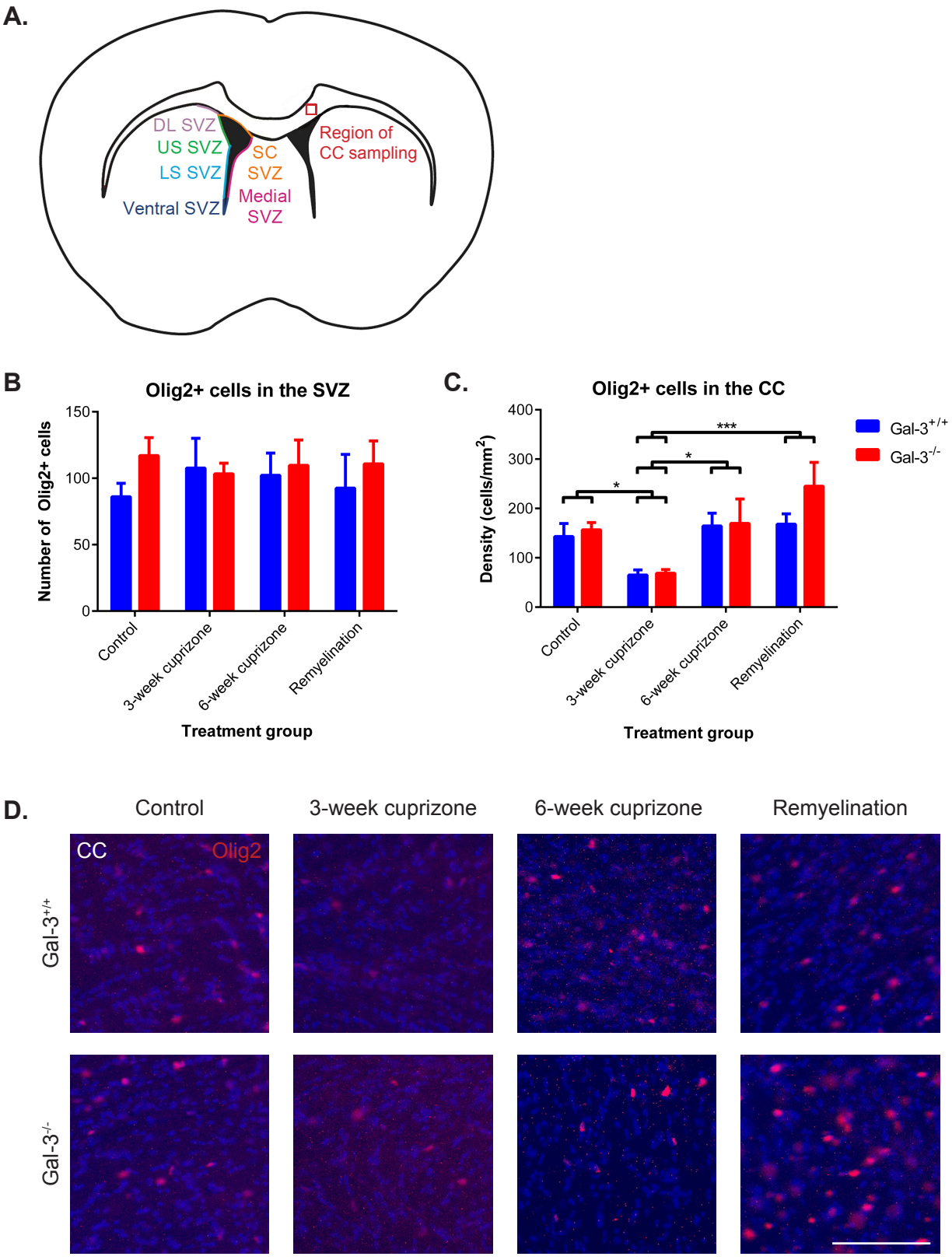


Figure 5.1: **The density of oligodendrocyte lineage cells changes after cuprizone treatment in the CC, but not in the SVZ or in the absence of Gal-3. A,** Diagram showing regions examined in the SVZ and CC. DL: dorsolateral, LS: lower striatal, SC: subcallosal, US: upper striatal. **B and C,** Graphs showing number of Olig2+ cells in the SVZ (B) and density in the CC (C). Statistics calculated using repeated measures ANOVA for SVZ and two-way ANOVA for CC with N $\geq$ 6 for each group. Graphs show mean $\pm$ SEM. *p $\leq$ 0.05, ***p $\leq$ 0.001. **D,** Representative images of Olig2+ immunohistochemistry from the CC. Scale bar 100μm.

5.2.2 Gal-3 presence does not enhance oligodendrocyte differentiation after cuprizone treatment

While the number or density of Olig2+ cells provides information on the number of oligodendrocyte lineage cells, it does not indicate how mature these cells are. I therefore performed co-immunohistochemistry with the mature oligodendrocyte marker CC1 (Figure 5.2A; Bhat et al., 1996). The labelling demonstrated CC1 with low and high fluorescence ($CC1^{low}$ and $CC1^{high}$; Figure 5.2B). The $CC1^{high}$ cells were interpreted as mature, myelinating oligodendrocytes. The $CC1^{low}$ cells were interpreted as less mature, non-myelinating oligodendrocytes that were beginning to express CC1.

The proportion of $CC1^{high}$ oligodendrocytes increased with cuprizone treatment and then remyelination, but not with Gal-3 presence (Figure 5.2C). A two-way ANOVA revealed a main effect for the difference between treatment groups ($F(3,47) = 5.361$, $p = 0.003$) with post-hoc comparisons showing the effect occurred between the control and remyelination groups ($p = 0.002$). The ANOVA showed no significant difference between genotypes (either main effect ($F(1,47) = 0.222$, $p = 0.640$) or interaction with treatment ($F(3,47) = 0.245$, $p = 0.865$)).

The proportion of $CC1^{low}$ oligodendrocytes was roughly constant in control, 3-week cuprizone and 6-week cuprizone mice before decreasing in remyelination mice (Figure 5.2D). The effect between treatment groups was not significant (either main effect ($F(3,47) = 0.745$, $p = 0.531$) or interaction with genotype ($F(3,47) = 0.342$, $p = 0.795$)). There was also no significant difference between genotypes (either main effect ($F(1,47) = 0.007$, $p = 0.936$) or interaction with treatment as before).

5.2.3 Gal-3 enhances neuronal differentiation in vitro

To further assess the capacity of Gal-3 to influence SVZ cells, I conducted in vitro differentiation assays. Tertiary neurospheres, initially obtained from P4-5 Gal-$3^{+/+}$ and Gal-$3^{-/-}$ mice, were dissociated then cultured without growth factors (Figure 5.3A).

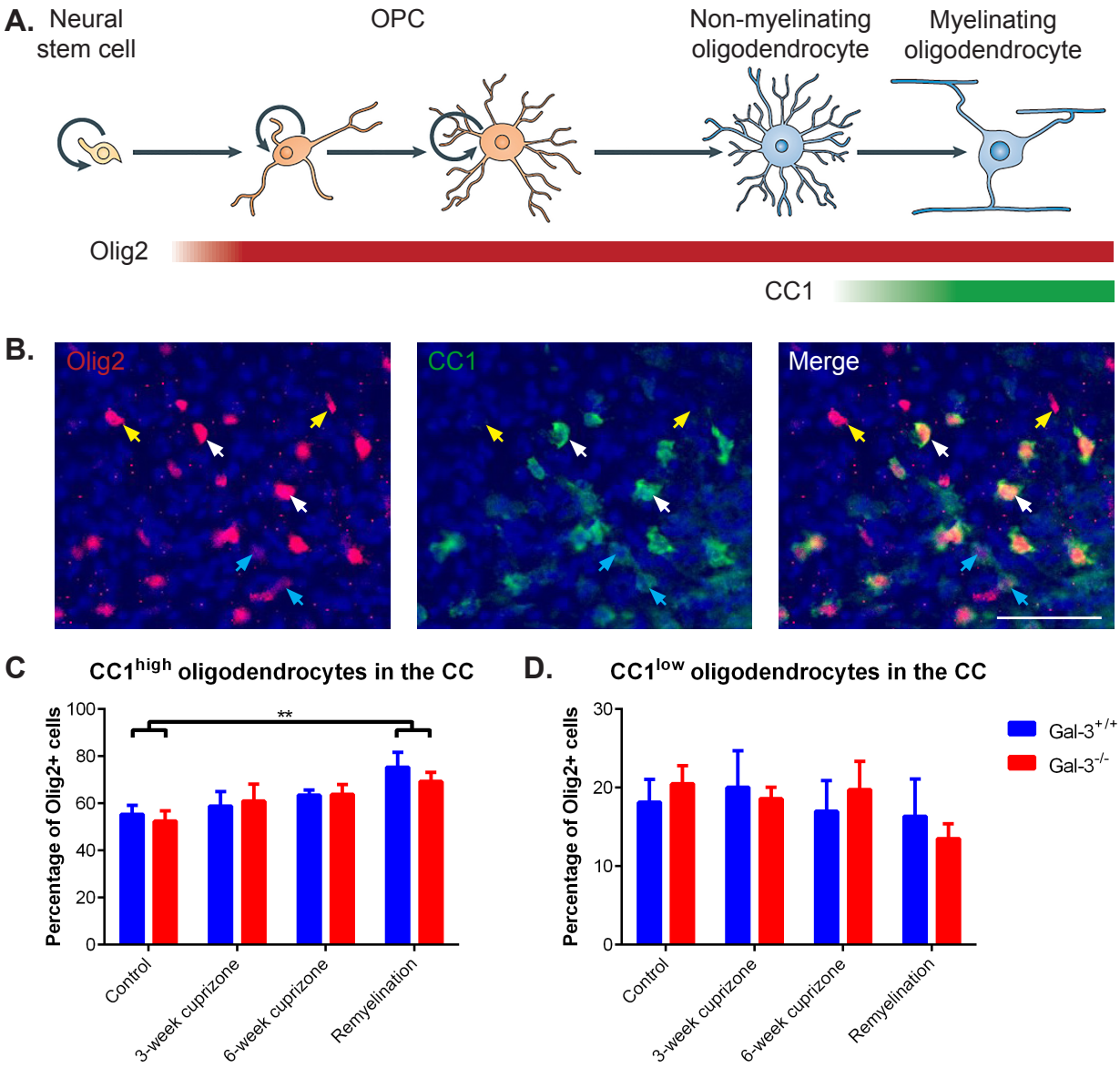


Figure 5.2: **Gal-3 presence does not enhance oligodendrocyte differentiation after cuprizone treatment. A,** Diagram showing differential expression of Olig2 and CC1 as oligodendrocytes mature. Adapted from Nishiyama et al. (2009). **B,** Images demonstrating immunohistochemistry of CC1 and Olig2. White arrows: $CC1^{high}$/Olig2+. Blue arrows: $CC1^{low}$/Olig2+. Yellow arrows: $CC1^{none}$/Olig2+. Scale bar 50μm. **C and D,** Graphs showing percentage of Olig2+ cells that are $CC1^{high}$ (C) and $CC1^{low}$ (D). Statistics were calculated as two-way ANOVA with N $\geq$ 6. Graphs show mean $\pm$ SEM. **p $\leq$ 0.01.

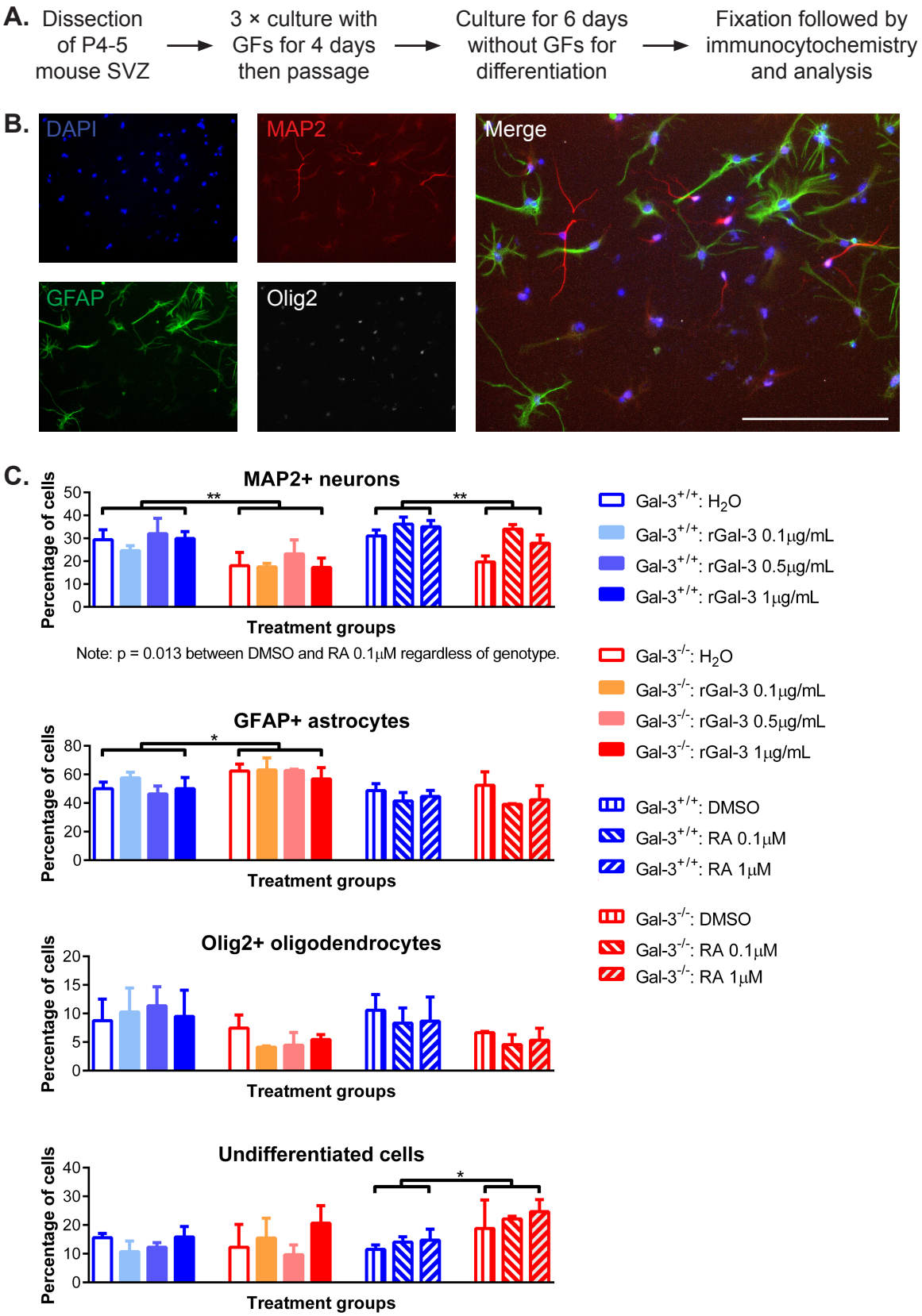


Figure 5.3: **Gal-3 enhances neuronal differentiation in vitro.** **A,** Diagram showing experiment design. **B,** Representative images demonstrating immunocytochemical staining of cell types. Scale bar 200μm. **C,** Graphs showing percentage of neural stem cells that differentiate into particular cell types. Statistics calculated as two-way ANOVA with N $\geq$ 3 biological replicates and technical triplicates. Graphs show mean $\pm$ SEM. *p $\leq$ 0.05, **p $\leq$ 0.01. RA: retinoic acid.

The use of growth factors in vitro causes neural stem cells to proliferate and maintain an undifferentiated state (Reynolds and Weiss, 1992). Their absence therefore allows neural stem cells to differentiate. After six days, I fixed the neural stem cells and performed immunocytochemistry with antibodies directed against MAP2 (neurons), GFAP (astrocytes) and Olig2 (oligodendrocytes; Figure 5.3B). Strict criteria were used to account for bleed-through and overlap of staining (for details see Methods on p44).

In addition to comparing genotypes, I added rGal-3 (dissolved in H_2O) in different concentrations to establish a dose-response curve. The concentrations were proposed by Dr Rachel James, a former doctoral student in the Szele laboratory; data from multiple in vitro experiments suggested these concentrations had a biological effect, including a preliminary differentiation experiment that showed an astrocyte-to-neuron (neurogenic) fate-shift with higher rGal-3 concentrations (James, 2012). The biological activity of this lot of rGal-3 was verified by adding it to neurospheres and observing them adhere to each other. Retinoic acid (dissolved in DMSO) was used as a positive control as it had previously been shown to also cause a neurogenic fate-shift (Wang et al., 2005). These experiments were performed at least three times for both Gal-$3^{+/+}$ and Gal-$3^{-/-}$ mice. Within each experiment, there were three wells for each concentration of rGal-3 and retinoic acid. A sample image from each well was then used for counting. The data for each cell type in the rGal-3 experiment was analysed with a two-way ANOVA that compared genotype and rGal-3 concentration. The retinoic acid experiment was analysed similarly but separately.

Retinoic acid, as expected, caused an increase in the proportion of neurons (Figure 5.3C). The statistical analysis confirmed this increase with significance occurring between DMSO and retinoic acid 0.1μM ($F(2,15) = 5.799$, $p = 0.014$ for main effect of concentration; $p = 0.013$ for pairwise comparison). Both astrocytes and oligodendrocytes showed reciprocal decreases with the addition of retinoic acid. There was, however, no significance for these changes ($p \geq 0.05$ for all main effects and interactions for astrocytes and oligodendrocytes). The number of undifferentiated cells also increased with the addition of retinoic acid, although it too was non-significant

($p \geq 0.05$ for both main effect of concentration and interaction of concentration and genotype).

Gal-3 increased the proportion of neurons as well. This trend was seen by comparing Gal-$3^{+/+}$ and Gal-$3^{-/-}$ cells across all conditions in each of the rGal-3 and retinoic acid experiments. In the rGal-3 experiment, there was a significant increase in neurons and decrease in astrocytes in the presence of Gal-3 ($F(1,20) = 9.309$, $p = 0.006$ for main effect of genotype for neurons; $F(1,20) = 5.897$, $p = 0.025$ for astrocytes). In the retinoic acid experiment, there was a significant increase in neurons and decrease in undifferentiated cells in the presence of Gal-3 ($F(1,15) = 8.565$, $p = 0.010$ for main effect of genotype for neurons; $F(1,15) = 5.766$, $p = 0.030$ for undifferentiated cells). The addition of rGal-3 did not, however, result in similar findings. The proportion of neurons, astrocytes and undifferentiated cells remained approximately the same in the presence of rGal-3 ($p \geq 0.05$ for main effects of concentration and interactions of concentration and genotype for each cell type).

Interestingly, Gal-3 also appeared to increase the proportion of oligodendrocytes. This effect was once again seen by comparing Gal-$3^{+/+}$ and Gal-$3^{-/-}$ cells across all conditions, although was not significant in both the rGal-3 ($F(1,20) = 3.464$, $p = 0.077$ for main effect of genotype; $F(3,20) = 0.256$, $p = 0.856$ for interaction with concentration) and retinoic acid ($F(1,20) = 2.423$, $p = 0.140$ for main effect; $F(2,20) = 0.006$, $p = 0.994$ for interaction) experiments. The trend was, however, broadly consistent with Pasquini et al. (2011) who showed that the proportion of O4+ oligodendrocytes in SVZ neurosphere cultures decreases from $\sim$12% of Gal-$3^{+/+}$ cells to $\sim$8% of Gal-$3^{-/-}$ cells. The addition of rGal-3 surprisingly decreased the proportion of oligodendrocytes in Gal-$3^{-/-}$ cells. This effect was not significant ($F(3,20) = 0.028$, $p = 0.994$ for main effect of concentration; $F(3,20) = 0.256$, $p = 0.856$ for interaction with genotype), and did not occur in Gal-$3^{+/+}$ cells.

5.2.4 Gal-3 absence does not alter MBP levels in the CC after cuprizone treatment

Having investigated oligodendrocyte populations for density, differentiation and maturation, I wanted to examine their ability to myelinate. I therefore performed both qualitative and quantitative analysis using immunohistochemistry with an anti-MBP antibody. As previously described, MBP is one of the key proteins associated with the myelin sheath (Kornguth and Anderson, 1965; Laatsch et al., 1962).

The CC was the first region I analysed, and it showed a decrease but not absence of MBP fluorescence with demyelination (Figure 5.4A; with enhanced contrast in Figure 5.4B). In the remyelination group, there were regions of increased MBP fluorescence. These findings confirmed that CC demyelination and remyelination, as has been extensively reported after cuprizone treatment, occurred here (Taylor et al., 2010). Qualitatively there was no difference between Gal-$3^{+/+}$ and Gal-$3^{-/-}$ mice.

In quantifying MBP fluorescence in the CC, there was no clear threshold value for when MBP was present or absent. I therefore produced cumulative fluorescence histograms for Gal-$3^{+/+}$ and Gal-$3^{-/-}$ mice (Figure 5.4C and D), which were also normalised as described in the Methods on p38. In these graphs, the area under the curve reflects the extent of myelination. The histograms provide two main pieces of information. Firstly, they demonstrate that MBP levels decreased with demyelination before increasing with remyelination. Secondly, they suggest that the largest differences between treatment groups occurred around an intensity of 150. This value was therefore used for statistical comparisons between genotypes and treatment groups (Figure 5.4E). A two-way ANOVA suggested no differences between genotypes (either as a main effect ($F(1,48) = 0.387$, $p = 0.537$) or as an interaction with treatment groups ($F(3,48) = 1.155$, $p = 0.337$)). It did, however, indicate a main effect for treatment groups ($F(3,48) = 8.146$, $p \leq 0.0005$). This effect was between control and 6-week cuprizone ($p \leq 0.0005$), and 3-week and 6-week cuprizone ($p = 0.006$) groups.

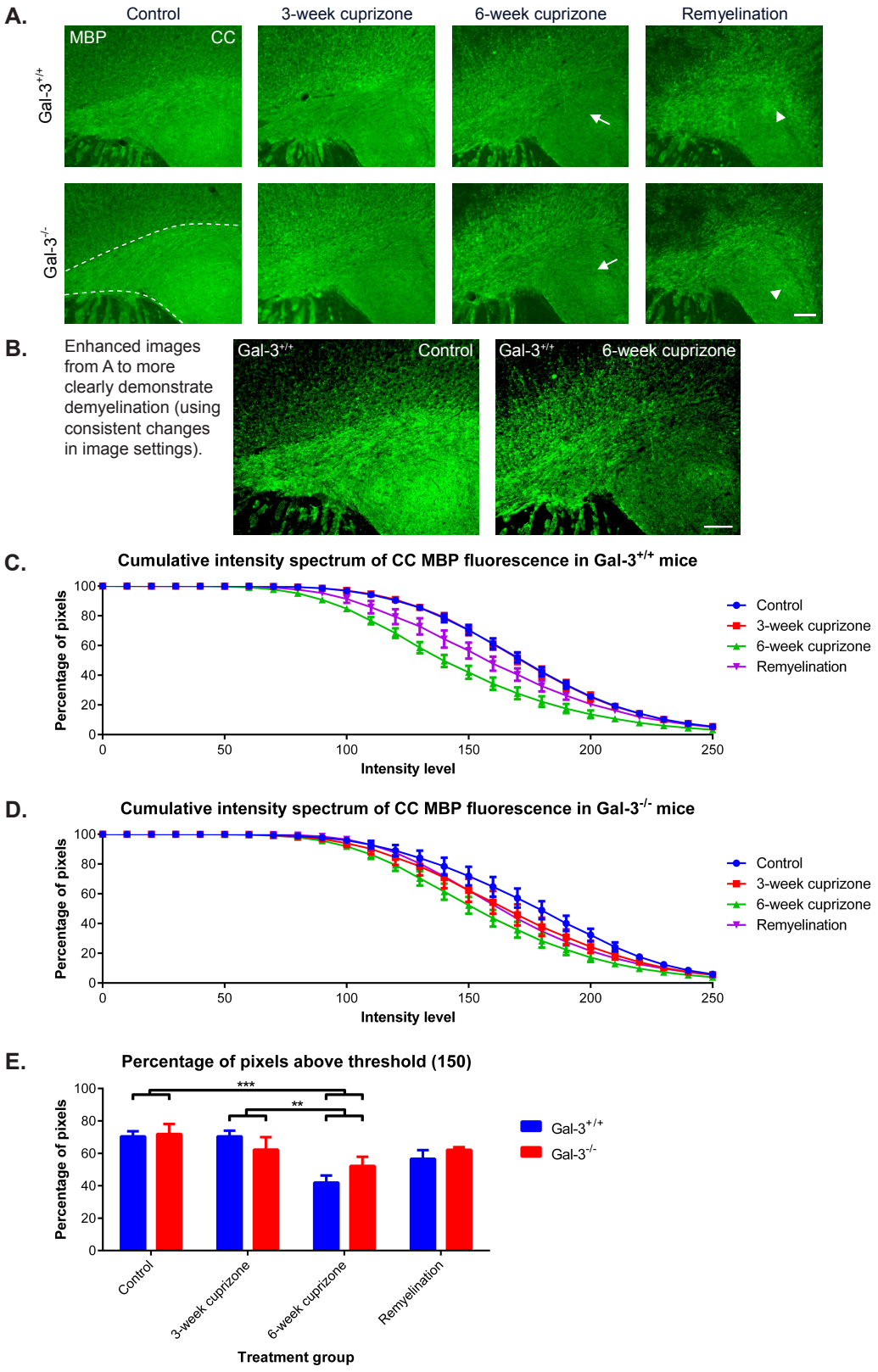


Figure 5.4: **Gal-3 absence does not alter MBP levels in the CC after cuprizone treatment.** **A,** Representative images of MBP immunohistochemistry including demyelination (arrows) and remyelination (arrowheads). Dotted line demonstrates region considered CC. **B,** Enhanced images from A that more clearly demonstrate demyelination. **C and D,** Graphs showing cumulative intensities in 10 point increments of MBP fluorescence in Gal-$3^{+/+}$ (C) and Gal-$3^{-/-}$ (D) mice. Statistics not performed on these graphs. **E,** Graph showing percentage of pixels above the MBP threshold of 150. Statistics calculated as two-way ANOVA with N $\geq$ 6. Graphs show mean $\pm$ SEM. **p $\leq$ 0.01, ***p $\leq$ 0.001. Scale bars 100μm.

5.2.5 Gal-3 absence increases MBP levels in layer six of the motor cortex after cuprizone treatment

While researching the CC, it became apparent that the cortex demonstrated more overt changes in MBP immunohistochemistry. The cortex also provided an opportunity to research grey matter demyelination, which is understudied yet functionally important. I therefore examined it with a focus on the motor and somatosensory regions (Figure 5.5A and B).

There was a consistent, qualitative effect across brains, with all brains in each treatment group demonstrating similar MBP expression (Figure 5.5C, $N \geq 6$ for each group). That effect involved little change between control and 3-week cuprizone brains, before a large decrease in MBP expression in 6-week cuprizone brains especially in layers 4 and 5. Following remyelination, there was a patchy return of MBP immunohistochemistry in layers 4 and 5. Interestingly, it appeared that layer 6 had a decrease in MBP expression from the 6-week cuprizone to remyelination groups. There was no clear qualitative difference between genotypes.

To quantitatively analyse the MBP immunohistochemistry, I used a similar thresholding technique to the CC (see Methods on p38 for details). It involved selecting regions on ImageJ for each of the layers with only the DAPI channel to avoid bias from knowing whether MBP staining was present. While intensity histograms were obtained for all layers, layer 1 was excluded from subsequent analysis because it contained a large amount of autofluorescence and it was not possible to establish a suitable threshold that distinguished whether MBP was present. Layers 2/3 were also excluded because they contained little MBP immunohistochemistry, which was difficult to separate from surrounding background fluorescence. Layers 4, 5 and 6 were analysed including with a repeated measures ANOVA (detailed statistics in Appendix C.3 on p211).

The quantitative measurements were broadly consistent with the qualitative observations (Figure 5.5D). Layers 4 and 5 demonstrated high levels of MBP in control and 3-week cuprizone brains, which then decreased in 6-week cuprizone and

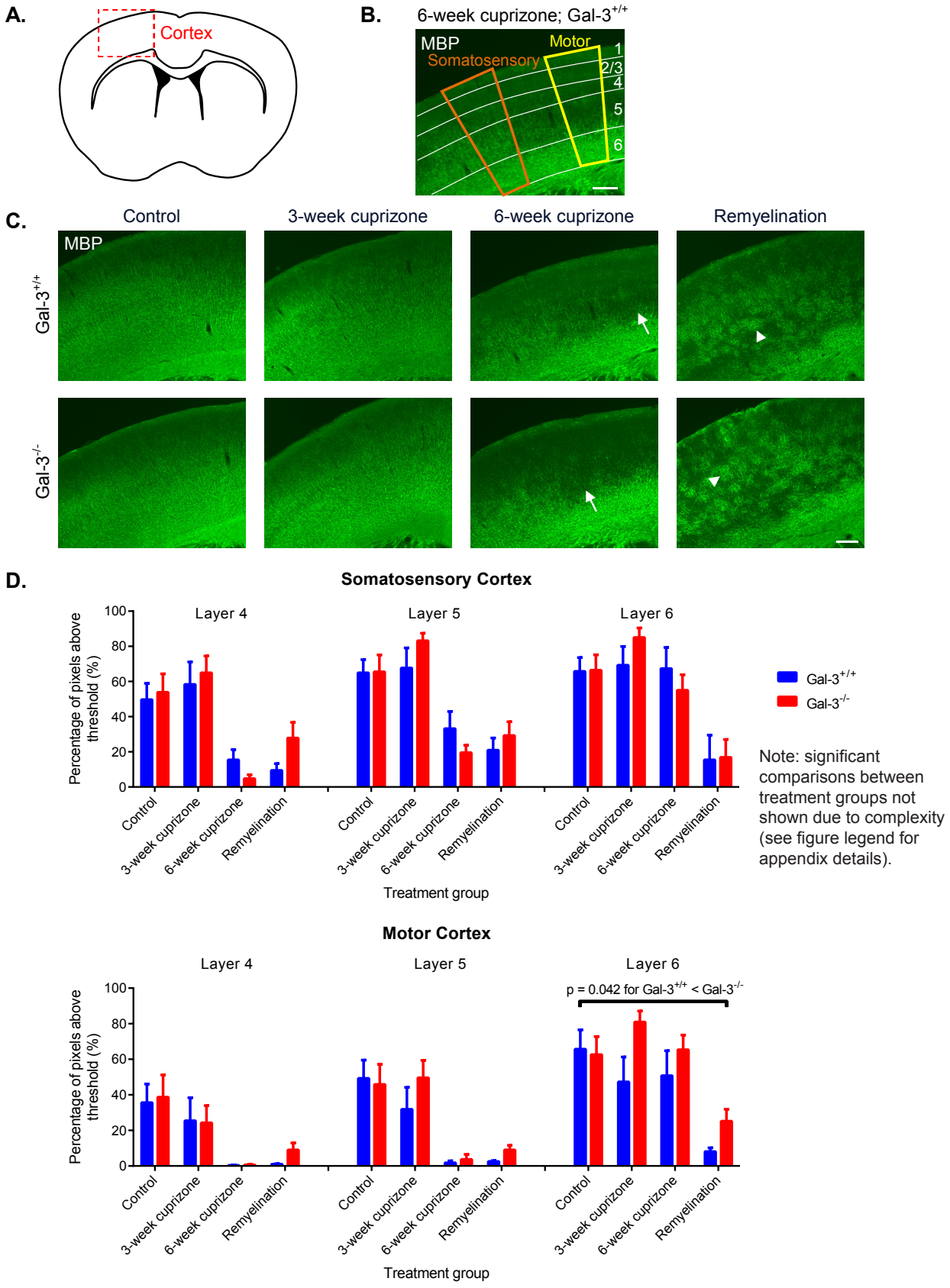


Figure 5.5: **Gal-3 absence increases MBP levels in layer six of the motor cortex after cuprizone treatment. A and B,** Diagrams showing cortical regions and layers examined. **C,** Representative images of MBP immunohistochemistry with demyelination (arrows) and remyelination (arrowheads). **D,** Graphs showing percentage of pixels with fluorescence intensity above threshold in separate cortical layers. Statistics calculated as repeated measures ANOVA with N $\geq$ 6 and reported in full in Appendix C.3 on p211. Graphs show mean $\pm$ SEM. Scale bars 200μm.

remyelination brains ($p \leq 0.004$ for each comparison; more detailed statistics in Table C.12 on p213). While there was often a trend for an increase between 6-week cuprizone and remyelination brains to reflect the patchy remyelination observed, these differences were not significant ($p = 1.000$). Layer 6 showed a huge decrease in the remyelination group ($p < 0.0005$ between every other treatment group).

The quantitative analysis revealed a difference between genotypes: in layer 6 in the motor cortex, Gal-$3^{-/-}$ mice had more MBP immunofluorescence than Gal-$3^{+/+}$ mice ($p = 0.042$; more detailed statistics in Table C.13 on p214). This effect was most prominent in the 3-week cuprizone and remyelination groups, although there was no statistically significant interaction between genotypes and treatment groups (Table C.11 on p212).

5.2.6 OB demyelination and remyelination occur in both the cuprizone and TMEV animal models

As described previously, I also wanted to determine if the extent of OB demyelination in the cuprizone and TMEV models is comparable to human MS (DeLuca et al., 2014). Once again I utilised MBP immunohistochemistry and performed both qualitative and quantitative analysis. Given the broader rationale for this experiment, I limited it to Gal-$3^{+/+}$ mice.

The cuprizone sections demonstrated qualitative decreases and subsequent increases in MBP levels in the glomerular, external plexiform and granular layers of the OB (Figure 5.6A and B). These findings were in line with the demyelination then remyelination phases of cuprizone treatment, and were consistent across all brains within a treatment group. The strongest effect appeared in the glomerular layer, which is where input from peripheral olfactory receptor neurons synapses with the central output neurons of the bulb, the mitral and tufted neurons. In addition, mice in the 3-week and 6-week cuprizone groups displayed rounded up MBP+ cells and fragmented fibres in the external plexiform layer, suggestive of oligodendrocytes undergoing apoptosis.

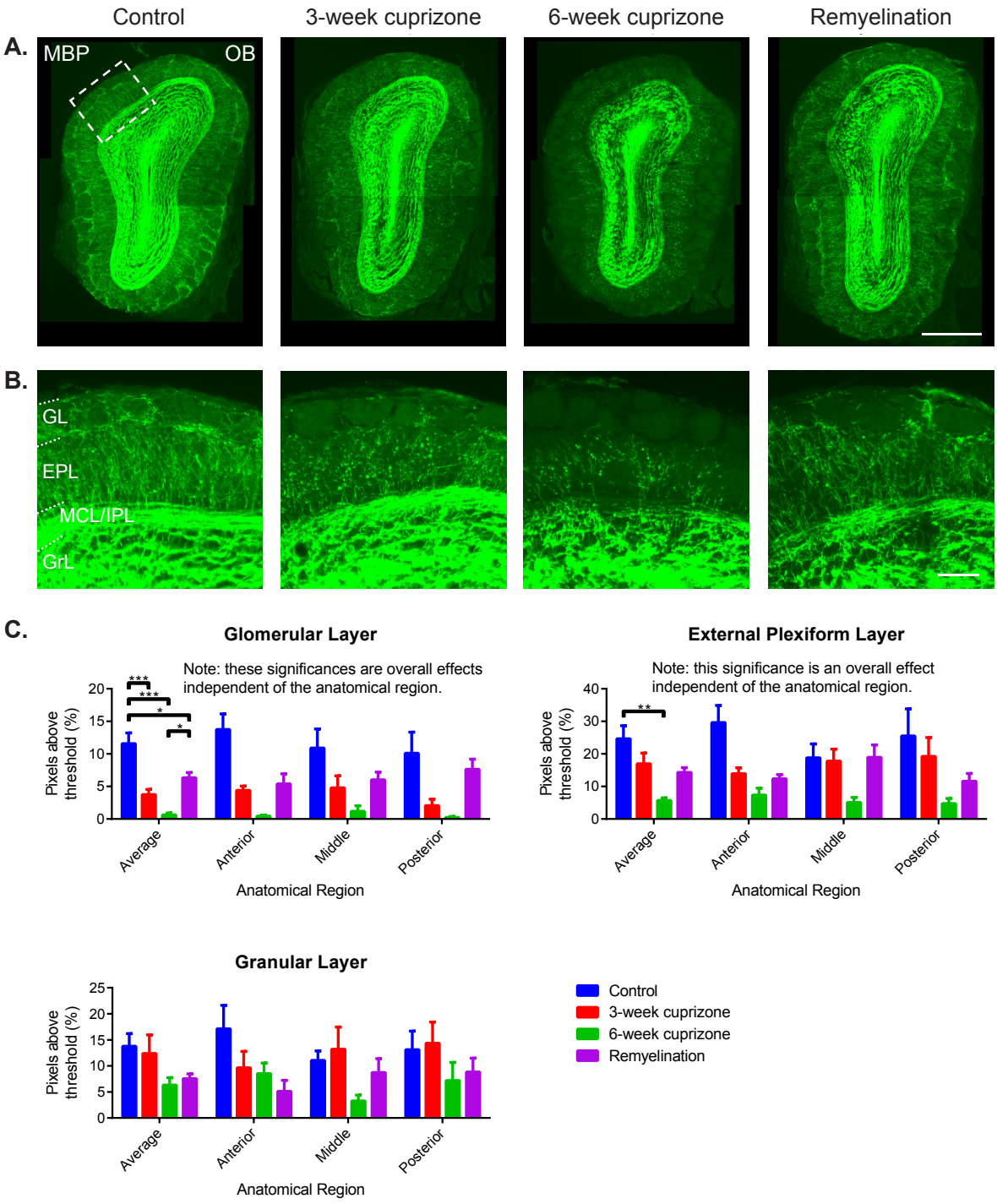


Figure 5.6: **Cuprizone causes consistent demyelination then remyelination in the OB. A and B,** OB sections with MBP immunohistochemistry. Dotted box shows region of images in B. GL: glomerular layer, EPL: external plexiform layer, MCL/IPL: mitral cell layer/internal plexiform layer, GrL: granular layer. Scale bars 500μm (A) and 100μm (B). **C,** Graphs showing percentage of pixels with fluorescence intensity above threshold in the glomerular, external plexiform and granular layers. Statistics calculated as repeated measures ANOVA with N = 6. Graphs show mean ± SEM. *p $\leq$ 0.05, **p $\leq$ 0.01, ***p $\leq$ 0.001.

The quantification process was similar to the CC and analysed the glomerular, external plexiform and granular layers of the anterior, middle and posterior OB. The antero-posterior regions were defined as follows: anterior had a circular OB (Bregma >5.3mm); middle had an hourglass OB (Bregma 4.0 to 5.3mm; as in Figure 5.6A); posterior had interrupted glomerular and external plexiform layers due to the anterior olfactory nucleus (Bregma 2.7 to 4.0mm). Once again, I produced intensity histograms and calculated the percentage of pixels above an appropriate threshold value.

Both the glomerular and external plexiform layers demonstrated a decrease in MBP levels during demyelination then an increase during remyelination (Figure 5.6C). A repeated measures ANOVA was used to determine significant differences (detailed statistics in Appendix C.4 on p215). These differences occurred in both the glomerular layer (decreases from control to 3-week cuprizone ($p = 0.001$), 6-week cuprizone ($p \leq 0.001$) or remyelination ($p = 0.041$) mice, and an increase from 6-week cuprizone to remyelination mice ($p = 0.048$)) and external plexiform layer (decrease between control and 6-week cuprizone mice ($p = 0.002$)). The granular layer followed similar trends, although there were greater SEMs and the trends were not always present. A subsequent review of granular layer images demonstrated heterogenous patches absent for MBP in all treatment groups, which would cause inconsistencies within groups and likely explain the non-significant results.

TMEV sections were obtained from SJL mice that received TMEV or sham injections and were sacrificed 3, 7 or 14 days later. This timeline fitted with the initial phase of TMEV-induced demyelination, and had the expectation of demyelination peaking after 7 days then resolving (described in the Introduction on p16). The sham brains were considered collectively for analysis.

In contrast to the consistent MBP immunohistochemistry following cuprizone treatment, TMEV varied greatly between mice within a given treatment group (Figure 5.7A and B). The trend in many layers and antero-posterior regions did, however, follow the expectation for MBP levels to be minimal in Day 7 TMEV sections (Figure 5.7C). A repeated measures ANOVA was once again used and only revealed significant

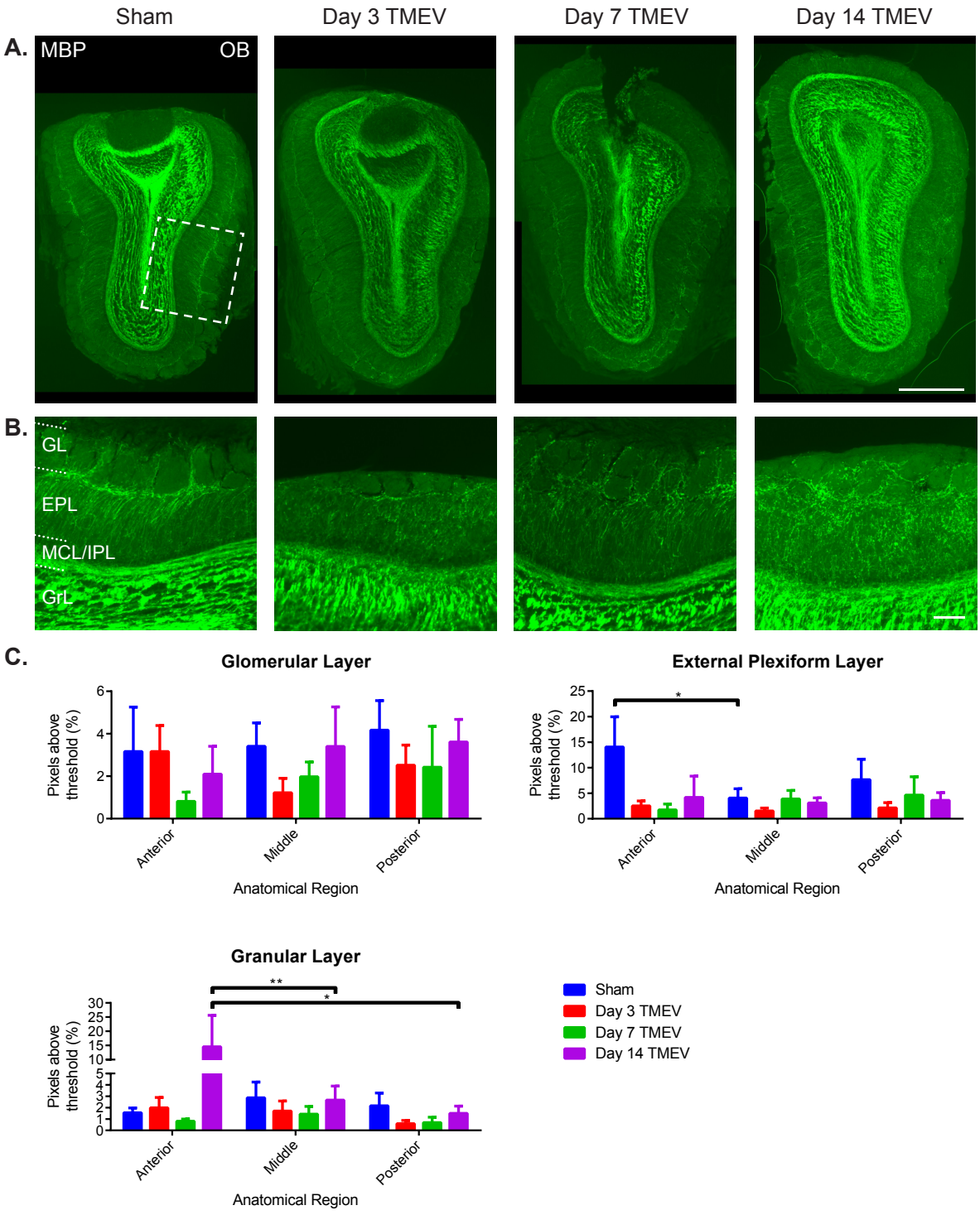


Figure 5.7: **TMEV causes less consistent demyelination then remyelination in the OB than cuprizone. A and B,** OB sections with MBP immunohistochemistry from mice 3, 7 and 14 days after TMEV or sham injection. Dotted box shows region of images in B. GL: glomerular layer, EPL: external plexiform layer, MCL/IPL: mitral cell layer/internal plexiform layer, GrL: granular layer. Scale bars 500μm (A) and 100μm (B). **C,** Graphs showing percentage of pixels with fluorescence intensity above threshold in the glomerular, external plexiform and granular layers. Statistics calculated as repeated measures ANOVA with N values detailed in Table C.18 on p218. Graphs show mean $\pm$ SEM. *p $\leq$ 0.05, **p $\leq$ 0.01.

differences between antero-posterior regions (detailed statistics in Appendix C.5 on p218). Those differences were between anterior and middle regions for the external plexiform layer in sham sections ($p = 0.022$), and between anterior and middle ($p = 0.010$) or anterior and posterior ($p = 0.014$) regions for the granular layer in Day 14 TMEV sections. There were no significant differences between treatment groups (Tables C.20 on p219 and C.22 on p222).

5.3 Discussion

In this chapter, I focused on the role of Gal-3 in oligodendrogenesis in the SVZ and CC. I showed that Gal-3 enhances neuronal differentiation in vitro, and its absence increases MBP levels in layer 6 of the motor cortex after cuprizone treatment. Gal-3 did not, however, affect oligodendrocyte density or maturation after cuprizone treatment.

5.3.1 Gal-3 role in neuronal differentiation

Through comparing Gal-$3^{+/+}$ and Gal-$3^{-/-}$ cells in a neurosphere differentiation assay, I demonstrated that Gal-3 enhances neuronal differentiation: the proportion of SVZ cells becoming neurons is ∼15% in Gal-$3^{-/-}$ cells compared to ∼30% in Gal-$3^{+/+}$ cells. A previous study had focused on oligodendrocytes, and reported that rGal-3 increases the oligodendrocyte proportion from ∼8% to ∼12% (Pasquini et al., 2011). My results showed a similar trend for oligodendrocytes between Gal-$3^{+/+}$ and Gal-$3^{-/-}$ cells but it was non-significant.

These results are relevant in considering the therapeutic potential of the SVZ. As an example, Cate et al. (2010) showed an opposite effect for BMP4, which increases the numbers of astrocytes derived from SVZ cells. This effect occurred both in vitro and in vivo during cuprizone-induced demyelination. By antagonising BMP4 during cuprizone treatment with an intraventricular infusion of Noggin, they decreased astrocyte and increased oligodendrocyte numbers in the SVZ. In a follow-up study, they showed that a Noggin infusion increased CC remyelination (Sabo et al., 2011). The same possibilities exist for Gal-3, and similar in vivo studies should be considered once an appropriate treatment dose is determined.

Interestingly, in one of the current experiments, the increase in neurons in Gal-$3^{+/+}$ cells was reciprocated by a decrease in astrocytes. This finding might explain the reactive astrocytosis seen in vivo in Gal-$3^{-/-}$ mice. Although that finding was not replicated in the previous chapter, both Comte et al. (2011) and Hoyos et al. (2014)

reported it.

A surprising result was that rGal-3 did not replicate the genotypic difference. It is possible that the concentrations (0.1 to 1μg/mL) were too low, especially when compared to the 5 to 10μg/mL typically used by Pasquini et al. (2011). Dr James had, however, used the current concentrations for in vitro experiments with significant biological effects (James, 2012). In particular, in a pilot differentiation experiment that she and I worked on, we found a similar neurogenic shift. It may be worthwhile attempting the experiment with higher concentrations of rGal-3 or with nucleofection of the pCAGIG-Gal-3 overexpression vector previously mentioned.

One intriguing finding from the oligodendrocyte cell line experiments by Pasquini et al. (2011) is their observation that mature oligodendrocytes upregulated Gal-3 expression. Dr James had shown a similar in vitro finding by performing co-immunohistochemistry with O4 and Gal-3 antibodies on neurospheres (James, 2012). In the previous chapter, however, I showed that Gal-3 is not expressed by Olig2+ oligodendrocytes in vivo. Comte et al. (2011) also did not report Gal-3 expression in oligodendrocytes in vivo. It is possible that Gal-3 behaves differently in vitro to in vivo. This limitation needs to be considered in interpreting these results.

5.3.2 Increased MBP in layer 6 of the Gal-3$^{-/-}$ motor cortex

While MBP levels increased in layer 6 of the Gal-3$^{-/-}$ motor cortex after cuprizone treatment, this finding requires careful interpretation. Preliminary electron microscopy results that I have obtained with Alec Noar, an undergraduate rotation student, suggest that myelin levels are higher after 6-weeks cuprizone in Gal-3$^{+/+}$ rather than Gal-3$^{-/-}$ mice. In the remyelination treatment group, electron microscopy suggests equal levels between genotypes. Electron microscopy is considered the 'gold-standard' for interpreting myelin levels and those results might invalidate this finding. At the same time, however, this MBP immunohistochemistry experiment was conducted under blinded and controlled conditions.

One aspect to consider is that MBP expression does not necessarily demonstrate the same outcome as electron microscopy. MBP is one of many proteins within the myelin sheath, whereas electron microscopy provides structural resolution of the myelin sheath layers (Smith, 1992). It is the latter that matters most physiologically in nerve conduction, which is why it is considered the 'gold standard'.

The existing literature does not definitively suggest that the result should be one or the other. As discussed in the Introduction and previous chapter, Gal-3 is broadly considered to increase inflammation, although it does not do so in the SVZ or CC here. If there is increased inflammation in the cortex in Gal-$3^{+/+}$ mice then a greater degree of demyelination might be expected. Hoyos et al. (2014) and Pasquini et al. (2011) both suggested that Gal-$3^{+/+}$ mice have better myelin integrity than Gal-$3^{-/-}$ mice, which presents an argument for a greater degree of demyelination in Gal-$3^{-/-}$ mice. It should be noted that in both the MBP and electron microscopy experiments, the extent of myelination appeared equal in control mice.

An appropriate biological question is whether the SVZ has any relevance to the cortex. Goings et al. (2004) used retroviruses to label SVZ cells and then showed their presence in cortical regions after cortical aspiration injury. In a subsequent study, Sundholm-Peters et al. (2005) showed that this cortical migration does not come at the expense of the usual RMS migration to the OB. It therefore appears possible for SVZ cells to migrate to the demyelinated cortex. The counter argument, however, is that local, parenchymal OPCs contribute to cortical remyelination. Dawson et al. (2003) showed that OPCs exist in the cortex, and separate studies have shown they are activated by demyelination (Fancy et al., 2004; Levine and Reynolds, 1999). As mentioned earlier though, Xing et al. (2014) demonstrated that SVZ neural stem cells contribute to better remyelination than OPCs in the CC. The current experiments may benefit from fate-mapping studies, to track SVZ cells during cuprizone treatment and confirm if they reach the cortex.

5.3.3 Lack of Gal-3 role in oligodendrocyte differentiation

While Gal-3 impacted on MBP levels in layer 6 after cuprizone treatment, there were a number measurements that it did not impact on. It did not alter Olig2+ cell number in the SVZ, Olig2+ cell density or differentiation in the CC, or MBP levels in the CC. These findings were in contrast to the published literature about Gal-3 enhancing oligodendrocyte differentiation both in vivo and in vitro (Hoyos et al., 2014; Pasquini et al., 2011). A simple explanation for this divergence is unfortunately not clear: possibilities include the use of a different transgenic mouse as well as sampling of different regions.

It is interesting to note that Olig2+ cell numbers remained constant in the SVZ across treatment groups. If the SVZ is contributing oligodendrocytes to myelin repair, one would expect the number of Olig2+ cells to increase. Chen et al. (2012) actually reported an increase of Olig2+ cell numbers in the SVZ after 6-weeks cuprizone, although the region of SVZ defined in images in that study encompassed what the current study considers CC. Jablonska et al. (2010), meanwhile, showed that SVZ neuroblasts can migrate into the demyelinated CC and transform into oligodendrocytes. It might be that the SVZ initially produces neuroblasts, which then migrate into the CC and differentiate into Olig2+ oligodendrocyte lineage cells at that stage.

It is also interesting to consider the different measurements across the treatment groups. Olig2+ cell density reaches a minimum after 3-weeks cuprizone, MBP reaches a minimum after 6-weeks cuprizone, and the proportion of $CC1^{high}$ oligodendrocytes continues to increase across treatment groups. It is not necessary for these measurements to follow the same pattern. For example, the increase in Olig2+ cell density between 3 and 6-weeks may represent non-myelinating oligodendrocyte lineage cells. These non-myelinating cells may then mature as $CC1^{high}$ oligodendrocytes and begin to myelinate once the cuprizone has ceased. Hoyos et al. (2014) actually referred to spontaneous remyelination occurring between 5 and 6-weeks of cuprizone treatment, even though cuprizone continued. This observation may be reflected in the current

study by the increase in Olig2+ cells between 3 and 6-weeks.

A question remains, however, about where the increase in Olig2+ cells comes from as well as how the majority are mostly mature. The sample region in these experiments was the medial CC, and the previous chapter showed a lack of increase in PHi3+ cells in the same location. It is possible that the cells migrate into the medial CC after proliferating elsewhere. It is also possible that the time points sampled missed a transient increase in proliferation as well as an increase in less mature oligodendrocytes. Future experiments may benefit from a broader range of time points as well as less mature oligodendrocyte markers like PDGF-Rα.

5.3.4 Demyelination in the OB in animal models

These experiments demonstrated demyelination and remyelination in the OB in both the cuprizone and TMEV demyelination models, which mapped onto human findings by DeLuca et al. (2014). In the current study, the cuprizone results were exceptionally consistent within treatment groups, while the TMEV results were less consistent. It is possible that there were slight variations in the anatomic location of TMEV inoculations, leading to differences in viral load, inflammation and demyelination. Goings et al. (2008) reported similar variability in CD45+ cell activation after TMEV. Cuprizone, in contrast, was administered in chow to all mice; assuming mice consumed a consistent amount of chow relative to their weight, they would receive a constant, weight-adjusted dose. The layer specific findings here provide more detail than Silvestroff et al. (2010) and Yang et al. (2009) previously reported after cuprizone treatment. They also add to the knowledge of TMEV having the capacity to infect the brain via the OB (Wada and Fujinami, 1993). The demyelination was most remarkable in the glomerular layer, which is where olfactory receptor neurons synapse with the central output neurons of the OB. Olfactory dysfunction is a known symptom of MS, which these results may also explain (Lutterotti et al., 2011; Rolet et al., 2012).

The reason for such extensive OB demyelination may be two-fold. Firstly, through

the demyelination that occurs there: the CD68-GFP+ cells in the OB in the previous chapter suggest that extensive inflammation is present. Secondly, through decreased regeneration from the SVZ: the previous chapter also showed decreased SVZ proliferation during cuprizone treatment. Tepavčević et al. (2011) suggested similar by demonstrating that EAE can decrease SVZ proliferation leading to reduced OB neurogenesis.

When comparing the extensive OB demyelination to other regions, it is interesting that the OB and cortex exhibit more change in MBP than the CC. It most likely reflects the larger quantity of MBP, and myelin, contained in the CC to begin with. It is in fact possible that there is more absolute demyelination in the CC but that it is masked by remaining myelin. Acs et al. (2013) also hypothesise that regional differences in copper containing enzymes cause different effects. Their results are, however, inconsistent in proving this hypothesis. As mentioned in the previous paragraph, the dual effect of increased inflammation and decreased neurogenesis may explain why OB demyelination is particularly prominent.

5.3.5 Conclusion

Gal-3 enhances neuronal differentiation, and its absence increases MBP levels in layer 6 of the motor cortex. Interestingly, the current study contradicted previous findings about Gal-3 having an effect on oligodendrocyte differentiation. It will be worthwhile revisiting the MBP results once the electron microscopy results are finalised. The prospect of using Gal-3 to enhance neurogenesis, or switching it off to enhance myelination, provides hope for future therapeutic application.

6

Galectin-3 and its role in migration

Contents

6.1 Introduction 127

6.1.1 Migration of SVZ neuroblasts to the CC 127

6.1.2 Migration of immune cells to the CC 128

6.1.3 Research questions 129

6.2 Results 130

6.2.1 Gal-3 absence increases the number of ectopic neuroblasts in the CC after TMEV in SJL mice 130

6.2.2 Gal-3 absence increases SVZ cells migrating to the CC after cuprizone treatment 132

6.2.3 Gal-3 does not demonstrate a motogenic or chemoattractive effect on neuroblasts in vitro 135

6.2.4 Gal-3 absence does not alter candidate migratory gene expression 137

6.2.5 Gal-3 does not attract murine macrophages in vitro 140

6.3 Discussion 143

6.3.1 Migration of SVZ cells to the CC in the cuprizone model 143

6.3.2 Increased migration to the CC in Gal-$3^{-/-}$ mice 144

6.3.3 Lack of in vitro effect of Gal-3 on migration 146

6.3.4 Conclusion 147

6.1 Introduction

For the SVZ to contribute to oligodendrogenesis in the CC, SVZ cells must migrate tangentially to the CC. This migration is in contrast to the usual rostral migration of SVZ neuroblasts along the RMS to the OB. Gal-3 is known to affect the migration of neuroblasts through the RMS under non-diseased conditions (Comte et al., 2011). This chapter therefore examines the role of Gal-3 on neuroblast migration to the CC in demyelination.

6.1.1 Migration of SVZ neuroblasts to the CC

It is worthwhile considering the normal migration of SVZ cells along the RMS to the OB. They migrate in chains and use astrocytes to guide them (Doetsch and Álvarez-Buylla, 1996; Rousselot et al., 1995). The fastest cells travel along the RMS at $\sim$80μm/hour (Nam et al., 2007). Their typical movement, however, can be extremely stochastic and involves them changing direction continuously (Martinez-Molina et al., 2011; Nam et al., 2007). Comte et al. (2011) showed that Gal-3 has a role in maintaining rostral migration under non-diseased conditions. They used two-photon microscopy to demonstrate that neuroblasts in Gal-$3^{-/-}$ mice migrate slower and with less directionality than in Gal-$3^{+/+}$ mice. Gal-$3^{-/-}$ mice then have fewer cells that reach the OB in vivo. Comte et al. also used explant RMS cultures to show increased migration with rGal-3 in vitro and decreased migration with a function blocking Gal-3 antibody.

The radial migration of SVZ cells to the CC after cuprizone treatment has been shown with a fate-mapping technique (Xing et al., 2014). The SVZ also contributes to CC oligodendrogenesis in the EAE and lysolecithin demyelination models (Nait-Oumesmar et al., 1999; Picard-Riera et al., 2002). There is unfortunately no published live imaging of adult SVZ cells migrating into the CC. There is, however, neonatal data that suggests SVZ cells migrate tangentially along blood vessels (Le Magueresse et al., 2012). Those authors hypothesise that the development of the RMS glial sheath and a decrease in

CC blood vessel density reduce radial migration as mice get older.

Multiple factors are known to contribute to the altered SVZ cell migration. Ciliary neurotrophic factor (CNTF) exemplifies a chemoattractant: its levels are raised in the CC after lysolecithin-induced demyelination, and it exerts a chemoattractive effect in vitro (Vernerey et al., 2013). When it is expressed in the non-diseased CC, through transplantation of CNTF-expressing HEK cells, it causes SVZ cells to migrate to the CC. In contrast, the chemokine receptor CXCR4 facilitates migration: it is expressed by Olig2+ oligodendrocytes and its knockdown with shRNA reduces the number of oligodendrocytes migrating to the CC (Banisadr et al., 2011). The growth factor EGF also plays a role: it increases SVZ cell proliferation generally, and its infusion into the lateral ventricles specifically enhances SVZ cell differentiation as oligodendrocytes and migration to the CC (Doetsch et al., 2002; Gonzalez-Perez et al., 2009).

The question arises whether Gal-3 has a similar effect, especially given its levels increase in the CC during cuprizone treatment. Paradoxically, however, Dr James showed in a preliminary experiment in TMEV treated C57Bl6 mice that Gal-3 absence increases the number of neuroblasts migrating into the CC (James, 2012). That experiment was, however, performed in the TMEV resistant C57Bl6 strain rather than the susceptible SJL strain. I was therefore keen to investigate that effect in the SJL strain, as well as the cuprizone model. I also wanted to investigate for potential mechanisms for this effect.

6.1.2 Migration of immune cells to the CC

The other key migration that occurs during cuprizone treatment involves microglia and macrophages. Sano et al. (2000) showed in human macrophages that rGal-3 was a motogen at low concentrations yet a chemoattractant at higher concentrations. The distinction is that a chemoattractant causes cells to migrate towards it, yet a motogen encourages movement in all directions. As Sano et al. investigated human cells, I wanted to see if this observation also occurred in mice.

6.1.3 Research questions

This chapter therefore aimed to answer the following questions:

- Does Gal-3 impact on the migration of neuroblasts to the CC in the cuprizone and TMEV demyelination models?
- Does Gal-3 act as a motogen or chemoattractant in vitro?
- What are the mechanisms by which Gal-3 exerts its effects on migration?
- Does Gal-3 chemoattract macrophages?

6.2 Results

6.2.1 Gal-3 absence increases the number of ectopic neuroblasts in the CC after TMEV in SJL mice

Initially I examined migration in sections obtained from TMEV treated SJL mice. As mentioned above, Dr James had demonstrated that TMEV treated C57Bl6 mice have more ectopic Dcx+ neuroblasts in the CC in the absence of Gal-3 (James, 2012). She also found an increase of ectopic neuroblasts in the striatum of Gal-$3^{-/-}$ mice. In counting the cells, the definition for an ectopic neuroblast involved it being at least 50μm from the neighbouring SVZ region.

The CC in the SJL strain revealed a similar increase of ectopic neuroblasts in Gal-$3^{-/-}$ compared to Gal-$3^{+/+}$ mice (Figure 6.1A; N $\geq$ 3 for each treatment group and genotype). While the levels were similar for shams (3.17 $\pm$ 1.13 cells for Gal-$3^{+/+}$ vs 3.24 $\pm$ 0.88 for Gal-$3^{-/-}$), they then diverged for mice inoculated with TMEV after 3 days (2.20 $\pm$ 0.92 vs 4.89 $\pm$ 1.09), 7 days (2.62 $\pm$ 0.83 vs 6.53 $\pm$ 2.23) and 14 days (2.19 $\pm$ 1.23 vs 8.44 $\pm$ 3.07). A two-way ANOVA demonstrated a significant main effect for genotype ($F(1,35) = 10.262$, $p = 0.003$). There was no significance for a difference relating to treatment group ($F(3,35) = 0.946$, $p = 0.429$ for main effect; $F(3,35) = 1.787$, $p = 0.168$ for interaction with genotype).

The striatum showed no difference in ectopic neuroblasts between Gal-$3^{+/+}$ and Gal-$3^{-/-}$ mice (Figure 6.1B). The cell counts were roughly equal in shams (0.50 $\pm$ 0.14 cells for Gal-$3^{+/+}$ vs 1.19 $\pm$ 0.51 for Gal-$3^{-/-}$), as well as mice inoculated with TMEV after 3 days (0.60 $\pm$ 0.31 vs 0.67 $\pm$ 0.33), 7 days (1.29 $\pm$ 0.75 vs 1.13 $\pm$ 0.45) and 14 days (2.29 $\pm$ 1.26 vs 2.56 $\pm$ 0.40). A one-way ANOVA demonstrated no significance for a main effect of treatment group ($F(3,35) = 1.761$, $p = 0.173$) or genotype ($F(1,35) = 0.147$, $p = 0.703$), nor an interaction between treatment group and genotype ($F(3,35) = 0.124$, $p = 0.945$).

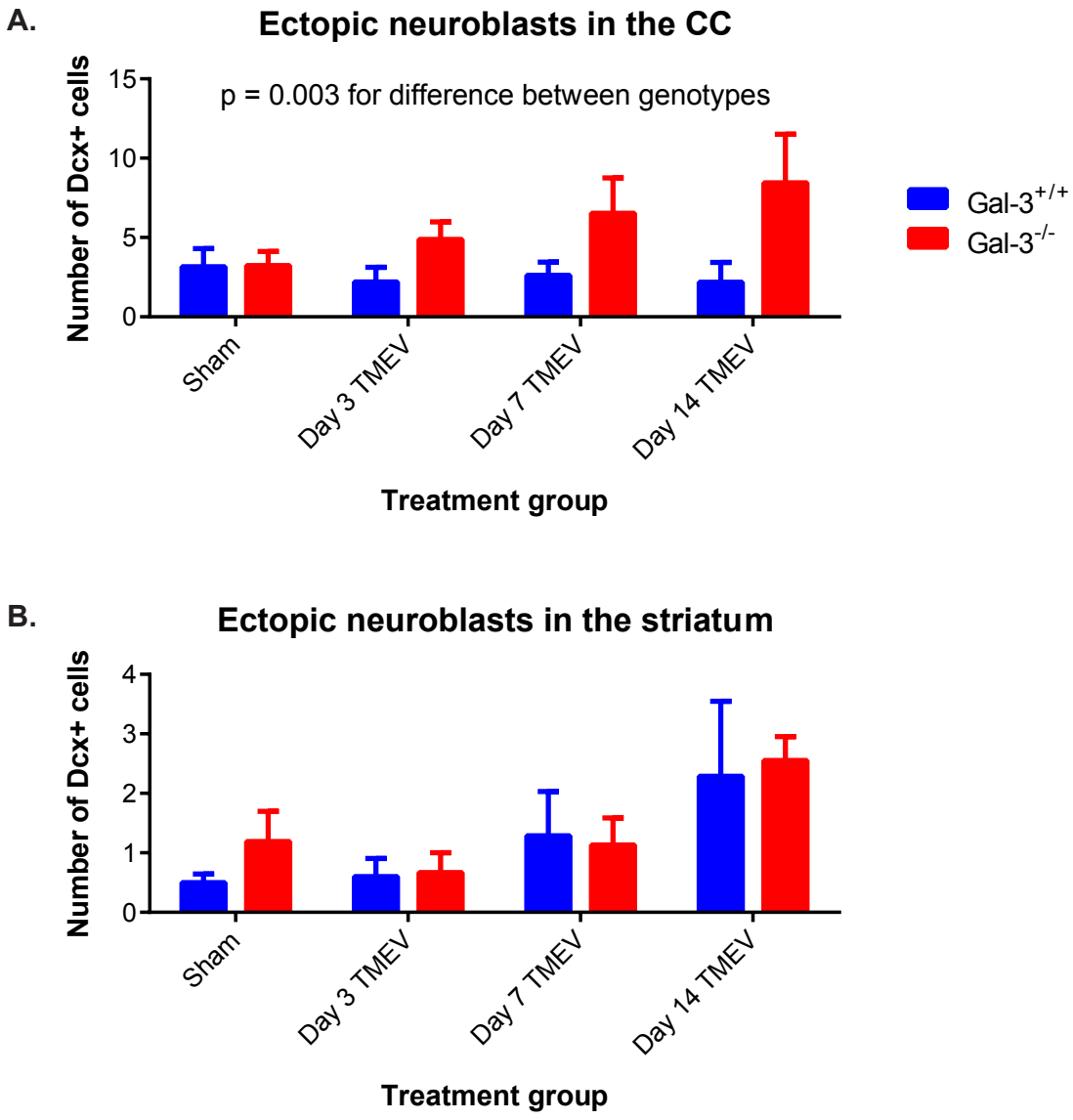


Figure 6.1: **Gal-3 absence increases the number of ectopic neuroblasts in the CC after TMEV in SJL mice. A and B,** Graphs demonstrating number of Dcx+ cells in the CC (A) and striatum (B) following TMEV in SJL Gal-$3^{+/+}$ and Gal-$3^{-/-}$ mice. Statistics calculated as two-way ANOVA with N $\geq$ 3. Graphs show mean $\pm$ SEM.

6.2.2 Gal-3 absence increases SVZ cells migrating to the CC after cuprizone treatment

Next I investigated if a similar migratory effect occurred after cuprizone treatment. To track SVZ cells, I administered six 12-hourly doses of IP BrdU to mice at the commencement of treatment (Figure 6.2A). As BrdU labels cells through incorporation into DNA as a thymidine analogue (Eidinoff et al., 1959), it only labels cells in S phase of the cell cycle. The majority of cells in the adult brain are quiescent and do not incorporate BrdU. As some SVZ cells are multiplying, they will incorporate BrdU and become label-retaining cells. The examination of BrdU+ cells at the time of sacrifice gives a readout of both SVZ cell proliferation and migration. There were, however, no genotypic differences in proliferation (see Section 4.2.7 on p84), suggesting that any differences in BrdU+ cells between Gal-$3^{+/+}$ and Gal-$3^{-/-}$ mice would be due to migration.

To analyse the BrdU+ cells, I counted cells in multiple SVZ and CC regions (Figure 6.2B), and then performed a repeated measures ANOVA. The results are quite complex and are detailed in Appendix C.6 on p224. There are, however, some important observations to point out.

Like the TMEV results, the data suggested a trend of BrdU+ cells increasing in the CC as well as decreasing in the SVZ in the absence of Gal-3 (Figure 6.2C to F). After statistical analysis though, the only significant differences for genotype occurred in the SVZ (Table C.25 on p225). With further breakdown using pairwise comparisons, the key genotypic difference was fewer BrdU+ cells in the Gal-$3^{-/-}$ compared to Gal-$3^{+/+}$ SVZ after 3-weeks cuprizone ($p < 0.0005$; Table C.26 on p226). Another statistical interaction revealed that this genotypic difference after 3-weeks occurred specifically in the dorsolateral ($p = 0.001$; Table C.30 on p228) and ventral ($p = 0.006$) SVZ.

As would be expected due to their migration away, the number of BrdU+ cells in the SVZ decreased with longer experiment duration. In all combinations of treatment (control or cuprizone) and genotype (Gal-$3^{+/+}$ or Gal-$3^{-/-}$), there were significant

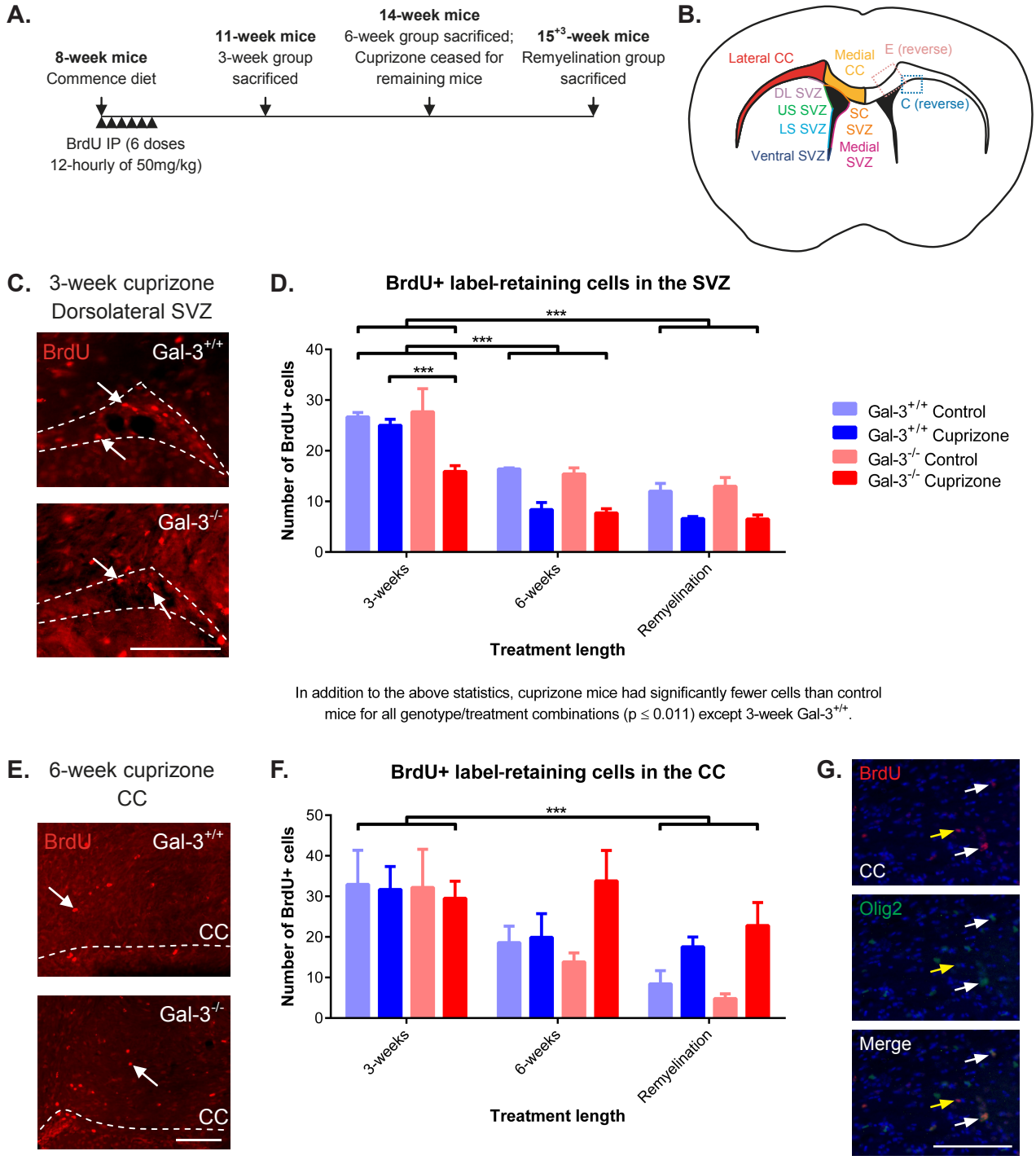


Figure 6.2: **Gal-3 absence increases SVZ cells migrating to the CC after cuprizone treatment. A,** BrdU regimen administered to mice. **B,** Coronal brain regions examined in the SVZ and CC. DL: dorsolateral, LS: lower striatal, SC: subcallosal, US: upper striatal. Dotted boxes show regions of images in C and E. **C and E,** Representative images showing differences in BrdU immunohistochemistry between Gal-$3^{+/+}$ and Gal-$3^{-/-}$ mice in the dorsolateral SVZ (C) and CC (E). White dotted lines delineate region of interest. White arrows show example BrdU+ cells. **D and F,** Quantification of BrdU+ cells overall in the SVZ (D) and CC (F). Statistics calculated as repeated measures ANOVA with N $\geq$ 3. Further statistics in Appendix C.6 on p224. Graphs show mean $\pm$ SEM. ***p $<$ 0.005. **G,** Images demonstrating co-localisation of BrdU and Olig2 immunohistochemistry. White arrows show BrdU+/Olig2+ cells. Yellow arrows show BrdU+/Olig2- cell. Scale bars 100μm.

decreases from 3-weeks to 6-weeks and 3-weeks to remyelination ($p < 0.0005$ for all; Table C.28 on p227). The decreases from the 6-week to remyelination treatment groups were not significant (p-values in Table C.28). A similar observation occurred for each combination of region (dorsolateral, upper striatal, lower striatal, ventral, septal and subcallosal SVZ) and genotype, whereby there were decreases from 3-weeks to 6-weeks and 3-weeks to remyelination. The p-values, including which comparisons were significant, are provided in Table C.31 on p229.

The number of BrdU+ cells in the SVZ mostly decreased from control to cuprizone mice, suggesting they had migrated away. This effect did not occur in Gal-$3^{+/+}$ mice after 3-weeks ($p = 0.344$). It resulted in significance for all other subgroup combinations of length (3-weeks, 6-weeks and remyelination) and genotype ($p \leq 0.011$; Table C.27 on p226). Interestingly, when looking at regions, the number of BrdU+ cells actually increased in the subcallosal SVZ from control to cuprizone mice ($p < 0.0005$). This region neighbours the CC and the increase could reflect proliferation as part of a reparative mechanism. For all other SVZ regions, the number of BrdU+ cells decreased ($p \leq 0.006$ for all; Table C.29 on p227).

The number of BrdU+ cells in the CC had its own patterns. There were decreases with longer experiment duration, although a significant decrease only occurred between the 3-week and remyelination treatment groups ($p = 0.001$; Table C.32 on p230). When comparing control and cuprizone mice, there was an increase after cuprizone treatment in the medial CC ($p = 0.007$; Table C.33 on p230). The number of cells in the lateral CC did not change significantly from control to cuprizone mice ($p = 0.852$).

While these changes in BrdU+ cells are interesting, a crucial question remains: what is the identity of these cells? Based on the TMEV results, I hypothesised that the BrdU+ cells in the CC could be Dcx+ neuroblasts. When performing a co-immunohistochemistry stain with anti-Dcx and BrdU antibodies, however, there were very few ectopic Dcx+ cells in the CC in any condition. In addition, the BrdU+ cells were often some distance from the SVZ, whereas Dcx+ ectopic neuroblasts in the CC are usually close to the SVZ. I therefore co-labelled with anti-Olig2 antibody and,

across a sample of brains (N = 3 per group), found most BrdU+ cells were Olig2+ (Figure 6.2G; 56%; 117 out of 208 cells). Occasionally BrdU+ cells were also CD45+.

6.2.3 Gal-3 does not demonstrate a motogenic or chemoattractive effect on neuroblasts in vitro

To determine how Gal-3 exerts its effect on migration, I performed in vitro RMS explant migration assays. They involved culturing RMS explants suspended in a 3D Matrigel structure in the presence of a chemical gradient. Neuroblasts migrated out in all directions, and were analysed by measuring the area occupied by neuroblasts in four quadrants (Figure 6.3A and B). Chemoattractive and chemorepulsive effects were examined by comparing the ratio of areas occupied in the proximal:distal quadrants, while motogenic effects were determined by calculating the total area the neuroblasts occupied.

A number of techniques were used to establish the chemical gradient. Initially vertical pipette tips were placed at each end of a well in a 12 well plate (described by Zhou et al., 2007). They were then filled with agarose, and the recombinant protein injected into the agarose so that it could diffuse out. It became apparent, however, that the recombinant protein would not diffuse in sufficient quantities from the agarose to the media and into the Matrigel. I therefore attempted injecting recombinant protein into the Matrigel using a Hamilton syringe, before switching to using agarose beads that were pre-soaked in the protein (described by Paratcha et al., 2006). The beads were placed on one side of the explant within the 3D Matrigel. I also attempted using a 2D Matrigel layer and securing the beads with vacuum grease (described by Theveneau and Mayor, 2011). Both the explants and beads, however, moved easily within the media and it was difficult to make them adhere. The agarose bead 3D Matrigel method was therefore used for the subsequent experiments.

In performing these experiments for rGal-3, I used a positive control of rSDF-1. It is a known chemoattractant of neuroblasts (Robin et al., 2006). The biological activity

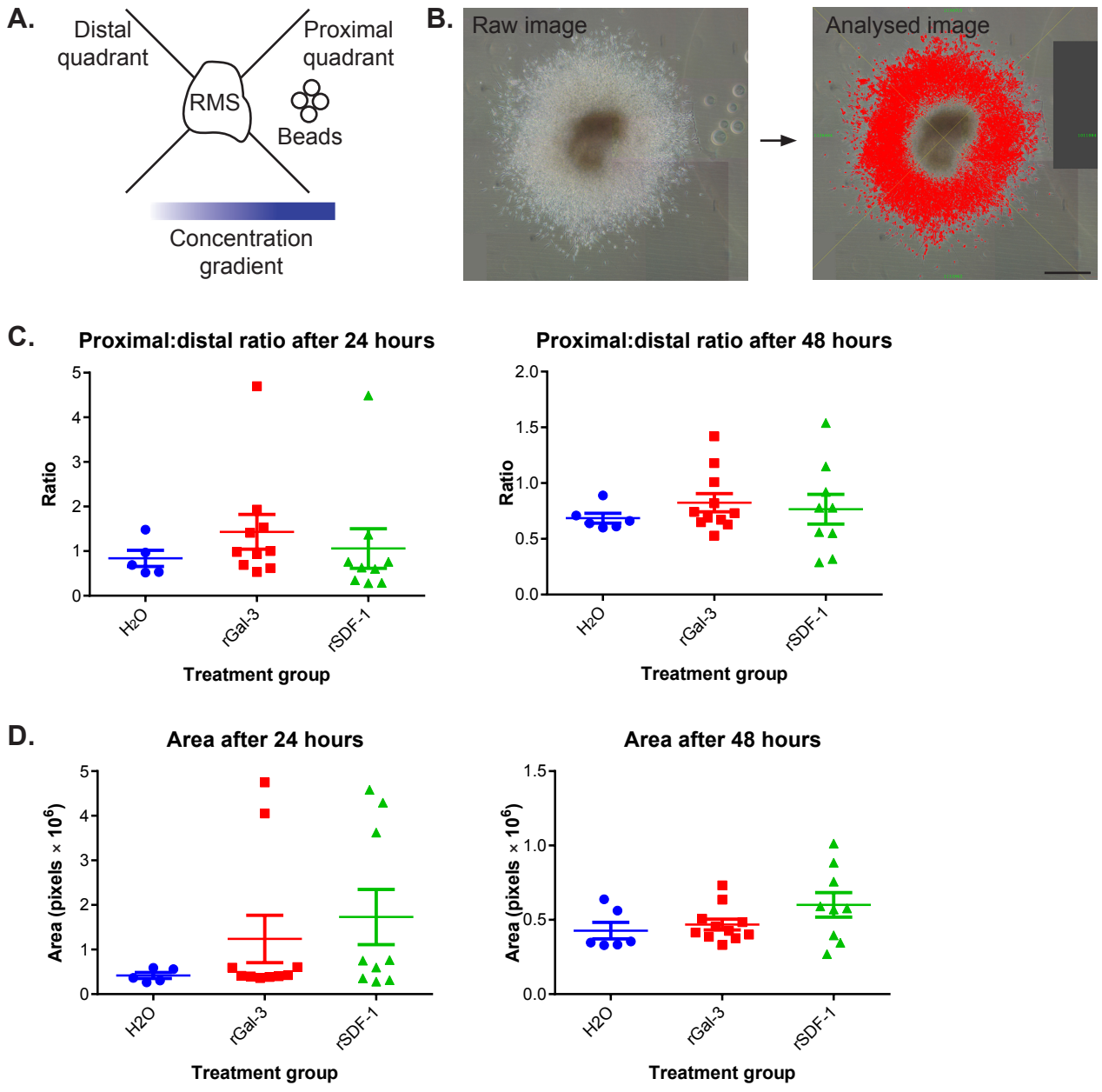


Figure 6.3: **Gal-3 does not demonstrate a motogenic or chemoattractive effect on neuroblasts in vitro. A and B,** Diagram (A) and images (B) demonstrating experiment design and analysis. Scale bar 250μm. **C and D,** Graphs showing proximal:distal ratio (C) and area of migrating neuroblasts (D) after 24 and 48-hours. Statistics were calculated using a one-way ANOVA and no significant differences occurred. Number of samples was 5 (H_2O 24-hours), 10 (rGal-3 24-hours), 9 (rSDF-1 24-hours), 6 (H_2O 48-hours), 11 (rGal-3 48-hours) and 9 (rSDF-1 48-hours). Graphs show individual data points and mean ± SEM.

of both it and rGal-3 was verified during an early pilot experiment, when the beads were inadvertently mixed thoroughly with the Matrigel. This combination resulted in recombinant protein being present throughout the Matrigel, and both the rGal-3 and rSDF-1 groups demonstrated greatly increased migration compared to H_2O controls.

In the experiments, I found a small trend for neuroblasts in the presence of both rGal-3 and rSDF-1 to migrate towards the agarose beads (Figure 6.3C, N values as per figure legend). When measured by the proximal:distal ratio, however, this trend was not significant after both 24-hours ($F(2,21) = 0.501$, $p = 0.613$ for one-way ANOVA) and 48-hours ($F(2,23) = 0.423$, $p = 0.660$). Interestingly, all explants in the control H_2O group, except for one, migrated distally. Both the rGal-3 and rSDF-1 had been diluted in H_2O, and were therefore compared to H_2O rather than considering if they were more or less than 1.

I also measured the total area migrated by the neuroblasts to see if rGal-3 or rSDF-1 impacted on motility regardless of direction. Once again there was a trend for rGal-3 and rSDF-1 to migrate further than H_2O (Figure 6.3D). It too was not significant after both 24-hours ($F(2,21) = 1.100$, $p = 0.351$) and 48-hours ($F(2,23) = 2.101$, $p = 0.145$).

6.2.4 Gal-3 absence does not alter candidate migratory gene expression

As the BrdU+ cell results suggested that Gal-3 impacts on SVZ migration, I considered possible mechanisms by comparing the SVZ expression of candidate genes in non-diseased Gal-$3^{+/+}$ and Gal-$3^{-/-}$ mice. Dr James and Dr Chris Young, another former Szele laboratory graduate student, had conducted an RT-PCR array on TMEV SVZ tissue and a proteomic array on MCAO brain homogenates respectively (James, 2012; Young et al., 2014). These arrays also compared Gal-$3^{+/+}$ and Gal-$3^{-/-}$ tissue, and provided a starting point for gene selection. The list of candidate genes was shortened to four using published literature.

The chemokine ligand CCL2 and receptor CCR2 revealed differential expression in

the arrays, and were previously shown to have a role in neuroblast migration. CCL2 increased following MCAO in Gal-$3^{+/+}$ mice (0.39 control vs 0.71 MCAO; units are pixel density as percentage of positive control), yet was increased in Gal-$3^{-/-}$ controls before decreasing in MCAO (1.33 vs 0.66). It was also upregulated following TMEV in both Gal-$3^{+/+}$ (277.6 fold expression change) and Gal-$3^{-/-}$ (187.9) mice. CCR2 had differential increases following TMEV: 17.3 in Gal-$3^{+/+}$ and 34.3 in Gal-$3^{-/-}$ mice. A previous study showed CCR2 is present on neuroblasts, while CCL2 is a neuroblast chemoattractant (Yan et al., 2007).

The matrix metallopeptidase MMP9 similarly revealed differential expression in the arrays. It increased following MCAO in Gal-$3^{+/+}$ mice (0.56 control vs 0.84 MCAO), and increased in Gal-$3^{-/-}$ controls before decreasing after MCAO (2.22 vs 1.28). It was not included in the TMEV array. It is, however, known to cleave Gal-3 and is a chemoattractant for neuroblasts (Barkho et al., 2008; Ochieng et al., 1994).

EGFR has been a longstanding interest of the Szele laboratory. It is expressed on a subset of neuroblasts that migrate slower and in more tortuous patterns (Kim et al., 2009). Its stimulation with transforming growth factor alpha also decreases motility. While EGFR was not measured in either array, its ligand EGF was only expressed in either control or MCAO Gal-$3^{-/-}$ mice: 0.00 control vs 0.00 MCAO in Gal-$3^{+/+}$ mice, 0.35 vs 0.60 in Gal-$3^{-/-}$ mice.

This experiment used the same SVZ lysates as the galectin compensation experiment between littermate Gal-$3^{+/+}$ and Gal-$3^{-/-}$ mice in Section 4.2.10 on p91 ($N = 3$ samples per genotype, each sample containing pooled SVZs from 4 mice). Once again B2m was used as a housekeeping gene and revealed no difference between genotypes ($p = 0.837$). The normalised values for the genes of the above proteins, Ccl2, Ccr2, Egfr and Mmp9, revealed no significant difference between genotypes ($p = 0.563$, $p = 0.650$, $p = 0.655$ and $p = 0.293$ respectively; Figure 6.4).



Figure 6.4: **Gal-3 absence does not alter candidate migratory gene expression** Graph showing RT-PCR comparison of SVZ Ccl2, Ccr2, Egfr and Mmp9 expression in Gal-$3^{+/+}$ and Gal-$3^{-/-}$ mice. It demonstrates fold change compared to Gal-$3^{+/+}$ mice for quantities normalised to the housekeeping gene B2m. Statistics calculated as t-test with N = 3 samples per genotype, each sample containing pooled SVZs from 4 mice. No significant differences. Graph shows mean ± SEM.

6.2.5 Gal-3 does not attract murine macrophages in vitro

This chapter also investigated the chemoattractive role of Gal-3 on murine macrophages. Sano et al. (2000) had previously shown that Gal-3 attracts human microglia and macrophages. In addition, Dr James had showed increased levels of the chemokines CCL2, CCL5, CCL8 and CXCL10 in Gal-$3^{+/+}$ compared to Gal-$3^{-/-}$ SVZ after TMEV treatment (James, 2012). She also demonstrated increased CD45+ cells in the Gal-$3^{+/+}$ compared to Gal-$3^{-/-}$ SVZ. An important mechanistic question was whether Gal-3 or the chemokines were attracting these cells. I helped to elucidate this mechanism through the ACEA xCELLigence chemotaxis assay. This experiment was done in collaboration with the Greaves laboratory, who had optimised the assay (Iqbal et al., 2013).

Initially macrophages were recruited through peritoneal irritation of mice following Biogel IP injection (Figure 6.5A). After 4 days, peritoneal lavage was performed to collect macrophages, and they were cultured overnight to enrich their proportion of total cells. Flow cytometry was used to determine the proportion: plots of forward scatter linear vs side scatter linear and forward scatter linear vs area were consistent with macrophage complexity and single-cell nature respectively (Figure 6.5B and C). Flow cytometry using the macrophage marker F4/80 confirmed the exact proportion (86.5% in this representative plot; Figure 6.5D).

The ACEA xCELLigence assay contains 8μm pores and gold electrodes below them. Cells are placed above the pores, while the chemoattractant is placed below. When cells migrate through the pores, they create an electrical impedance in the gold electrodes and that translates to an arbitrary cell index (Iqbal et al., 2013). Slope, which is calculated from the gradient between 15-90 minutes, and the difference between maximum and minimum are easily comparable parameters. Gal-3 at neither 300nM (N = 2), which had elicited an effect in human microglia and macrophages (Sano et al., 2000), nor 10nM (N = 1) exerted an effect compared to vehicle-only controls (N = 8, Figure 6.5E-G). Both CCL2 (N = 5) and CCL5 (N = 5) at 10nM were

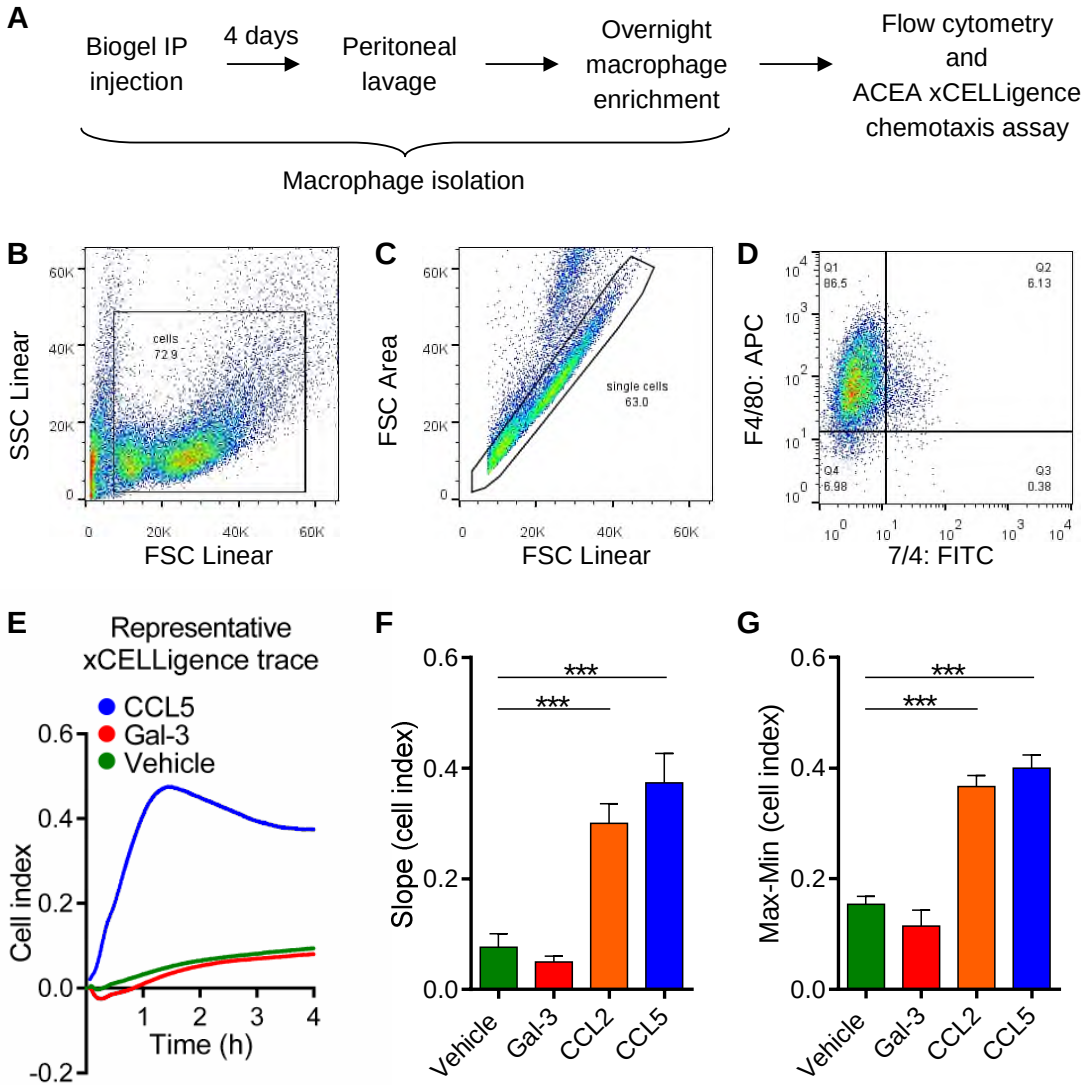


Figure 6.5: **Gal-3 does not attract murine macrophages in vitro. A** Schematic of the experiment. **B to D,** Flow cytometry graphs demonstrating successful isolation of macrophages. **E to G,** Graphs showing chemoattractive effect of Gal-3 (300nM), CCL2 (10nM) and CCL5 (10nM) with parameters as described on p140. Statistics calculated as one-way ANOVA with N values as per text. ***p $\leq$ 0.001.

chemoattractants, while CCL8 (N = 1) and CXCL10 (N = 2) at 10nM did not exert an effect (data not shown).

6.3 Discussion

In this chapter, I showed that Gal-3$^{-/-}$ mice have increased migration into the CC in both the cuprizone and TMEV demyelination models. Gal-3 did not, however, exert an effect on in vitro migration of neuroblasts or macrophages. I also found no difference in the expression of candidate migratory genes in Gal-3 absence.

6.3.1 Migration of SVZ cells to the CC in the cuprizone model

These experiments appeared to show that cuprizone caused migration of SVZ cells to the CC, regardless of the effect of Gal-3: the number of BrdU+ cells decreased in the SVZ and increased in the CC. The BrdU regimen aimed to create label-retaining cells with this purpose of tracking migration. One concern with the regimen, however, was that it could also demonstrate changes in proliferation. It needed to be considered carefully especially with correlations like both BrdU+ label-retaining cells and PHi3+ proliferating cells decreasing in the SVZ after 6-weeks cuprizone. There were, however, time points at which the BrdU+ and PHi3+ cells behaved differently. Most notably, the Gal-3$^{+/+}$ mice did not show a decrease in BrdU+ cells in the SVZ at 3-weeks or an increase in the CC at 6-weeks. PHi3+ cells did show these changes, which suggested the BrdU+ label-retaining cells reflected a different process to only proliferation. It was possible that apoptosis affected these results, and a future experiment could clarify that with TUNEL or Caspase-3 immunohistochemistry. An effect on SVZ cell migration was, however, also consistent with the literature (Xing et al., 2014).

One interesting finding was that the number of BrdU+ cells increased in the subcallosal SVZ with cuprizone treatment while decreasing in all other SVZ regions. The subcallosal SVZ is adjacent to the CC and this increase might reflect proliferation specifically for the CC. This region also reflects the developmental origin of Gsh2 derived oligodendrocytes (Kessaris et al., 2006). It is possible that they are reactivated selectively for the purpose of aiding remyelination.

6.3.2 Increased migration to the CC in Gal-3$^{-/-}$ mice

The finding of increased BrdU+ label-retaining cells in cuprizone treated Gal-3$^{-/-}$ mice could be attributed to migration with more certainty because there was no genotypic difference in proliferation. There was still the possibility of increased cell death. Once again, however, interpreting these results as a migration phenotype was consistent with the broader literature and the finding of ectopic Dcx+ neuroblasts in the CC after TMEV (Xing et al., 2014). A possible future experiment involves fluorescently labelling SVZ cells in Gal-3$^{+/+}$ and Gal-3$^{-/-}$ mice similar to Xing et al. (described on p101), which would provide a definitive answer about migration. Such an experiment could also visualise layer 6 of the motor cortex to determine if SVZ cells contribute to the increased MBP levels in Gal-3$^{-/-}$ mice.

Based on the TMEV experiments, it seemed likely that the migrating SVZ cells represented Dcx+ neuroblasts. It was therefore a surprise to see so few Dcx+ neuroblasts in the CC after cuprizone treatment. Initially I thought it might be due to the hydrochloric acid antigen retrieval used for BrdU. The limited number of Dcx+ cells was, however, consistent with the Gal-3 co-localisation studies that showed only 42 Dcx+ cells in the CC compared to 337 Gal-3+ and 436 Olig2+ cells. This co-immunohistochemistry experiment had not used hydrochloric acid. At the same time, it was interesting that more than 50% of the BrdU+ cells were in fact Olig2+ oligodendrocytes. Jablonska et al. (2010) demonstrated the capacity for Dcx+ cells to become oligodendrocytes, which possibly occurred here. One limitation in interpreting BrdU+ label-retaining cells as Olig2+ oligodendrocytes, however, is that CC Olig2+ densities did not show a significant genotypic difference. The Olig2/BrdU co-immunohistochemistry was only performed in a small number of sections and mice, and the sample size should be increased to clarify an effect.

The mechanism for the role of Gal-3 in migration requires some thought. The simple hypothesis is that Gal-3 is a chemorepellant or chemoattractant. The trouble with this hypothesis, however, is that it is not consistent with both in vivo and in vitro

findings. Ex vivo and in vitro experiments, separate to this study, suggest that Gal-3 is motogenic or chemoattractive (Comte et al., 2011). In vivo experiments suggest that Gal-3 is chemorepulsive: its level increased in the CC with cuprizone treatment, yet migration to the CC increased when Gal-3 was absent. In addition, Gal-3 was expressed in very low levels in the OB in the developmental RT-PCR, suggesting that it has little role in routine SVZ migration along the RMS.

A more complex hypothesis is that Gal-3 facilitates transport without being a chemoattractant or chemorepellant. Comte et al. (2011) showed that Gal-$3^{-/-}$ neuroblasts are more exploratory. Here I show that more SVZ cells make it to the CC. In a perplexing way, their lack of directionality could increase the likelihood of them making it to the demyelinated CC. Furthermore, Gal-3 is not actually expressed by Dcx+ neuroblasts or Olig2+ oligodendrocytes. Instead it is expressed by GFAP+ astrocytes, which are known to guide neuroblast migration (Jankovski and Sotelo, 1996). It therefore appears that Gal-3 is having a paracrine effect on these migrating cells. In the discussion below about in vitro results, I detail a possible experiment to confirm this hypothesis.

One limitation of the current experiments is the BrdU dosing. Normally when BrdU is used to create label-retaining cells, it is given before any experimental intervention. The Procedure Project Licence here, however, required the mice to have commenced cuprizone chow before an additional procedure such as BrdU injection could occur. As cuprizone was administered over 6 weeks, it was hoped that biological differences would occur after the first 60 hours and that it would not matter that BrdU was administered then. The 3-week cuprizone results suggested that was the case: there were no differences between cuprizone and control mice in both the SVZ and CC, except for Gal-$3^{-/-}$ mice in the SVZ.

6.3.3 Lack of in vitro effect of Gal-3 on migration

It was surprising that both in vitro experiments delivered negative results. Gal-3 had previously been shown to enhance macrophage migration in humans and increase the immune cell infiltrate in TMEV and EAE (James, 2012; Jiang et al., 2009; Sano et al., 2000). It had also been shown to have an effect on neuroblast migration (Comte et al., 2011). The doses used here were based on those studies. A concern is that the rGal-3, as well as the rSDF-1, were simply inactive. The increased migratory effect seen when these proteins were mixed with the 3D Matrigel was unequivocal though. The aggregation assay, whereby neurospheres clumped in the presence of rGal-3, was also unequivocal. It therefore seems unlikely that these recombinant proteins were completely inactive. Future experiments may, however, wish to try a new batch.

The RMS explant cultures also require refinement. Although the agarose bead 3D Matrigel assay has previously been described (Paratcha et al., 2006), it did not produce a robust response with rGal-3 or the positive control rSDF-1. The method received much troubleshooting attention including minimising the distance between the beads and explant. Another alternative method involves using a neurosphere that overexpresses Gal-3 to produce the chemical gradient.

An experiment that I would like to have performed involved adding rGal-3 to Matrigel while using Gal-$3^{+/+}$ and Gal-$3^{-/-}$ explants. This experiment would evaluate the effects of neuroblasts using Gal-3 as a substrate to migrate, similar to my hypothesis of them being guided by Gal-3 on astrocytes. The absence of Gal-3 in the neuroblasts should not affect their migration. The presence of a higher concentration of Gal-3 in the Matrigel should, however, increase migration. It was disappointing that no candidate migratory genes showed a difference in SVZ expression between Gal-$3^{+/+}$ and Gal-$3^{-/-}$ mice. Otherwise antibodies directed against their respective proteins could have been used to determine a mechanism for the migratory effects too.

6.3.4 Conclusion

Gal-3 appears to have a role in migration with its absence leading to more SVZ cells migrating to the CC in both the TMEV and cuprizone demyelination models. This effect could benefit demyelination greatly by recruiting more SVZ stem cells to demyelinated lesions. The experiments performed here did not confirm the results in vitro, and also did not identify a candidate gene that Gal-3 might interact with. Future experiments are therefore required to clarify these results and their mechanisms.

7

Discussion

Contents

7.1 Overall comments 149

7.1.1 SVZ response to demyelination 149

7.1.2 Gal-3 impact on the SVZ response to demyelination 151

7.1.3 Gal-3 as a therapeutic candidate 152

7.2 Limitations 154

7.2.1 Postmortem tissue samples 154

7.2.2 Cuprizone as a demyelination model 154

7.2.3 Lack of behavioural studies 156

7.3 Future ideas 156

7.3.1 Immunohistochemistry in cuprizone experiments 156

7.3.2 Floxed Gal-3 mouse 157

7.3.3 Molecular manipulation of Gal-3 157

7.3.4 Heterogeneity between SVZ regions 157

7.3.5 Exogenous stem cells 158

7.4 Concluding remarks 159

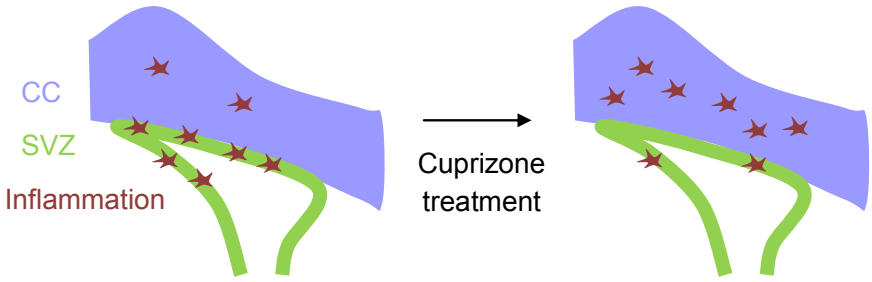
7.1 Overall comments

This thesis explored the role of Gal-3 in the SVZ response to demyelination. It specifically examined questions relating to inflammation, oligodendrogenesis and migration. An understanding of these three processes is paramount in recruiting SVZ cells to remyelinate the neighbouring CC: inflammation influences the SVZ response including proliferation; the cells arising from the SVZ need to become mature, myelinating oligodendrocytes; and these cells also need to migrate from the SVZ to the CC. The literature suggested that Gal-3 might have a role in each of these processes, which this thesis investigated through postmortem human experiments, and in vivo and in vitro murine experiments. Key findings included a role for Gal-3 in neuronal differentiation, myelination and SVZ cell migration. The thesis also demonstrated a decrease in SVZ inflammation yet increase in CC inflammation during cuprizone treatment. These key findings are summarised in Figure 7.1.

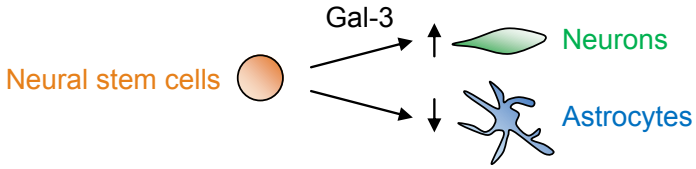
7.1.1 SVZ response to demyelination

A previous study reported that SVZ cells contribute to CC remyelination after cuprizone treatment, and in fact provide thicker myelin than local OPCs (Xing et al., 2014). The current study similarly showed that BrdU+ label-retaining cells migrate from the SVZ to the CC, and most of these cells are Olig2+ oligodendrocytes. The intriguing finding, however, was that inflammation decreased in the SVZ as it increased in the CC during cuprizone treatment (Figure 7.1A). This juxtaposition was evident through changes in the densities of CD45+ and Gal-3+ cells as well as the number of PHi3+ proliferative cells. It remains unclear whether the inflammatory effects caused, or simply correlated with, the subsequent migration from the SVZ to the CC. One possibility, which is expanded on below, is that Gal-3 normally guides neuroblasts in rostral migration along the RMS. Its decrease in the SVZ, as was apparent during cuprizone treatment, might allow more neuroblasts to migrate tangentially to the CC instead.

A. Inflammation: The SVZ becomes less inflamed, while the CC becomes more inflamed after cuprizone treatment. This effect occurs with Gal-3+ astrocytes and microglia, CD45+ haematopoietic cells, and PHi3+ proliferating cells.



B. Differentiation: Gal-3 enhances neuronal differentiation in vitro.



C. Migration: Gal-3, which is expressed by astrocytes, helps guide neuroblasts in the SVZ and RMS to the OB. Gal-3 absence can be beneficial in demyelination by allowing some neuroblasts to migrate to demyelinated regions. They may then transform into oligodendrocytes and aid remyelination.

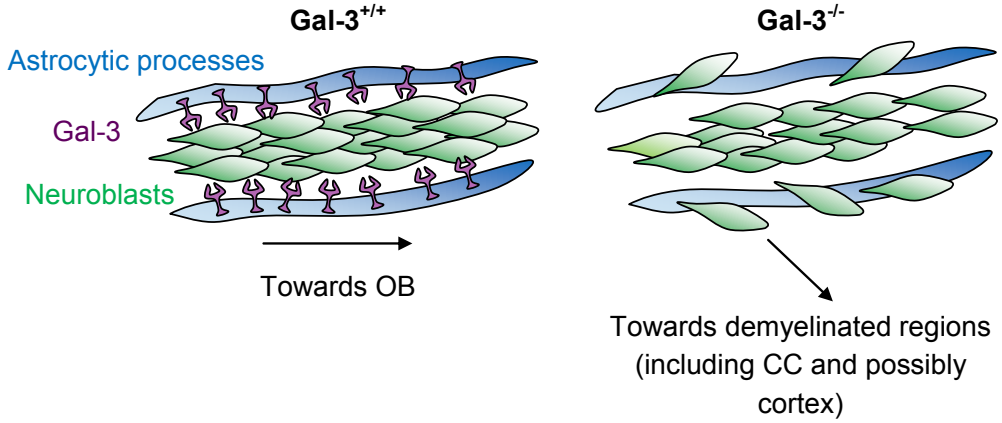


Figure 7.1: **Key findings of thesis.** Diagrams demonstrating key findings of this thesis with respect to inflammation (A), differentiation (B) and migration (C).

The role of SVZ microglia in the CC inflammatory response is also intriguing. Goings et al. (2006) reported that the SVZ contains activated microglia under normal conditions, and also showed that SVZ microglia can migrate into the CC after cortical aspiration injury. The juxtaposition between the SVZ and CC seen here suggests that the SVZ may respond to the demyelination in the CC by providing microglia. The SVZ then becomes deficient in microglia itself. This mechanism is important to understand given the potential influence of inflammation on SVZ cell migration described above, as well as the known influence of microglia on SVZ proliferation (Walton et al., 2006). The hypothesis of microglia migrating from the SVZ to the CC could be tested by tracking SVZ microglia during cuprizone treatment, including through intraventricular injection of rhodamine-labelled latex microspheres. A preliminary experiment should also clarify the proportion of pro-inflammatory M1 and anti-inflammatory M2 microglia in the SVZ and CC. It is possible that M1 microglia migrate to the CC, while M2 microglia remain in the SVZ.

7.1.2 Gal-3 impact on the SVZ response to demyelination

This thesis initially confirmed Gal-3 expression in the CC both in human MS and in mice after cuprizone treatment. Its expression also occurred constitutively in the SVZ in humans and mice, although did not increase in MS and decreased during cuprizone. The main cells to express Gal-3 were ependymal cells, astrocytes and microglia in the SVZ, and microglia, macrophages and astrocytes in the CC. These findings were largely consistent with known Gal-3 expression (Comte et al., 2011; Ho and Springer, 1982; Liu et al., 1995; Stancic et al., 2011). They importantly provide a translational link from the murine cuprizone model to human MS.

The thesis then investigated roles for Gal-3 by comparing Gal-$3^{+/+}$ and Gal-$3^{-/-}$ mice in both in vitro and in vivo experiments. Two key in vivo findings were that Gal-$3^{-/-}$ mice demonstrated more MBP fluorescence in layer 6 of the motor cortex after cuprizone treatment, and contained more emigrating SVZ cells in the CC after cuprizone and TMEV (Figure 7.1C). The proposed mechanism for these results is based

on the normal astrocyte guidance of neuroblast chain migration along the RMS to the OB (Jankovski and Sotelo, 1996). It involves Gal-3 presence on astrocytes guiding neuroblasts, which do not express Gal-3 themselves. In the absence of Gal-3, the neuroblasts can instead migrate in 'aberrant' directions including tangentially to the CC and cortex. While aberrant for routine rostral migration, this radial migration is beneficial for regeneration of the damaged CC and cortex. An experiment investigating candidate proteins, which Gal-3 might interact with for this mechanism, did not show any expression difference between Gal-$3^{+/+}$ and Gal-$3^{-/-}$ mice.

The thesis also showed that Gal-3 did not appear to have a role in inflammation, proliferation or oligodendrocyte differentiation during cuprizone treatment. Interestingly, Hoyos et al. (2014) published contradictory results as these experiments were in progress: they showed that Gal-3 enhances both microglial activation and oligodendrocyte differentiation. There was no simple explanation for these differences. Hoyos et al. did, however, perform experiments in a Gal-3 knockout mouse with exon V removed as opposed to the current knockout mouse with exons II, III and IV removed. The current project also expanded on the in vitro finding from Pasquini et al. (2011) that Gal-3 enhances oligodendrocyte differentiation. It showed that Gal-3 enhances neuronal differentiation in vitro (Figure 7.1B). The current experiments showed a non-significant trend for enhanced oligodendrocyte differentiation in vitro.

7.1.3 Gal-3 as a therapeutic candidate

Having conducted experiments on a murine disease model, an important consideration is how the findings will translate to human treatments. There are many results here that would be beneficial, at least conceptually, for MS: by increasing Gal-3 it could be possible to increase the proportion of neurons produced by the SVZ; by decreasing Gal-3 it might be possible to increase the number of neuroblasts reaching the CC. In addition, current drug candidates that inhibit Gal-3 are being developed as cancer treatments (Galectin Therapeutics, 2015). The next step in progressing towards human

therapy would involve further clarifying the effects of Gal-3 before performing animal experiments that pharmacologically alter Gal-3 levels. These experiments might involve systemic administration of pharmaceuticals intravenously or localised administration intraventricularly. The results would need to demonstrate unequivocal benefit before human trials could be considered.

The key concern with using Gal-3, however, is that it is not clearly beneficial or detrimental overall. It may be that the effect of inhibiting or enhancing Gal-3 needs to be limited to specific cell types. For example, if the main way that Gal-3 exerts an effect on migration is through its presence on astrocytes, its expression could be downregulated specifically in astrocytes. Fortunately, the use of cell-targeted technology to alter gene expression is becoming more common. Adenoviruses that express dystrophin specifically in muscle to treat Duchenne's muscular dystrophy have been researched for over twenty years (Hauser et al., 1997; Quantin et al., 1992). The CRISPR/Cas9 system holds plenty of potential for allowing genome editing (Jinek et al., 2012); as this thesis was being finalised, a controversial study reported the use of CRISPR/Cas9 to alter β-globin expression in human embryos with the view to treating β-thalassaemia (Liang et al., 2015). Before any therapeutic technique is used to alter Gal-3 in MS, however, further clarification about the role of Gal-3 is required.

The finding from this study that might be most relevant for near-future therapies is the juxtaposition of inflammation in the SVZ and CC. If inflammation influences SVZ proliferation, which both the current and previous studies suggest it does (Walton et al., 2006), then manipulating inflammation may be an easy method of altering SVZ behaviour. Lau et al. (2007) showed that corticosteroids, which are anti-inflammatory, reduce proliferation in the SVZ. Alonso (2000) similarly showed that an adrenalectomy, which decreases endogenous corticosteroid production and is thus pro-inflammatory, causes a non-significant increase in proliferation in the SVZ and a significant increase in the anterior CC. Admittedly Alonso also reported equal SVZ proliferation after corticosteroids, although Lau et al. have since demonstrated otherwise. These findings are consistent with the correlation of decreased SVZ inflammation and proliferation,

and increased CC inflammation and proliferation observed here. Corticosteroids are already a mainstay of MS treatment (see Introduction on p14), and it would be interesting to evaluate their effect on the SVZ in postmortem tissue. It might also be worthwhile investigating their effect in cuprizone treated animals.

7.2 Limitations

7.2.1 Postmortem tissue samples

The postmortem studies confirmed the expression of Gal-3 around the lateral ventricles in MS. As with any postmortem study, however, the number of cases available was limited. The eight cases and eight controls here had a variety of PMIs as well as fixation lengths. The tissue was consistent in demonstrating observed results, such as expression in acute lesions, within sections. There were, however, differences when comparing across sections and brains. It would be informative to count Gal-3+ cells in the SVZ and the CC: it would provide quantification to confirm Gal-3 increase in the CC, and would also provide preliminary evidence about an inflammatory juxtaposition in MS. This experiment was not possible with the current postmortem samples because Gal-3 DAB immunohistochemistry varied so significantly.

7.2.2 Cuprizone as a demyelination model

Cupizone is one of many animal demyelination models (see Introduction on p15 for review). They generally aim to replicate MS, although none appear to do so entirely. They therefore each have similarities and differences with MS, and these limitations must be considered in interpreting experiments.

The main advantage of cuprizone is that it causes consistent demyelination and remyelination. These experiments demonstrated that effect, especially with the clear qualitative differences in the cortex and OB. There was, however, a smaller degree of demyelination in the CC. It might be considered that the SVZ was only responding to

a mild degree of CC demyelination. At the same time, the robust difference between treatment groups for most other SVZ parameters suggests that there was a substantial SVZ response. The cuprizone dose used (0.2%) was also based on previous studies that reported more complete demyelination (Taylor et al., 2010). One difference was that these mice were 129Sv strain rather than the usual C57Bl6 strain, although the literature suggested they should in fact be affected more (Taylor et al., 2009; VonDran et al., 2011). In addition, these results were obtained with MBP immunohistochemistry and should be confirmed with electron microscopy.

The main disadvantage of cuprizone is that it maintains a BBB and lacks adaptive immune system involvement (Bakker and Ludwin, 1987; Kondo et al., 1987). The adaptive immune system roles of Gal-3 could therefore not be evaluated in the current experiments (see Introduction on p26 for review). Many Gal-3 functions are, however, to do with macrophages, which still cross the BBB during cuprizone treatment (McMahon et al., 2002). In these experiments, the Gal-3 increase in the CC was mostly associated with macrophages and microglia. Gal-3 immunohistochemistry in human tissue also predominantly appeared in macrophages. There was, however, a lack of Gal-3 influence on the inflammation present, when Gal-3 presence is known to increase immune cells present in TMEV and EAE (James, 2012; Jiang et al., 2009). These demyelination models both involve the adaptive immune system, which might be why Gal-3 causes an effect with them and not cuprizone.

Another disadvantage of this cuprizone regimen is that demyelination and remyelination occur in sequential order. A key issue in recruiting stem cells to become oligodendrocytes is progressive remyelination failure. It results from oligodendrocytes failing to mature, and is believed to be because of accumulated myelin debris and the effect of ageing (Kotter et al., 2006; Ruckh et al., 2012; Wolswijk, 1998). As the current regimen has sequential demyelination then remyelination, it does not have the same degree of remyelination failure as an alternating regimen would. Johnson and Ludwin (1981) performed an alternating regimen, and found that remyelination was slower and more varied in completeness after multiple cuprizone administration

periods. Baxi et al. (2014) proposed transferring myelin reactive effector T-cells after 4-weeks of cuprizone treatment. This intervention resulted in more CD4+ T-cells in the brain and reduced endogenous remyelination. Baxi et al. therefore suggested it provided a model to study the immune mechanisms of remyelination failure. In addition, Lampron et al. (2015) showed CX3CR1-deficient mice fail to clear myelin debris in the cuprizone model, preventing proper remyelination. In evaluating the role of Gal-3 or the SVZ more broadly after demyelination, consideration should be given to remyelination failure occurring outside the cuprizone model.

7.2.3 Lack of behavioural studies

This thesis did not conduct behavioural studies as very few isolate a CC endophenotype. Hibbits et al. (2009) previously suggested two studies after cuprizone treatment. The first involves mice running on a 'complex' wheel with varied rung intervals. It requires sensorimotor coordination between hemispheres to determine how to run and therefore tests CC functionality. The second examines the frequency of social interactions with other mice. Hibbits et al. showed differences for both studies in cuprizone treated mice compared to controls. Future experiments on Gal-3 may wish to include more behavioural studies. Given the small differences between Gal-$3^{+/+}$ and Gal-$3^{-/-}$ mice in the current experiments, however, it seems unlikely that behavioural differences would occur.

7.3 Future ideas

7.3.1 Immunohistochemistry in cuprizone experiments

As reasoned throughout this thesis, there are immunohistochemistry experiments that would further the current cuprizone findings. The inflammation juxtaposition could be extended by determining the proportions of M1 and M2 microglia in the SVZ and CC. The lack of effect of Gal-3 on oligodendrocyte maturation could be confirmed with the OPC marker PDGF-Rα. The migration experiments would benefit from comparing

the number of BrdU+ cells that reach the OB in Gal-$3^{+/+}$ and Gal-$3^{-/-}$ mice.

7.3.2 Floxed Gal-3 mouse

The characterisation of the Gal-$3^{fl/fl}$ mouse suggests that it expresses the transgene in the correct location. This mouse was unfortunately only available in the latter part of my research, and could not be incorporated into more substantial experiments. It does, however, provide two crucial opportunities for future experiments. Firstly, it can knockout Gal-3 in restricted cell populations through using a specific promoter driven Cre-recombinase. The hypothesis of ensheathing astrocytes using Gal-3 to direct migration could in theory be checked. The difficulty with this experiment, however, will be that many of the genes and corresponding promoters that specify astrocytes are also expressed in neural stem cells. Secondly, this mouse can knockout Gal-3 at a specific time by using tamoxifen inducible Cre-recombinase. Tamoxifen could, for example, be given in remyelination mice that have just ceased cuprizone. The Gal-3 specific effects on remyelination could then be evaluated.

7.3.3 Molecular manipulation of Gal-3

As discussed in the section about Gal-3 therapeutic potential, future experiments must investigate how manipulating Gal-3 levels affects demyelination outcomes. The shRNA plasmids designed will allow knockdown both in vivo and in vitro. One way to deliver them in vivo is through intraventricular injection and electroporation. The co-electroporation with fluorescent plasmids, which are normally incorporated by the same cells, will permit tracking of the Gal-3 depleted cells.

7.3.4 Heterogeneity between SVZ regions

An evolving concept is the heterogeneity within the SVZ. Merkle et al. (2007) reported that individual OB interneuron subtypes develop from specific SVZ regions. In a follow-up study, the same authors examined promoters associated with those regions

(Merkle et al., 2014). One promoter in the ventral SVZ was Nkx2.1, which is also associated with the first wave of oligodendrocytes during development (see Figure 1.2 on p3; Kessaris et al., 2006). It would be interesting to see if these Nkx2.1+ cells give rise to oligodendrocytes in the adult, and similar responses might be expected from Gsh2+ cells in the striatal SVZ or Emx1+ cells in the subcallosal and septal SVZ. The increase here of BrdU+ cells in the subcallosal SVZ after cuprizone treatment was an indication of SVZ regional specificity. The current experiments would benefit from fate-mapping studies to determine how SVZ cells contribute to oligodendrogenesis in the CC in Gal-$3^{+/+}$ and Gal-$3^{-/-}$ mice. In the broader context of oligodendrogenesis, it would be interesting to determine the molecular identity of the cells they arise from.

7.3.5 Exogenous stem cells

In addition to recruiting SVZ cells, researchers have investigated transplanting neural stem cells into the brain to treat demyelination (Pluchino et al., 2003). These cells face many of the same issues as endogenous stem cells including migration and proliferation. Given the current experiments suggest Gal-3 has a role in migration, it would be interesting to see if altering Gal-3 expression in cells before transplantation changes their site of integration. In addition, increasing Gal-3 expression could be used to drive more transplanted cells to become neurons.

Transplanted stem cells also provide the opportunity to use iPSCs or iPSC derived neurons. In thinking towards permissible human stem cell treatments, the cells used must be easily accessible. The use of dermal fibroblasts to create iPSCs is now common, and neurons can then be derived (Hu et al., 2010). It may therefore be that transplanted stem cells will have therapeutic relevance sooner than the recruitment of endogenous stem cells. In the interests of best utilising these stem cells, the knowledge of Gal-3 function in SVZ stem cells may be transferrable and should be considered in them too.

7.4 Concluding remarks

MS continues to be a debilitating disease that affects individuals and their families around the world. The progressive forms of MS, in particular, do not currently have viable treatments. The possibility of using neural stem cells provides hope to affected individuals, clinicians and researchers alike. With the aim of better utilising these cells, this thesis investigated the role of Gal-3 in the SVZ after demyelination. It demonstrated that Gal-3 has a role in neuronal differentiation and migration, and uncovered an intriguing juxtaposition of inflammation in the SVZ and CC. The hope remains that one day these cells will provide an efficient, effective and practical method of treating such disease.

Bibliography

Abrahamsson, S. V., Angelini, D. F., Dubinsky, A. N., Morel, E., Oh, U., Jones, J. L., Carassiti, D., Reynolds, R., Salvetti, M., Calabresi, P. A., et al. (2013). Non-myeloablative autologous haematopoietic stem cell transplantation expands regulatory cells and depletes IL-17 producing mucosal-associated invariant T cells in multiple sclerosis. *Brain*, 136(9):2888–2903.

Acikalin, M. F., Etiz, D., Gurbuz, M. K., Ozudogru, E., Canaz, F., and Colak, E. (2012). Prognostic significance of galectin-3 and cyclin D1 expression in undifferentiated nasopharyngeal carcinoma. *Medical Oncology*, 29(2):742–749.

Acosta-Rodríguez, E. V., Montes, C. L., Motrán, C. C., Zuniga, E. I., Liu, F.-T., Rabinovich, G. A., and Gruppi, A. (2004). Galectin-3 mediates IL-4-induced survival and differentiation of B cells: functional cross-talk and implications during trypanosoma cruzi infection. *Journal of Immunology*, 172(1):493–502.

Acs, P., Selak, M., Komoly, S., and Kalman, B. (2013). Distribution of oligodendrocyte loss and mitochondrial toxicity in the cuprizone-induced experimental demyelination model. *Journal of Neuroimmunology*, 262(1):128–131.

Adachi, K., Mirzadeh, Z., Sakaguchi, M., Yamashita, T., Nikolcheva, T., Gotoh, Y., Peltz, G., Gong, L., Kawase, T., Álvarez-Buylla, A., et al. (2007). β-catenin signaling promotes proliferation of progenitor cells in the adult mouse subventricular zone. *Stem Cells*, 25(11):2827–2836.

Ahn, S. and Joyner, A. L. (2005). In vivo analysis of quiescent adult neural stem cells responding to sonic hedgehog. *Nature*, 437(7060):894–897.

Alonso, A. and Hernán, M. A. (2008). Temporal trends in the incidence of multiple sclerosis a systematic review. *Neurology*, 71(2):129–135.

Alonso, G. (2000). Prolonged corticosterone treatment of adult rats inhibits the proliferation of oligodendrocyte progenitors present throughout white and gray matter regions of the brain. *Glia*, 31(3):219–231.

Altman, J. and Das, G. D. (1965). Autoradiographic and histological evidence of postnatal hippocampal neurogenesis in rats. *Journal of Comparative Neurology*, 124(3):319–335.

Apatoff, B. (2014). Overview of demyelinating disorders. *Merck Manual*. Retrieved from http://www.merckmanuals.com/professional/neurologic_disorders/demyelinating_disorders/overview_of_demyelinating_disorders.html.

Asgarian-Omran, H., Forghani, P., Hojjat-Farsangi, M., Roohi, A., Sharifian, R. A., Razavi, S. M., Jeddi-Tehrani, M., Rabbani, H., and Shokri, F. (2010). Expression profile of galectin-1 and galectin-3 molecules in different subtypes of chronic lymphocytic leukemia. *Cancer Investigation*, 28(7):717–725.

Azim, K., Raineteau, O., and Butt, A. M. (2012). Intraventricular injection of FGF-2 promotes generation of oligodendrocyte-lineage cells in the postnatal and adult forebrain. *Glia*, 60(12):1977–1990.

Bagert, B. A. (2009). Epstein-Barr virus in multiple sclerosis. *Current Neurology and Neuroscience Reports*, 9(5):405–410.

Bain, G., Kitchens, D., Yao, M., Huettner, J. E., and Gottlieb, D. I. (1995). Embryonic stem cells express neuronal properties in vitro. *Developmental Biology*, 168(2):342–357.

Bakker, D. A. and Ludwin, S. K. (1987). Blood-brain barrier permeability during cuprizone-induced demyelination: implications for the pathogenesis of immune-mediated demyelinating diseases. *Journal of the Neurological Sciences*, 78(2):125–137.

Banik, N. L., Gohil, K., and Davison, A. (1976). The action of snake venom, phospholipase A and trypsin on purified myelin in vitro. *Biochemical Journal*, 159:273–277.

Banisadr, G., Frederick, T. J., Freitag, C., Ren, D., Jung, H., Miller, S. D., and Miller, R. J. (2011). The role of CXCR4 signaling in the migration of transplanted oligodendrocyte progenitors into the cerebral white matter. *Neurobiology of Disease*, 44(1):19–27.

Barkho, B. Z., Munoz, A. E., Li, X., Li, L., Cunningham, L. A., and Zhao, X. (2008). Endogenous matrix metalloproteinase (MMP)-3 and MMP-9 promote the differentiation and migration of adult neural progenitor cells in response to chemokines. *Stem Cells*, 26(12):3139–3149.

Barnes, D., Hughes, R., Morris, R., Wade-Jones, O., Brown, P., Britton, T., Francis, D., Perkin, G., Rudge, P., Swash, M., et al. (1997). Randomised trial of oral and intravenous methylprednisolone in acute relapses of multiple sclerosis. *Lancet*, 349(9056):902–906.

Barros, M. H. M., Hauck, F., Dreyer, J. H., Kempkes, B., and Niedobitek, G. (2013). Macrophage polarisation: an immunohistochemical approach for identifying M1 and M2 macrophages. *PLOS ONE*, 8(11):e80908.

Baxi, E. G., Tosi, D., Kirby, L., Derbruin, J., Grishkan, I., Fairchild, A., Calabresi, P., and Gocke, A. (2014). Assessing remyelination in an inflammatory environment: a novel adoptive transfer cuprizone model. Nanosymposium 12.07. *2014 Neuroscience Meeting Planner*. Washington: Society for Neuroscience, 2014.

Bergles, D. E., Roberts, J. D. B., Somogyi, P., and Jahr, C. E. (2000). Glutamatergic synapses on oligodendrocyte precursor cells in the hippocampus. *Nature*, 405(6783):187–191.

Bernard, C. C. and Carnegie, P. R. (1975). Experimental autoimmune encephalomyelitis in mice: immunologic response to mouse spinal cord and myelin basic proteins. *Journal of Immunology*, 114(5):1537–1540.

Bernardes, E. S., Silva, N. M., Ruas, L. P., Mineo, J. R., Loyola, A. M., Hsu, D. K., Liu, F.-T., Chammas, R., and Roque-Barreira, M. C. (2006). Toxoplasma gondii infection reveals a novel regulatory role for galectin-3 in the interface of innate and adaptive immunity. *American Journal of Pathology*, 168(6):1910–1920.

Bhat, R. V., Axt, K. J., Fosnaugh, J. S., Smith, K. J., Johnson, K. A., Hill, D. E., Kinzler, K. W., and Baraban, J. M. (1996). Expression of the APC tumor suppressor protein in oligodendroglia. *Glia*, 17(2):169–174.

Bieber, A. J., Kerr, S., and Rodriguez, M. (2003). Efficient central nervous system remyelination requires T cells. *Annals of Neurology*, 53(5):680–684.

Billiau, A., Heremans, H., Vandekerckhove, F., Dijkmans, R., Sobis, H., Meulepas, E., and Carton, H. (1988). Enhancement of experimental allergic encephalomyelitis in mice by antibodies against IFN-gamma. *Journal of Immunology*, 140(5):1506–1510.

Black, J. A., Liu, S., Hains, B. C., Saab, C. Y., and Waxman, S. G. (2006). Long-term protection of central axons with phenytoin in monophasic and chronic-relapsing EAE. *Brain*, 129(12):3196–3208.

Blakemore, W. (1972). Observations on oligodendrocyte degeneration, the resolution of status spongiosus and remyelination in cuprizone intoxication in mice. *Journal of Neurocytology*, 1(4):413–426.

Blakemore, W. (1977). Remyelination of CNS axons by Schwann cells transplanted from the sciatic nerve. *Nature*, 266(5597):68–69.

Boda, E., Pini, A., Hoxha, E., Parolisi, R., and Tempia, F. (2009). Selection of reference genes for quantitative real-time rt-pcr studies in mouse brain. *Journal of Molecular Neuroscience*, 37(3):238–253.

Bonde, S., Ekdahl, C. T., and Lindvall, O. (2006). Long-term neuronal replacement in adult rat hippocampus after status epilepticus despite chronic inflammation. *European Journal of Neuroscience*, 23(4):965–974.

Boscher, C., Dennis, J. W., and Nabi, I. R. (2011). Glycosylation, galectins and cellular signaling. *Current Opinion in Cell Biology*, 23(4):383–392.

Bradley, A., Anastassiadis, K., Ayadi, A., Battey, J. F., Bell, C., Birling, M.-C., Bottomley, J., Brown, S. D., Bürger, A., Bult, C. J., et al. (2012). The mammalian gene function resource: the international knockout mouse consortium. *Mammalian Genome*, 23(9-10):580–586.

Brinkmann, B. G., Agarwal, A., Sereda, M. W., Garratt, A. N., Müller, T., Wende, H., Stassart, R. M., Nawaz, S., Humml, C., Velanac, V., et al. (2008). Neuregulin-1/erbb signaling serves distinct functions in myelination of the peripheral and central nervous system. *Neuron*, 59(4):581–595.

Brown, E. R., Doig, T., Anderson, N., Brenn, T., Doherty, V., Xu, Y., Bartlett, J. M., Smyth, J. F., and Melton, D. W. (2012). Association of galectin-3 expression with melanoma progression and prognosis. *European Journal of Cancer*, 48(6):865–874.

Brynedal, B., Wojcik, J., Esposito, F., Debailleul, V., Yaouanq, J., Martinelli-Boneschi, F., Edan, G., Comi, G., Hillert, J., and Abderrahim, H. (2010). Mgat5 alters the severity of multiple sclerosis. *Journal of Neuroimmunology*, 220(1):120–124.

Califice, S., Castronovo, V., Bracke, M., and van den Brûle, F. (2004). Dual activities of galectin-3 in human prostate cancer: tumor suppression of nuclear galectin-3 vs tumor promotion of cytoplasmic galectin-3. *Oncogene*, 23(45):7527–7536.

Carlton, W. W. (1967). Studies on the induction of hydrocephalus and spongy degeneration by cuprizone feeding and attempts to antidote the toxicity. *Life Sciences*, 6(1):11–19.

Carswell, R. (1838). *Pathological Anatomy: Illustrations of the Elementary Forms of Disease*. London: Longman, Orme, Brown, Green and Longman.

Castronovo, V., Van Den Brûle, F. A., Jackers, P., Clausse, N., Liu, F.-T., Gillet, C., and Sobel, M. E. (1996). Decreased expression of galectin-3 is associated with progression of human breast cancer. *Journal of Pathology*, 179(1):43–48.

Cate, H. S., Sabo, J. K., Merlo, D., Kemper, D., Aumann, T. D., Robinson, J., Merson, T. D., Emery, B., Perreau, V. M., and Kilpatrick, T. J. (2010). Modulation of bone morphogenic protein signalling alters numbers of astrocytes and oligodendroglia in the subventricular zone during cuprizone-induced demyelination. *Journal of Neurochemistry*, 115(1):11–22.

Charcot, J.-M. (1868). Histologie de la sclérose en plaques. *Gazette des Hopitaux, Paris*, 41:554–555.

Chen, L., Li, Z., Ping, M., Li, R., Liu, J., Xie, X., Song, X., and Guo, L. (2012). Regulation of Olig2 during astroglial differentiation in the subventricular zone of a cuprizone-induced demyelination mouse model. *Neuroscience*, 221:96–107.

Chong, S. C., Rosenberg, S. S., Fancy, S. P., Zhao, C., Shen, Y.-A. A., Hahn, A. T., McGee, A. W., Xu, X., Zheng, B., Zhang, L. I., et al. (2012). Neurite outgrowth inhibitor Nogo-A establishes spatial segregation and extent of oligodendrocyte myelination. *Proceedings of the National Academy of Sciences*, 109(4):1299–1304.

Chung, A.-Y., Kim, S., Kim, E., Kim, D., Jeong, I., Cha, Y. R., Bae, Y.-k., Park, S. W., Lee, J., and Park, H.-C. (2013). Indian hedgehog B function is required for the specification of oligodendrocyte progenitor cells in the zebrafish CNS. *Journal of Neuroscience*, 33(4):1728–1733.

Citterio, A., La Mantia, L., Ciucci, G., Candelise, L., Brusaferri, F., Midgard, R., and Filippini, G. (2000). Corticosteroids or ACTH for acute exacerbations in multiple sclerosis. *Cochrane Database of Systematic Reviews*, (4):CD001331.

Codega, P., Silva-Vargas, V., Paul, A., Maldonado-Soto, A. R., DeLeo, A. M., Pastrana, E., and Doetsch, F. (2014). Prospective identification and purification of quiescent adult neural stem cells from their in vivo niche. *Neuron*, 82(3):545–559.

Cohen, J. A., Coles, A. J., Arnold, D. L., Confavreux, C., Fox, E. J., Hartung, H.-P., Havrdova, E., Selmaj, K. W., Weiner, H. L., Fisher, E., et al. (2012). Alemtuzumab versus interferon beta 1a as first-line treatment for patients with relapsing-remitting multiple sclerosis: a randomised controlled phase 3 trial. *Lancet*, 380(9856):1819–1828.

Coles, A. J., Twyman, C. L., Arnold, D. L., Cohen, J. A., Confavreux, C., Fox, E. J., Hartung, H.-P., Havrdova, E., Selmaj, K. W., Weiner, H. L., et al. (2012). Alemtuzumab for patients with relapsing multiple sclerosis after disease-modifying therapy: a randomised controlled phase 3 trial. *Lancet*, 380(9856):1829–1839.

Colnot, C., Fowlis, D., Ripoche, M.-A., Bouchaert, I., and Poirier, F. (1998). Embryonic implantation in galectin 1/galectin 3 double mutant mice. *Developmental Dynamics*, 211(4):306–313.

Coman, I., Aigrot, M., Seilhean, D., Reynolds, R., Girault, J., Zalc, B., and Lubetzki, C. (2006). Nodal, paranodal and juxtaparanodal axonal proteins during demyelination and remyelination in multiple sclerosis. *Brain*, 129(12):3186–3195.

Compston, A. and Coles, A. (2008). Multiple sclerosis. *Lancet*, 372(9648):1502–1517.

Comte, I., Kim, Y., Young, C. C., Van Der Harg, J. M., Hockberger, P., Bolam, P. J., Poirier, F., and Szele, F. G. (2011). Galectin-3 maintains cell motility from the subventricular zone to the olfactory bulb. *Journal of Cell Science*, 124(14):2438–2447.

Confavreux, C. and Vukusic, S. (2006). Age at disability milestones in multiple sclerosis. *Brain*, 129(3):595–605.

Connick, P., Kolappan, M., Crawley, C., Webber, D. J., Patani, R., Michell, A. W., Du, M.-Q., Luan, S.-L., Altmann, D. R., Thompson, A. J., et al. (2012). Autologous mesenchymal stem cells for the treatment of secondary progressive multiple sclerosis: an open-label phase 2a proof-of-concept study. *Lancet Neurology*, 11(2):150–156.

Constantinescu, C. S., Farooqi, N., O'Brien, K., and Gran, B. (2011). Experimental autoimmune encephalomyelitis (EAE) as a model for multiple sclerosis (MS). *British Journal of Pharmacology*, 164(4):1079–1106.

Crain, J. M., Nikodemova, M., and Watters, J. J. (2013). Microglia express distinct M1 and M2 phenotypic markers in the postnatal and adult central nervous system in male and female mice. *Journal of Neuroscience Research*, 91(9):1143–1151.

Craner, M. J., Newcombe, J., Black, J. A., Hartle, C., Cuzner, M. L., and Waxman, S. G. (2004). Molecular changes in neurons in multiple sclerosis: altered axonal expression of Nav1.2 and Nav1.6 sodium channels and Na+/Ca2+ exchanger. *Proceedings of the National Academy of Sciences*, 101(21):8168–8173.

Cua, D. J., Sherlock, J., Chen, Y., Murphy, C. A., Joyce, B., Seymour, B., Lucian, L., To, W., Kwan, S., Churakova, T., et al. (2003). Interleukin-23 rather than interleukin-12 is the critical cytokine for autoimmune inflammation of the brain. *Nature*, 421(6924):744–748.

Cunningham, C. L., Martínez-Cerdeño, V., and Noctor, S. C. (2013). Microglia regulate the number of neural precursor cells in the developing cerebral cortex. *Journal of Neuroscience*, 33(10):4216–4233.

Cyranoski, D. (2014). Next-generation stem cells cleared for human trial. *Nature*. Retrieved from http://www.nature.com/news/next-generation-stem-cells-cleared-for-human-trial-1.15897.

Darlington, P. J., Touil, T., Doucet, J.-S., Gaucher, D., Zeidan, J., Gauchat, D., Corsini, R., Kim, H. J., Duddy, M., Jalili, F., et al. (2013). Diminished Th17 (not Th1) responses underlie multiple sclerosis disease abrogation after hematopoietic stem cell transplantation. *Annals of Neurology*, 73(3):341–354.

Dawson, M. R., Polito, A., Levine, J. M., and Reynolds, R. (2003). NG2-expressing glial progenitor cells: an abundant and widespread population of cycling cells in the adult rat CNS. *Molecular and Cellular Neuroscience*, 24(2):476–488.

Dean, G., Yeo, T., Goris, A., Taylor, C., Goodman, R., Elian, M., Galea-Debono, A., Aquilina, A., Felice, A., Vella, M., et al. (2008). HLA-DRB1 and multiple sclerosis in Malta. *Neurology*, 70(2):101–105.

Debray, C., Vereecken, P., Belot, N., Teillard, P., Brion, J.-P., Pandolfo, M., and Pochet, R. (2004). Multifaceted role of galectin-3 on human glioblastoma cell motility. *Biochemical and Biophysical Research Communications*, 325(4):1393–1398.

DeLuca, G. C., Joseph, A., George, J., Yates, R. L., Hamard, M., Hofer, M., and Esiri, M. M. (2014). Olfactory pathology in central nervous system demyelinating diseases. *Brain Pathology*.

Demetriou, M., Granovsky, M., Quaggin, S., and Dennis, J. W. (2001). Negative regulation of T-cell activation and autoimmunity by Mgat5 N-glycosylation. *Nature*, 409(6821):733–739.

Denic, A., Johnson, A. J., Bieber, A. J., Warrington, A. E., Rodriguez, M., and Pirko, I. (2011). The relevance of animal models in multiple sclerosis research. *Pathophysiology*, 18(1):21–29.

Dhib-Jalbut, S. and Marks, S. (2010). Interferon-β mechanisms of action in multiple sclerosis. *Neurology*, 74(Supplement 1):S17–S24.

Di Bello, I. C., Dawson, M., Levine, J., and Reynolds, R. (1999). Generation of oligodendroglial progenitors in acute inflammatory demyelinating lesions of the rat brain stem is associated with demyelination rather than inflammation. *Journal of Neurocytology*, 28(4-5):365–381.

Dimos, J. T., Rodolfa, K. T., Niakan, K. K., Weisenthal, L. M., Mitsumoto, H., Chung, W., Croft, G. F., Saphier, G., Leibel, R., Goland, R., et al. (2008). Induced pluripotent stem cells generated from patients with ALS can be differentiated into motor neurons. *Science*, 321(5893):1218–1221.

Dobson, R., Giovannoni, G., and Ramagopalan, S. (2012). The month of birth effect in multiple sclerosis: systematic review, meta-analysis and effect of latitude. *Journal of Neurology, Neurosurgery & Psychiatry*, 84(4):427–432.

Doetsch, F. and Álvarez-Buylla, A. (1996). Network of tangential pathways for neuronal migration in adult mammalian brain. *Proceedings of the National Academy of Sciences*, 93(25):14895–14900.

Doetsch, F., Caille, I., Lim, D. A., García-Verdugo, J. M., and Álvarez-Buylla, A. (1999). Subventricular zone astrocytes are neural stem cells in the adult mammalian brain. *Cell*, 97(6):703–716.

Doetsch, F., García-Verdugo, J. M., and Álvarez-Buylla, A. (1997). Cellular composition and three-dimensional organization of the subventricular germinal zone in the adult mammalian brain. *Journal of Neuroscience*, 17(13):5046–5061.

Doetsch, F., Petreanu, L., Caille, I., Garcia-Verdugo, J.-M., and Álvarez-Buylla, A. (2002). EGF converts transit-amplifying neurogenic precursors in the adult brain into multipotent stem cells. *Neuron*, 36(6):1021–1034.

Dutta, R., McDonough, J., Yin, X., Peterson, J., Chang, A., Torres, T., Gudz, T., Macklin, W. B., Lewis, D. A., Fox, R. J., et al. (2006). Mitochondrial dysfunction as a cause of axonal degeneration in multiple sclerosis patients. *Annals of Neurology*, 59(3):478–489.

Dyment, D., Yee, I., Ebers, G., and Sadovnick, A. (2006). Multiple sclerosis in stepsiblings: recurrence risk and ascertainment. *Journal of Neurology, Neurosurgery & Psychiatry*, 77(2):258–259.

Dziedzic, T., Metz, I., Dallenga, T., König, F. B., Müller, S., Stadelmann, C., and Brück, W. (2010). Wallerian degeneration: a major component of early axonal pathology in multiple sclerosis. *Brain Pathology*, 20(5):976–985.

Ebers, G., Sadovnick, A., and Risch, N. (1995). A genetic basis for familial aggregation in multiple sclerosis. *Nature*, 377(6545):150–151.

Ebers, G. C. et al. (1998). Randomised double-blind placebo-controlled study of interferon β-1a in relapsing/remitting multiple sclerosis. *Lancet*, 352(9139):1498–1504.

Eidinoff, M., Cheong, L., and Rich, M. (1959). Incorporation of unnatural pyrimidine bases into deoxyribonucleic acid of mammalian cells. *Science*, 129(3362):1550–1551.

Ekdahl, C. T., Claasen, J.-H., Bonde, S., Kokaia, Z., and Lindvall, O. (2003). Inflammation is detrimental for neurogenesis in adult brain. *Proceedings of the National Academy of Sciences*, 100(23):13632–13637.

Elola, M., Wolfenstein-Todel, C., Troncoso, M., Vasta, G., and Rabinovich, G. (2007). Galectins: matricellular glycan-binding proteins linking cell adhesion, migration, and survival. *Cellular and Molecular Life Sciences*, 64(13):1679–1700.

Emerson, M. R., Biswas, S., and LeVine, S. M. (2001). Cuprizone and piperonyl butoxide, proposed inhibitors of T-cell function, attenuate experimental allergic encephalomyelitis in SJL mice. *Journal of Neuroimmunology*, 119(2):205–213.

Emery, B., Agalliu, D., Cahoy, J. D., Watkins, T. A., Dugas, J. C., Mulinyawe, S. B., Ibrahim, A., Ligon, K. L., Rowitch, D. H., and Barres, B. A. (2009). Myelin gene regulatory factor is a critical transcriptional regulator required for CNS myelination. *Cell*, 138(1):172–185.

Endo, K., Kohnoe, S., Tsujita, E., Watanabe, A., Nakashima, H., Baba, H., and Maehara, Y. (2005). Galectin-3 expression is a potent prognostic marker in colorectal cancer. *Anticancer Research*, 25(4):3117–3121.

Ernst, A., Alkass, K., Bernard, S., Salehpour, M., Perl, S., Tisdale, J., Possnert, G., Druid, H., and Frisén, J. (2014). Neurogenesis in the striatum of the adult human brain. *Cell*, 156(5):1072–1083.

Fancy, S. P., Chan, J. R., Baranzini, S. E., Franklin, R. J., and Rowitch, D. H. (2011). Myelin regeneration: a recapitulation of development? *Annual Review of Neuroscience*, 34:21–43.

Fancy, S. P., Zhao, C., and Franklin, R. J. (2004). Increased expression of Nkx2.2 and Olig2 identifies reactive oligodendrocyte progenitor cells responding to demyelination in the adult CNS. *Molecular and Cellular Neuroscience*, 27(3):247–254.

Farnworth, S. L., Henderson, N. C., MacKinnon, A. C., Atkinson, K. M., Wilkinson, T., Dhaliwal, K., Hayashi, K., Simpson, A. J., Rossi, A. G., Haslett, C., et al. (2008). Galectin-3 reduces the severity of pneumococcal pneumonia by augmenting neutrophil function. *American Journal of Pathology*, 172(2):395–405.

Finean, J. (1957). The role of water in the structure of peripheral nerve myelin. *Journal of Biophysical and Biochemical Cytology*, 3(1):95–102.

Finzsch, M., Stolt, C. C., Lommes, P., and Wegner, M. (2008). Sox9 and Sox10 influence survival and migration of oligodendrocyte precursors in the spinal cord by regulating PDGF receptor α expression. *Development*, 135(4):637–646.

Flores, A. I., Narayanan, S. P., Morse, E. N., Shick, H. E., Yin, X., Kidd, G., Avila, R. L., Kirschner, D. A., and Macklin, W. B. (2008). Constitutively active Akt induces enhanced myelination in the CNS. *Journal of Neuroscience*, 28(28):7174–7183.

Folch, J. and Lees, M. (1951). Proteolipides, a new type of tissue lipoproteins their isolation from brain. *Journal of Biological Chemistry*, 191(2):807–817.

Fowlis, D., Colnot, C., Ripoche, M.-A., and Poirier, F. (1995). Galectin-3 is expressed in the notochord, developing bones, and skin of the postimplantation mouse embryo. *Developmental Dynamics*, 203(2):241–251.

Franco, S. J., Gil-Sanz, C., Martinez-Garay, I., Espinosa, A., Harkins-Perry, S. R., Ramos, C., and Müller, U. (2012). Fate-restricted neural progenitors in the mammalian cerebral cortex. *Science*, 337(6095):746–749.

Franklin, R. J. and Ffrench-Constant, C. (2010). Stem cell treatments and multiple sclerosis. *British Medical Journal*, 340:c1387.

Friese, M. A., Schattling, B., and Fugger, L. (2014). Mechanisms of neurodegeneration and axonal dysfunction in multiple sclerosis. *Nature Reviews Neurology*, 10(4):225–238.

Frigeri, L. G., Zuberi, R. I., and Liu, F. T. (1993). Epsilon BP, a beta-galactoside-binding animal lectin, recognizes IgE receptor (Fc epsilon RI) and activates mast cells. *Biochemistry*, 32(30):7644–7649.

Fukumori, T., Takenaka, Y., Yoshii, T., Kim, H.-R. C., Hogan, V., Inohara, H., Kagawa, S., and Raz, A. (2003). CD29 and CD7 mediate galectin-3-induced type II T-cell apoptosis. *Cancer Research*, 63(23):8302–8311.

Fünfschilling, U., Supplie, L. M., Mahad, D., Boretius, S., Saab, A. S., Edgar, J., Brinkmann, B. G., Kassmann, C. M., Tzvetanova, I. D., Möbius, W., et al. (2012). Glycolytic oligodendrocytes maintain myelin and long-term axonal integrity. *Nature*, 485(7399):517–521.

Gajera, C. R., Emich, H., Lioubinski, O., Christ, A., Beckervordersandforth-Bonk, R., Yoshikawa, K., Bachmann, S., Christensen, E. I., Götz, M., Kempermann, G., et al. (2010). LRP2 in ependymal cells regulates BMP signaling in the adult neurogenic niche. *Journal of Cell Science*, 123(11):1922–1930.

Galectin Therapeutics (2015). *Develop Proprietary Compounds*. Retrieved from http://galectintherapeutics.com/what-we-do/develop-proprietary-compounds-for-disease/.

Gao, Z., Ure, K., Ables, J. L., Lagace, D. C., Nave, K. A., Goebbels, S., Eisch, A. J., and Hsieh, J. (2009). Neurod1 is essential for the survival and maturation of adult-born neurons. *Nature Neuroscience*, 12(9):1090–1092.

Gasser, H. S. and Erlanger, J. (1927). The role played by the sizes of the constituent fibers of a nerve trunk in determining the form of its action potential wave. *American Journal of Physiology*, 80(3):522–547.

Gencic, S., Abuelo, D., Ambler, M., and Hudson, L. (1989). Pelizaeus-Merzbacher disease: an X-linked neurologic disorder of myelin metabolism with a novel mutation in the gene encoding proteolipid protein. *American Journal of Human Genetics*, 45(3):435–442.

Gerdoni, E., Gallo, B., Casazza, S., Musio, S., Bonanni, I., Pedemonte, E., Mantegazza, R., Frassoni, F., Mancardi, G., Pedotti, R., et al. (2007). Mesenchymal stem cells effectively modulate pathogenic immune response in experimental autoimmune encephalomyelitis. *Annals of Neurology*, 61(3):219–227.

Goings, G. E., Greisman, A., James, R. E., Abram, L. K., Begolka, W. S., Miller, S. D., and Szele, F. G. (2008). Hematopoietic cell activation in the subventricular zone after Theiler's virus infection. *Journal of Neuroinflammation*, 5(1):44.

Goings, G. E., Kozlowski, D. A., and Szele, F. G. (2006). Differential activation of microglia in neurogenic versus non-neurogenic regions of the forebrain. *Glia*, 54(4):329–342.

Goings, G. E., Sahni, V., and Szele, F. G. (2004). Migration patterns of subventricular zone cells in adult mice change after cerebral cortex injury. *Brain Research*, 996(2):213–226.

Goings, G. E., Wibisono, B. L., and Szele, F. G. (2002). Cerebral cortex lesions decrease the number of bromodeoxyuridine-positive subventricular zone cells in mice. *Neuroscience Letters*, 329(2):161–164.

Goldschmidt, T., Antel, J., König, F., Brück, W., and Kuhlmann, T. (2009). Remyelination capacity of the MS brain decreases with disease chronicity. *Neurology*, 72(22):1914–1921.

Gonzalez-Perez, O., Romero-Rodriguez, R., Soriano-Navarro, M., Garcia-Verdugo, J. M., and Álvarez-Buylla, A. (2009). Epidermal growth factor induces the progeny of subventricular zone type B cells to migrate and differentiate into oligodendrocytes. *Stem Cells*, 27(8):2032–2043.

Goodin, D. S. (2014). The epidemiology of multiple sclerosis: insights to disease pathogenesis. *Handbook of Clinical Neurology*, 122:231–266.

Goodkin, D., Rooney, W., Sloan, R., Bacchetti, P., Gee, L., Vermathen, M., Waubant, E., Abundo, M., Majumdar, S., Nelson, S., et al. (1998). A serial study of new MS lesions and the white matter from which they arise. *Neurology*, 51(6):1689–1697.

GraphPad Software (2015). *GraphPad Statistics Guide*. Retrieved from http://www.graphpad.com/guides/prism/6/statistics/index.htm?stat_testing_for_equivalence_with_c.htm.

Griffiths, I., Klugmann, M., Anderson, T., Yool, D., Thomson, C., Schwab, M. H., Schneider, A., Zimmermann, F., McCulloch, M., Nadon, N., et al. (1998). Axonal swellings and degeneration in mice lacking the major proteolipid of myelin. *Science*, 280(5369):1610–1613.

Gu, H., Marth, J. D., Orban, P. C., Mossmann, H., and Rajewsky, K. (1994). Deletion of a DNA polymerase beta gene segment in T cells using cell type-specific gene targeting. *Science*, 265(5168):103–106.

Guglielmetti, C., Praet, J., Rangarajan, J. R., Vreys, R., De Vocht, N., Maes, F., Verhoye, M., Ponsaerts, P., and Van der Linden, A. (2014). Multimodal imaging of subventricular zone neural stem/progenitor cells in the cuprizone mouse model reveals increased neurogenic potential for the olfactory bulb pathway, but no contribution to remyelination of the corpus callosum. *Neuroimage*, 86:99–110.

Gupta, N., Henry, R. G., Strober, J., Kang, S.-M., Lim, D. A., Bucci, M., Caverzasi, E., Gaetano, L., Mandelli, M. L., Ryan, T., et al. (2012). Neural stem cell engraftment and myelination in the human brain. *Science Translational Medicine*, 4(155):155ra137.

Hack, M. A., Saghatelyan, A., de Chevigny, A., Pfeifer, A., Ashery-Padan, R., Lledo, P. M., and Gotz, M. (2005). Neuronal fate determinants of adult olfactory bulb neurogenesis. *Nature Neuroscience*, 8(7):865–872.

Haider, L., Fischer, M. T., Frischer, J. M., Bauer, J., Höftberger, R., Botond, G., Esterbauer, H., Binder, C. J., Witztum, J. L., and Lassmann, H. (2011). Oxidative damage in multiple sclerosis lesions. *Brain*, 134(7):1914–1924.

Hall, S. M. (1972). The effect of injections of lysophosphatidyl choline into white matter of the adult mouse spinal cord. *Journal of Cell Science*, 10(2):535–546.

Harrington, E. P., Zhao, C., Fancy, S. P., Kaing, S., Franklin, R. J., and Rowitch, D. H. (2010). Oligodendrocyte pten is required for myelin and axonal integrity, not remyelination. *Annals of Neurology*, 68(5):703–716.

Hauser, M., Amalfitano, A., Kumar-Singh, R., Hauschka, S., and Chamberlain, J. (1997). Improved adenoviral vectors for gene therapy of Duchenne muscular dystrophy. *Neuromuscular Disorders*, 7(5):277–283.

Henderson, N. C., Mackinnon, A. C., Farnworth, S. L., Poirier, F., Russo, F. P., Iredale, J. P., Haslett, C., Simpson, K. J., and Sethi, T. (2006). Galectin-3 regulates myofibroblast activation and hepatic fibrosis. *Proceedings of the National Academy of Sciences*, 103(13):5060–5065.

Herder, V., Iskandar, C. D., Kegler, K., Hansmann, F., Elmarabet, S. A., Khan, M. A., Kalkuhl, A., Deschl, U., Baumgärtner, W., Ulrich, R., et al. (2015). Dynamic changes of microglia/macrophage M1 and M2 polarization in Theiler's murine encephalomyelitis. *Brain Pathology*.

Hermann, A., Gastl, R., Liebau, S., Popa, M. O., Fiedler, J., Boehm, B. O., Maisel, M., Lerche, H., Schwarz, J., Brenner, R., et al. (2004). Efficient generation of neural stem cell-like cells from adult human bone marrow stromal cells. *Journal of Cell Science*, 117(19):4411–4422.

Hibbits, N., Pannu, R., Wu, T. J., and Armstrong, R. C. (2009). Cuprizone demyelination of the corpus callosum in mice correlates with altered social interaction and impaired bilateral sensorimotor coordination. *ASN NEURO*, 1(3):AN20090032.

Ho, M.-K. and Springer, T. (1982). Mac-2, a novel 32,000 Mr mouse macrophage subpopulation-specific antigen defined by monoclonal antibodies. *Journal of Immunology*, 128(3):1221–1228.

Howell, O., Palser, A., Polito, A., Melrose, S., Zonta, B., Scheiermann, C., Vora, A., Brophy, P., and Reynolds, R. (2006). Disruption of neurofascin localization reveals early changes preceding demyelination and remyelination in multiple sclerosis. *Brain*, 129(12):3173–3185.

Howng, S. Y. B., Avila, R. L., Emery, B., Traka, M., Lin, W., Watkins, T., Cook, S., Bronson, R., Davisson, M., Barres, B. A., et al. (2010). ZFP191 is required by oligodendrocytes for CNS myelination. *Genes & Development*, 24(3):301–311.

Hoyos, H., Rinaldi, M., Mendez-Huergo, S., Marder, M., Rabinovich, G., Pasquini, J., and Pasquini, L. (2014). Galectin-3 controls the response of microglial cells to limit cuprizone-induced demyelination. *Neurobiology of Disease*, 62:441–455.

Hsu, D. K., Chernyavsky, A. I., Chen, H.-Y., Yu, L., Grando, S. A., and Liu, F.-T. (2009). Endogenous galectin-3 is localized in membrane lipid rafts and regulates migration of dendritic cells. *Journal of Investigative Dermatology*, 129(3):573–583.

Hsu, D. K., Yang, R.-Y., Pan, Z., Yu, L., Salomon, D. R., Fung-Leung, W.-P., and Liu, F.-T. (2000). Targeted disruption of the galectin-3 gene results in attenuated peritoneal inflammatory responses. *American Journal of Pathology*, 156(3):1073–1083.

Hu, B.-Y., Weick, J. P., Yu, J., Ma, L.-X., Zhang, X.-Q., Thomson, J. A., and Zhang, S.-C. (2010). Neural differentiation of human induced pluripotent stem cells follows developmental principles but with variable potency. *Proceedings of the National Academy of Sciences*, 107(9):4335–4340.

Hume, D. A., Summers, K. M., Raza, S., Baillie, J. K., and Freeman, T. C. (2010). Functional clustering and lineage markers: insights into cellular differentiation and gene function from large-scale microarray studies of purified primary cell populations. *Genomics*, 95(6):328–338.

Huxley, A. and Stämpfli, R. (1949). Evidence for saltatory conduction in peripheral myelinated nerve fibres. *Journal of Physiology*, 108(3):315–339.

IFNB Multiple Sclerosis Study Group et al. (1993). Interferon beta-1b is effective in relapsing-remitting multiple sclerosis I. clinical results of a multicenter, randomized, double-blind, placebo-controlled trial. *Neurology*, 43(4):655–655.

Ihrie, R. A. and Álvarez-Buylla, A. (2011). Lake-front property: a unique germinal niche by the lateral ventricles of the adult brain. *Neuron*, 70(4):674–686.

Ikehara, S., Good, R. A., Nakamura, T., Sekita, K., Inoue, S., Oo, M. M., Muso, E., Ogawa, K., and Hamashima, Y. (1985). Rationale for bone marrow transplantation in the treatment of autoimmune diseases. *Proceedings of the National Academy of Sciences*, 82(8):2483–2487.

International Mouse Phenotyping Consortium (2014). *Gene:Lgals3*. Retrieved from http://www.mousephenotype.org/data/genes/MGI:96778.

International Multiple Sclerosis Genetics Consortium et al. (2013). MANBA, CXCR5, SOX8, RPS6KB1 and ZBTB46 are genetic risk loci for multiple sclerosis. *Brain*, 136(6):1778–1782.

International Multiple Sclerosis Genetics Consortium, Wellcome Trust Case Control Consortium 2, et al. (2011). Genetic risk and a primary role for cell-mediated immune mechanisms in multiple sclerosis. *Nature*, 476(7359):214–219.

Iqbal, A. J., McNeill, E., Kapellos, T. S., Regan-Komito, D., Norman, S., Burd, S., Smart, N., Machemer, D. E., Stylianou, E., McShane, H., et al. (2014). Human CD68 promoter directs GFP transgene expression in mouse myeloid cells, allowing analysis of monocyte to macrophage differentiation in vivo. *Blood*, 124(15):e33–44.

Iqbal, A. J., Regan-Komito, D., Christou, I., White, G. E., McNeill, E., Kenyon, A., Taylor, L., Kapellos, T. S., Fisher, E. A., Channon, K. M., et al. (2013). A real time chemotaxis assay unveils unique migratory profiles amongst different primary murine macrophages. *PLOS ONE*, 8(3):e58744.

Ishibashi, S., Kuroiwa, T., Sakaguchi, M., Sun, L., Kadoya, T., Okano, H., and Mizusawa, H. (2007). Galectin-1 regulates neurogenesis in the subventricular zone and promotes functional recovery after stroke. *Experimental Neurology*, 207(2):302–313.

Ito, D., Imai, Y., Ohsawa, K., Nakajima, K., Fukuuchi, Y., and Kohsaka, S. (1998). Microglia-specific localisation of a novel calcium binding protein, Iba1. *Molecular Brain Research*, 57(1):1–9.

Jablonska, B., Aguirre, A., Raymond, M., Szabo, G., Kitabatake, Y., Sailor, K. A., Ming, G.-L., Song, H., and Gallo, V. (2010). Chordin-induced lineage plasticity of adult SVZ neuroblasts after demyelination. *Nature Neuroscience*, 13(5):541–550.

Jackson, E. L., Garcia-Verdugo, J. M., Gil-Perotin, S., Roy, M., Quinones-Hinojosa, A., VandenBerg, S., and Álvarez-Buylla, A. (2006). PDGFR alpha-positive B cells are neural stem cells in the adult SVZ that form glioma-like growths in response to increased PDGF signaling. *Neuron*, 51(2):187–199.

James, R. E. (2012). *The effects of neuroinflammation on the subventricular zone neurogenic compartment following Theiler's murine encephalomyelitis virus infection and its regulation by Galectin-3.* DPhil thesis, St Cross College, University of Oxford, United Kingdom.

Jankovski, A. and Sotelo, C. (1996). Subventricular zone-olfactory bulb migratory pathway in the adult mouse: cellular composition and specificity as determined by heterochronic and heterotopic transplantation. *Journal of Comparative Neurology*, 371(3):376–396.

Jeffery, N. and Blakemore, W. (1995). Remyelination of mouse spinal cord axons demyelinated by local injection of lysolecithin. *Journal of Neurocytology*, 24(10):775–781.

Jia, S. and Wang, J. (1988). Carbohydrate binding protein 35. complementary DNA sequence reveals homology with proteins of the heterogeneous nuclear RNP. *Journal of Biological Chemistry*, 263(13):6009–6011.

Jiang, H.-R., Al Rasebi, Z., Mensah-Brown, E., Shahin, A., Xu, D., Goodyear, C. S., Fukada, S. Y., Liu, F.-T., Liew, F. Y., and Lukic, M. L. (2009). Galectin-3 deficiency reduces the severity of experimental autoimmune encephalomyelitis. *Journal of Immunology*, 182(2):1167–1173.

Jinek, M., Chylinski, K., Fonfara, I., Hauer, M., Doudna, J. A., and Charpentier, E. (2012). A programmable dual-RNA–guided DNA endonuclease in adaptive bacterial immunity. *Science*, 337(6096):816–821.

Johnson, E. S. and Ludwin, S. (1981). The demonstration of recurrent demyelination and remyelination of axons in the central nervous system. *Acta Neuropathologica*, 53(2):93–98.

Johnson, K., Brooks, B., Cohen, J., Ford, C., Goldstein, J., Lisak, R., Myers, L., Panitch, H., Rose, J., Schiffer, R., et al. (1995). Copolymer 1 reduces relapse rate and improves disability in relapsing-remitting multiple sclerosis results of a phase III multicenter, double-blind, placebo-controlled trial. *Neurology*, 45(7):1268–1276.

Kandel, E. R., Schwartz, J. H., and Jessell, T. M. (2000). *Principles of Neural Science*. New York: McGraw-Hill, fourth edition.

Kapoor, R., Davies, M., Blaker, P. A., Hall, S. M., and Smith, K. J. (2003). Blockers of sodium and calcium entry protect axons from nitric oxide-mediated degeneration. *Annals of Neurology*, 53(2):174–180.

Karlsson, A., Christenson, K., Matlak, M., Björstad, Å., Brown, K. L., Telemo, E., Salomonsson, E., Leffler, H., and Bylund, J. (2009). Galectin-3 functions as an opsonin and enhances the macrophage clearance of apoptotic neutrophils. *Glycobiology*, 19(1):16–20.

Katsimpardi, L., Litterman, N. K., Schein, P. A., Miller, C. M., Loffredo, F. S., Wojtkiewicz, G. R., Chen, J. W., Lee, R. T., Wagers, A. J., and Rubin, L. L. (2014). Vascular and neurogenic rejuvenation of the aging mouse brain by young systemic factors. *Science*, 344(6184):630–634.

Kebir, H., Kreymborg, K., Ifergan, I., Dodelet-Devillers, A., Cayrol, R., Bernard, M., Giuliani, F., Arbour, N., Becher, B., and Prat, A. (2007). Human TH17 lymphocytes promote blood-brain barrier disruption and central nervous system inflammation. *Nature Medicine*, 13(10):1173–1175.

Kennebecasis Valley High School (2015). *Myelin Sheath*. Retrieved from http://kvhs.nbed.nb.ca/gallant/biology/schwann_myelin.html.

Kessaris, N., Fogarty, M., Iannarelli, P., Grist, M., Wegner, M., and Richardson, W. D. (2006). Competing waves of oligodendrocytes in the forebrain and postnatal elimination of an embryonic lineage. *Nature Neuroscience*, 9(2):173–179.

Kigerl, K. A., Gensel, J. C., Ankeny, D. P., Alexander, J. K., Donnelly, D. J., and Popovich, P. G. (2009). Identification of two distinct macrophage subsets with divergent effects causing either neurotoxicity or regeneration in the injured mouse spinal cord. *Journal of Neuroscience*, 29(43):13435–13444.

Kim, Y., Comte, I., Szabo, G., Hockberger, P., and Szele, F. G. (2009). Adult mouse subventricular zone stem and progenitor cells are sessile and epidermal growth factor receptor negatively regulates neuroblast migration. *PLOS ONE*, 4(12):e8122.

Kim, Y., Wang, W.-Z., Comte, I., Pastrana, E., Tran, P. B., Brown, J., Miller, R. J., Doetsch, F., Molnár, Z., and Szele, F. G. (2010). Dopamine stimulation of postnatal murine subventricular zone neurogenesis via the D3 receptor. *Journal of Neurochemistry*, 114(3):750–760.

Koenning, M., Jackson, S., Hay, C. M., Faux, C., Kilpatrick, T. J., Willingham, M., and Emery, B. (2012). Myelin gene regulatory factor is required for maintenance of myelin and mature oligodendrocyte identity in the adult CNS. *Journal of Neuroscience*, 32(36):12528–12542.

Kokoeva, M. V., Yin, H., and Flier, J. S. (2005). Neurogenesis in the hypothalamus of adult mice: potential role in energy balance. *Science*, 310(5748):679–683.

Kondo, A., Nakano, T., and Suzuki, K. (1987). Blood-brain barrier permeability to horseradish peroxidase in twitcher and cuprizone-intoxicated mice. *Brain Research*, 425(1):186–190.

Kopen, G. C., Prockop, D. J., and Phinney, D. G. (1999). Marrow stromal cells migrate throughout forebrain and cerebellum, and they differentiate into astrocytes after injection into neonatal mouse brains. *Proceedings of the National Academy of Sciences*, 96(19):10711–10716.

Kornek, B., Storch, M. K., Bauer, J., Djamshidian, A., Weissert, R., Wallstroem, E., Stefferl, A., Zimprich, F., Olsson, T., Linington, C., et al. (2001). Distribution of a calcium channel subunit in dystrophic axons in multiple sclerosis and experimental autoimmune encephalomyelitis. *Brain*, 124(6):1114–1124.

Kornguth, S. E. and Anderson, J. W. (1965). Localization of a basic protein in the myelin of various species with the aid of fluorescence and electron microscopy. *Journal of Cell Biology*, 26(1):157–166.

Kotter, M. R., Li, W.-W., Zhao, C., and Franklin, R. J. (2006). Myelin impairs CNS remyelination by inhibiting oligodendrocyte precursor cell differentiation. *Journal of Neuroscience*, 26(1):328–332.

Kuhn, H. G., Winkler, J., Kempermann, G., Thal, L. J., and Gage, F. H. (1997). Epidermal growth factor and fibroblast growth factor-2 have different effects on neural progenitors in the adult rat brain. *Journal of Neuroscience*, 17(15):5820–5829.

Kuwabara, I. and Liu, F.-T. (1996). Galectin-3 promotes adhesion of human neutrophils to laminin. *Journal of Immunology*, 156(10):3939–3944.

Laatsch, R. H., Kies, M. W., Gordon, S., and Alvord, E. C. (1962). The encephalomyelitic activity of myelin isolated by ultracentrifugation. *Journal of Experimental Medicine*, 115(4):777–788.

Lacar, B., Herman, P., Platel, J.-C., Kubera, C., Hyder, F., and Bordey, A. (2012). Neural progenitor cells regulate capillary blood flow in the postnatal subventricular zone. *Journal of Neuroscience*, 32(46):16435–16448.

Lampron, A., Larochelle, A., Laflamme, N., Préfontaine, P., Plante, M.-M., Sánchez, M. G., Yong, V. W., Stys, P. K., Tremblay, M.-È., and Rivest, S. (2015). Inefficient clearance of myelin debris by microglia impairs remyelinating processes. *Journal of Experimental Medicine*, 212(4):481–495.

Langrish, C. L., Chen, Y., Blumenschein, W. M., Mattson, J., Basham, B., Sedgwick, J. D., McClanahan, T., Kastelein, R. A., and Cua, D. J. (2005). IL-23 drives a pathogenic T cell population that induces autoimmune inflammation. *Journal of Experimental Medicine*, 201(2):233–240.

Lappe-Siefke, C., Goebbels, S., Gravel, M., Nicksch, E., Lee, J., Braun, P. E., Griffiths, I. R., and Nave, K.-A. (2003). Disruption of Cnp1 uncouples oligodendroglial functions in axonal support and myelination. *Nature Genetics*, 33(3):366–374.

Larsen, P. D., Bloomer, L. C., and Bray, P. F. (1985). Epstein-Barr nuclear antigen and viral capsid antigen antibody titers in multiple sclerosis. *Neurology*, 35(3):435–435.

Lau, W.-M., Qiu, G., Helmeste, D. M., Lee, T. M., Tang, S.-W., So, K.-F., and Tang, S.-W. (2007). Corticosteroid decreases subventricular zone cell proliferation, which could be reversed by paroxetine. *Restorative Neurology and Neuroscience*, 25(1):17–23.

Le Magueresse, C., Alfonso, J., Bark, C., Eliava, M., Khrulev, S., and Monyer, H. (2012). Subventricular zone-derived neuroblasts use vasculature as a scaffold to migrate radially to the cortex in neonatal mice. *Cerebral Cortex*, 22(10):2285–2296.

Lee, Y., Morrison, B. M., Li, Y., Lengacher, S., Farah, M. H., Hoffman, P. N., Liu, Y., Tsingalia, A., Jin, L., Zhang, P.-W., et al. (2012). Oligodendroglia metabolically support axons and contribute to neurodegeneration. *Nature*, 487(7408):443–448.

Lein, E. S., Hawrylycz, M. J., Ao, N., Ayres, M., Bensinger, A., Bernard, A., Boe, A. F., Boguski, M. S., Brockway, K. S., Byrnes, E. J., et al. (2007). Genome-wide atlas of gene expression in the adult mouse brain. *Nature*, 445(7124):168–176.

Levine, J. M. and Reynolds, R. (1999). Activation and proliferation of endogenous oligodendrocyte precursor cells during ethidium bromide-induced demyelination. *Experimental Neurology*, 160(2):333–347.

Levison, S. W. and Goldman, J. E. (1993). Both oligodendrocytes and astrocytes develop from progenitors in the subventricular zone of postnatal rat forebrain. *Neuron*, 10(2):201–212.

Lewis, R. (2012). Chronic inflammatory demyelinating polyneuropathy: Etiology, clinical features, and diagnosis. *UpToDate*. Retrieved from http://www.uptodate.com/contents/chronic-inflammatory-demyelinating-polyneuropathy-etiology-clinical-features-and-diagnosis.

Liang, P., Xu, Y., Zhang, X., Ding, C., Huang, R., Zhang, Z., Lv, J., Xie, X., Chen, Y., Li, Y., et al. (2015). CRISPR/Cas9-mediated gene editing in human tripronuclear zygotes. *Protein & Cell*.

Lim, D. A. and Álvarez-Buylla, A. (2014). Adult neural stem cells stake their ground. *Trends in Neurosciences*, 37(10):563–571.

Lim, D. A., Tramontin, A. D., Trevejo, J. M., Herrera, D. G., García-Verdugo, J. M., and Álvarez-Buylla, A. (2000). Noggin antagonizes BMP signaling to create a niche for adult neurogenesis. *Neuron*, 28(3):713–726.

Lin, Y.-H., Lin, L.-Y., Wu, Y.-W., Chien, K.-L., Lee, C.-M., Hsu, R.-B., Chao, C.-L., Wang, S.-S., Hsein, Y.-C., Liao, L.-C., et al. (2009). The relationship between serum galectin-3 and serum markers of cardiac extracellular matrix turnover in heart failure patients. *Clinica Chimica Acta*, 409(1):96–99.

Lipton, H. L. (1975). Theiler's virus infection in mice: an unusual biphasic disease process leading to demyelination. *Infection and Immunity*, 11(5):1147–1155.

Liu, F.-T., Hsu, D. K., Zuberi, R. I., Kuwabara, I., Chi, E. Y., and Henderson Jr, W. R. (1995). Expression and function of galectin-3, a beta-galactoside-binding lectin, in human monocytes and macrophages. *American Journal of Pathology*, 147(4):1016.

Liu, F.-T. and Rabinovich, G. A. (2010). Galectins: regulators of acute and chronic inflammation. *Annals of the New York Academy of Sciences*, 1183(1):158–182.

Liu, R., Cai, J., Hu, X., Tan, M., Qi, Y., German, M., Rubenstein, J., Sander, M., and Qiu, M. (2003). Region-specific and stage-dependent regulation of Olig gene expression and oligodendrogenesis by Nkx6.1 homeodomain transcription factor. *Development*, 130(25):6221–6231.

Liu, X., Wang, Q., Haydar, T. F., and Bordey, A. (2005). Nonsynaptic GABA signaling in postnatal subventricular zone controls proliferation of GFAP-expressing progenitors. *Nature Neuroscience*, 8(9):1179–1187.

Liu, Z., Hu, X., Cai, J., Liu, B., Peng, X., Wegner, M., and Qiu, M. (2007). Induction of oligodendrocyte differentiation by Olig2 and Sox10: evidence for reciprocal interactions and dosage-dependent mechanisms. *Developmental Biology*, 302(2):683–693.

Llufriu, S., Sepúlveda, M., Blanco, Y., Marín, P., Moreno, B., Berenguer, J., Gabilondo, I., Martínez-Heras, E., Sola-Valls, N., Arnaiz, J.-A., et al. (2014). Randomized placebo-controlled phase II trial of autologous mesenchymal stem cells in multiple sclerosis. *PLOS ONE*, 9(12):e113936.

Lois, C. and Álvarez-Buylla, A. (1994). Long-distance neuronal migration in the adult mammalian brain. *Science*, 264(5162):1145–1148.

Lok, D. J., Van Der Meer, P., Lipsic, E., Van Wijngaarden, J., Hillege, H. L., van Veldhuisen, D. J., et al. (2010). Prognostic value of galectin-3, a novel marker of fibrosis, in patients with chronic heart failure: data from the DEAL-HF study. *Clinical Research in Cardiology*, 99(5):323–328.

Lu, L., Chen, X., Zhang, C.-W., Yang, W.-L., Wu, Y.-J., Sun, L., Bai, L.-M., Gu, X.-S., Ahmed, S., Dawe, G. S., et al. (2008). Morphological and functional characterization of predifferentiation of myelinating glia-like cells from human bone marrow stromal cells through activation of F3/Notch signaling in mouse retina. *Stem Cells*, 26(2):580–590.

Lu, Q. R., Sun, T., Zhu, Z., Ma, N., Garcia, M., Stiles, C. D., and Rowitch, D. H. (2002). Common developmental requirement for Olig function indicates a motor neuron/oligodendrocyte connection. *Cell*, 109(1):75–86.

Lu, Q. R., Yuk, D.-i., Alberta, J. A., Zhu, Z., Pawlitzky, I., Chan, J., McMahon, A. P., Stiles, C. D., and Rowitch, D. H. (2000). Sonic hedgehog–regulated oligodendrocyte lineage genes encoding bhlh proteins in the mammalian central nervous system. *Neuron*, 25(2):317–329.

Lublin, F. D., Reingold, S. C., et al. (1996). Defining the clinical course of multiple sclerosis results of an international survey. *Neurology*, 46(4):907–911.

Lucchinetti, C., Bruck, W., Parisi, J., Scheithauer, B., Rodriguez, M., Lassman, H., et al. (2000). Heterogeneity of multiple sclerosis lesions: implications for the pathogenesis of demyelination. *Annals of Neurology*, 47(6):707–717.

Lutterotti, A., Vedovello, M., Reindl, M., Ehling, R., DiPauli, F., Kuenz, B., Gneiss, C., Deisenhammer, F., and Berger, T. (2011). Olfactory threshold is impaired in early, active multiple sclerosis. *Multiple Sclerosis Journal*, 17(8):964–969.

Ma, W., Rogers, K., Zbar, B., and Schmidt, L. (2002). Effects of different fixatives on β-galactosidase activity. *Journal of Histochemistry & Cytochemistry*, 50(10):1421–1424.

Machold, R., Hayashi, S., Rutlin, M., Muzumdar, M. D., Nery, S., Corbin, J. G., Gritli-Linde, A., Dellovade, T., Porter, J. A., Rubin, L. L., et al. (2003). Sonic hedgehog is required for progenitor cell maintenance in telencephalic stem cell niches. *Neuron*, 39(6):937–950.

MacKinnon, A. C., Farnworth, S. L., Hodkinson, P. S., Henderson, N. C., Atkinson, K. M., Leffler, H., Nilsson, U. J., Haslett, C., Forbes, S. J., and Sethi, T. (2008). Regulation of alternative macrophage activation by galectin-3. *Journal of Immunology*, 180(4):2650–2658.

Mancardi, G. and Saccardi, R. (2008). Autologous haematopoietic stem-cell transplantation in multiple sclerosis. *Lancet Neurology*, 7(7):626–636.

Markakis, E. A., Palmer, T. D., Randolph-Moore, L., Rakic, P., and Gage, F. H. (2004). Novel neuronal phenotypes from neural progenitor cells. *Journal of Neuroscience*, 24(12):2886–2897.

Markowska, A. I., Liu, F.-T., and Panjwani, N. (2010). Galectin-3 is an important mediator of VEGF- and bFGF-mediated angiogenic response. *Journal of Experimental Medicine*, 207(9):1981–1993.

Marmont, A. M. (1994). Immune ablation followed by allogeneic or autologous bone marrow transplantation: a new treatment for severe autoimmune diseases? *Stem Cells*, 12(1):125–135.

Marshall, C. A., Novitch, B. G., and Goldman, J. E. (2005). Olig2 directs astrocyte and oligodendrocyte formation in postnatal subventricular zone cells. *Journal of Neuroscience*, 25(32):7289–7298.

Martinez-Molina, N., Kim, Y., Hockberger, P., and Szele, F. G. (2011). Rostral migratory stream neuroblasts turn and change directions in stereotypic patterns. *Cell Adhesion & Migration*, 5(1):83–95.

Mason, J., Jones, J., Taniike, M., Morell, P., Suzuki, K., and Matsushima, G. (2000). Mature oligodendrocyte apoptosis precedes IGF-1 production and oligodendrocyte progenitor accumulation and differentiation during demyelination/remyelination. *Journal of Neuroscience Research*, 61(3):251–262.

Matarrese, P., Tinari, N., Semeraro, M. L., Natoli, C., Iacobelli, S., and Malorni, W. (2000). Galectin-3 overexpression protects from cell damage and death by influencing mitochondrial homeostasis. *FEBS Letters*, 473(3):311–315.

Mathey, E. K., Derfuss, T., Storch, M. K., Williams, K. R., Hales, K., Woolley, D. R., Al-Hayani, A., Davies, S. N., Rasband, M. N., Olsson, T., et al. (2007). Neurofascin as a novel target for autoantibody-mediated axonal injury. *Journal of Experimental Medicine*, 204(10):2363–2372.

Matsushima, G. K. and Morell, P. (2001). The neurotoxicant, cuprizone, as a model to study demyelination and remyelination in the central nervous system. *Brain Pathology*, 11(1):107–116.

McDonald, W. I., Compston, A., Edan, G., Goodkin, D., Hartung, H.-P., Lublin, F. D., McFarland, H. F., Paty, D. W., Polman, C. H., Reingold, S. C., et al. (2001). Recommended diagnostic criteria for multiple sclerosis: guidelines from the international panel on the diagnosis of multiple sclerosis. *Annals of Neurology*, 50(1):121–127.

McMahon, E. J., Suzuki, K., and Matsushima, G. K. (2002). Peripheral macrophage recruitment in cuprizone-induced CNS demyelination despite an intact blood–brain barrier. *Journal of Neuroimmunology*, 130(1):32–45.

Menn, B., Garcia-Verdugo, J. M., Yaschine, C., Gonzalez-Perez, O., Rowitch, D., and Álvarez-Buylla, A. (2006). Origin of oligodendrocytes in the subventricular zone of the adult brain. *Journal of Neuroscience.*, 26(30):7907–7918.

Merkle, F. T., Fuentealba, L. C., Sanders, T. A., Magno, L., Kessaris, N., and Álvarez-Buylla, A. (2014). Adult neural stem cells in distinct microdomains generate previously unknown interneuron types. *Nature Neuroscience*, 17(2):207–214.

Merkle, F. T., Mirzadeh, Z., and Álvarez-Buylla, A. (2007). Mosaic organization of neural stem cells in the adult brain. *Science*, 317(5836):381–384.

Merzbacher, L. (1910). Eine eigenartige familiär-hereditäre erkrankungsform (aplasia axialis extracorticalis congenita). *Zeitschrift für die gesamte Neurologie und Psychiatrie*, 3(1):1–138.

Metzger, D., Clifford, J., Chiba, H., and Chambon, P. (1995). Conditional site-specific recombination in mammalian cells using a ligand-dependent chimeric Cre recombinase. *Proceedings of the National Academy of Sciences*, 92(15):6991–6995.

Middeldorp, J. and Hol, E. (2011). GFAP in health and disease. *Progress in Neurobiology*, 93(3):421–443.

Miller, S. D., Vanderlugt, C. L., Begolka, W. S., Pao, W., Yauch, R. L., Neville, K. L., Katz-Levy, Y., Carrizosa, A., and Kim, B. S. (1997). Persistent infection with Theiler's virus leads to CNS autoimmunity via epitope spreading. *Nature Medicine*, 3(10):1133–1136.

Milting, H., Ellinghaus, P., Seewald, M., Cakar, H., Bohms, B., Kassner, A., Körfer, R., Klein, M., Krahn, T., Kruska, L., et al. (2008). Plasma biomarkers of myocardial fibrosis and remodeling in terminal heart failure patients supported by mechanical circulatory support devices. *Journal of Heart and Lung Transplantation*, 27(6):589–596.

Miron, V. E., Boyd, A., Zhao, J.-W., Yuen, T. J., Ruckh, J. M., Shadrach, J. L., van Wijngaarden, P., Wagers, A. J., Williams, A., Franklin, R. J., et al. (2013). M2 microglia and macrophages drive oligodendrocyte differentiation during CNS remyelination. *Nature Neuroscience*, 16(9):1211–1218.

Mirzadeh, Z., Merkle, F. T., Soriano-Navarro, M., Garcia-Verdugo, J. M., and Álvarez-Buylla, A. (2008). Neural stem cells confer unique pinwheel architecture to the ventricular surface in neurogenic regions of the adult brain. *Cell Stem Cell*, 3(3):265–278.

Mo, Z. and Zecevic, N. (2009). Human fetal radial glia cells generate oligodendrocytes in vitro. *Glia*, 57(5):490–498.

Monje, M. L., Toda, H., and Palmer, T. D. (2003). Inflammatory blockade restores adult hippocampal neurogenesis. *Science*, 302(5651):1760–1765.

Morshead, C. M., Reynolds, B. A., Craig, C. G., McBurney, M. W., Staines, W. A., Morassutti, D., Weiss, S., and van der Kooy, D. (1994). Neural stem cells in the adult mammalian forebrain: a relatively quiescent subpopulation of subependymal cells. *Neuron*, 13(5):1071–1082.

Multiple Sclerosis International Federation (2013). *Atlas of MS 2013*. Retrieved from www.msif.org/wp-content/uploads/2014/09/Atlas-of-MS.pdf.

Multiple Sclerosis Society (2014). *MS Info, Research, News and Support || Multiple Sclerosis Society UK*. Retrieved from http://www.mssociety.org.uk/.

Munger, K. L., Zhang, S., O'Reilly, E., Hernán, M., Olek, M., Willett, W., and Ascherio, A. (2004). Vitamin D intake and incidence of multiple sclerosis. *Neurology*, 62(1):60–65.

Muraro, P. A., Douek, D. C., Packer, A., Chung, K., Guenaga, F. J., Cassiani-Ingoni, R., Campbell, C., Memon, S., Nagle, J. W., Hakim, F. T., et al. (2005). Thymic output generates a new and diverse TCR repertoire after autologous stem cell transplantation in multiple sclerosis patients. *Journal of Experimental Medicine*, 201(5):805–816.

Nait-Oumesmar, B., Decker, L., Lachapelle, F., Avellana-Adalid, V., Bachelin, C., Evercooren, V., and Baron, A. (1999). Progenitor cells of the adult mouse subventricular zone proliferate, migrate and differentiate into oligodendrocytes after demyelination. *European Journal of Neuroscience*, 11(12):4357–4366.

Nait-Oumesmar, B., Picard-Riera, N., Kerninon, C., Decker, L., Seilhean, D., Höglinger, G. U., Hirsch, E. C., Reynolds, R., and Baron-Van Evercooren, A. (2007). Activation of the subventricular zone in multiple sclerosis: evidence for early glial progenitors. *Proceedings of the National Academy of Sciences*, 104(11):4694–4699.

Nam, S. C., Kim, Y., Dryanovski, D., Walker, A., Goings, G., Woolfrey, K., Kang, S. S., Chu, C., Chenn, A., Erdelyi, F., et al. (2007). Dynamic features of postnatal subventricular zone cell motility: a two-photon time-lapse study. *Journal of Comparative Neurology*, 505(2):190–208.

Nangia-Makker, P., Honjo, Y., Sarvis, R., Akahani, S., Hogan, V., Pienta, K. J., and Raz, A. (2000). Galectin-3 induces endothelial cell morphogenesis and angiogenesis. *American Journal of Pathology*, 156(3):899–909.

Narayanan, S. P., Flores, A. I., Wang, F., and Macklin, W. B. (2009). Akt signals through the mammalian target of rapamycin pathway to regulate CNS myelination. *Journal of Neuroscience*, 29(21):6860–6870.

Nave, K.-A. (2010). Myelination and the trophic support of long axons. *Nature Reviews Neuroscience*, 11(4):275–283.

Newcombe, J., Uddin, A., Dove, R., Patel, B., Turski, L., Nishizawa, Y., and Smith, T. (2008). Glutamate receptor expression in multiple sclerosis lesions. *Brain Pathology*, 18(1):52–61.

Nishiyama, A., Komitova, M., Suzuki, R., and Zhu, X. (2009). Polydendrocytes (NG2 cells): multifunctional cells with lineage plasticity. *Nature Reviews Neuroscience*, 10(1):9–22.

Norton, W. T. and Autilio, L. A. (1966). The lipid composition of purified bovine brain melin. *Journal of Neurochemistry*, 13(4):213–222.

Novitch, B. G., Chen, A. I., and Jessell, T. M. (2001). Coordinate regulation of motor neuron subtype identity and pan-neuronal properties by the bHLH repressor Olig2. *Neuron*, 31(5):773–789.

Ochieng, J., Fridman, R., Nangia-Makker, P., Kleiner, D. E., Liotta, L. A., Stetler-Stevenson, W. G., and Raz, A. (1994). Galectin-3 is a novel substrate for human matrix metalloproteinases-2 and-9. *Biochemistry*, 33(47):14109–14114.

O'Driscoll, L., Linehan, R., Liang, Y., Joyce, H., Oglesby, I., and Clynes, M. (2001). Galectin-3 expression alters adhesion, motility and invasion in a lung cell line (DLKP), in vitro. *Anticancer Research*, 22(6A):3117–3125.

O'Gorman, C., Lin, R., Stankovich, J., and Broadley, S. A. (2012). Modelling genetic susceptibility to multiple sclerosis with family data. *Neuroepidemiology*, 40(1):1–12.

Ohsawa, K., Imai, Y., Sasaki, Y., and Kohsaka, S. (2004). Microglia/macrophage-specific protein Iba1 binds to fimbrin and enhances its actin-bundling activity. *Journal of Neurochemistry*, 88(4):844–856.

Oksenberg, J. R., Panzara, M. A., Begovich, A. B., Mitchell, D., Erlich, H. A., Murray, R. S., Shimonkevitz, R., Sherritt, M., Rothbard, J., and Bernard, C. C. (1993). Selection for T-cell receptor V beta-D beta-J beta gene rearrangements with specificity for a myelin basic protein peptide in brain lesions of multiple sclerosis. *Nature*, 362(6415):68–70.

Olek, M. (2014). Treatment of progressive multiple sclerosis in adults. *UpToDate*. Retrieved from http://www.uptodate.com/contents/treatment-of-progressive-multiple-sclerosis-in-adults.

Oluich, L.-J., Stratton, J. A. S., Xing, Y. L., Ng, S. W., Cate, H. S., Sah, P., Windels, F., Kilpatrick, T. J., and Merson, T. D. (2012). Targeted ablation of oligodendrocytes induces axonal pathology independent of overt demyelination. *Journal of Neuroscience*, 32(24):8317–8330.

Orentas, D. M., Hayes, J. E., Dyer, K. L., and Miller, R. H. (1999). Sonic hedgehog signaling is required during the appearance of spinal cord oligodendrocyte precursors. *Development*, 126(11):2419–2429.

Ortega, J. A., Radonjić, N. V., and Zecevic, N. (2013). Sonic hedgehog promotes generation and maintenance of human forebrain Olig2 progenitors. *Frontiers in Cellular Neuroscience*, 7:254.

Paez-Gonzalez, P., Asrican, B., Rodriguez, E., and Kuo, C. T. (2014). Identification of distinct ChAT+ neurons and activity-dependent control of postnatal SVZ neurogenesis. *Nature Neuroscience*, 17(7):934–942.

Panitch, H., Haley, A., Hirsch, R., and Johnson, K. (1987). Exacerbations of multiple sclerosis in patients treated with gamma interferon. *Lancet*, 329(8538):893–895.

Paratcha, G., Ibánez, C. F., and Ledda, F. (2006). GDNF is a chemoattractant factor for neuronal precursor cells in the rostral migratory stream. *Molecular and Cellular Neuroscience*, 31(3):505–514.

Parras, C. M., Galli, R., Britz, O., Soares, S., Galichet, C., Battiste, J., Johnson, J. E., Nakafuku, M., Vescovi, A., and Guillemot, F. (2004). Mash1 specifies neurons and oligodendrocytes in the postnatal brain. *EMBO Journal*, 23(22):4495–4505.

Pasquini, L., Millet, V., Hoyos, H., Giannoni, J., Croci, D., Marder, M., Liu, F., Rabinovich, G., and Pasquini, J. (2011). Galectin-3 drives oligodendrocyte differentiation to control myelin integrity and function. *Cell Death & Differentiation*, 18(11):1746–1756.

Patani, R., Balaratnam, M., Vora, A., and Reynolds, R. (2007). Remyelination can be extensive in multiple sclerosis despite a long disease course. *Neuropathology and Applied Neurobiology*, 33(3):277–287.

Patrikios, P., Stadelmann, C., Kutzelnigg, A., Rauschka, H., Schmidbauer, M., Laursen, H., Sorensen, P. S., Brück, W., Lucchinetti, C., and Lassmann, H. (2006). Remyelination is extensive in a subset of multiple sclerosis patients. *Brain*, 129(12):3165–3172.

Pelizaeus, F. (1885). Ueber eine eigenthümliche form spastischer lähmung mit cerebralerscheinungen auf hereditärer grundlage (multiple sklerose). *European Archives of Psychiatry and Clinical Neuroscience*, 16(3):698–710.

Pencea, V., Bingaman, K. D., Wiegand, S. J., and Luskin, M. B. (2001). Infusion of brain-derived neurotrophic factor into the lateral ventricle of the adult rat leads to new neurons in the parenchyma of the striatum, septum, thalamus, and hypothalamus. *Journal of Neuroscience*, 21(17):6706–6717.

Penderis, J., Shields, S. A., and Franklin, R. J. (2003a). Impaired remyelination and depletion of oligodendrocyte progenitors does not occur following repeated episodes of focal demyelination in the rat central nervous system. *Brain*, 126(6):1382–1391.

Penderis, J., Woodruff, R. H., Lakatos, A., Li, W.-W., Dunning, M. D., Zhao, C., Marchionni, M., and Franklin, R. J. (2003b). Increasing local levels of neuregulin (glial growth factor-2) by direct infusion into areas of demyelination does not alter remyelination in the rat CNS. *European Journal of Neuroscience*, 18(8):2253–2264.

Petryniak, M. A., Potter, G. B., Rowitch, D. H., and Rubenstein, J. L. (2007). Dlx1 and Dlx2 control neuronal versus oligodendroglial cell fate acquisition in the developing forebrain. *Neuron*, 55(3):417–433.

Pettitt, S. J., Liang, Q., Rairdan, X. Y., Moran, J. L., Prosser, H. M., Beier, D. R., Lloyd, K. C., Bradley, A., Skarnes, W. C., Newell, E. W., et al. (2009). Agouti C57BL/6N embryonic stem cells for mouse genetic resources. *Nature Methods*, 6(7):493–495.

Picard-Riera, N., Decker, L., Delarasse, C., Goude, K., Nait-Oumesmar, B., Liblau, R., Pham-Dinh, D., and Baron-Van Evercooren, A. (2002). Experimental autoimmune encephalomyelitis mobilizes neural progenitors from the subventricular zone to undergo oligodendrogenesis in adult mice. *Proceedings of the National Academy of Sciences*, 99(20):13211–13216.

Piccin, D. and Morshead, C. M. (2011). Wnt signaling regulates symmetry of division of neural stem cells in the adult brain and in response to injury. *Stem Cells*, 29(3):528–538.

Pittenger, M. F., Mackay, A. M., Beck, S. C., Jaiswal, R. K., Douglas, R., Mosca, J. D., Moorman, M. A., Simonetti, D. W., Craig, S., and Marshak, D. R. (1999). Multilineage potential of adult human mesenchymal stem cells. *Science*, 284(5411):143–147.

Pluchino, S., Gritti, A., Blezer, E., Amadio, S., Brambilla, E., Borsellino, G., Cossetti, C., Del Carro, U., Comi, G., t Hart, B., et al. (2009). Human neural stem cells ameliorate autoimmune encephalomyelitis in non-human primates. *Annals of Neurology*, 66(3):343–354.

Pluchino, S., Quattrini, A., Brambilla, E., Gritti, A., Salani, G., Dina, G., Galli, R., Del Carro, U., Amadio, S., Bergami, A., et al. (2003). Injection of adult neurospheres induces recovery in a chronic model of multiple sclerosis. *Nature*, 422(6933):688–694.

Pluchino, S., Zanotti, L., Rossi, B., Brambilla, E., Ottoboni, L., Salani, G., Martinello, M., Cattalini, A., Bergami, A., Furlan, R., et al. (2005). Neurosphere-derived multipotent precursors promote neuroprotection by an immunomodulatory mechanism. *Nature*, 436(7048):266–271.

Polman, C. H., Reingold, S. C., Banwell, B., Clanet, M., Cohen, J. A., Filippi, M., Fujihara, K., Havrdova, E., Hutchinson, M., Kappos, L., et al. (2011). Diagnostic criteria for multiple sclerosis: 2010 revisions to the McDonald criteria. *Annals of Neurology*, 69(2):292–302.

Poncet, C., Soula, C., Trousse, F., Kan, P., Hirsinger, E., Pourquié, O., Duprat, A.-M., and Cochard, P. (1996). Induction of oligodendrocyte progenitors in the trunk neural tube by ventralizing signals: effects of notochord and floor plate grafts, and of sonic hedgehog. *Mechanisms of Development*, 60(1):13–32.

Ponti, G., Obernier, K., Guinto, C., Jose, L., Bonfanti, L., and Álvarez-Buylla, A. (2013). Cell cycle and lineage progression of neural progenitors in the ventricular-subventricular zones of adult mice. *Proceedings of the National Academy of Sciences*, 110(11):E1045–E1054.

Popescu, B. F. G. and Lucchinetti, C. F. (2012). Pathology of demyelinating diseases. *Annual Review of Pathology: Mechanisms of Disease*, 7:185–217.

Pringle, N. P., Yu, W.-P., Guthrie, S., Roelink, H., Lumsden, A., Peterson, A. C., and Richardson, W. D. (1996). Determination of neuroepithelial cell fate: induction of the oligodendrocyte lineage by ventral midline cells and sonic hedgehog. *Developmental Biology*, 177(1):30–42.

Qi, Y., Cai, J., Wu, Y., Wu, R., Lee, J., Fu, H., Rao, M., Sussel, L., Rubenstein, J., and Qiu, M. (2001). Control of oligodendrocyte differentiation by the Nkx2.2 homeodomain transcription factor. *Development*, 128(14):2723–2733.

Quantin, B., Perricaudet, L. D., Tajbakhsh, S., and Mandel, J.-L. (1992). Adenovirus as an expression vector in muscle cells in vivo. *Proceedings of the National Academy of Sciences*, 89(7):2581–2584.

Quarles, R. H., Everly, J. L., and Brady, R. O. (1972). Demonstration of a glycoprotein which is associated with a purified myelin fraction from rat brain. *Biochemical and Biophysical Research Communications*, 47(2):491–497.

Ramagopalan, S. V., Maugeri, N. J., Handunnetthi, L., Lincoln, M. R., Orton, S.-M., Dyment, D. A., DeLuca, G. C., Herrera, B. M., Chao, M. J., Sadovnick, A. D., et al. (2009). Expression of the multiple sclerosis-associated MHC class II allele HLA-DRB1*1501 is regulated by vitamin D. *PLOS Genetics*, 5(2):e1000369.

Ray, J., Peterson, D. A., Schinstine, M., and Gage, F. H. (1993). Proliferation, differentiation, and long-term culture of primary hippocampal neurons. *Proceedings of the National Academy of Sciences*, 90(8):3602–3606.

Reichert, F., Saada, A., and Rotshenker, S. (1994). Peripheral nerve injury induces Schwann cells to express two macrophage phenotypes: phagocytosis and the galactose-specific lectin MAC-2. *Journal of Neuroscience*, 14(5):3231–3245.

Reston, J. T., Uhl, S., Treadwell, J. R., Nash, R. A., and Schoelles, K. (2011). Autologous hematopoietic cell transplantation for multiple sclerosis: a systematic review. *Multiple Sclerosis Journal*, 17(2):204–213.

Reynolds, B. A. and Weiss, S. (1992). Generation of neurons and astrocytes from isolated cells of the adult mammalian central nervous system. *Science*, 255(5052):1707–1710.

Riise, T., Nortvedt, M. W., and Ascherio, A. (2003). Smoking is a risk factor for multiple sclerosis. *Neurology*, 61(8):1122–1124.

Rinholm, J. E., Hamilton, N. B., Kessaris, N., Richardson, W. D., Bergersen, L. H., and Attwell, D. (2011). Regulation of oligodendrocyte development and myelination by glucose and lactate. *Journal of Neuroscience*, 31(2):538–548.

Rivera, F. J., Couillard-Despres, S., Pedre, X., Ploetz, S., Caioni, M., Lois, C., Bogdahn, U., and Aigner, L. (2006). Mesenchymal stem cells instruct oligodendrogenic fate decision on adult neural stem cells. *Stem Cells*, 24(10):2209–2219.

Rivers, T. M. and Schwentker, F. F. (1935). Encephalomyelitis accompanied by myelin destruction experimentally produced in monkeys. *Journal of Experimental Medicine*, 61(5):689–702.

Rivers, T. M., Sprunt, D., and Berry, G. (1933). Observations on attempts to produce acute disseminated encephalomyelitis in monkeys. *Journal of Experimental Medicine*, 58(1):39–53.

Robin, A. M., Zhang, Z. G., Wang, L., Zhang, R. L., Katakowski, M., Zhang, L., Wang, Y., Zhang, C., and Chopp, M. (2006). Stromal cell-derived factor 1α mediates neural progenitor cell motility after focal cerebral ischemia. *Journal of Cerebral Blood Flow & Metabolism*, 26(1):125–134.

Rodriguez, M., Leibowitz, J. L., and Lampert, P. W. (1983). Persistent infection of oligodendrocytes in Theiler's virus-induced encephalomyelitis. *Annals of Neurology*, 13(4):426–433.

Rolet, A., Magnin, E., Millot, J., Berger, E., Vidal, C., Sileman, G., and Rumbach, L. (2012). Olfactory dysfunction in multiple sclerosis: evidence of a decrease in different aspects of olfactory function. *European Neurology*, 69(3):166–170.

Rousselot, P., Lois, C., and Álvarez-Buylla, A. (1995). Embryonic (psa) n-cam reveals chains of migrationg neuroblasts between the lateral ventricle and the olfactory bulb of adult mice. *Journal of Comparative Neurology*, 351(1):51–61.

Ruckh, J. M., Zhao, J.-W., Shadrach, J. L., van Wijngaarden, P., Rao, T. N., Wagers, A. J., and Franklin, R. J. (2012). Rejuvenation of regeneration in the aging central nervous system. *Cell Stem Cell*, 10(1):96–103.

Sabo, J. K., Aumann, T. D., Merlo, D., Kilpatrick, T. J., and Cate, H. S. (2011). Remyelination is altered by bone morphogenic protein signaling in demyelinated lesions. *Journal of Neuroscience*, 31(12):4504–4510.

Sakaguchi, M., Shingo, T., Shimazaki, T., Okano, H. J., Shiwa, M., Ishibashi, S., Oguro, H., Ninomiya, M., Kadoya, T., Horie, H., et al. (2006). A carbohydrate-binding protein, Galectin-1, promotes proliferation of adult neural stem cells. *Proceedings of the National Academy of Sciences*, 103(18):7112–7117.

Sakamoto, M., Ieki, N., Miyoshi, G., Mochimaru, D., Miyachi, H., Imura, T., Yamaguchi, M., Fishell, G., Mori, K., Kageyama, R., et al. (2014). Continuous postnatal neurogenesis contributes to formation of the olfactory bulb neural circuits and flexible olfactory associative learning. *Journal of Neuroscience*, 34(17):5788–5799.

Samanta, J. and Kessler, J. A. (2004). Interactions between ID and OLIG proteins mediate the inhibitory effects of BMP4 on oligodendroglial differentiation. *Development*, 131(17):4131–4142.

Sanai, N., Nguyen, T., Ihrie, R. A., Mirzadeh, Z., Tsai, H.-H., Wong, M., Gupta, N., Berger, M. S., Huang, E., Garcia-Verdugo, J.-M., et al. (2011). Corridors of migrating neurons in the human brain and their decline during infancy. *Nature*, 478(7369):382–386.

Sanai, N., Tramontin, A. D., Quiñones-Hinojosa, A., Barbaro, N. M., Gupta, N., Kunwar, S., Lawton, M. T., McDermott, M. W., Parsa, A. T., Verdugo, J. M.-G., et al. (2004). Unique astrocyte ribbon in adult human brain contains neural stem cells but lacks chain migration. *Nature*, 427(6976):740–744.

Sano, H., Hsu, D. K., Yu, L., Apgar, J. R., Kuwabara, I., Yamanaka, T., Hirashima, M., and Liu, F.-T. (2000). Human galectin-3 is a novel chemoattractant for monocytes and macrophages. *Journal of Immunology*, 165(4):2156–2164.

Sato, S., Ouellet, N., Pelletier, I., Simard, M., Rancourt, A., and Bergeron, M. G. (2002). Role of galectin-3 as an adhesion molecule for neutrophil extravasation during streptococcal pneumonia. *Journal of Immunology*, 168(4):1813–1822.

Sawcer, S., Franklin, R. J., and Ban, M. (2014). Multiple sclerosis genetics. *Lancet Neurology*, 13(7):700–709.

Schattling, B., Steinbach, K., Thies, E., Kruse, M., Menigoz, A., Ufer, F., Flockerzi, V., Brück, W., Pongs, O., Vennekens, R., et al. (2012). TRPM4 cation channel mediates axonal and neuronal degeneration in experimental autoimmune encephalomyelitis and multiple sclerosis. *Nature Medicine*, 18(12):1805–1811.

Sharma, U. C., Pokharel, S., van Brakel, T. J., van Berlo, J. H., Cleutjens, J. P., Schroen, B., André, S., Crijns, H. J., Gabius, H.-J., Maessen, J., et al. (2004). Galectin-3 marks activated macrophages in failure-prone hypertrophied hearts and contributes to cardiac dysfunction. *Circulation*, 110(19):3121–3128.

Shen, S., Sandoval, J., Swiss, V. A., Li, J., Dupree, J., Franklin, R. J., and Casaccia-Bonnefil, P. (2008). Age-dependent epigenetic control of differentiation inhibitors is critical for remyelination efficiency. *Nature Neuroscience*, 11(9):1024–1034.

Shibata, K. and Ajiro, K. (1993). Cell cycle-dependent suppressive effect of histone H1 on mitosis-specific H3 phosphorylation. *Journal of Biological Chemistry*, 268(25):18431–18434.

Shields, S. A., Gilson, J. M., Blakemore, W. F., and Franklin, R. J. (1999). Remyelination occurs as extensively but more slowly in old rats compared to young rats following gliotoxin-induced CNS demyelination. *Glia*, 28(1):77–83.

Shields, S. D., Cheng, X., Gasser, A., Saab, C. Y., Tyrrell, L., Eastman, E. M., Iwata, M., Zwinger, P. J., Black, J. A., Dib-Hajj, S. D., et al. (2012). A channelopathy contributes to cerebellar dysfunction in a model of multiple sclerosis. *Annals of Neurology*, 71(2):186–194.

Siegel, G., Agranoff, B., Albers, R., Fisher, S., and Uhler, M. (1999). *Basic Neurochemistry: Molecular, Cellular and Medical Aspects.* Philadelphia: Lippincott-Raven, sixth edition.

Silvestroff, L., Bartucci, S., Soto, E., Gallo, V., Pasquini, J., and Franco, P. (2010). Cuprizone-induced demyelination in CNP::GFP transgenic mice. *Journal of Comparative Neurology*, 518(12):2261–2283.

Simpson, S., Blizzard, L., Otahal, P., van der Mei, I., and Taylor, B. (2011). Latitude is significantly associated with the prevalence of multiple sclerosis: a meta-analysis. *Journal of Neurology, Neurosurgery & Psychiatry*, 82(10):1132–1141.

Skarnes, W. C., Rosen, B., West, A. P., Koutsourakis, M., Bushell, W., Iyer, V., Mujica, A. O., Thomas, M., Harrow, J., Cox, T., et al. (2011). A conditional knockout resource for the genome-wide study of mouse gene function. *Nature*, 474(7351):337–342.

Smith, K., Blakemore, W., and McDonald, W. (1979). Central remyelination restores secure conduction. *Nature*, 280(5721):395–396.

Smith, K. J. (2006). Axonal protection in multiple sclerosis–a particular need during remyelination? *Brain*, 129(12):3147–3149.

Smith, R. (1992). The basic protein of CNS myelin: its structure and ligand binding. *Journal of Neurochemistry*, 59(5):1589–1608.

Sohn, J., Selvaraj, V., Wakayama, K., Orosco, L., Lee, E., Crawford, S. E., Guo, F., Lang, J., Horiuchi, M., Zarbalis, K., et al. (2012). PEDF is a novel oligodendrogenic morphogen acting on the adult SVZ and corpus callosum. *Journal of Neuroscience*, 32(35):12152–12164.

Sola-Valls, N., Sepúlveda, M., Blanco, Y., and Saiz, A. (2015). Current role of chemotherapy and bone marrow transplantation in multiple sclerosis. *Current Treatment Options in Neurology*, 17(1):1–20.

Song, L., Tang, J.-W., Owusu, L., Sun, M.-Z., Wu, J., and Zhang, J. (2014). Galectin-3 in cancer. *Clinica Chimica Acta*, 431:185–191.

Spassky, N., Merkle, F. T., Flames, N., Tramontin, A. D., García-Verdugo, J. M., and Álvarez-Buylla, A. (2005). Adult ependymal cells are postmitotic and are derived from radial glial cells during embryogenesis. *Journal of Neuroscience*, 25(1):10–18.

Spitzer, T. (2001). Engraftment syndrome following hematopoietic stem cell transplantation. *Bone Marrow Transplantation*, 27(9):893–898.

Sriram, S. and Steiner, I. (2005). Experimental allergic encephalomyelitis: a misleading model of multiple sclerosis. *Annals of Neurology*, 58(6):939–945.

Srivastava, R., Aslam, M., Kalluri, S. R., Schirmer, L., Buck, D., Tackenberg, B., Rothhammer, V., Chan, A., Gold, R., Berthele, A., et al. (2012). Potassium channel KIR4.1 as an immune target in multiple sclerosis. *New England Journal of Medicine*, 367(2):115–123.

Stancic, M., van Horssen, J., Thijssen, V., Gabius, H.-J., van der Valk, P., Hoekstra, D., and Baron, W. (2011). Increased expression of distinct galectins in multiple sclerosis lesions. *Neuropathology and Applied Neurobiology*, 37(6):654–671.

Staples, J., Ponsonby, A.-L., and Lim, L. (2010). Low maternal exposure to ultraviolet radiation in pregnancy, month of birth, and risk of multiple sclerosis in offspring: longitudinal analysis. *British Medical Journal*, 340:c1640.

Stillman, B. N., Hsu, D. K., Pang, M., Brewer, C. F., Johnson, P., Liu, F.-T., and Baum, L. G. (2006). Galectin-3 and galectin-1 bind distinct cell surface glycoprotein receptors to induce T cell death. *Journal of Immunology*, 176(2):778–789.

Stolt, C. C., Lommes, P., Friedrich, R. P., and Wegner, M. (2004). Transcription factors Sox8 and Sox10 perform non-equivalent roles during oligodendrocyte development despite functional redundancy. *Development*, 131(10):2349–2358.

Stolt, C. C., Lommes, P., Sock, E., Chaboissier, M.-C., Schedl, A., and Wegner, M. (2003). The Sox9 transcription factor determines glial fate choice in the developing spinal cord. *Genes & Development*, 17(13):1677–1689.

Stolt, C. C., Rehberg, S., Ader, M., Lommes, P., Riethmacher, D., Schachner, M., Bartsch, U., and Wegner, M. (2002). Terminal differentiation of myelin-forming oligodendrocytes depends on the transcription factor Sox10. *Genes & Development*, 16(2):165–170.

Storan, M. J., Magnaldo, T., Biol-N'Garagba, M.-C., Zick, Y., and Key, B. (2004). Expression and putative role of lactoseries carbohydrates present on NCAM in the rat primary olfactory pathway. *Journal of Comparative Neurology*, 475(3):289–302.

Sundholm-Peters, N. L., Yang, H. K., Goings, G. E., Walker, A. S., and Szele, F. G. (2005). Subventricular zone neuroblasts emigrate toward cortical lesions. *Journal of Neuropathology & Experimental Neurology*, 64(12):1089–1100.

Swinnen, N., Smolders, S., Avila, A., Notelaers, K., Paesen, R., Ameloot, M., Brône, B., Legendre, P., and Rigo, J.-M. (2013). Complex invasion pattern of the cerebral cortex bymicroglial cells during development of the mouse embryo. *Glia*, 61(2):150–163.

Takahashi, K. and Yamanaka, S. (2006). Induction of pluripotent stem cells from mouse embryonic and adult fibroblast cultures by defined factors. *Cell*, 126(4):663–676.

Tavazoie, M., Van der Veken, L., Silva-Vargas, V., Louissaint, M., Colonna, L., Zaidi, B., Garcia-Verdugo, J. M., and Doetsch, F. (2008). A specialized vascular niche for adult neural stem cells. *Cell Stem Cell*, 3(3):279–288.

Taveggia, C., Thaker, P., Petrylak, A., Caporaso, G. L., Toews, A., Falls, D. L., Einheber, S., and Salzer, J. L. (2008). Type III neuregulin-1 promotes oligodendrocyte myelination. *Glia*, 56(3):284–293.

Taylor, L. C., Gilmore, W., and Matsushima, G. K. (2009). SJL mice exposed to cuprizone intoxication reveal strain and gender pattern differences in demyelination. *Brain Pathology*, 19(3):467–479.

Taylor, L. C., Gilmore, W., Ting, J. P.-Y., and Matsushima, G. K. (2010). Cuprizone induces similar demyelination in male and female C57BL/6 mice and results in disruption of the estrous cycle. *Journal of Neuroscience Research*, 88(2):391–402.

Teitelbaum, D., Meshorer, A., Hirshfeld, T., Arnon, R., and Sela, M. (1971). Suppression of experimental allergic encephalomyelitis by a synthetic polypeptide. *European Journal of Immunology*, 1(4):242–248.

Teng, Y. D., Yu, D., Ropper, A. E., Li, J., Kabatas, S., Wakeman, D. R., Wang, J., Sullivan, M. P., Redmond Jr, D. E., Langer, R., et al. (2011). Functional multipotency of stem cells: a conceptual review of neurotrophic factor-based evidence and its role in translational research. *Current Neuropharmacology*, 9(4):574–585.

Tepavčević, V., Lazarini, F., Alfaro-Cervello, C., Kerninon, C., Yoshikawa, K., Garcia-Verdugo, J. M., Lledo, P.-M., Nait-Oumesmar, B., and Baron-Van Evercooren, A. (2011). Inflammation-induced subventricular zone dysfunction leads to olfactory deficits in a targeted mouse model of multiple sclerosis. *Journal of Clinical Investigation*, 121(12):4722–4734.

Thacker, E. L., Mirzaei, F., and Ascherio, A. (2006). Infectious mononucleosis and risk for multiple sclerosis: a meta-analysis. *Annals of Neurology*, 59(3):499–503.

Theiler, M. (1937). Spontaneous encephalomyelitis of mice, a new virus disease. *Journal of Experimental Medicine*, 65(5):705–719.

Theveneau, E. and Mayor, R. (2011). Beads on the run: beads as alternative tools for chemotaxis assays. *Methods in Molecular Biology*, 769:449–460.

Tong, C. K., Han, Y.-G., Shah, J. K., Obernier, K., Guinto, C. D., and Álvarez-Buylla, A. (2014). Primary cilia are required in a unique subpopulation of neural progenitors. *Proceedings of the National Academy of Sciences*, 111(34):12438–12443.

Touahri, Y., Escalas, N., Benazeraf, B., Cochard, P., Danesin, C., and Soula, C. (2012). Sulfatase 1 promotes the motor neuron-to-oligodendrocyte fate switch by activating Shh signaling in Olig2 progenitors of the embryonic ventral spinal cord. *Journal of Neuroscience*, 32(50):18018–18034.

Tribulatti, M. V., Figini, M. G., Carabelli, J., Cattaneo, V., and Campetella, O. (2012). Redundant and antagonistic functions of galectin-1,-3, and-8 in the elicitation of T cell responses. *Journal of Immunology*, 188(7):2991–2999.

Tripathi, R. B., Clarke, L. E., Burzomato, V., Kessaris, N., Anderson, P. N., Attwell, D., and Richardson, W. D. (2011). Dorsally and ventrally derived oligodendrocytes have similar electrical properties but myelinate preferred tracts. *Journal of Neuroscience*, 31(18):6809–6819.

Trowbridge, I. S. and Thomas, M. L. (1994). CD45: an emerging role as a protein tyrosine phosphatase required for lymphocyte activation and development. *Annual Review of Immunology*, 12(1):85–116.

Truong, M.-J., Gruart, V., Liu, F.-T., Prin, L., Capron, A., and Capron, M. (1993). IgE-binding molecules (Mac-2/epsilon BP) expressed by human eosinophils. implication in IgE-dependent eosinophil cytotoxicity. *European Journal of Immunology*, 23(12):3230–3235.

Tsai, C.-M., Guan, C.-H., Hsieh, H.-W., Hsu, T.-L., Tu, Z., Wu, K.-J., Lin, C.-H., and Lin, K.-I. (2011). Galectin-1 and galectin-8 have redundant roles in promoting plasma cell formation. *Journal of Immunology*, 187(4):1643–1652.

Tzartos, J. S., Friese, M. A., Craner, M. J., Palace, J., Newcombe, J., Esiri, M. M., and Fugger, L. (2008). Interleukin-17 production in central nervous system-infiltrating T cells and glial cells is associated with active disease in multiple sclerosis. *American Journal of Pathology*, 172(1):146–155.

Vaknin-Dembinsky, A., Balashov, K., and Weiner, H. L. (2006). IL-23 is increased in dendritic cells in multiple sclerosis and down-regulation of IL-23 by antisense oligos increases dendritic cell IL-10 production. *Journal of Immunology*, 176(12):7768–7774.

van den Brûle, F. A., Waltregny, D., Liu, F.-T., and Castronovo, V. (2000). Alteration of the cytoplasmic/nuclear expression pattern of galectin-3 correlates with prostate carcinoma progression. *International Journal of Cancer*, 89(4):361–367.

van der Mei, I., Ponsonby, A., Dwyer, T., Blizzard, L., Simmons, R., Taylor, B., Butzkueven, H., and Kilpatrick, T. (2003). Past exposure to sun, skin phenotype, and risk of multiple sclerosis: case-control study. *British Medical Journal*, 327(7410):316.

van Kimmenade, R. R., Januzzi, J. L., Ellinor, P. T., Sharma, U. C., Bakker, J. A., Low, A. F., Martinez, A., Crijns, H. J., MacRae, C. A., Menheere, P. P., et al. (2006). Utility of amino-terminal pro-brain natriuretic peptide, galectin-3, and apelin for the evaluation of patients with acute heart failure. *Journal of the American College of Cardiology*, 48(6):1217–1224.

Venturini, G. (1973). Enzymic activities and sodium, potassium and copper concentrations in mouse brain and liver after cuprizone treatment in vivo. *Journal of Neurochemistry*, 21(5):1147–1151.

Vergo, S., Craner, M. J., Etzensperger, R., Attfield, K., Friese, M. A., Newcombe, J., Esiri, M., and Fugger, L. (2011). Acid-sensing ion channel 1 is involved in both axonal injury and demyelination in multiple sclerosis and its animal model. *Brain*, 134(2):571–584.

Vernerey, J., Macchi, M., Magalon, K., Cayre, M., and Durbec, P. (2013). Ciliary neurotrophic factor controls progenitor migration during remyelination in the adult rodent brain. *Journal of Neuroscience*, 33(7):3240–3250.

Vieira, P. L., Heystek, H. C., Wormmeester, J., Wierenga, E. A., and Kapsenberg, M. L. (2003). Glatiramer acetate (copolymer-1, copaxone) promotes Th2 cell development and increased IL-10 production through modulation of dendritic cells. *Journal of Immunology*, 170(9):4483–4488.

Vierbuchen, T., Ostermeier, A., Pang, Z. P., Kokubu, Y., Südhof, T. C., and Wernig, M. (2010). Direct conversion of fibroblasts to functional neurons by defined factors. *Nature*, 463(7284):1035–1041.

Viglietta, V., Baecher-Allan, C., Weiner, H. L., and Hafler, D. A. (2004). Loss of functional suppression by CD4+ CD25+ regulatory T cells in patients with multiple sclerosis. *Journal of Experimental Medicine*, 199(7):971–979.

von Virchow, R. (1854). Über das ausgebreitete vorkommen einer dem nervenmark analogen substanz in den tierischen geweben (on the wide-spread occurance of a substance analogous to nerve marrow in animal tissues). *Virchows Archiv für Pathologische Anatomie*, 6:562–568.

VonDran, M. W., Singh, H., Honeywell, J. Z., and Dreyfus, C. F. (2011). Levels of BDNF impact oligodendrocyte lineage cells following a cuprizone lesion. *Journal of Neuroscience*, 31(40):14182–14190.

Vriesendorp, F. J. (2014). Clinical features and diagnosis of Guillain-Barré syndrome in adults. *UpToDate*. Retrieved from http://www.uptodate.com/contents/clinical-features-and-diagnosis-of-guillain-barre-syndrome-in-adults.

Wada, Y. and Fujinami, R. S. (1993). Viral infection and dissemination through the olfactory pathway and the limbic system by Theiler's virus. *American Journal of Pathology*, 143(1):221.

Walton, N. M., Sutter, B. M., Laywell, E. D., Levkoff, L. H., Kearns, S. M., Marshall, G. P., Scheffler, B., and Steindler, D. A. (2006). Microglia instruct subventricular zone neurogenesis. *Glia*, 54(8):815–825.

Wang, C., You, Y., Qi, D., Zhou, X., Wang, L., Wei, S., Zhang, Z., Huang, W., Liu, Z., Liu, F., et al. (2014). Human and monkey striatal interneurons are derived from the medial ganglionic eminence but not from the adult subventricular zone. *Journal of Neuroscience*, 34(33):10906–10923.

Wang, S., Sdrulla, A., Johnson, J. E., Yokota, Y., and Barres, B. A. (2001). A role for the helix-loop-helix protein Id2 in the control of oligodendrocyte development. *Neuron*, 29(3):603–614.

Wang, T.-W., Zhang, H., and Parent, J. M. (2005). Retinoic acid regulates postnatal neurogenesis in the murine subventricular zone-olfactory bulb pathway. *Development*, 132(12):2721–2732.

Ward, M. E. and Rao, Y. (2005). Investigations of neuronal migration in the central nervous system. *Methods in Molecular Biology*, 294:137–156.

Webb, C., Teitelbaum, D., Arnon, R., and Sela, M. (1973). In vivo and in vitro immunological cross-reactions between basic encephalitogen and synthetic basic polypeptides capable of suppressing experimental allergic encephalomyelitis. *European Journal of Immunology*, 3(5):279–286.

Weinshenker, B. G., O'Brien, P. C., Petterson, T. M., Noseworthy, J. H., Lucchinetti, C. F., Dodick, D. W., Pineda, A. A., Stevens, L. N., and Rodriguez, M. (1999). A randomized trial of plasma exchange in acute central nervous system inflammatory demyelinating disease. *Annals of Neurology*, 46(6):878–886.

Wolswijk, G. (1998). Chronic stage multiple sclerosis lesions contain a relatively quiescent population of oligodendrocyte precursor cells. *Journal of Neuroscience*, 18(2):601–609.

Woodbury, D., Schwarz, E. J., Prockop, D. J., and Black, I. B. (2000). Adult rat and human bone marrow stromal cells differentiate into neurons. *Journal of Neuroscience Research*, 61(4):364–370.

Xie, L., Ni, W.-K., Chen, X.-D., Xiao, M.-B., Chen, B.-Y., He, S., Lu, C.-H., Li, X.-Y., Jiang, F., and Ni, R.-Z. (2012). The expressions and clinical significances of tissue and serum galectin-3 in pancreatic carcinoma. *Journal of Cancer Research and Clinical Oncology*, 138(6):1035–1043.

Xin, M., Yue, T., Ma, Z., Wu, F.-f., Gow, A., and Lu, Q. R. (2005). Myelinogenesis and axonal recognition by oligodendrocytes in brain are uncoupled in Olig1-null mice. *Journal of Neuroscience*, 25(6):1354–1365.

Xing, Y. L., Röth, P. T., Stratton, J. A. S., Chuang, B. H., Danne, J., Ellis, S. L., Ng, S. W., Kilpatrick, T. J., and Merson, T. D. (2014). Adult neural precursor cells from the subventricular zone contribute significantly to oligodendrocyte regeneration and remyelination. *Journal of Neuroscience*, 34(42):14128–14146.

Yamane, J., Nakamura, M., Iwanami, A., Sakaguchi, M., Katoh, H., Yamada, M., Momoshima, S., Miyao, S., Ishii, K., Tamaoki, N., et al. (2010). Transplantation of galectin-1-expressing human neural stem cells into the injured spinal cord of adult common marmosets. *Journal of Neuroscience Research*, 88(7):1394–1405.

Yan, Y.-P., Sailor, K. A., Lang, B. T., Park, S.-W., Vemuganti, R., and Dempsey, R. J. (2007). Monocyte chemoattractant protein-1 plays a critical role in neuroblast migration after focal cerebral ischemia. *Journal of Cerebral Blood Flow & Metabolism*, 27(6):1213–1224.

Yang, H.-J., Wang, H., Zhang, Y., Xiao, L., Clough, R. W., Browning, R., Li, X.-M., and Xu, H. (2009). Region-specific susceptibilities to cuprizone-induced lesions in the mouse forebrain: implications for the pathophysiology of schizophrenia. *Brain Research*, 1270:121–130.

Yang, R.-Y., Hsu, D. K., and LIu, F.-T. (1996). Expression of galectin-3 modulates T-cell growth and apoptosis. *Proceedings of the National Academy of Sciences*, 93(13):6737–6742.

Yeung, M. S., Zdunek, S., Bergmann, O., Bernard, S., Salehpour, M., Alkass, K., Perl, S., Tisdale, J., Possnert, G., Brundin, L., et al. (2014). Dynamics of oligodendrocyte generation and myelination in the human brain. *Cell*, 159(4):766–774.

Young, C. C. (2011). *The adult neural stem cell niche in ischaemic stroke.* DPhil thesis, University College, University of Oxford, United Kingdom.

Young, C. C., Al-Dalahmah, O., Lewis, N. J., Brooks, K. J., Jenkins, M. M., Poirier, F., Buchan, A. M., and Szele, F. G. (2014). Blocked angiogenesis in Galectin-3 null mice does not alter cellular and behavioral recovery after middle cerebral artery occlusion stroke. *Neurobiology of Disease*, 63:155–164.

Young, K. M., Psachoulia, K., Tripathi, R. B., Dunn, S.-J., Cossell, L., Attwell, D., Tohyama, K., and Richardson, W. D. (2013). Oligodendrocyte dynamics in the healthy adult CNS: evidence for myelin remodeling. *Neuron*, 77(5):873–885.

Yu, Y., Chen, Y., Kim, B., Wang, H., Zhao, C., He, X., Liu, L., Liu, W., Wu, L. M. N., Mao, M., et al. (2013). Olig2 targets chromatin remodelers to enhancers to initiate oligodendrocyte differentiation. *Cell*, 152(1):248–261.

Yue, T., Xian, K., Hurlock, E., Xin, M., Kernie, S. G., Parada, L. F., and Lu, Q. R. (2006). A critical role for dorsal progenitors in cortical myelination. *Journal of Neuroscience*, 26(4):1275–1280.

Zajicek, J., Wing, M., Scolding, N., and Compston, D. (1992). Interactions between oligodendrocytes and microglia a major role for complement and tumour necrosis factor in oligodendrocyte adherence and killing. *Brain*, 115(6):1611–1631.

Zappia, E., Casazza, S., Pedemonte, E., Benvenuto, F., Bonanni, I., Gerdoni, E., Giunti, D., Ceravolo, A., Cazzanti, F., Frassoni, F., et al. (2005). Mesenchymal stem cells ameliorate experimental autoimmune encephalomyelitis inducing T-cell anergy. *Blood*, 106(5):1755–1761.

Zeis, T., Probst, A., Steck, A. J., Stadelmann, C., Brück, W., and Schaeren-Wiemers, N. (2009). Molecular changes in white matter adjacent to an active demyelinating lesion in early multiple sclerosis. *Brain Pathology*, 19(3):459–466.

Zhang, H., Vutskits, L., Pepper, M. S., and Kiss, J. Z. (2003). VEGF is a chemoattractant for FGF-2-stimulated neural progenitors. *Journal of Cell Biology*, 163(6):1375–1384.

Zhang, J., Markovic-Plese, S., Lacet, B., Raus, J., Weiner, H., and Hafler, D. (1994). Increased frequency of interleukin 2-responsive T cells specific for myelin basic protein and proteolipid protein in peripheral blood and cerebrospinal fluid of patients with multiple sclerosis. *Journal of Experimental Medicine*, 179(3):973–984.

Zhou, P., Porcionatto, M., Pilapil, M., Chen, Y., Choi, Y., Tolias, K. F., Bikoff, J. B., Hong, E. J., Greenberg, M. E., and Segal, R. A. (2007). Polarized signaling endosomes coordinate BDNF-induced chemotaxis of cerebellar precursors. *Neuron*, 55(1):53–68.

Zhou, Q., Choi, G., and Anderson, D. J. (2001). The bHLH transcription factor Olig2 promotes oligodendrocyte differentiation in collaboration with Nkx2.2. *Neuron*, 31(5):791–807.

Ziv, Y., Ron, N., Butovsky, O., Landa, G., Sudai, E., Greenberg, N., Cohen, H., Kipnis, J., and Schwartz, M. (2006). Immune cells contribute to the maintenance of neurogenesis and spatial learning abilities in adulthood. *Nature Neuroscience*, 9(2):268–275.

Appendices

Appendix A. Reagent preparation

A.1 Animal tissue preparation

Bromodeoxyuridine (BrdU) 10mg/mL	
Sterile normal saline (NaCl 0.9%)	15mL
Sodium hydroxide 10M	15μL
BrdU (Sigma-Aldrich)	150mg
Mix on vortexer until dissolved; also heat to a maximum of 37°C in water bath to aid solubility.	
Final volume	15mL

Cryoprotectant	
Sucrose	300g
Ethylene glycol	300mL
PB 0.1M	fill to 1000mL
Final volume	1000mL

Paraformaldehyde (PFA) 4%	
PFA	40g
PBS 0.1M pH 7.40	1000mL
Heat with 750mL PBS to 65°C on magnetic stirrer for 5 minutes. Add remaining PBS to cool then filter.	
Final volume	1000mL

A.2 Cell culture

Neurobasal A+ (NB-A+)	
Neurobasal-A media 1× (Life Technologies)	480mL
B27 supplement 50× (Life Technologies)	10mL
Glutamax 100× (Life Technologies)	5mL
Penicillin/Streptomycin 100× (Life Technologies)	5mL
Final volume	500mL

Neurobasal with growth factors (NB-GF)	
Neurobasal A+	25mL
EGF (100μg/mL, Sigma)	5μL
bFGF (100μg/mL, R&D Systems)	5μL
Final volume	25mL

10× Polyheme	
Polyheme	600mg
Ethanol	47.5mL
Distilled water	2.5mL
Final volume	50mL

A.3 Common laboratory solutions

Phosphate buffer (PB) 0.1M pH 7.20

Monobasic solution A	
Sodium phosphate monobasic (NaH_2PO_4)	27.8g
Distilled water	Fill to 1000mL
Final volume	1000mL
Dibasic solution B	
Sodium phosphate dibasic (Na_2HPO_4)	28.4g
Distilled water	Fill to 1000mL
Final volume	1000mL
PB 0.1M pH 7.20	
Monobasic solution A	140mL
Dibasic solution B	360mL
Distilled water	500mL
Final volume	1000mL

10× Phosphate buffered saline (PBS) 0.1M pH 7.40

Sodium chloride	80g
Potassium phosphate monobasic (KH_2PO_4)	2.4g
Sodium phosphate dibasic (Na_2HPO_4)	14.4g
Potassium chloride	2g
Distilled water	1000mL
Final volume	1000mL

10× Tris-buffered saline (TBS)

Tris	60.6g
Sodium chloride	87.6g
Distilled water	Fill to 1000mL
Final volume	1000mL

A.4 Immunohistochemistry

X-gal detergent rinse

Igepal	100μL (0.02%)
Sodium deoxycholate	50mg (0.01%)
Magnesium chloride	0.0952g (2mM)
PB 0.1M pH 7.30	500mL
Final volume	500mL

X-gal staining solution

X-gal detergent rinse	50mL
Potassium ferricyanide ($K_3Fe(CN)_6$)	0.0823g (5mM)
Potassium ferrocyanide ($K_4Fe(CN)_6$)	0.1056g (5mM)
Final volume	50mL

A.5 Molecular biology

Genotyping mastermix	
PCR buffer 10× (Sigma-Aldrich)	2.5μL (1×)
Deoxynucleotides	1.25μL (0.2mM)
Primers (×3)	1μL (0.4μM)
Magnesium chloride	1.25μL (2.5mM)
RedTaq polymerase (Sigma-Aldrich, D4309)	1.25μL (1.25 units)
Dimethyl sulfoxide	1.25μL (5%)
Endonuclease free water	9.5μL
Final volume (added to 5μL DNA)	20μL per sample

50× TAE recipe	
Tris	242g
Glacial acetic acid	57.1mL
EDTA 0.5M	100mL
Distilled water	Fill to 1000mL
Final volume	1000mL

Triton X-100 lysis buffer	
Sodium chloride 5M	1.5mL (150mM)
Triton X-100	500μL (1%)
Tris-hydrochloride 1M pH 8	2.5mL (50mM)
Distilled water	45.5mL
Final volume	50mL

A.6 Western blot

A.6.1 Buffers

10× Running buffer pH 8.3	
Glycine	144g
Tris	30.3g
Sodium dodecyl sulphate	10g
Distilled water	Up to 1L
Final volume	1L

10× Stripping buffer	
Sodium dodecyl sulphate 10%	20mL
Tris-hydrochloride 0.5M	12.5mL
Distilled water	67.5mL
β-mercaptoethanol	0.8mL
Final volume	∼100mL

10× Transfer buffer	
Glycine	144g
Tris	30.3g
Distilled water	Up to 1L
Final volume	1L

1× Transfer buffer	
10× Transfer buffer	100mL
Methanol	150mL
Distilled water	750mL
Final volume	1L

A.6.2 Gels

Resolving gel 10%	
Distilled water	5.9mL
Acrylamide mix 30%	5.0mL
Tris 1.5M pH 8.8	3.8mL
Sodium dodecyl sulphate 10%	150μL
Ammonium phosphate 10%	150μL
TEMED	6μL
Final volume (for 2 gels)	$\sim$15mL

Stacking gel	
Distilled water	4.1mL
Acrylamide mix 30%	1.0mL
Tris 1.0M pH 6.8	0.75mL
Sodium dodecyl sulphate 10%	60μL
Ammonium phosphate 10%	60μL
TEMED	6μL
Final volume (for 2 gels)	$\sim$6mL

Appendix B. Computer scripts

B.1 ImageJ macros

B.1.1 CC immunohistochemistry quantification

See description in Methods on p37.

```
macro “Display DAPI [f1]” {
run(“Make Composite”);
Stack.setActiveChannels(“001”);}

macro “Draw box [f2]” {
getCursorLoc(x, y, z, flags);
run(“Select None”);
u = x-200;
v = y-200;
makeRectangle(u, v, 400, 400);}

macro “Clear outside [f3]” {
run(“Clear Outside”);
Stack.setActiveChannels(“110”);}
```

B.1.2 MBP threshold quantification

See description in Methods on p38.

```
macro “Display Dcx [f1]” {
run(“Make Composite”);
Stack.setActiveChannels(“100”);}

macro “OB Regions [f3]” {
getCursorLoc(x, y, z, flags);
run(“Select None”);
setRGBWeights(1,0,0);
getStatistics(area, mean, min, max, std,
   ghistA);
u = x-200;
v = y-200;
makeRectangle(u, v, 400, 400);
setRGBWeights(1,0,0);
getStatistics(area, mean, min, max, std,
   ghistB);
run(“Clear Results”)
for (i=0; i<256; i++) {
setResult(“Value”,i,i);
setResult(“Select Histogram”,i,ghistB[i]);
setResult(“Total Histogram”,i,ghistA[i]);}
setOption(“ShowRowNumbers”, false);
updateResults; }

macro “Cortical Regions [f5]” {
run(“Select None”);
setRGBWeights(1,0,0);
getStatistics(area, mean, min, max, std,
   rhistA);
roiManager(“Select”, 0);
setRGBWeights(1,0,0);
getStatistics(area, mean, min, max, std,
   rhistB);
roiManager(“Deselect”);
roiManager(“Select”, 1);
setRGBWeights(1,0,0);
getStatistics(area, mean, min, max, std,
   rhistC);
roiManager(“Deselect”);
roiManager(“Select”, 2);
setRGBWeights(1,0,0);
getStatistics(area, mean, min, max, std,
   rhistD);
roiManager(“Deselect”);
roiManager(“Select”, 3);
setRGBWeights(1,0,0);
getStatistics(area, mean, min, max, std,
   rhistE);
roiManager(“Deselect”);
roiManager(“Select”, 4);
setRGBWeights(1,0,0);
getStatistics(area, mean, min, max, std,
   rhistF);
roiManager(“Deselect”);
```

```
roiManager("Select", 5);
setRGBWeights(1,0,0);
getStatistics(area, mean, min, max, std,
   rhistG);
roiManager("Deselect");
roiManager("Select", 6);
setRGBWeights(1,0,0);
getStatistics(area, mean, min, max, std,
   rhistH);
roiManager("Deselect");
roiManager("Select", 7);
setRGBWeights(1,0,0);
getStatistics(area, mean, min, max, std,
   rhistI);
roiManager("Deselect");
roiManager("Select", 8);
setRGBWeights(1,0,0);
getStatistics(area, mean, min, max, std,
   rhistJ);
roiManager("Deselect");
roiManager("Select", 9);
setRGBWeights(1,0,0);
getStatistics(area, mean, min, max, std,
   rhistK);
roiManager("Deselect");
run("Clear Results")
for (i=0; i<256; i++) {
setResult("Value",i,i);
setResult("Overall",i,rhistA[i]);
setResult("Layer 1 - motor
   cortex",i,rhistB[i]);
setResult("Layers 2/3 - motor
   cortex",i,rhistC[i]);
setResult("Layer 4 - motor
   cortex",i,rhistD[i]);
setResult("Layer 5 - motor
   cortex",i,rhistE[i]);
setResult("Layer 6 - motor
   cortex",i,rhistF[i]);
setResult("Layer 1 - somatosensory
   cortex",i,rhistG[i]);
setResult("Layers 2/3 - somatosensory
   cortex",i,rhistH[i]);
setResult("Layer 4 - somatosensory
   cortex",i,rhistI[i]);
setResult("Layer 5 - somatosensory
   cortex",i,rhistJ[i]);
setResult("Layer 6 - somatosensory
   cortex",i,rhistK[i]);}
setOption("ShowRowNumbers", false);
updateResults;
title = getString("Brain ID:", "Letter")
roiManager("Draw")
Stack.setActiveChannels("111");
saveAs("JPEG", title); }
```

B.1.3 Neuorosphere proliferation quantification

See description in Methods on p43.

Using Stack Sorter plugin available from http://www.optinav.com/Stack-Sorter.htm. (Downloaded 05 November 2014.)

```
var title = "a string";
var imagedir = "a string";

macro "Clear [c]" {
run("Clear Results");
roiManager("Reset");}

macro "Merge images [1]" {
title = getTitle();
imagedir = getDirectory("image");
run("Images to Stack", "name=Stack
   title=[] use");
run("Stack Sorter");
waitForUser("Switch layers 3 and 4.");
run("Make Montage...", "columns=2
   rows=3 scale=1 first=1 last=6
   increment=0 border=0 font=12");}

macro "Measure [2]" {
run("Measure");
roiManager("Add");
run("Label");
a = nResults;
x = getResult("Length",a-1);
setResult("Calibrated Length (um)", a-1,
   x*1000/462.062);}
```

```
macro “Save [3]” {
imagpath = imagedir+title+“ marked
   up”;
roipath = imagedir+title+“.zip”;
respath = imagedir+title+“.xls”;
saveAs(“JPEG”,imagpath);
saveAs(“Results”, respath);
roiManager(“Save”,roipath);}
```

B.1.4 Explant assay quantification

See description in Methods on p46.

```
macro “Quadrants [f1]” {
r1 = nResults;
u = (getWidth()-6);
v = (getHeight()-6);
makeRectangle(3, 3, u, v);
run(“Crop”);
roiManager(“Reset”);
run(“Color Threshold...”);
waitForUser(“Set threshold for
   determining centroid.”);
Dialog.create(“Threshold values”);
Dialog.addNumber(“Hue minimum:”,0);
Dialog.addNumber(“Hue
   maximum:”,255);
Dialog.addNumber(“Saturation
   minimum:”,0);
Dialog.addNumber(“Saturation
   maximum:”,255);
Dialog.addNumber(“Brightness
   minimum:”,0);
Dialog.addNumber(“Brightness
   maximum:”,255);
Dialog.show();
hueminex = Dialog.getNumber();
huemaxex = Dialog.getNumber();
satminex = Dialog.getNumber();
satmaxex = Dialog.getNumber();
briminex = Dialog.getNumber();
brimaxex = Dialog.getNumber();
roiManager(“Reset”);
run(“Analyze Particles...”,
   “size=100000-Infinity
   circularity=0.00-1.00 show=Nothing
   display add”);
updateResults();
region = getNumber(“Appropriate
   Region of Interest:”, 0);
roiManager(“Reset”);
x = getResult(“X”,r1+region-1);
y = getResult(“Y”,r1+region-1);
explarea =
   getResult(“Area”,r1+region-1);
r2 = nResults-1;
IJ.deleteRows(r1, r2);
run(“Color Threshold...”);
waitForUser(“Set threshold for migrating
   neuroblasts.”);
Dialog.create(“Threshold values”);
Dialog.addNumber(“Hue minimum:”,0);
Dialog.addNumber(“Hue
   maximum:”,255);
Dialog.addNumber(“Saturation
   minimum:”,0);
Dialog.addNumber(“Saturation
   maximum:”,255);
Dialog.addNumber(“Brightness
   minimum:”,0);
Dialog.addNumber(“Brightness
   maximum:”,255);
Dialog.show();
hueminnb = Dialog.getNumber();
huemaxnb = Dialog.getNumber();
satminnb = Dialog.getNumber();
satmaxnb = Dialog.getNumber();
briminnb = Dialog.getNumber();
brimaxnb = Dialog.getNumber();
if (x>y) {
a = 0;
b = y-x;
} else {
a = x-y;
b = 0;}
if ((u-x)>y) {
c = u;
d = y+x-u;
} else {
c = x+y;
d = 0;}
if ((u-x)>(v-y)) {
e = u;
```

```
f = u+y-x;
} else {
e = v+x-y;
f = v;}
if (x>(v-y)) {
g = 0;
h = x+y;
} else {
g = x+y-v;
h = v;}
makePolygon(x,y,a,b,c,d);
roiManager("Add");
makePolygon(x,y,c,d,e,f);
roiManager("Add");
makePolygon(x,y,e,f,g,h);
roiManager("Add");
makePolygon(x,y,g,h,a,b);
roiManager("Add");
roiManager("Select", 0);
setRGBWeights(1,0,0);
getStatistics(area, mean, min, max, std,
   rhist0);
roiManager("Select", 1);
setRGBWeights(1,0,0);
getStatistics(area, mean, min, max, std,
   rhist1);
roiManager("Select", 2);
setRGBWeights(1,0,0);
getStatistics(area, mean, min, max, std,
   rhist2);
roiManager("Select", 3);
setRGBWeights(1,0,0);
getStatistics(area, mean, min, max, std,
   rhist3);
setColor("yellow");
setLineWidth(2);
drawLine(a,b,e,f);
drawLine(c,d,g,h);
setColor("green");
setFont("Monospaced", 72);
drawString(rhist0[255],x,92);
drawString(rhist1[255],(u-getStringWidth
   (rhist1[255])-20),y);
drawString(rhist2[255],x,v-20);
drawString(rhist3[255],20,y);
title = getTitle();
imagedir = getDirectory("image");
path = imagedir+title+" - processed";
saveAs("JPEG", path);
setResult("Label", r1, title);
setResult("Area", r1, explarea);
setResult("X", r1, x);
setResult("Y", r1, y);
setResult("TopQ", r1, rhist0[255]);
setResult("RightQ", r1, rhist1[255]);
setResult("BottomQ", r1, rhist2[255]);
setResult("LeftQ", r1, rhist3[255]);
setResult("HueMinEx", r1, hueminex);
setResult("HueMaxEx", r1, huemaxex);
setResult("SatMinEx", r1, satminex);
setResult("SatMaxEx", r1, satmaxex);
setResult("BriMinEx", r1, briminex);
setResult("BriMaxEx", r1, brimaxex);
setResult("HueMinNB", r1, hueminnb);
setResult("HueMaxNB", r1, huemaxnb);
setResult("SatMinNB", r1, satminnb);
setResult("SatMaxNB", r1, satmaxnb);
setResult("BriMinNB", r1, briminnb);
setResult("BriMaxNB", r1, brimaxnb);
updateResults();}
```

B.2 SPSS syntax

B.2.1 Student's t-test

Example used for comparing the RT-PCR cDNA quantities for four genes (VAR00001, VAR00002, VAR00003, VAR00004) between two genotypes (Genotype; 1 = Gal-$3^{+/+}$, 2 = Gal-$3^{-/-}$).

```
EXAMINE VARIABLES=VAR00001, VAR00002, VAR00003, VAR00004 BY
   Genotype
   /PLOT BOXPLOT NPPLOT
   /COMPARE GROUPS
   /STATISTICS DESCRIPTIVES
   /CINTERVAL 95
   /MISSING LISTWISE
   /NOTOTAL.
T-TEST GROUPS=Genotype(1 2)
   /MISSING=ANALYSIS
   /VARIABLES=VAR00001, VAR00002, VAR00003, VAR00004
   /CRITERIA=CI(.95).
```

B.2.2 One-way ANOVA

Example used for comparing the density of Gal-3+ cells in the SVZ (VAR00001) across four treatment groups (Treatment; control, 3-week cuprizone, 6-week cuprizone, remyelination).

```
SORT CASES BY Treatment (A).
SPLIT FILE SEPARATE BY Treatment.
EXAMINE VARIABLES=VAR00001
   /PLOT BOXPLOT NPPLOT
   /COMPARE GROUPS
   /STATISTICS NONE
   /CINTERVAL 95
   /MISSING LISTWISE
   /NOTOTAL.
SPLIT FILE OFF.
MEANS TABLES=VAR00001 BY Treatment
   /CELLS MEAN STDDEV SEMEAN COUNT.
UNIANOVA VAR00001 BY Treatment
   /METHOD=SSTYPE(3)
   /INTERCEPT=INCLUDE
   /SAVE=SRESID
   /POSTHOC=Treatment (BONFERRONI)
   /EMMEANS=TABLES(Treatment) COMPARE ADJ(BONFERRONI)
   /PRINT=HOMOGENEITY DESCRIPTIVE
   /CRITERIA=ALPHA(.05)
   /DESIGN=Treatment.
EXAMINE VARIABLES=SRE_1
```

```
  /PLOT BOXPLOT NPPLOT
  /COMPARE GROUPS
  /STATISTICS NONE
  /CINTERVAL 95
  /MISSING LISTWISE
  /NOTOTAL.
```

B.2.3 Two-way ANOVA

Example used for comparing the density of CD45+ cells in the SVZ (VAR00001) across two genotypes (Genotype; Gal-$3^{+/+}$, Gal-$3^{-/-}$) and four treatment groups (Treatment; control, 3-week cuprizone, 6-week cuprizone, remyelination).

```
SORT CASES BY Genotype(A) Treatment(A).
SPLIT FILE SEPARATE BY Genotype Treatment.
EXAMINE VARIABLES=VAR00001
  /PLOT BOXPLOT NPPLOT
  /COMPARE GROUPS
  /STATISTICS NONE
  /CINTERVAL 95
  /MISSING LISTWISE
  /NOTOTAL.
SPLIT FILE OFF.
MEANS TABLES=VAR00001 BY Treatment BY Genotype
  /CELLS MEAN STDDEV SEMEAN COUNT.
UNIANOVA VAR00001 BY Treatment Genotype
  /METHOD=SSTYPE(3)
  /INTERCEPT=INCLUDE
  /SAVE=SRESID
  /POSTHOC=Treatment Genotype(BONFERRONI)
  /EMMEANS=TABLES(Treatment) COMPARE ADJ(BONFERRONI)
  /EMMEANS=TABLES(Genotype) COMPARE ADJ(BONFERRONI)
  /EMMEANS=TABLES(Treatment*Genotype) COMPARE(Treatment)
     ADJ(BONFERRONI)
  /EMMEANS=TABLES(Treatment*Genotype) COMPARE(Genotype)
     ADJ(BONFERRONI)
  /PRINT=HOMOGENEITY DESCRIPTIVE
  /CRITERIA=ALPHA(.05)
  /DESIGN=Treatment Genotype Treatment*Genotype.
EXAMINE VARIABLES=SRE_1
  /PLOT BOXPLOT NPPLOT
  /COMPARE GROUPS
  /STATISTICS NONE
  /CINTERVAL 95
  /MISSING LISTWISE
  /NOTOTAL.
```

B.2.4 Repeated measures ANOVA

Example used for comparing the number of PHi3+ cells in two CC regions (Regions; VAR00001, VAR00002) across two genotypes (Genotype; Gal-$3^{+/+}$, Gal-$3^{-/-}$) and four treatment groups (Treatment; control, 3-week cuprizone, 6-week cuprizone, remyelination).

```
SORT CASES BY Genotype(A) Treatment(A).
SPLIT FILE SEPARATE BY Genotype Treatment.
EXAMINE VARIABLES=VAR00001
  /PLOT BOXPLOT NPPLOT
  /COMPARE GROUPS
  /STATISTICS NONE
  /CINTERVAL 95
  /MISSING LISTWISE
  /NOTOTAL.
EXAMINE VARIABLES=VAR00002
  /PLOT BOXPLOT NPPLOT
  /COMPARE GROUPS
  /STATISTICS NONE
  /CINTERVAL 95
  /MISSING LISTWISE
  /NOTOTAL.
SPLIT FILE OFF.
MEANS TABLES=VAR00001 BY Treatment BY Genotype
  /CELLS MEAN STDDEV SEMEAN COUNT.
MEANS TABLES=VAR00002 BY Treatment BY Genotype
  /CELLS MEAN STDDEV SEMEAN COUNT.
GLM VAR00001 VAR00002 BY Treatment Genotype
  /WSFACTOR=Regions 2 Polynomial
  /MEASURE=CC
  /METHOD=SSTYPE(3)
  /SAVE=SRESID
  /POSTHOC=Treatment(BONFERRONI)
  /EMMEANS=TABLES(Treatment) COMPARE ADJ(BONFERRONI)
  /EMMEANS=TABLES(Genotype) COMPARE ADJ(BONFERRONI)
  /EMMEANS=TABLES(Regions) COMPARE ADJ(BONFERRONI)
  /EMMEANS=TABLES(Treatment*Genotype) COMPARE(Treatment)
     ADJ(BONFERRONI)
  /EMMEANS=TABLES(Treatment*Genotype) COMPARE(Genotype)
     ADJ(BONFERRONI)
  /EMMEANS=TABLES(Treatment*Regions) COMPARE(Treatment)
     ADJ(BONFERRONI)
  /EMMEANS=TABLES(Treatment*Regions) COMPARE(Regions)
     ADJ(BONFERRONI)
  /EMMEANS=TABLES(Genotype*Regions) COMPARE(Genotype)
     ADJ(BONFERRONI)
  /EMMEANS=TABLES(Genotype*Regions) COMPARE(Regions)
     ADJ(BONFERRONI)
  /EMMEANS=TABLES(Treatment*Genotype*Regions) COMPARE(Treatment)
```

```
    ADJ(BONFERRONI)
  /EMMEANS=TABLES(Treatment*Genotype*Regions) COMPARE(Genotype)
    ADJ(BONFERRONI)
  /EMMEANS=TABLES(Treatment*Genotype*Regions) COMPARE(Regions)
    ADJ(BONFERRONI)
  /PRINT=DESCRIPTIVE
  /CRITERIA=ALPHA(.05)
  /WSDESIGN=Regions
  /DESIGN= Treatment Genotype Treatment*Genotype.
EXAMINE VARIABLES=SRE_1
  /PLOT BOXPLOT NPPLOT
  /COMPARE GROUPS
  /STATISTICS NONE
  /CINTERVAL 95
  /MISSING LISTWISE
  /NOTOTAL.
EXAMINE VARIABLES=SRE_2
  /PLOT BOXPLOT NPPLOT
  /COMPARE GROUPS
  /STATISTICS NONE
  /CINTERVAL 95
  /MISSING LISTWISE
  /NOTOTAL.
```

Appendix C. Repeated measures ANOVA statistics

C.1 PHi3+ cells in the SVZ and CC after cuprizone treatment

PHi3 immunohistochemistry was used to quantify the number of proliferating cells (Section 4.2.7 on p84). Differences were analysed using a repeated measures ANOVA for SVZ or CC Region (dorsolateral, striatal, ventral or septal; or medial or lateral) that also compared Genotype (Gal-$3^{+/+}$ or Gal-$3^{-/-}$) and Treatment (control, 3-week cuprizone, 6-week cuprizone or remyelination).

Table C.1: **Means.** Table displays mean ± SEM.

	Control		3-week cuprizone		6-week cuprizone		Remyelination	
	Gal-$3^{+/+}$	Gal-$3^{-/-}$	Gal-$3^{+/+}$	Gal-$3^{-/-}$	Gal-$3^{+/+}$	Gal-$3^{-/-}$	Gal-$3^{+/+}$	Gal-$3^{-/-}$
Number (N)	10	9	6	6	6	6	6	6
Dosolateral SVZ	67.50 ± 8.55	69.33 ± 4.98	39.67 ± 7.89	31.17 ± 7.30	28.33 ± 4.54	35.83 ± 6.35	101.00 ± 11.94	89.83 ± 11.21
Striatal SVZ	50.30 ± 4.05	53.11 ± 5.25	11.50 ± 3.42	14.33 ± 6.44	7.67 ± 1.31	7.33 ± 1.96	54.00 ± 7.69	61.00 ± 9.52
Ventral SVZ	32.70 ± 3.71	33.00 ± 5.79	2.50 ± 0.72	3.67 ± 1.33	2.83 ± 1.08	4.50 ± 1.59	31.33 ± 6.50	37.17 ± 6.26
Septal SVZ	29.60 ± 3.98	24.56 ± 3.59	4.50 ± 1.15	7.00 ± 1.93	4.33 ± 0.88	4.83 ± 1.11	36.00 ± 4.78	47.50 ± 5.78
Medial CC	0.60 ± 0.22	0.44 ± 0.24	0.50 ± 0.34	0.17 ± 0.17	0.67 ± 0.21	2.83 ± 2.24	1.00 ± 0.63	0.33 ± 0.21
Lateral CC	1.10 ± 0.31	1.44 ± 0.38	0.33 ± 0.21	0.50 ± 0.34	18.00 ± 4.63	16.83 ± 4.51	12.00 ± 5.07	14.50 ± 5.57

Table C.2: **Sphericity testing.** Table displays sphericity of data with the conclusion that future analysis of SVZ data should use the Greenhouse-Geisser correction; sphericity testing could not be completed for CC as there were only two variables.

	Within Subjects Effect	Approx. Chi-Square	Degrees of Freedom (df)	Significance	Epsilon (Greenhouse-Geisser)	Epsilon (Huynh-Feldt)
SVZ	Region	50.750	5	**0.000**	0.591	0.704
CC	Region	0.000	0	.	1.000	1.000

Table C.3: **Main effects and interactions.** Table displays main effects and interactions for different comparisons. The most complex interaction was for Region * Treatment for both SVZ and CC. It was used for the pairwise comparisons.

	Comparison	df	F	Significance
SVZ	Treatment	3	49.754	**0.000**
	Genotype	1	0.166	0.685
	Treatment * Genotype	3	0.084	0.968
	Error	47		
	Region	1.773	140.262	**0.000**
	Region * Treatment	5.320	5.566	**0.000**
	Region * Genotype	1.773	0.710	0.478
	Region * Treatment * Genotype	5.320	1.097	0.370
	Error(Region)	83.354		
CC	Treatment	3	13.970	**0.000**
	Genotype	1	0.086	0.770
	Treatment * Genotype	3	0.032	0.992
	Error	47		
	Region	1	49.757	**0.000**
	Region * Treatment	3	15.275	**0.000**
	Region * Genotype	1	0.010	0.920
	Region * Treatment * Genotype	3	0.383	0.766
	Error(Region)	47		

Table C.4: **Pairwise comparisons for Region * Treatment in the SVZ.** Table displays the pairwise comparisons for different regions and treatments in the SVZ. The pairwise comparisons focus on differences between treatments. The differences between regions were ignored as they were expected due to anatomic heterogeneity. Bonferroni adjustment was used for multiple comparisons.

Region	Treatment A	Treatment B	Mean Difference (A-B)	Standard Error	Significance
Dorsolateral SVZ	Control	3-week cuprizone	33.000	7.930	**0.001**
	Control	6-week cuprizone	36.333	7.930	**0.000**
	Control	Remyelination	-27.000	7.930	**0.008**
	3-week cuprizone	6-week cuprizone	3.333	8.775	1.000
	3-week cuprizone	Remyelination	-60.000	8.775	**0.000**
	6-week cuprizone	Remyelination	-63.333	8.775	**0.000**
Striatal SVZ	Control	3-week cuprizone	38.789	5.306	**0.000**
	Control	6-week cuprizone	44.206	5.306	**0.000**
	Control	Remyelination	-5.794	5.306	1.000
	3-week cuprizone	6-week cuprizone	5.417	5.871	1.000
	3-week cuprizone	Remyelination	-44.583	5.871	**0.000**
	6-week cuprizone	Remyelination	-50.000	5.871	**0.000**
Ventral SVZ	Control	3-week cuprizone	29.767	4.262	**0.000**
	Control	6-week cuprizone	29.183	4.262	**0.000**
	Control	Remyelination	-1.400	4.262	1.000
	3-week cuprizone	6-week cuprizone	-0.583	4.716	1.000
	3-week cuprizone	Remyelination	-31.167	4.716	**0.000**
	6-week cuprizone	Remyelination	-30.583	4.716	**0.000**
Septal SVZ	Control	3-week cuprizone	21.328	3.511	**0.000**
	Control	6-week cuprizone	22.494	3.511	**0.000**
	Control	Remyelination	-14.672	3.511	**0.001**
	3-week cuprizone	6-week cuprizone	1.167	3.886	1.000
	3-week cuprizone	Remyelination	-36.000	3.886	**0.000**
	6-week cuprizone	Remyelination	-37.167	3.886	**0.000**

Table C.5: **Pairwise comparisons for Region * Treatment in the CC.** Table displays the pairwise comparisons for the interaction between Region * Treatment in the CC. Given the anatomic heterogeneity between regions, those pairwise comparisons were ignored. Instead the pairwise comparisons focus on differences between treatments. Bonferroni adjustment was used for multiple comparisons.

Region	Treatment A	Treatment B	Mean Difference (A-B)	Standard Error	Significance
Medial CC	Control	3-week cuprizone	0.189	0.719	1.000
	Control	6-week cuprizone	-1.228	0.719	0.566
	Control	Remyelination	-0.144	0.719	1.000
	3-week cuprizone	6-week cuprizone	-1.417	0.796	0.488
	3-week cuprizone	Remyelination	-0.333	0.796	1.000
	6-week cuprizone	Remyelination	1.083	0.796	1.000
Lateral CC	Control	3-week cuprizone	0.856	2.937	1.000
	Control	6-week cuprizone	-16.144	2.937	**0.000**
	Control	Remyelination	-11.978	2.937	**0.001**
	3-week cuprizone	6-week cuprizone	-17.000	3.250	**0.000**
	3-week cuprizone	Remyelination	-12.833	3.250	**0.002**
	6-week cuprizone	Remyelination	4.167	3.250	1.000

C.2 Olig2+ cells in the SVZ after cuprizone treatment

Olig2 immunohistochemistry was used to quantify the number of oligodendrocyte lineage cells (Section 5.2.1 on p104). Differences were analysed using a repeated measures ANOVA for SVZ Region (dorsolateral, upper striatal, lower striatal, ventral, septal or subcallosal) that also compared Genotype (Gal-$3^{+/+}$ or Gal-$3^{-/-}$) and Treatment (control, 3-week cuprizone, 6-week cuprizone or remyelination).

Table C.6: **Means.** Table displays mean ± SEM.

	Control		3-week cuprizone		6-week cuprizone		Remyelination	
	Gal-$3^{+/+}$	Gal-$3^{-/-}$	Gal-$3^{+/+}$	Gal-$3^{-/-}$	Gal-$3^{+/+}$	Gal-$3^{-/-}$	Gal-$3^{+/+}$	Gal-$3^{-/-}$
Number (N)	10	9	6	6	6	6	6	6
Dorsolateral SVZ	16.30 ± 2.60	23.22 ± 2.87	21.50 ± 3.77	23.83 ± 3.56	24.33 ± 3.41	26.00 ± 5.56	20.50 ± 4.72	23.83 ± 5.58
Upper striatal SVZ	8.90 ± 1.29	11.44 ± 1.09	13.50 ± 2.62	15.33 ± 1.82	12.67 ± 2.91	14.83 ± 3.75	10.50 ± 2.46	12.67 ± 2.78
Lower striatal SVZ	17.90 ± 3.31	24.44 ± 4.27	21.83 ± 4.09	20.00 ± 1.18	15.67 ± 3.40	20.33 ± 5.31	20.83 ± 7.67	21.67 ± 2.43
Ventral SVZ	14.10 ± 1.81	19.67 ± 3.69	14.83 ± 4.70	12.83 ± 1.35	18.33 ± 4.32	13.00 ± 1.41	17.67 ± 4.33	18.67 ± 4.45
Septal SVZ	15.70 ± 2.25	22.00 ± 3.70	20.00 ± 3.27	17.33 ± 2.28	16.00 ± 3.63	18.50 ± 4.73	15.67 ± 7.37	21.17 ± 3.88
Subcallosal SVZ	13.20 ± 1.44	16.22 ± 1.37	16.00 ± 4.89	14.00 ± 2.07	15.17 ± 2.40	17.00 ± 1.86	7.33 ± 2.35	12.83 ± 3.45

Table C.7: **Sphericity testing.** Table displays sphericity of data with the conclusion that future analysis of SVZ data should use the Huynh-Feldt correction.

Within Subjects Effect	Approx. Chi-Square	df	Significance	Epsilon (Greenhouse-Geisser)	Epsilon (Huynh-Feldt)
Region	37.475	14	**0.001**	0.785	0.993

Table C.8: **Main effects and interactions.** Table displays main effects and interactions for different comparisons. There were no interactions and the only main effect occurred for Region. Given the heterogeneity between regions, this result was not investigated further with pairwise comparisons.

Comparison	df	F	Significance
Genotype	1	1.220	0.275
Treatment	3	0.041	0.989
Genotype * Treatment	3	0.452	0.717
Error	47		
Region	4.965	20.515	**0.000**
Region * Genotype	4.965	0.583	0.712
Region * Treatment	14.896	1.519	0.100
Region * Genotype * Treatment	14.896	0.533	0.920
Error(Region)	233.368		

C.3 MBP threshold values in the cortex after cuprizone treatment

MBP immunohistochemistry was quantified by calculating the percentage of pixels above a given intensity (Section 5.2.5 on p113). Differences were then analysed using a repeated measures ANOVA for Cortical Region (motor or somatosensory) and Cortical Layer (Layer 4, 5 or 6) that also compared Genotype (Gal-$3^{+/+}$ or Gal-$3^{-/-}$) and Treatment (control, 3-week cuprizone, 6-week cuprizone or remyelination).

Table C.9: **Means.** Table displays mean ± SEM.

		Control		3-week cuprizone		6-week cuprizone		Remyelination	
		Gal-$3^{+/+}$	Gal-$3^{-/-}$	Gal-$3^{+/+}$	Gal-$3^{-/-}$	Gal-$3^{+/+}$	Gal-$3^{-/-}$	Gal-$3^{+/+}$	Gal-$3^{-/-}$
Number (N)		10	9	6	6	6	6	6	6
Motor cortex	Layer 4	35.63 ± 10.50	38.71 ± 12.46	25.48 ± 12.92	24.33 ± 9.66	0.34 ± 0.21	0.62 ± 0.33	1.03 ± 0.29	9.07 ± 3.86
	Layer 5	49.30 ± 10.22	45.85 ± 11.39	31.88 ± 12.31	49.64 ± 9.74	1.83 ± 1.02	3.71 ± 2.83	2.56 ± 0.49	9.04 ± 2.57
	Layer 6	65.72 ± 10.84	62.61 ± 10.19	47.30 ± 13.98	80.98 ± 6.14	50.80 ± 13.96	65.34 ± 8.30	8.10 ± 2.15	25.19 ± 6.78
Somato-sensory cortex	Layer 4	49.69 ± 9.23	53.90 ± 10.47	58.34 ± 12.83	65.00 ± 9.54	15.44 ± 5.83	4.76 ± 2.19	9.46 ± 3.83	27.86 ± 8.92
	Layer 5	64.95 ± 7.51	65.51 ± 9.63	67.72 ± 11.36	83.23 ± 4.26	33.17 ± 9.77	19.58 ± 4.24	20.98 ± 6.89	29.28 ± 7.89
	Layer 6	65.78 ± 7.85	66.43 ± 8.77	69.30 ± 10.69	85.06 ± 5.37	67.38 ± 12.04	55.01 ± 8.88	15.48 ± 14.08	16.91 ± 10.10

Table C.10: **Sphericity testing.** Table displays sphericity of data with the conclusion that future analysis of Cortical Layer and Cortical Layer * Cortical Region data should use the Greenhouse-Geisser correction; sphericity testing could not be completed for Cortical Region as there were only two variables.

Within Subjects Effect	Approx. Chi-Square	df	Significance	Epsilon (Greenhouse-Geisser)	Epsilon (Huynh-Feldt)
Cortical Layer	36.171	2	**0.000**	0.647	0.757
Cortical Region	0.000	0	.	1.000	1.000
Cortical Layer * Cortical Region	19.418	2	**0.000**	0.744	0.877

Table C.11: **Main effects and interactions.** Table displays main effects and interactions for different comparisons. The most complex interactions were for Cortical Layer * Treatment and Cortical Layer * Cortical Region * Genotype, which were used for the pairwise comparisons.

Comparison	df	F	Significance
Genotype	1	1.022	0.317
Treatment	3	15.838	**0.000**
Genotype * Treatment	3	0.587	0.627
Error	47		
Cortical Layer	1.295	114.406	**0.000**
Cortical Layer * Genotype	1.295	1.101	0.315
Cortical Layer * Treatment	3.885	20.122	**0.000**
Cortical Layer * Genotype * Treatment	3.885	1.650	0.175
Error(Cortical Layer)	60.862		
Cortical Region	1	24.357	**0.000**
Cortical Region * Genotype	1	0.629	0.432
Cortical Region * Treatment	3	1.657	0.189
Cortical Region * Genotype * Treatment	3	0.518	0.672
Error(Cortical Region)	47		
Cortical Layer * Cortical Region	1.488	21.657	**0.000**
Cortical Layer * Cortical Region * Genotype	1.488	3.714	**0.042**
Cortical Layer * Cortical Region * Treatment	4.463	0.859	0.503
Cortical Layer * Cortical Region * Genotype * Treatment	4.463	0.740	0.582
Error(Cortical Layer * Cortical Region)	69.922		

Table C.12: **Pairwise comparisons for Cortical Layer * Treatment.** Table displays the pairwise comparisons for the interaction between Cortical Layer * Treatment. Given different threshold values were used between cortical layers, those pairwise comparisons were ignored. Instead the pairwise comparisons focus on differences between treatments. Bonferroni adjustment was used for multiple comparisons.

Cortical Layer	Treatment A	Treatment B	Mean Difference (A-B)	Standard Error	Significance
Layer 4	Control	3-week cuprizone	1.196	7.768	1.000
	Control	6-week cuprizone	39.195	7.768	**0.000**
	Control	Remyelination	32.629	7.768	**0.001**
	3-week cuprizone	6-week cuprizone	37.999	8.595	**0.000**
	3-week cuprizone	Remyelination	31.433	8.595	**0.004**
	6-week cuprizone	Remyelination	-6.567	8.595	1.000
Layer 5	Control	3-week cuprizone	-1.717	7.142	1.000
	Control	6-week cuprizone	41.829	7.142	**0.000**
	Control	Remyelination	40.938	7.142	**0.000**
	3-week cuprizone	6-week cuprizone	43.546	7.903	**0.000**
	3-week cuprizone	Remyelination	42.655	7.903	**0.000**
	6-week cuprizone	Remyelination	-0.891	7.903	1.000
Layer 6	Control	3-week cuprizone	-5.525	8.141	1.000
	Control	6-week cuprizone	5.504	8.141	1.000
	Control	Remyelination	48.717	8.141	**0.000**
	3-week cuprizone	6-week cuprizone	11.029	9.009	1.000
	3-week cuprizone	Remyelination	54.243	9.009	**0.000**
	6-week cuprizone	Remyelination	43.213	9.009	**0.000**

Table C.13: **Pairwise comparisons for Cortical Region * Cortical Layer * Genotype.** Table displays the pairwise comparisons for the interaction between Cortical Region * Cortical Layer * Genotype. Given different threshold values were used between cortical layers and cortical regions, those pairwise comparisons were ignored. Instead the pairwise comparisons focus on differences between genotypes. Bonferroni adjustment was used for multiple comparisons.

Cortical Region	Cortical Layer	Genotype A	Genotype B	Mean Difference (=A-B)	Standard Error	Significance
Motor Cortex	Layer 4	Gal-$3^{+/+}$	Gal-$3^{-/-}$	-2.558	6.877	0.712
	Layer 5	Gal-$3^{+/+}$	Gal-$3^{-/-}$	-5.669	6.547	0.391
	Layer 6	Gal-$3^{+/+}$	Gal-$3^{-/-}$	-15.548	7.452	**0.042**
Somatosensory Cortex	Layer 4	Gal-$3^{+/+}$	Gal-$3^{-/-}$	-4.647	6.621	0.486
	Layer 5	Gal-$3^{+/+}$	Gal-$3^{-/-}$	-2.692	6.068	0.659
	Layer 6	Gal-$3^{+/+}$	Gal-$3^{-/-}$	-1.367	7.077	0.848

C.4 MBP threshold values in the OB after cuprizone treatment

MBP immunohistochemistry was quantified by calculating the percentage of pixels above a given intensity (Section 5.2.6 on p115). Differences were then analysed using a repeated measures ANOVA for Anterior-Posterior (A-P) Axis (anterior, middle or posterior) and OB Region (glomerular layer, external plexiform layer or granular layer) that also compared Treatment (control, 3-week cuprizone, 6-week cuprizone or remyelination).

Table C.14: **Means.** Table displays mean ± SEM.

		Control	3-week cuprizone	6-week cuprizone	Remyelination
Number (N)		10	6	6	6
Glomerular layer	Anterior	13.75 ± 2.40	4.42 ± 0.64	0.45 ± 0.17	5.39 ± 1.56
	Middle	10.90 ± 2.92	4.80 ± 1.82	1.19 ± 0.85	6.02 ± 1.20
	Posterior	10.11 ± 3.25	2.07 ± 0.99	0.25 ± 0.14	7.65 ± 1.54
External plexiform layer	Anterior	29.65 ± 5.28	13.92 ± 1.82	7.36 ± 2.12	12.38 ± 1.28
	Middle	18.83 ± 4.23	17.80 ± 3.70	5.08 ± 1.57	18.98 ± 3.82
	Posterior	25.56 ± 8.30	19.27 ± 5.76	4.76 ± 1.55	11.63 ± 2.37
Granular layer	Anterior	17.13 ± 4.49	9.64 ± 3.16	8.52 ± 2.02	5.12 ± 2.11
	Middle	11.08 ± 1.80	13.20 ± 4.26	3.28 ± 1.10	8.75 ± 2.65
	Posterior	13.13 ± 3.54	14.35 ± 4.07	7.19 ± 3.48	8.83 ± 2.67

Table C.15: **Sphericity testing.** Table displays that data has sphericity and future calculations can be performed without corrections.

Within Subjects Effect	Approx. Chi-Square	df	Significance
A-P Axis	3.733	2	0.155
OB Region	1.243	2	0.537
A-P Axis * OB Region	15.737	9	0.073

Table C.16: **Main effects and interactions.** Table displays main effects and interactions for different comparisons. The most complex interaction was OB Region * Treatment, which was used for the pairwise comparisons.

Comparison	df	F	Significance
Treatment	3	7.045	**0.001**
Error (Treatment)	24		
A-P Axis	2	0.053	0.948
A-P Axis * Treatment	6	0.823	0.557
Error(A-P Axis)	48		
OB Region	2	29.948	**0.000**
OB Region * Treatment	6	2.729	**0.023**
Error(OB Region)	48		
A-P Axis * OB Region	4	0.291	0.883
A-P Axis * OB Region * Treatment	12	1.006	0.450
Error(A-P Axis * OB Region)	96		

Table C.17: **Pairwise comparisons for OB Region * Treatment.** Table displays the pairwise comparisons for the interaction between OB Region * Treatment. Given different threshold values were used between OB regions, those pairwise comparisons were ignored. Instead the pairwise comparisons focus on differences between treatments. Bonferroni adjustment was used for multiple comparisons.

OB Region	Treatment A	Treatment B	Mean Difference (=A-B)	Standard Error	Significance
Glomerular layer	Control	3-week cuprizone	7.820	1.769	**0.001**
	Control	6-week cuprizone	10.955	1.769	**0.000**
	Control	Remyelination	5.234	1.769	**0.041**
	3-week cuprizone	6-week cuprizone	3.135	1.978	0.757
	3-week cuprizone	Remyelination	-2.586	1.978	1.000
	6-week cuprizone	Remyelination	-5.720	1.978	**0.048**
External plexiform layer	Control	3-week cuprizone	7.682	4.531	0.618
	Control	6-week cuprizone	18.943	4.531	**0.002**
	Control	Remyelination	10.348	4.531	0.189
	3-week cuprizone	6-week cuprizone	11.260	5.066	0.215
	3-week cuprizone	Remyelination	2.666	5.066	1.000
	6-week cuprizone	Remyelination	-8.594	5.066	0.616
Granular layer	Control	3-week cuprizone	1.380	3.318	1.000
	Control	6-week cuprizone	7.445	3.318	0.206
	Control	Remyelination	6.214	3.318	0.440
	3-week cuprizone	6-week cuprizone	6.065	3.710	0.691
	3-week cuprizone	Remyelination	4.834	3.710	1.000
	6-week cuprizone	Remyelination	-1.231	3.710	1.000

C.5 MBP threshold values in the OB after TMEV

MBP immunohistochemistry was quantified by calculating the percentage of pixels above a given intensity (Section 5.2.6 on p115). Differences were then analysed using a repeated measures ANOVA for A-P Axis (anterior, middle or posterior) and OB Region (glomerular layer, external plexiform layer or granular layer) that also compared Treatment (sham, day 3 TMEV, day 7 TMEV or day 14 TMEV).

Table C.18: **Means.** Table displays mean ± SEM.

		Sham	Day 3 TMEV	Day 7 TMEV	Day 14 TMEV
Number (N)	Anterior	4	4	3	2
	Middle	6	4	7	6
	Posterior	5	4	6	7
Glomerular layer	Anterior	3.16 ± 2.09	3.17 ± 1.22	0.82 ± 0.43	2.10 ± 1.31
	Middle	3.41 ± 1.10	1.22 ± 0.68	1.98 ± 0.69	3.40 ± 1.86
	Posterior	4.17 ± 1.39	2.52 ± 0.94	2.42 ± 1.93	3.61 ± 1.07
External plexiform layer	Anterior	14.07 ± 5.91	2.51 ± 0.97	1.73 ± 1.15	4.18 ± 4.16
	Middle	4.07 ± 1.79	1.53 ± 0.57	3.88 ± 1.65	3.08 ± 1.00
	Posterior	7.65 ± 4.02	2.14 ± 1.03	4.62 ± 3.61	3.61 ± 1.52
Granular layer	Anterior	1.55 ± 0.42	1.99 ± 0.90	0.80 ± 0.20	14.52 ± 11.10
	Middle	2.86 ± 1.39	1.70 ± 0.89	1.42 ± 0.68	2.66 ± 1.24
	Posterior	2.16 ± 1.12	0.59 ± 0.28	0.68 ± 0.47	1.49 ± 0.63

Table C.19: **Sphericity testing.** Table displays sphericity of data with the conclusions that OB Region and A-P Axis * OB Region have sphericity, and future calculations can be performed without corrections; and A-P Axis does not have sphericity and future calculations should use the Greenhouse-Geisser correction.

Within Subjects Effect	Approx. Chi-Square	df	Significance	Epsilon (Greenhouse-Geisser)	Epsilon (Huynh-Feldt)
A-P Axis	6.499	2	**0.039**	0.643	0.953
OB Region	1.585	2	0.453	0.848	1.000
A-P Axis * OB Region	16.588	9	0.061	0.538	0.949

Table C.20: **Main effects and interactions.** Table displays main effects and interactions for different comparisons. The most complex interaction was A-P Axis * OB Region * Treatment, which was used for the pairwise comparisons.

Comparison	df	F	Significance
Treatment	3	1.050	0.417
Error (Treatment)	9		
A-P Axis	1.285	4.395	0.051
A-P Axis * Treatment	3.856	1.398	0.295
Error(A-P Axis)	11.567		
OB Region	2	2.012	0.163
OB Region * Treatment	6	3.087	**0.029**
Error(OB Region)	18		
A-P Axis * OB Region	4	1.878	0.135
A-P Axis * OB Region * Treatment	12	3.456	**0.002**
Error(A-P Axis * OB Region)	36		

Table C.21: **Pairwise comparisons for A-P Axis within A-P Axis * OB Region * Treatment interaction.** Table displays the pairwise comparisons for the interaction between A-P Axis * OB Region * Treatment. Given different threshold values were used between OB regions, those pairwise comparisons were ignored. Instead the pairwise comparisons focus on A-P Axis and Treatment (next table). Bonferroni adjustment was used for multiple comparisons.

OB Region	Treatment	A-P Axis A	A-P Axis B	Mean Difference (=A-B)	Standard Error	Significance
Glomerular layer	Sham	Anterior	Middle	-0.020	1.456	1.000
		Anterior	Posterior	-0.164	1.455	1.000
		Middle	Posterior	-0.144	0.727	1.000
	Day 3 TMEV	Anterior	Middle	1.946	1.456	0.642
		Anterior	Posterior	0.645	1.455	1.000
		Middle	Posterior	-1.302	0.727	0.321
	Day 7 TMEV	Anterior	Middle	-1.682	1.681	1.000
		Anterior	Posterior	0.347	1.680	1.000
		Middle	Posterior	2.029	0.840	0.117
	Day 14 TMEV	Anterior	Middle	1.369	2.059	1.000
		Anterior	Posterior	1.404	2.057	1.000
		Middle	Posterior	0.035	1.028	1.000
External plexiform layer	Sham	Anterior	Middle	10.269	2.990	**0.022**
		Anterior	Posterior	10.278	3.908	0.082
		Middle	Posterior	0.009	2.235	1.000
	Day 3 TMEV	Anterior	Middle	0.983	2.990	1.000
		Anterior	Posterior	0.369	3.908	1.000
		Middle	Posterior	-0.614	2.235	1.000
	Day 7 TMEV	Anterior	Middle	-4.666	3.453	0.629
		Anterior	Posterior	1.073	4.513	1.000
		Middle	Posterior	5.739	2.581	0.160
	Day 14 TMEV	Anterior	Middle	1.595	4.229	1.000
		Anterior	Posterior	4.093	5.527	1.000
		Middle	Posterior	2.498	3.161	1.000

Granular layer	Sham	Anterior	Middle	-0.539	1.874	1.000
		Anterior	Posterior	0.446	2.731	1.000
		Middle	Posterior	0.985	1.299	1.000
	Day 3 TMEV	Anterior	Middle	0.290	1.874	1.000
		Anterior	Posterior	1.395	2.731	1.000
		Middle	Posterior	1.104	1.299	1.000
	Day 7 TMEV	Anterior	Middle	0.282	2.164	1.000
		Anterior	Posterior	0.705	3.153	1.000
		Middle	Posterior	0.424	1.501	1.000
	Day 14 TMEV	Anterior	Middle	10.413	2.650	**0.010**
		Anterior	Posterior	14.358	3.862	**0.014**
		Middle	Posterior	3.945	1.838	0.181

Table C.22: **Pairwise comparisons for Treatment within A-P Axis * OB Region * Treatment interaction.** Table displays the pairwise comparisons for the interaction between A-P Axis * OB Region * Treatment. Given different threshold values were used between OB regions, those pairwise comparisons were ignored. Instead the pairwise comparisons focus on A-P Axis (previous table) and Treatment. Bonferroni adjustment was used for multiple comparisons.

A-P Axis	OB Region	Treatment A	Treatment B	Mean Difference (=A-B)	Standard Error	Significance
Anterior	Glomerular layer	Sham	Day 3 TMEV	-0.002	2.041	1.000
		Sham	Day 7 TMEV	2.346	2.205	1.000
		Sham	Day 14 TMEV	1.067	2.500	1.000
		Day 3 TMEV	Day 7 TMEV	2.348	2.205	1.000
		Day 3 TMEV	Day 14 TMEV	1.069	2.500	1.000
		Day 7 TMEV	Day 14 TMEV	-1.279	2.635	1.000
	External plexiform layer	Sham	Day 3 TMEV	11.555	5.123	0.303
		Sham	Day 7 TMEV	12.333	5.533	0.317
		Sham	Day 14 TMEV	9.884	6.274	0.898
		Day 3 TMEV	Day 7 TMEV	0.778	5.533	1.000
		Day 3 TMEV	Day 14 TMEV	-1.671	6.274	1.000
		Day 7 TMEV	Day 14 TMEV	-2.450	6.614	1.000
	Granular layer	Sham	Day 3 TMEV	-0.433	3.790	1.000
		Sham	Day 7 TMEV	0.755	4.094	1.000
		Sham	Day 14 TMEV	-12.965	4.642	0.126
		Day 3 TMEV	Day 7 TMEV	1.187	4.094	1.000
		Day 3 TMEV	Day 14 TMEV	-12.533	4.642	0.146
		Day 7 TMEV	Day 14 TMEV	-13.720	4.893	0.123
	Glomerular layer	Sham	Day 3 TMEV	1.964	1.322	1.000
		Sham	Day 7 TMEV	0.684	1.428	1.000
		Sham	Day 14 TMEV	2.456	1.620	0.982
		Day 3 TMEV	Day 7 TMEV	-1.280	1.428	1.000
		Day 3 TMEV	Day 14 TMEV	0.492	1.620	1.000
		Day 7 TMEV	Day 14 TMEV	1.772	1.707	1.000

Middle	External plexiform layer	Sham	Day 3 TMEV	2.268	3.135	1.000
		Sham	Day 7 TMEV	-2.602	3.386	1.000
		Sham	Day 14 TMEV	1.210	3.840	1.000
		Day 3 TMEV	Day 7 TMEV	-4.870	3.386	1.000
		Day 3 TMEV	Day 14 TMEV	-1.059	3.840	1.000
		Day 7 TMEV	Day 14 TMEV	3.812	4.048	1.000
	Granular layer	Sham	Day 3 TMEV	0.397	1.658	1.000
		Sham	Day 7 TMEV	1.576	1.791	1.000
		Sham	Day 14 TMEV	-2.013	2.031	1.000
		Day 3 TMEV	Day 7 TMEV	1.179	1.791	1.000
		Day 3 TMEV	Day 14 TMEV	-2.409	2.031	1.000
		Day 7 TMEV	Day 14 TMEV	-3.588	2.141	0.768
Posterior	Glomerular layer	Sham	Day 3 TMEV	0.807	1.419	1.000
		Sham	Day 7 TMEV	2.857	1.533	0.571
		Sham	Day 14 TMEV	2.635	1.738	0.983
		Day 3 TMEV	Day 7 TMEV	2.050	1.533	1.000
		Day 3 TMEV	Day 14 TMEV	1.829	1.738	1.000
		Day 7 TMEV	Day 14 TMEV	-0.222	1.832	1.000
	External plexiform layer	Sham	Day 3 TMEV	1.646	1.453	1.000
		Sham	Day 7 TMEV	3.128	1.569	0.464
		Sham	Day 14 TMEV	3.699	1.779	0.405
		Day 3 TMEV	Day 7 TMEV	1.483	1.569	1.000
		Day 3 TMEV	Day 14 TMEV	2.053	1.779	1.000
		Day 7 TMEV	Day 14 TMEV	0.570	1.876	1.000
	Granular layer	Sham	Day 3 TMEV	0.516	0.487	1.000
		Sham	Day 7 TMEV	1.014	0.526	0.516
		Sham	Day 14 TMEV	0.947	0.597	0.882
		Day 3 TMEV	Day 7 TMEV	0.498	0.526	1.000
		Day 3 TMEV	Day 14 TMEV	0.431	0.597	1.000
		Day 7 TMEV	Day 14 TMEV	-0.067	0.629	1.000

C.6 BrdU+ cells in the SVZ and CC after cuprizone treatment

BrdU immunohistochemistry was used to quantify the number of migrating cells (Section 6.2.2 on p132). Differences were analysed using a repeated measures ANOVA for SVZ or CC Region (dorsolateral, upper striatal, lower striatal, ventral, septal or subcallosal; or medial or lateral) that also compared Genotype (Gal-$3^{+/+}$ or Gal-$3^{-/-}$), Treatment (control or cuprizone) and Length (3-weeks, 6-weeks or remyelination).

Table C.23: **Means.** Table displays mean ± SEM.

		3-weeks		6-weeks		Remyelination	
		Gal-$3^{+/+}$	Gal-$3^{-/-}$	Gal-$3^{+/+}$	Gal-$3^{-/-}$	Gal-$3^{+/+}$	Gal-$3^{-/-}$
Number (N)	Control	5	3	3	3	3	3
	Cuprizone	6	6	6	6	6	6
Dosolateral SVZ	Control	5.23 ± 0.45	4.44 ± 0.53	2.94 ± 0.34	3.19 ± 0.28	2.17 ± 0.25	3.00 ± 0.50
	Cuprizone	6.12 ± 0.85	3.41 ± 0.31	1.54 ± 0.47	2.11 ± 0.46	1.03 ± 0.11	1.29 ± 0.28
Upper striatal SVZ	Control	2.85 ± 0.72	3.44 ± 0.55	1.86 ± 0.77	1.89 ± 0.39	1.44 ± 0.53	1.34 ± 0.16
	Cuprizone	2.61 ± 0.19	2.24 ± 0.33	1.15 ± 0.20	1.16 ± 0.33	0.86 ± 0.19	0.75 ± 0.21
Lower striatal SVZ	Control	3.34 ± 0.35	4.08 ± 0.21	1.92 ± 0.29	1.89 ± 0.59	1.56 ± 0.49	2.17 ± 0.25
	Cuprizone	2.81 ± 0.69	2.31 ± 0.46	0.73 ± 0.24	0.69 ± 0.20	0.58 ± 0.15	0.89 ± 0.09
Ventral SVZ	Control	10.89 ± 1.08	10.61 ± 2.72	6.58 ± 0.34	5.61 ± 0.59	4.50 ± 0.98	5.31 ± 0.90
	Cuprizone	8.34 ± 1.13	3.56 ± 0.87	1.66 ± 0.56	1.19 ± 0.20	1.22 ± 0.16	1.21 ± 0.25
Septal SVZ	Control	2.59 ± 0.45	2.69 ± 0.40	2.17 ± 0.44	1.31 ± 0.37	1.28 ± 0.34	0.41 ± 0.05
	Cuprizone	1.86 ± 0.18	1.70 ± 0.33	1.03 ± 0.33	0.76 ± 0.21	0.71 ± 0.17	0.79 ± 0.11
Subcallosal SVZ	Control	1.78 ± 0.25	2.39 ± 0.68	0.94 ± 0.29	1.53 ± 0.46	1.06 ± 0.15	0.74 ± 0.30
	Cuprizone	3.28 ± 0.30	2.70 ± 0.46	2.27 ± 0.39	1.81 ± 0.47	2.21 ± 0.22	1.58 ± 0.22
Medial CC	Control	20.46 ± 4.30	24.67 ± 6.88	14.06 ± 2.80	8.75 ± 0.73	5.44 ± 1.99	3.06 ± 0.75
	Cuprizone	23.28 ± 5.40	23.42 ± 3.14	15.78 ± 4.62	25.48 ± 5.09	15.08 ± 2.28	19.49 ± 4.31
Lateral CC	Control	12.46 ± 5.15	7.50 ± 2.69	4.56 ± 1.26	5.11 ± 1.84	3.00 ± 1.58	1.77 ± 0.49
	Cuprizone	8.43 ± 1.33	6.08 ± 1.69	4.11 ± 1.23	8.32 ± 3.19	2.46 ± 0.88	3.35 ± 1.40

Table C.24: **Sphericity testing.** Table displays sphericity of data with the conclusion that future analysis of SVZ data should use the Greenhouse-Geisser correction; sphericity testing could not be completed for CC as there were only two variables.

	Within Subjects Effect	Approx. Chi-Square	df	Significance	Epsilon (Greenhouse-Geisser)	Epsilon (Huynh-Feldt)
SVZ	Region	91.523	14	**0.000**	0.533	0.712
CC	Region	0.000	0	.	1.000	1.000

Table C.25: **Main effects and interactions.** Table displays main effects and interactions for different comparisons. The most complex interactions were Length * Treatment * Genotype, Region * Treatment and Region * Length * Genotype for SVZ; and Length and Region * Treatment for CC. They were used for the pairwise comparisons.

	SVZ			CC		
Comparison	df	F	Significance	df	F	Significance
Length	2	122.626	**0.000**	2	8.358	**0.001**
Treatment	1	70.315	**0.000**	1	4.034	0.051
Genotype	1	3.318	0.075	1	0.127	0.723
Length * Treatment	2	0.457	0.636	2	1.735	0.188
Length * Genotype	2	2.814	0.071	2	0.232	0.794
Treatment * Genotype	1	4.898	**0.032**	1	1.395	0.244
Length * Treatment * Genotype	2	4.194	**0.022**	2	0.636	0.534
Error	44			44		
Region	2.664	80.755	**0.000**	1	91.096	**0.000**
Region * Length	5.328	11.317	**0.000**	2	2.563	0.089
Region * Treatment	2.664	33.584	**0.000**	1	11.951	**0.001**
Region * Genotype	2.664	1.682	0.180	1	0.974	0.329
Region * Length * Treatment	5.328	0.718	0.619	2	1.306	0.281
Region * Length * Genotype	5.328	2.417	**0.037**	2	0.654	0.525
Region * Treatment * Genotype	2.664	1.221	0.304	1	0.456	0.503
Region * Length * Treatment * Genotype	5.328	0.753	0.594	2	1.352	0.269
Error(Region)	117.217			44		

Table C.26: **Pairwise comparisons for Genotype within Length * Treatment * Genotype interaction in the SVZ.** Table displays the pairwise comparisons between genotypes for the interaction between Length * Treatment * Genotype in the SVZ. Bonferroni adjustment was used for multiple comparisons.

Length	Treatment	Genotype A	Genotype B	Mean Difference (A-B)	Standard Error	Significance
3-weeks	Control	Gal-$3^{+/+}$	Gal-$3^{-/-}$	-0.163	0.352	0.645
	Cuprizone	Gal-$3^{+/+}$	Gal-$3^{-/-}$	1.517	0.278	**0.000**
6-weeks	Control	Gal-$3^{+/+}$	Gal-$3^{-/-}$	0.167	0.393	0.674
	Cuprizone	Gal-$3^{+/+}$	Gal-$3^{-/-}$	0.111	0.278	0.691
Remyelination	Control	Gal-$3^{+/+}$	Gal-$3^{-/-}$	-0.163	0.393	0.680
	Cuprizone	Gal-$3^{+/+}$	Gal-$3^{-/-}$	0.016	0.278	0.954

Table C.27: **Pairwise comparisons for Treatment within Length * Treatment * Genotype interaction in the SVZ.** Table displays the pairwise comparisons between treatments for the interaction of Length * Treatment * Genotype. Bonferroni adjustment was used for multiple comparisons.

Length	Genotype	Treatment A	Treatment B	Mean Difference (A-B)	Standard Error	Significance
3-weeks	Gal-$3^{+/+}$	Control	Cuprizone	0.279	0.292	0.344
	Gal-$3^{-/-}$	Control	Cuprizone	1.959	0.340	**0.000**
6-weeks	Gal-$3^{+/+}$	Control	Cuprizone	1.339	0.340	**0.000**
	Gal-$3^{-/-}$	Control	Cuprizone	1.283	0.340	**0.000**
Remyelination	Gal-$3^{+/+}$	Control	Cuprizone	0.898	0.340	**0.011**
	Gal-$3^{-/-}$	Control	Cuprizone	1.077	0.340	**0.003**

Table C.28: **Pairwise comparisons for Length within Length * Treatment * Genotype interaction in the SVZ.** Table displays the pairwise comparisons between lengths for the interaction of Length * Treatment * Genotype. Bonferroni adjustment was used for multiple comparisons.

Treatment	Genotype	Length A	Length B	Mean Difference (A-B)	Standard Error	Significance
Control	Gal-$3^{+/+}$	3-weeks	6-weeks	1.712	0.352	**0.000**
		3-weeks	Remyelination	2.448	0.352	**0.000**
		6-weeks	Remyelination	0.736	0.393	0.203
	Gal-$3^{-/-}$	3-weeks	6-weeks	2.042	0.393	**0.000**
		3-weeks	Remyelination	2.448	0.393	**0.000**
		6-weeks	Remyelination	0.406	0.393	0.920
Cuprizone	Gal-$3^{+/+}$	3-weeks	6-weeks	2.772	0.278	**0.000**
		3-weeks	Remyelination	3.067	0.278	**0.000**
		6-weeks	Remyelination	0.295	0.278	0.881
	Gal-$3^{-/-}$	3-weeks	6-weeks	1.366	0.278	**0.000**
		3-weeks	Remyelination	1.566	0.278	**0.000**
		6-weeks	Remyelination	0.200	0.278	1.000

Table C.29: **Pairwise comparisons for Region * Treatment interaction in the SVZ.** Table displays the pairwise comparisons for the interaction between Region * Treatment in the SVZ. Given the anatomic heterogeneity between regions, those pairwise comparisons were ignored. Instead the pairwise comparisons focus on differences between lengths. Bonferroni adjustment was used for multiple comparisons.

Region	Treatment A	Treatment B	Mean Difference (A-B)	Standard Error	Significance
Dorsolateral SVZ	Control	Cuprizone	0.914	0.297	**0.004**
Upper striatal SVZ	Control	Cuprizone	0.677	0.232	**0.006**
Lower striatal SVZ	Control	Cuprizone	1.158	0.239	**0.000**
Ventral SVZ	Control	Cuprizone	4.390	0.530	**0.000**
Septal SVZ	Control	Cuprizone	0.599	0.179	**0.002**
Subcallosal SVZ	Control	Cuprizone	-0.902	0.232	**0.000**

Table C.30: **Pairwise comparisons for Genotype within Region * Length * Genotype interaction in the SVZ.** Table displays the pairwise comparisons for the interaction between Region * Length * Genotype in the SVZ. Given the anatomic heterogeneity between regions, those pairwise comparisons were ignored. Instead the pairwise comparisons focus on Genotype and Length (next table). Bonferroni adjustment was used for multiple comparisons.

Region	Length	Genotype A	Genotype B	Mean Difference (A-B)	Standard Error	Significance
Dorsolateral SVZ	3-weeks	Gal-3$^{+/+}$	Gal-3$^{-/-}$	1.749	0.491	**0.001**
	6-weeks	Gal-3$^{+/+}$	Gal-3$^{-/-}$	-0.406	0.527	0.446
	Remyelination	Gal-3$^{+/+}$	Gal-3$^{-/-}$	-0.549	0.527	0.304
Upper striatal SVZ	3-weeks	Gal-3$^{+/+}$	Gal-3$^{-/-}$	-0.116	0.383	0.764
	6-weeks	Gal-3$^{+/+}$	Gal-3$^{-/-}$	-0.019	0.411	0.963
	Remyelination	Gal-3$^{+/+}$	Gal-3$^{-/-}$	0.106	0.411	0.799
Lower striatal SVZ	3-weeks	Gal-3$^{+/+}$	Gal-3$^{-/-}$	-0.122	0.395	0.759
	6-weeks	Gal-3$^{+/+}$	Gal-3$^{-/-}$	0.036	0.424	0.933
	Remyelination	Gal-3$^{+/+}$	Gal-3$^{-/-}$	-0.458	0.424	0.286
Ventral SVZ	3-weeks	Gal-3$^{+/+}$	Gal-3$^{-/-}$	2.533	0.874	**0.006**
	6-weeks	Gal-3$^{+/+}$	Gal-3$^{-/-}$	0.719	0.939	0.447
	Remyelination	Gal-3$^{+/+}$	Gal-3$^{-/-}$	-0.399	0.939	0.673
Septal SVZ	3-weeks	Gal-3$^{+/+}$	Gal-3$^{-/-}$	0.031	0.295	0.916
	6-weeks	Gal-3$^{+/+}$	Gal-3$^{-/-}$	0.564	0.317	0.082
	Remyelination	Gal-3$^{+/+}$	Gal-3$^{-/-}$	0.392	0.317	0.223
Subcallosal SVZ	3-weeks	Gal-3$^{+/+}$	Gal-3$^{-/-}$	-0.014	0.383	0.971
	6-weeks	Gal-3$^{+/+}$	Gal-3$^{-/-}$	-0.061	0.411	0.883
	Remyelination	Gal-3$^{+/+}$	Gal-3$^{-/-}$	0.468	0.411	0.261

Table C.31: **Pairwise comparisons for Length within Region * Length * Genotype interaction in the SVZ.** Table displays the pairwise comparisons for the interaction between Region * Length * Genotype in the SVZ. Given the anatomic heterogeneity between regions, those pairwise comparisons were ignored. Instead the pairwise comparisons focus on Genotype (previous table) and Length. Bonferroni adjustment was used for multiple comparisons.

Region	Genotype	Length A	Length B	Mean Difference (A-B)	Standard Error	Significance
Dorsolateral SVZ	Gal-$3^{+/+}$	3-weeks	6-weeks	3.432	0.491	**0.000**
		3-weeks	Remyelination	4.079	0.491	**0.000**
		6-weeks	Remyelination	0.647	0.527	0.678
	Gal-$3^{-/-}$	3-weeks	6-weeks	1.278	0.527	0.059
		3-weeks	Remyelination	1.782	0.527	**0.005**
		6-weeks	Remyelination	0.504	0.527	1.000
Upper striatal SVZ	Gal-$3^{+/+}$	3-weeks	6-weeks	1.221	0.383	**0.008**
		3-weeks	Remyelination	1.573	0.383	**0.001**
		6-weeks	Remyelination	0.353	0.411	1.000
	Gal-$3^{-/-}$	3-weeks	6-weeks	1.317	0.411	**0.008**
		3-weeks	Remyelination	1.794	0.411	**0.000**
		6-weeks	Remyelination	0.478	0.411	0.755
Lower striatal SVZ	Gal-$3^{+/+}$	3-weeks	6-weeks	1.748	0.395	**0.000**
		3-weeks	Remyelination	2.003	0.395	**0.000**
		6-weeks	Remyelination	0.256	0.424	1.000
	Gal-$3^{-/-}$	3-weeks	6-weeks	1.906	0.424	**0.000**
		3-weeks	Remyelination	1.667	0.424	**0.001**
		6-weeks	Remyelination	-0.239	0.424	1.000
Ventral SVZ	Gal-$3^{+/+}$	3-weeks	6-weeks	5.497	0.874	**0.000**
		3-weeks	Remyelination	6.755	0.874	**0.000**
		6-weeks	Remyelination	1.258	0.939	0.561
	Gal-$3^{-/-}$	3-weeks	6-weeks	3.683	0.939	**0.001**
		3-weeks	Remyelination	3.824	0.939	**0.001**
		6-weeks	Remyelination	0.140	0.939	1.000

Septal SVZ	Gal-$3^{+/+}$	3-weeks	6-weeks	0.631	0.295	0.114
		3-weeks	Remyelination	1.236	0.295	**0.000**
		6-weeks	Remyelination	0.604	0.317	0.190
	Gal-$3^{-/-}$	3-weeks	6-weeks	1.164	0.317	**0.002**
		3-weeks	Remyelination	1.596	0.317	**0.000**
		6-weeks	Remyelination	0.432	0.317	0.540
Subcallosal SVZ	Gal-$3^{+/+}$	3-weeks	6-weeks	0.922	0.383	0.061
		3-weeks	Remyelination	0.898	0.383	0.070
		6-weeks	Remyelination	-0.024	0.411	1.000
	Gal-$3^{-/-}$	3-weeks	6-weeks	0.875	0.411	0.117
		3-weeks	Remyelination	1.381	0.411	**0.005**
		6-weeks	Remyelination	0.506	0.411	0.676

Table C.32: **Pairwise comparisons for Length in the CC.** Table displays the pairwise comparisons for the main effect of Length in the CC. Bonferroni adjustment was used for multiple comparisons.

Length A	Length B	Mean Difference (A-B)	Standard Error	Significance
3-weeks	6-weeks	5.016	2.232	0.089
3-weeks	Remyelination	9.081	2.232	**0.001**
6-weeks	Remyelination	4.065	2.310	0.256

Table C.33: **Pairwise comparisons for Region * Treatment in the CC.** Table displays the pairwise comparisons for the interaction between Region * Treatment in the CC. Given the anatomic heterogeneity between regions, those pairwise comparisons were ignored. Instead the pairwise comparisons focus on differences between treatments. Bonferroni adjustment was used for multiple comparisons.

Region	Treatment A	Treatment B	Mean Difference (A-B)	Standard Error	Significance
Medial CC	Control	Cuprizone	-7.683	2.701	**0.007**
Lateral CC	Control	Cuprizone	0.275	1.468	0.852